The Prediction of Nociceptive Neural Activity in Passive Tissues Following Lumbar Spine Flexion

by

Daniel Viggiani

A thesis

presented to the University of Waterloo

in fulfillment of the

thesis requirement for the degree of

Doctor of Philosophy

in

Kinesiology

Waterloo, Ontario, Canada, 2021

Examining Committee Membership

The following served on the Examining Committee for this thesis. The decision of the Examining Committee is by majority vote.

External Examiner	Laura A. Frey Law, MPT, PhD Associate Professor, Physical Therapy and Rehabilitation Sciences University of Iowa
Supervisor	Jack P. Callaghan, PhD Professor, Kinesiology and Health Sciences
Internal Members	Steven L. Fischer, PhD Associate Professor, Kinesiology and Health Sciences
	Joe Quadrilatero, PhD Professor, Kinesiology and Health Sciences
Internal-external Member	Stewart D. McLachlin, PhD Assistant Professor, Mechatronics and Mechanical Engineering

Author’s Declaration

I hereby declare that I am the sole author of this thesis. This is a true copy of the thesis, including any required final revisions, as accepted by my examiners.

I understand that my thesis may be made electronically available to the public.

Abstract

Low back pain is a costly and debilitating disorder; however, most cases are categorized as being non-specific: low back pain without an identifiable origin or cause. Non-specific low back pain can be broadly considered and treated as either musculoskeletal disorders or pain disorders. In the musculoskeletal case, mechanics and loading history are believed to disrupt or damage tissues in the low back, which then generate nociceptive signals to be interpreted as pain. If the low back pain is a pain disorder, the disruption or damage is not with the tissues of the lower back, but rather the nervous system that transmits or interprets these nociceptive signals. Additionally, these subcategories of non-specific low back pain are not wholly independent since mechanical exposures can influence nervous system activity and vice versa. A specific outcome of this interconnectedness between mechanics and neural encoding is that a mechanical exposure can alter our ability to detect mechanical loads or mechanical sensitivity. One mechanical exposure that is linked to low back pain development and has been documented to alter neural activity is lumbar spine flexion. The purpose of this thesis was to determine the extent and mechanisms underlying how lumbar spine flexion can alter lower back mechanical sensitivity through a combination of viscoelastic creep and muscle activity, and to determine the implications those changes could have on the development of low back pain. The methods undertaken to achieve this thesis' purpose were a combination of *in-vivo* human laboratory experiments, *ex-vivo* benchtop histology and mechanical testing, and *in-silico* modelling across four studies. Studies 1 and 2 quantified how mechanical sensitivity was altered over time in response to static and repetitive lumbar spine flexion respectively, Study 3 quantified the innervation properties of lumbar spine tissues, and Study 4 simulated mechanical exposures before and after lumbar spine flexion exposures to determine the nociceptive neural activity those exposures and conditions could generate.

The first two studies employed a similar design and methodology measuring mechanical sensitivity and biomechanical variables before and up to 40 minutes after a 10-minute lumbar spine flexion exposure. For Study 1, the exposure was a static, seated, maximal lumbar spine flexion exposure and for Study 2, the exposure was a repetitive, standing, maximal lumbar spine flexion exposure. A custom motorized pressure algometer was constructed for these studies and used to track three measures of mechanical sensitivity—pressure-pain threshold, stimulus intensity, and stimulus unpleasantness—in the lower back and tibial shaft. Accelerometry was used in both studies to track the development and recovery from viscoelastic creep through lumbar spine flexion range of motion, and surface electromyography was used to determine flexion-relaxation (mean amplitude) in Study 1, and muscle fatigue (mean power frequency) in Study 2. Isometric joint strength and ratings of perceived exertion were also measured in Study 2. These data were fed into two main statistical processes: the first aimed to determine the time-course of mechanical sensitivity changes in the lower back relative to the tibial control site, and the second was to determine if any of the biomechanical variables (creep, muscle use, strength) or tibial mechanical sensitivities could predict lower back mechanical sensitivity changes.

The static exposure generated a 10.3% creep response (4.4 ± 2.7°) in flexion range of motion that lasted for at least 40 minutes after the exposure. This exposure caused a transient increase in lower back stimulus unpleasantness but otherwise did not affect mechanical sensitivity nor did it affect flexion-relaxation. The strongest predictor of lower back mechanical sensitivity throughout the static exposure was the tibial surrogate; however, the magnitude of creep was also a significant predictor of changes in lower back pressure-pain thresholds. Despite being significant, these significant predictors could not explain the majority to the variance in mechanical sensitivity, and these changes appear more related to emotional

affect than a physiological response. Study 1 concluded that a static lumbar spine flexion exposure that did not incorporate muscle activity did not alter nociceptive activity but could shape how nociceptive activity is experienced.

The repetitive exposure generated a 5.0% creep response (2.7 ± 1.4°) in flexion range of motion dissipated within 5 minutes of the exposure ending. This exposure caused an immediate and transient decrease in lumbar spine extensor mean power frequency (5.1%) and lower back joint strength (9.8%) indicative of muscle fatigue, and a delayed 13.6% increase in lower back pressure-pain thresholds occurring 10 minutes after the exposure ended. Like Study 1, tibial mechanical sensitivities were the strongest predictor of lower back mechanical sensitivities, however interaction terms between these tibial surrogates and either creep magnitude or fatigue indicators (mean power frequency and strength) were also significant predictors. The delayed desensitization following this repetitive exposure was believed to arise from a combination of creep development and muscle use.

The third study used lumbar spine tissues harvested from four cadaveric donors to determine the relative concentration of four neural membrane molecules (Protein Gene Product 9.5 (PGP9.5), Calcitonin Gene-Related Peptide, Bradykinin B1-Receptor, and Acid-Sensing Ion Channel 3 (ASIC3)) relevant to detecting mechanical stimuli in three tissues (dermal skin, superficial posterior annulus fibrosus, and the supraspinous-interspinous ligament complex) using Western Blotting. Only PGP9.5 and ASIC3 were found consistently in any of the three tissues. PGP9.5 had similar concentrations in skin and ligament, both of which were at least 12.8 times higher than in annular tissues. ASIC3 was most common in skin, followed by ligament, then annulus fibrosus, however the ratio of ASIC3:PGP9.5 was highest in annular tissue.

The fourth study documents a model of nociceptive activity that predicts the likelihood that three exposures (pressure-pain threshold, flexion range of motion, and tissue failure) would generate nociceptive activity in the brainstem given a tissue (skin, annulus, or ligament), a viscoelastic state, $\zeta(t)$, and a muscle activity state, $\phi(t)$. The model simulated a single tissue-exposure combination for a sample of 100 mechanical sensitivities derived from the data in Studies 1 and 2. The model itself consisted of a Sensitivity Module that converted a tissue stress to an electrical current and a Neurological Module that used the electrical current to simulate the behaviour of a network of Hodgkin-Huxley neurons. The pressure-pain threshold exposure was used to validate the model and derive values for $\zeta(t)$ and $\phi(t)$, which were then applied to the other two exposures in annular and ligament tissues. While $\zeta(t)$, representing any effects related to creep following lumbar spine flexion, had minimal effects on nociceptive neural activity, $\phi(t)$, representing muscle activity-related effects of lumbar spine flexion, could inhibit nociceptive activity substantially. A major prediction from the model is that annulus fibrosus failure would be unlikely to generate any nociceptive activity in 12% of the population, and that characteristics of the exposure could increase that percentage to as many as 99.9% depending on the mode of failure. Flexion range of motion consistently generated no nociceptive activity in all tissues and conditions, and ligament failure consistently generated nociceptive activity regardless of other factors.

While both viscoelastic creep and muscle activity related to lumbar spine flexion can influence mechanical sensitivity, the effects of muscle activity were more prominent, and could meaningfully influence the connection between tissue disruption and low back pain. These effects were most notable in exposures that have the potential to damage the annulus fibrosus.

Acknowledgements

I am deeply indebted to my supervisor, Dr. Jack Callaghan, for supporting, encouraging, and generally believing in me through the nine years we've worked together over the course of three degrees. In addition to the scientific training as well as the prompted and unprompted advice—all of which has been valuable—you've helped me grow from being that awkward kid in your lab into a slightly-less-awkward adult. Your lab has been a blast to be a part of and I wish you the powderiest of snow to ski through and the smoothest of pavement to ride on.

I'd like to thank my examining committee for not only improving the quality of the work and stimulating critical reflection, but also for helping revitalize my interest in this project through their enthusiasm and feedback. Specifically, Drs. Steven Fischer and Stewart McLachlin pushed me towards a more nuanced understanding of viscoelasticity, Dr. Joe Quadrilatero lent me his lab and provided big-picture and technical advice on benchtop physiology, and Dr. Laura Frey Law helped show me how this thesis matters by offering valuable clinical and modelling perspectives.

The topic for and contents of this thesis were heavily inspired by a six-month visiting scholarship to Regis University and the University of Denver, which would not have been possible without the trust and support of Drs. Bradley Davidson, Erika Nelson-Wong, and Erin Mannen, but mostly Erika. From hiking/climbing lab meetings to concert-and-hipster-doughnuts to mid-conference snowball fights; it was an unforgettable experience for me both personally and professionally. At least you got a cookbook out of it. Lydia van Vleet deserves a shout-out for being an awesome roommate/host/tour guide/co-host and Dr. Jim Wong deserves a shout-out for being voluntold to fix my car. Twice.

I could not have collected the data for this thesis on my own, or at least it would not have been as clean or useful data. Anna-Mae Dueck and Zackary Tsang were instrumental during the piloting and testing of the data collected for Chapters 3 to 5 and were also my two biggest cheerleaders that I didn't deserve. You're both all-stars and I should've chosen a more obscure code than Corrin… Fasih Rahman aka Buckaroo aka One-Man-Quad-Squad trained me first on Immunofluorescence and then on Western Blotting and then on how manga can be superior to anime. Good lord, were all of those rabbit holes or what? Jeff Rice lent me his shop, gave me metal cutting/shaping contacts, and did the wiring I was too incompetent to do myself for the pressure algometer/flexion rig used in Chapter 3, Chapter 4, and Appendix C. Zinnia Chung made the crispiest gels, Emma Dare and Jenny Davey ordered/maintained all the supplies, and Erinn Frangakis and Raymond Tran made excellent photo models.

I have had no shortage of lab mates, peers, and colleagues provide insight, feedback, and advice throughout my doctorate, many of whom became my closest friends. Let's start with Drs. Alan Cudlip, Dave Kingston, Kayla Fewster, and Kristina Gruevski for leading the way through the maze of comps, proposals, and defenses; and always being open to chatting about just anything. Next are my current (and former) lab mates: Brendan Pinto, Graham Mayberry, Jackie Zehr, Jessa Buchman-Pearle, Johnny Park, Lia Tennant, Mamiko Noguchi, and Mike Glinka; all of whom helped me in and out of the lab while tolerating my bubble tea and baked pastry obsessions. You can keep the fridge but I'll be back for the sign. There is my RPG crew including Dan Martel, Natasha Ivanochko, and Taylor Winberg for training me how to improvise and contributing heavily to a more sustainable work-life balance. Then there's the talented and outspoken Evan Sauve and the talented and much-less outspoken Dr. Collin Roberts who demonstrated how to simultaneously be musicians, writers, teachers, and academics. Lastly, there's Annmarie Laudanski,

Binh Ngo, Carmen Liang, Dan Armstrong, Dan Lamontagne-Kam, Egor Avrutin, Gary Mangan, and Risa Hall who deserve a mention but didn't fit into any of the other categories. Thank you, and best of luck.

If you're reading this and feel shafted so far, your name is probably Jeffery Barrett; don't worry, this is your paragraph. In addition to being a part of most of the categories outlined thus far (Appendix E Data Collection, RPG crew, Lab mate, and Academic inspiration) and plenty of unique ones (Trivia/Podcasting, Body Improvement Club, Project Crustulum, Speedbaking, and Homebrew Editor to name a few), your help in implementing ODE solvers and insights on the optimal model-duct-tape locations shaped the latter part of this thesis. Not to mention literally coding the robot interface used in Appendix E, kind of a big thing to have almost forgotten to acknowledge. I'm sorry this isn't written in LaTeX and don't forget to water James.

I would formally like to use this space to acknowledge the Acknowledgments Section of Jonathan Park's Master's Thesis.

Ross and Doris Dixon Charitable Foundation, and the Doctoral Thesis Completion Award. I am also grateful to Marg Burnett and the administrative staff in the Department of Kinesiology and Health Studies for arranging sessional instructor opportunities to help support my doctorate training.

Lastly, I'd like to thank my family: my parents Anne and Jon, my sister Sam, my brother Pat, and my girlfriend Jen, along with Betty, Charlie, Lily, and Maddie. You might have no technical understanding of what I've been dedicating this huge chunk of my life to doing, but you've always had faith in me and supported me throughout it all. I'm more grateful for that than I've probably ever told you.

Thank you.

Table of Contents

List of Figures

List of Tables

Chapter 1 - Introduction

Musculoskeletal pain is highly prevalent and burdensome on affected individuals and the healthcare system that attempts to mitigate pain (Murray and Lopez, 2013; Woolf and Pfleger, 2003). Musculoskeletal pain is the worldwide leading source of years living with disability (Vos et al., 2012), and a major source of lost time from work in high-income countries. While often an indicator of injury (bone fractures, ligament tear) or other pathology (osteoarthritis), pain can also be a disorder unto itself (fibromyalgia, chronic regional pain syndrome) (Arendt-Nielsen et al., 2011; Loeser and Melzack, 1999). There is an identifiable mechanical or biochemical initiator responsible for generating pain in many musculoskeletal disorders (Gallagher and Heberger, 2012; Kumar, 2001; Solomonow, 2004); the disorder is with the tissue and not the sensation of pain itself. In contrast, pain disorders are disorders where there are no clearly identifiable sources of pain other than the nervous system responsible for transmitting, modulating or interpreting pain (Ehrlich, 2003; Sterling et al., 2001).

Low back pain occupies a problematic position in between a musculoskeletal injury or pathology, and a pain disorder since it may have mixed origins dependent on the specific case. A by-product of these mixed origins is that while cases related to an injury (disc herniation; (Gooyers et al., 2015; Veres et al., 2009)) or diseased state (disc degeneration; (Hansen et al., 2015; Lao et al., 2015)) are given specific names and aetiologies, those stemming from pain disorders are lumped together as non-specific low back pain. Further complicating this issue, injuries or pathologies that cannot be adequately diagnosed are amalgamated into the definition of non-specific low back pain and may be treated as a pain disorder despite mechanical or biochemical origins or vice versa (Balagué et al., 2012; Foster et al., 2011). Misalignment of the underlying causes and treatments for low back pain results in people who live with low back pain seeking multiple treatment options and staying in the healthcare system for longer (Fritz et al., 2003; Gore et al., 2012), causing high treatment costs per person.

Despite the uncertainty around its mechanisms, non-specific low back pain is often assumed to be related to the musculoskeletal system and have mechanical origins. The rationale for this conclusion is as follows:

1) The main purpose of a functioning pain system is to alert the person to an actual or potential threat of tissue damage (Basbaum et al., 2009; Braz et al., 2014; Brodal, 2017; Loeser and Melzack, 1999).
2) One of the main functions of the musculoskeletal system is to support and transfer loads during motion (Kumar, 2001; Mammoto and Ingber, 2010; Panjabi, 2003; Solomonow, 2011); the presence of pain as an internal “alarm system” would only be useful if a painful component of the musculoskeletal system had its ability to transmit or support loads altered in some fashion.
3) Mechanical loads applied to the musculoskeletal system can activate neurons and receptors capable of encoding painful stimuli (Braz et al., 2014; Ghitani et al., 2017; Ochoa and Torebjörk, 1989; Schmidt et al., 1995; Xu et al., 2008b).
4) Epidemiology has related mechanical exposures to the prevalence of low back pain (Cole and Grimshaw, 2003; Lis et al., 2007; Sterud et al., 2016; Sterud and Tynes, 2013; Tissot et al., 2009), with some empirical support for biomechanical theories relating potential mechanisms of injury to these exposures (Nelson-Wong and Callaghan, 2010; O’Sullivan et al., 2013; Shin and Mirka, 2007).

5) Successful treatments and interventions for non-specific low back pain are grounded in either directly or indirectly altering the loads on the painful tissues (Delitto et al., 1995; Stanton et al., 2011; Van Dillen et al., 2003), increasing the ability of painful tissues to tolerate loads (McGill et al., 2000; Scotti et al., 2016), or disrupting the transmission of pain itself (Kumar et al., 2007; Taylor et al., 2006; van den Beuken-van Everdingen et al., 2017).

The first two rationales are widely agreed upon by the scientific community related to acute pain. However, chronic pain states often run counter to these two rationales where pain is present in the absence of any detectable threat of tissue damage to the musculoskeletal system (Adams et al., 1999; Balagué et al., 2012; Cordero-Erausquin et al., 2016; Loeser and Melzack, 1999). Many of the features present in a person transitioning from an acute to a chronic pain patient are sociological or psychological (Costa et al., 2009; Sterling et al., 2001), suggesting a reweighting of the perception of pain relative to the strength of nociceptive stimuli (Cordero-Erausquin et al., 2016; Latremoliere and Woolf, 2009). Rationale three has been repeatedly supported in animal models (Arcourt et al., 2017; Lima et al., 2017; Ochoa and Torebjörk, 1983; Winkelstein and DeLeo, 2004) and authors must test for and identify neurons that encode mechanical pain in order to study any pain-related interventions in these animal models (Chen et al., 2006; Kashiwadani et al., 2017; Namer et al., 2015; Pitcher and Henry, 2004; Toda et al., 2004). However, the specific genes responsible for the production of membrane receptor proteins and the function of those proteins that detect painful (and non-painful) mechanical stimuli are better understood in earthworm and flea models (Bianchi and Driscoll, 2002; Geffeney and Goodman, 2012) than in mammalian homologues (Qi et al., 2015; Wetzel et al., 2017). The widespread use of pressure-pain thresholds (Hägg and Åström, 1997; Hoeger Bement et al., 2009; Jones et al., 2017; Petrini et al., 2015) and electrophysiological testing (Schmidt et al., 1995; Staud et al., 2007) confirms the presence of these neurons in humans, although the specific membrane receptor proteins are not understood to the same level of detail as in animal models (Osmakov et al., 2014). Within rationale four, the psychosocial factors related to pain in workplace or clinical settings can confound the biomechanical predictors (Roffey et al., 2010a; Wai et al., 2010). However, there have been fairly strong exposure-pain likelihood correlations in multiple workplace scenarios, where workers exposed to longer duration tasks and higher loads are more likely to develop low back pain (Cole and Grimshaw, 2003; Lis et al., 2007; Tissot et al., 2009; Xu et al., 1997). Rationale five does not consider the episodic nature and favourable prognosis of the natural history of low back pain (Costa et al., 2009; Schiottz-Christensen et al., 1999). However, studies that sort low back pain patients based on how their symptoms change with sets of conservative or surgical treatments have resulted in more efficient (Fritz et al., 2003) and better pain reduction (Fairbank et al., 2011; Foster et al., 2011; Hall et al., 2009) than general pain-mediating and physical activity-driven treatments.

Despite the rationale for a mechanical origin of non-specific musculoskeletal low back pain, attempts to isolate a specific tissue as generating a specific instance of pain has been elusive. Ligaments and joint capsules are often cited as the inciting tissues based on an analysis of forces and moments applied to systems within the low back (Cavanaugh et al., 1996; Solomonow et al., 2003), however their depth in the body prevents *in-vivo* validation of these predictions. Attempts to invasively measure the internal loads on these tissues involve modifying the mechanical properties of the tissue itself and are not feasible across large numbers of participants with current technology. *In-vitro* or *ex-vivo* studies are suitable for characterizing mechanical behavior of these tissues (Busscher et al., 2011; Callaghan and McGill, 2001; Fick et al., 2015), but require a dissociation from the brain and spinal cord in order to conduct these tests, therefore the sensation of these loads cannot be determined. Models that attempt to predict the loads within these tissues

do not generate neural outputs to the brain in order to assess whether those loads could be perceived as painful (Arjmand and Shirazi-Adl, 2006; Cholewicki and McGill, 1994; Reynaud and Quinn, 2006; van Dieën and Kingma, 2005), but may be expanded in order to include this feature (Argüello et al., 2015; Britton and Skevington, 1989; Xu et al., 2008b). While *in-situ* studies have been able to combine the ability to manipulate controlled loads with measures of sensory afferent information, these animal studies involve terminating the subject after the procedure is completed due to the level of invasiveness that prevents its use on humans (Cavanaugh et al., 1996; Lima et al., 2017; Winkelstein and DeLeo, 2004). Therefore, a predictive model of pain combining biomechanical and neurophysiological foundations is the most feasible currently available method to validate if non-specific musculoskeletal low back pain can be caused by loading, injury, or damage to a particular tissue.

The intrinsic properties of passive tissues in the spine may affect how sensory information is transmitted to the brain and perceived by the person (Abboud et al., 2016; Sánchez-Zuriaga et al., 2010). Ligaments, joint capsules and other passive collagenous tissues are considered viscoelastic—they have viscous/fluid and elastic/solid attributes (Provenzano et al., 2002, 2001). One phenomenon that arises from the interplay of solid and fluid elements is viscoelastic creep: a time-dependent increase in deformation for a given force (McGill and Brown, 1992; Shin et al., 2009; Thornton et al., 2002). Creep occurring in the posterior ligaments of the spine is prominently featured in discussions of low back pain arising from repetitive or prolonged trunk flexion (Arjmand and Shirazi-Adl, 2006; Parkinson et al., 2004; Shin et al., 2009; Shin and Mirka, 2007). Ligamentous creep is associated with local inflammatory responses (Pinski et al., 2010; Yang et al., 2011), which can interact with pain-sensing neurons to affect a person's pain perception to a given magnitude of stress or strain (Braz et al., 2014; Kidd and Urban, 2001; Solomonow, 2004). There is evidence that ligament creep can affect the electrical activity generated by muscles surrounding the tissues undergoing creep (Andersen et al., 1995; Claude et al., 2003; Granata et al., 2005). Furthermore, the modality (static or repetitive) and stresses producing ligament creep have resulted in different neuromuscular adaptations during the development and recovery from creep exposures (Little and Khalsa, 2005; Toosizadeh et al., 2012; Toosizadeh and Nussbaum, 2013). Other muscular- (Kennedy et al., 2015; Taylor et al., 2000) or physical activity-related factors (Ellingson et al., 2014; Koltyn et al., 2014) that arise from moving into and about spinal postures that generate creep can also affect pain sensitivity.

A global objective of this thesis is to develop a more complete understanding of how mechanical loads in passive linkages of the musculoskeletal system can result in pain. The thesis focuses on passive tissue creep in the low back because of its prevalence (Boschman et al., 2011; Grant et al., 1995; Thiede et al., 2014) and the theorized relevance of these tissues to clinical low back pain (Arendt-Nielsen et al., 2011; Solomonow, 2004; Thornton et al., 2002). The first two studies determined how the accumulation and recovery from tissue creep affected low back pain sensitivity in two models of tissue creep: passive static spine flexion (Chapter 3) and active repetitive spine flexion (Chapter 4). The third study documented innervation characteristics of lower back passive tissues in cadavers (Chapter 6). The fourth study took measurements from the first three studies to generate a mechanism-driven model of mechanical ligamentous pain in the low back accounting for viscoelastic creep (Chapter 7).

Chapter 2 - Literature Review

This chapter is intended to provide a general framework that will support the studies outlined in this thesis. The literature specific to each study is discussed in the Introduction sections of each chapter. This section starts with explicit definitions of terminology used throughout the document, followed by an overview of low back anatomy and general neuron function. A current understanding of the sensation of mechanical pain is then described considering the definitions, anatomy, and neurophysiology. The subsequent sections focus on the problem of low back pain and viscoelastic properties of the tissues in the low back. A final section summarizing outstanding problems from the literature review are provided to frame the position of the studies proposed for Chapters 3 through 6 within the existing knowledge.

2.1 Definitions and Terminology

This section serves to introduce the reader to terminology and provide high-level details from the literature, more depth is provided in later sections.

2.1.1 Pain-Related Terminology

The terminology used here draws heavily from the International Association for the Study of Pain, who published a formal list of definitions in 2008 (Loeser and Treede, 2008), which was updated in 2020 (Raja et al., 2020).

Pain

The International Association for the Study of Pain defines pain as "an unpleasant sensory and emotional experience associated with actual or potential tissue damage, or described in terms of such damage" (Loeser and Treede, 2008; Raja et al., 2020). This definition acknowledges a somatic and cognitive element, and that pain itself does not require any actual damage to have occurred (Williams and Craig, 2016). However this definition also implies a massive amount of personal variability and subjectivity inherent in pain being an experience (Dennett, 1978). The phrase "… or described in terms of such damage" also implicates that people often link pain to some form of damage, a practice with historical and linguistic origins (Duncan, 2017). There have been calls to revise this definition despite its thoroughness. Williams and Craig (2016) have suggested that pain be a "distressing experience" and that it has "sensory, emotional, cognitive and social components", arguing that "unpleasant" is not a strong enough descriptor and that the "cognitive and social" elements of a painful experience not be lumped together with the emotional elements. Pain has been argued to be a homeostatic perturbation detector, where it warns a person of disruptions to homeostasis, which could be physical or emotional (Craig, 2003). Abstracting further, it has also been argued that pain is a "conjectured entity" that cannot be observed directly yet can emerge naturally from a "dynamic and complex interaction" of organs and tissues, the neurons that innervate them, and cognitive, emotional, physical, social, or other brain states (Doleys, 2017). Despite an intricate and debated conceptual definition, pain has a relatively straightforward functional definition: it is believed to serve as a "warning system" to prevent excessive damage to the individual (Brodal, 2017; Julius and Basbaum, 2001). Cases where pain is no longer useful as a warning system, such as in those with phantom limb pain, reveal that plastic changes have occurred in the central nervous system causing people to experience pain without any "actual or potential tissue damage" (Flor et al., 2006). This corresponds with emerging evidence that there could be a neurological "signature" of brain activity unique to the experience of pain (Baliki and Apkarian, 2015; Kucyi and Davis, 2017; Wager et al., 2013) further expanded in Section 2.4.3.

Despite multifactorial definitions, attempts to quantify pain frequently reduce it to a unidimensional intensity (Duncan, 2017; Hjermstad et al., 2011; Kemp et al., 2012), often assuming ratio properties in discrete or continuous numerical scales (Gallagher et al., 2001; Hägg et al., 2003; Kelly, 2001; Price et al., 1983; Todd et al., 1996). Since clinicians frequently assess pain with unidimensional scales, lay people seeking pain treatments can believe this to be a useful metric, and in turn frame their own thinking about pain in this way, which can affect their prognosis (Atlas and Wager, 2012; Moseley and Butler, 2015). Similar to how knowledge about one's heart rate can affect their heart rate (Blanchard et al., 1984), the knowledge and manner of thinking about pain can affect their experience of pain (Moseley and Butler, 2015). Arguments for simplifying pain to an intensity are based on external validity; they allow for a quick and reliable way to assess an overall meaningful change in those living with pain (Gallagher et al., 2001; Kelly, 2001). The reported sensitivity and reliability of numerical rating (Hjermstad et al., 2011) or visual analog scales (Bird and Dickson, 2001) in providing clinically meaningful representations is remarkable considering they involve a numerical or spatial summary of a subjective interpretation of an individual-specific experience derived from a large diversity of physiological responses. Additionally, comprehensive assessments of pain designed for clinical or chronic pain (Melzack, 1987, 1975) lack the temporal resolution required for most studies involving repeated measures that instead focus on one (Cecchi et al., 2012; Gallagher et al., 2014; Rabey et al., 2017) or two dimensions (Ellingson et al., 2014; Petrini et al., 2015) of pain. When researchers include a second dimension of pain, the "unpleasantness", interpreted to represent the emotional or experiential side of pain (Ellingson et al., 2014; Petrini et al., 2015), is tracked in addition to the "intensity", which refers to the physiological strength of that stimulus.

For the purposes of this thesis, pain will be defined conceptually as the subjective interpretation of an unpleasant physiological stimulus (Loeser and Treede, 2008; Raja et al., 2020), and functionally as a means to inform a person of potential impending damage (Brodal, 2017). A person will be in pain if they consider themselves to be in pain (Dennett, 1978; Nagel, 1974), and can ascribe at least an intensity and unpleasantness to that pain (Duncan, 2017; Ellingson et al., 2014; Petrini et al., 2015).

Noxious Stimuli, Nociception, Nociceptive Neurons, and Nociceptors

The terms noxious stimulus, nociception, nociceptive neuron, and nociceptor are all related to the physiological responses associated with painful experiences. First, all sensory stimuli can be split into noxious, and non-noxious stimuli; noxious stimuli will or have the potential to damage tissues (Loeser and Treede, 2008). A noxious stimulus can be mechanical (e.g. pinching, stretch, ripping) (Garell et al., 1996; Schmidt et al., 1995; Staud et al., 2007), thermal (excessive heat or cold) (Caterina et al., 1997; Xu et al., 2008b), or chemical (e.g. inflammatory molecules, capsaicin, ATP) (Ahern et al., 2005; Brain, 2011; Song and Varner, 2009). All modalities of noxious stimuli can be non-noxious if the intensity of the stimulus is small enough that there is no threat of any tissue damage (Basbaum et al., 2009; Chalfie, 2009; Cordero-Erausquin et al., 2016; Julius and Basbaum, 2001; Namer et al., 2015). Therefore, a noxious stimulus must be of a certain modality and possess a minimum intensity.

Nociception is defined as "the neural process of encoding and processing noxious stimuli" (Loeser and Treede, 2008) and is often used to refer to the activities of the peripheral nervous system and spinal cord that usually generate the experience of pain (Cordero-Erausquin et al., 2016; Heinricher et al., 2009; Julius and Basbaum, 2001; Sperry et al., 2017). Nociceptive neuron is the label given to neurons that are responsible for nociception; non-nociceptive neurons encode other sensory information (Loeser and Treede, 2008). A nociceptor is a receptor on nociceptive neurons in the peripheral nervous system that transforms a noxious stimulus into a membrane potential (Dubin and Patapoutian, 2010; Loeser and Treede, 2008;

Woolf and Ma, 2007). In other words, nociceptors detect noxious stimuli in the periphery that are encoded and transmitted along nociceptive neurons throughout the peripheral nervous system and spinal cord; this entire process is called nociception. Unlike pain, nociception is not an experience, and can be quantified by the time-history of action potentials (Arcourt et al., 2017; Duan et al., 2014; Pitcher and Henry, 2004) or macromolecule concentrations within and around nociceptive neurons (Saxler et al., 2008; Weisshaar et al., 2017). This makes nociception a more objective measure of painful stimuli, where nociception is often assumed to result in painful experiences (Andersen et al., 1995; Frahm et al., 2013; Namer et al., 2015) or behaviours (Caterina et al., 2000; Kashiwadani et al., 2017). This is a safe assumption in healthy individuals (Loeser and Melzack, 1999).

Acute and Chronic Pain

Acute pain is functionally useful—it serves to warn the person of a threat to, or the existence of tissue damage or some other noxious stimulus (Dunn et al., 2006; Julius and Basbaum, 2001; Tamcan et al., 2010). Acute pain is defined as pain lasting less than two to six months dependent on the author (Airaksinen et al., 2006; Doleys, 2017; Duncan, 2017; Hansson et al., 1985). Chronic (or sometimes "persistent") pain refers to pain that may no longer be related to any noxious stimulus despite still being "described in terms of such damage" (Williams and Craig, 2016). Chronic pain is similar with the term "pain disorder" used in the Introduction; chronic pain often indicates a disorder with the person's ability to experience pain (Balagué et al., 2012; Boström et al., 2015), and can indicate changes in neural connectivity or unusual activity in nociceptive neurons (Baliki and Apkarian, 2015; Coderre et al., 1993; Tanasescu et al., 2016). Although acute pain does require an identifiable noxious stimulus, it can be associated with shorter-scale plastic changes in neural connectivity (Heinricher et al., 2009; Latremoliere and Woolf, 2009).

Chronic pain is considered the largest worldwide burden on health care systems in terms of years lived with disability (Vos et al., 2012); it is highly prevalent (Hoy et al., 2012; Murray and Lopez, 2013; Phillips, 2009), and is highly co-morbid with psychological disorders (Gore et al., 2012). The direct annual medical costs of a person with chronic pain has been estimated to be 2 to 3 times greater than someone without chronic pain (Gore et al., 2012; Roberts et al., 2015), with much larger indirect costs (Phillips, 2009). Despite chronic pain being a more prominent problem in society than acute pain, the majority of mechanistic studies on pain systems have used acute pain models. These include: nerve ligation (Joshi et al., 2006; Winkelstein and DeLeo, 2004), chemical irritants (Ahern et al., 2005; Caterina et al., 1997; Ciubotariu et al., 2007; Torisu et al., 2006), direct neural stimulation (Frahm et al., 2013; Namer et al., 2015), transient mechanical exposures (Beissner et al., 2010; Ghitani et al., 2017; Melia et al., 2015; Micalos and Arendt-Nielsen, 2016; Nelson-Wong and Callaghan, 2010), or skin heating/cooling (Arntz and Claassens, 2004; Cai et al., 2016; Lawson et al., 2008; Rabey et al., 2017; Wager et al., 2013). Additionally, the outcomes of these acute pain studies are often nociception-based rather than pain-based since they are easier to define and quantify (Barrot, 2012; Mogil et al., 2010).

Although the studies within this thesis are concerned exclusively with noxious stimuli that inform acute pain, the findings will be extrapolated to inform and address the problem of chronic low back pain. The assumption in this extrapolation is founded in preventing the development of chronic pain through understanding the noxious stimuli that triggers its precursor, acute pain.

Pain Sensitivity

Pain sensitivity relates the intensity of the noxious stimulus to the intensity of the painful experience, and can manifest as: a change in pain thresholds, a different response for a fixed stimulus, or an altered rate of

spontaneous activity in the absence of any stimulus (Loeser and Treede, 2008; Rukwied et al., 2013; Woolf and Salter, 2000). Hyperalgesia and hypoalgesia refer to an increased or decreased pain sensitivity respectively, regardless of the mechanism underlying those changes (Loeser and Treede, 2008). Central and peripheral sensitization refer to the location within the nervous system that a given change in sensitivity occurs; local inflammatory responses are one form of peripheral sensitization (Kidd and Urban, 2001), and neurogenesis in the spinal cord is an example of central sensitization (Coderre et al., 1993). Allodynia refers to the specific case where a known non-noxious stimulus causes pain, the only agreed upon example is pain in response to light stroking of the skin following a previous noxious stimulus (Loeser and Treede, 2008; Pitcher and Henry, 2004; Winkelstein and DeLeo, 2004). Pain thresholds refer to the minimum stimulus that can evoke a painful response, and the pain tolerance is the maximum stimulus intensity a person is willing to tolerate (Loeser and Treede, 2008; Melia et al., 2015; Petrini et al., 2015).

2.1.2 Neuroscience-Related Terminology

Primary Afferent Neurons, Projection Neurons, and Interneurons

Three broad classes of neurons that convey sensory information from the periphery to the brain (afferent direction) are primary afferent neurons, projection neurons, and interneurons. Primary afferent neurons are the first neuron in the signaling chain, containing a set of receptors within the periphery, and a single axon carrying information into the spinal cord (Gregory et al., 2016; Saeed and Ribeiro-da-Silva, 2012; Slugg et al., 2000). They are structurally different from other neurons because they lack true dendrites and are excited by external stimuli rather than another neuron. Projection neurons are those that ascend the spinal column and enter the brain. For the purposes of this thesis, projection neurons represent the output of nociceptive processes and function as the input to pain processes (Braz et al., 2014; Guo and Hu, 2014; Prince et al., 2005). Interneurons connect two neurons to each other, and are often implied to be an intermediate neuron in a signaling pathway or tract within the spinal cord (Braz et al., 2014). Complementary to this classification are numerical orders of neurons where the *n*th order neuron is the *n*th neuron in series; by definition, a first order afferent neuron is a primary afferent neuron.

Neurotransmitters and Neuropeptides

Neurotransmitters and neuropeptides are two similar types of neurochemicals released from a neuron that affect the membrane voltage of adjacent neurons. Excitatory neurochemicals increase the membrane voltage potential of the postsynaptic (receiving) neuron while inhibitory ones decrease it (Platkiewicz and Brette, 2010). Neurotransmitters are released quickly, diffuse short distances before activating a receptor, and are immediately transported back into a neuron or broken down (van den Pol, 2012). Glutamate (El Mestikawy et al., 2011; Li et al., 2017), gamma-aminobutyric acid (GABA) (François et al., 2017; Guo and Hu, 2014), glycine (Polgár et al., 2003), and ATP (Jo and Schlichter, 1999; Saeed and Ribeiro-da-Silva, 2012; Song and Varner, 2009) are all examples of neurotransmitters in nociceptive pathways. A given neurotransmitter tends to always be excitatory (e.g. glutamate) or inhibitory (e.g. GABA) in that it affects the postsynaptic membrane voltage consistently (Boyle et al., 2017; Braz et al., 2014; Duan et al., 2014). However, a given neuron may release multiple neurotransmitters (De Biasi and Rustioni, 1988; Jo and Schlichter, 1999) and has the ability to modulate the release of each neurotransmitter separately (Keller et al., 2001).

Neuropeptides are short amino acid chains (usually less than 20) released in tandem with neurotransmitters that linger outside of neuron for longer periods of time than neurotransmitters (Basbaum et al., 2009), and can diffuse beyond a single synapse (van den Pol, 2012). Unlike neurotransmitters that

have a fast and specific response, the effects of neuropeptides accumulate more slowly over time and can affect more neurons (van den Pol, 2012). Calcitonin gene-related peptide (CGRP) (Corey et al., 2011; Mense and Hoheisel, 2016) and Substance P (Kallakuri et al., 1998; Nederpelt et al., 2016) are two excitatory neuropeptides linked to nociception. Only a subset of neurons contain neuropeptides, termed peptidergic neurons (Saxler et al., 2008; Stucky and Lewin, 1999); other neurons are non-peptidergic (Saeed and Ribeiro-da-Silva, 2012; Weisshaar et al., 2017).

Neural Activity

The phrase "neural activity" will be used throughout this thesis to describe the overall intensity of a neuron's metabolism. Neural activity will be increased when action potentials occur more frequently or when a neuron is releasing a larger amount of neurotransmitter or neuropeptide. Neural activity can be used to describe a single neuron or a population of neurons, in the latter case, neural activity will refer to the average rates of action potentials and neurochemical release among that population.

2.1.3 Biomechanical Terminology

Tissue

"Tissue" will be used in this thesis as a generic term for distinct anatomical structures, or subsets of those structures. A tissue's type indicates its rough composition and function (e.g. muscle, ligament, tendon, neuron, skin). The term "passive tissues" will generally refer to ligaments, tendons, fascia, joint structures (discs, capsules), and skin.

Viscoelasticity

A viscoelastic material is one that simultaneously exhibits mechanical properties of solids and liquids (Fung, 1994; Provenzano et al., 2001). Pure solids respond to external loads by deforming in proportion to the magnitude of the applied load, store the energy of that applied load in the chemical bonds between molecules, and release that energy when the load is removed (Fung, 1994). The specific amount of deformation an object has for a given load is referred to as its elasticity (Lu and Mow, 2008; Yang et al., 2016). Pure liquids respond to external loads by flowing in proportion to the rate of the applied load, and do not store the energy of applied loads as solids do (Fung, 1994). The resistance of a fluid to flow in response to a change in applied loads is its viscosity. All tissues in the body are viscoelastic, with varying proportions of viscous (liquid) and elastic (solid) elements.

Viscoelastic Creep

Viscoelastic creep, referred to in this thesis as "creep", is an emergent phenomenon where viscoelastic materials have larger deformations for a given load as a result of their loading history (Fung, 1994; Solomonow, 2004; Thornton et al., 2002). Viscoelastic materials with smaller viscosity coefficients, representing less resistance to flow, exhibit larger amounts of creep. Creep is often reported as a percent increase in initial length or deformation at a predetermined load (Howarth et al., 2013b; Little and Khalsa, 2005; Shin and Mirka, 2007; Solomonow et al., 2000; Toosizadeh and Nussbaum, 2013), meaning that a load must be applied in order to assess the current level of creep.

Acute and Chronic Injury

There are two gross mechanisms of injury. An acute injury involves a single instance of a large load or deformation exceeding the undamaged tolerance of a tissue (Kumar, 2001). A chronic injury involves repeated (Callaghan and McGill, 2001; Gedalia et al., 1999), cumulative (Parkinson and Callaghan, 2009), or static loading (Busscher et al., 2011; Little and Khalsa, 2005) deteriorating the integrity of a tissue,

resulting in a sub-maximal load exceeding the reduced tolerance of a tissue. These terms are explicitly distinguished from acute and chronic pain as defined in Section 2.1.1. Injuries often cause acute pain regardless of injury mechanism. If both the injury and pain persist beyond a certain time criterion, that injury has then caused persistent pain; chronic pain results from the pain continuing to exist in the absence of an identifiable injury. Theoretically, the occurrence of persistent or chronic pain can be independent of injury mechanism in this paradigm shown in Figure 2-1.

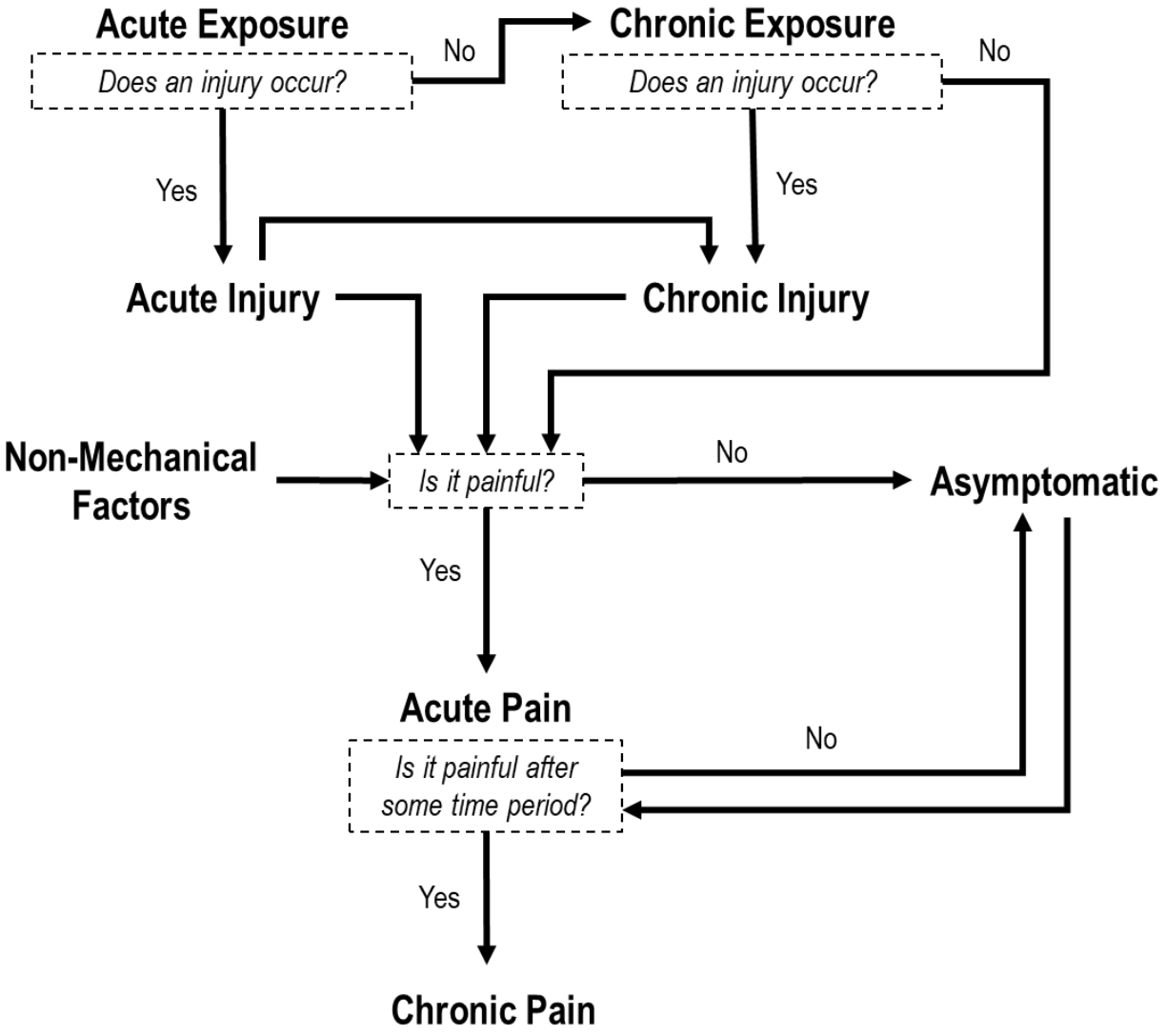

Figure 2-1: Theoretical Model Relating Injuries and Pain. Based on the Definitions provided in text. Note that a chronic exposure is one that involves some combination of static or repetitive loading that modifies the tolerance of the tissues being loaded, an acute exposure does not affect tissue tolerances (Kumar, 2001). There is also a means for the development of chronic pain after acute pain has become asymptotic.

2.2 Lumbar Spine Anatomy

The anatomy of the lumbar spine reflects its overall functions: transferring loads between the upper body and pelvis while protecting the spinal cord and allowing motion (White III and Panjabi, 1990). The spine itself consists of an alternating series of vertebrae and intervertebral discs supported by muscles and

ligaments and surrounded by fascia, subcutaneous fat and skin. Each of the six joints in the human lumbar spine consists of three parts: an anterior intervertebral joint consisting of the interface of two adjacent vertebral bodies and the intervening disc, and two posterior facet joints consisting of the bony interface of the inferior articulating surface of the superior vertebrae and the superior articulating surface of the inferior vertebrae. The facet joints contain synovial joint capsules while the intervertebral joints do not (White III and Panjabi, 1990). The components of the lumbar spine relevant to this review are the vertebrae, intervertebral disc, and ligaments with an overview presented of the innervation and mechanical properties of each component.

The vertebrae of the lumbar spine have larger vertebral bodies, more vertically-oriented facet joints, and more rectangular spinous processes than other vertebrae in the spine (White III and Panjabi, 1990). The vertebral bodies bear most of the compressive loads of the vertebrae and are highly innervated by primary afferent neurons (Bailey et al., 2011), however are not often implicated to cause low back pain outside of fractures or other high-energy impacts (Dempsey and Hashemi, 1999; Ehrlich, 2003). The vertebral bodies interface with the intervertebral disc through cartilaginous endplates (Tang et al., 2016; Van Der Houwen et al., 2010), which are more sparsely innervated than the vertebral bodies themselves (Bailey et al., 2011; Fields et al., 2014), but have been implicated as a source of discogenic low back pain (Braithwaite et al., 1998). The more posterior elements of lumbar vertebrae serve mainly as an attachment point for soft tissues and muscles (the transverse and spinous processes), as well as providing protection to the spinal cord (vertebral laminae and pedicles; Figure 2-2).

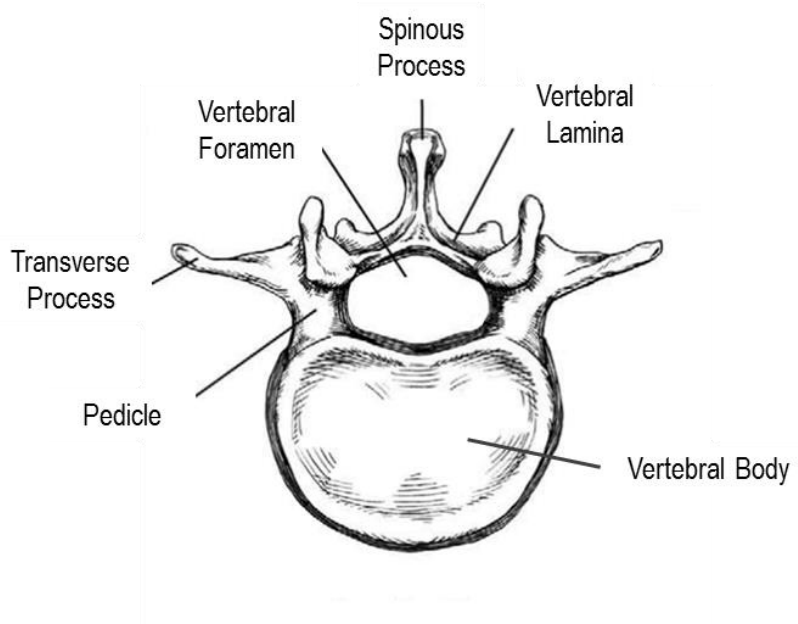

Figure 2-2: Superior View of Generic Lumbar Vertebrae. Components discussed in text are shown. Adapted from Figure 1 of Ebraheim, Hassan, Lee, & Xu (2004).

The intervertebral disc consists of an outer annulus fibrosis and an inner nucleus pulposus (White III and Panjabi, 1990) (Figure 2-3, Panel A). The annulus fibrosis consists of concentric layers of collagen fibres called lamina (the same name but a different structure from the vertebral lamina), with adjacent lamina having non-parallel collagen fibre orientations (Newell et al., 2017) (Figure 2-3 Panel B). The

nucleus pulposus consists of proteoglycans bound to collagen, surrounded by water which results in a gel-like consistency that exerts a hydrostatic pressure outwards when compressive loads are applied to it (Newell et al., 2017). The nerve supply to the intervertebral disc is limited to the outer annular laminae (Bogduk et al., 1981; Morinaga et al., 1996), however the branches of the sinu-vertebral nerve supplying these outer layers are known to transmit nociceptive information (Raoul et al., 2002). Repeated spine flexion can cause the nucleus to herniate posteriorly (Callaghan and McGill, 2001; Veres et al., 2009) and may compress the nerves innervating the outer annular layers.

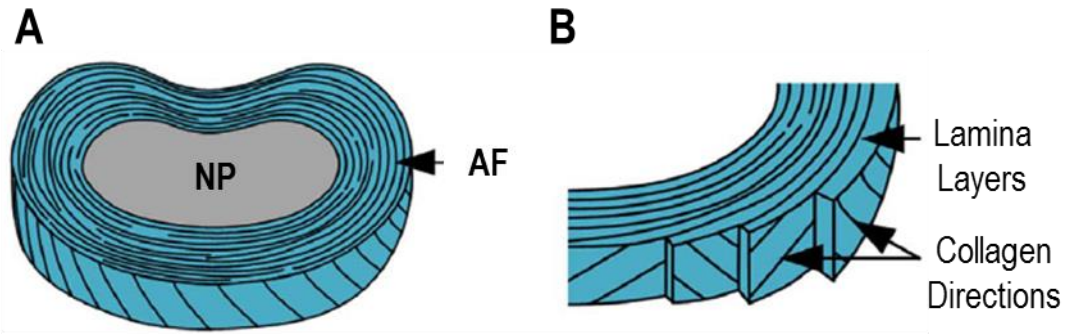

Figure 2-3: Depiction of the Annulus Fibrosis and Nucleus Pulposus of an Intervertebral Disc. Adapted from Figure 2 of Newell et al. (2017). Panel A shows an overview of the whole disc, Panel B shows the hatching-pattern of obliquely oriented collagen fibres in adjacent laminae of the annulus fibrosis. AF – Annulus Fibrosis; NP – Nucleus Pulposus.

The ligaments of the lumbar spine serve to restrain excessive tensile loads based on their position relative to the intervertebral and facet joints (Figure 2-4). All ligaments are highly innervated by a variety of receptor types (Kallakuri et al., 1998; Kiter et al., 2010; Rhalmi et al., 1993), allowing them to provide proprioceptive (Solomonow, 2004) and nociceptive (Sperry et al., 2017; Weisshaar et al., 2017) information to the brain and spinal cord. The anterior and posterior longitudinal ligaments course the entire length of the spine (Higuchi and Sato, 2002; Pintar et al., 1992), with their name indicating their position relative to the vertebral bodies (Figure 2-4). The posterior longitudinal ligament is stiffer than the anterior longitudinal ligament (Sharma et al., 1995), although both are stiffer than other lumbar spine ligaments (Pintar et al., 1992). The interspinous ligament and ligamentum flavum connect adjacent vertebrae posterior to the spinal cord, with the more posterior interspinous ligament connecting adjacent spinous processes (Hindle et al., 1990), and the ligamentum flavum connecting adjacent vertebral laminae (Chau et al., 2014) (Figure 2-4). The supraspinous ligament courses along the spinal column posterior to the spinous processes and interspinous ligament (Figure 2-4). The supraspinous ligament is the stiffest non-longitudinal ligament (Heylings, 1978; Pintar et al., 1992), and the anterior portion of the ligament is stiffer than the posterior portion (Robertson et al., 2013a). The supraspinous and interspinous ligaments tend to form a complex due to their proximity to each other (Heylings, 1978). Both undergo large physiological strains (Hindle et al., 1990) and combined offer the greatest resistance to peak flexion moments in animal spinal models (Gillespie and Dickey, 2004). As a result, these ligaments are often implicated in creep-related injuries stemming from lumbar spine flexion (Kumar, 2001; Solomonow, 2004).

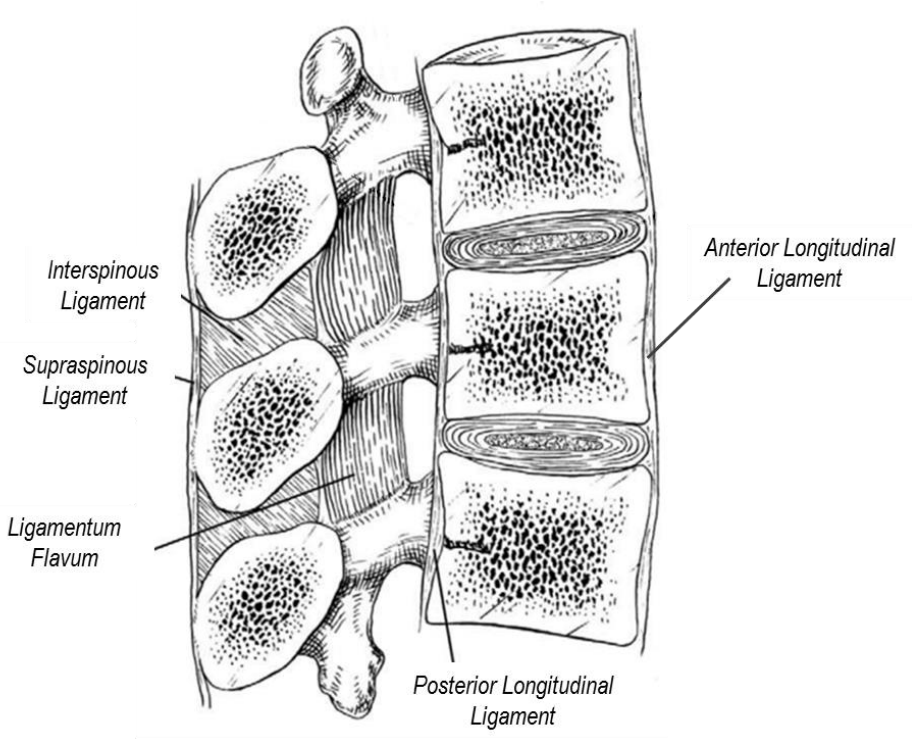

Figure 2-4: Ligaments of the Lumbar Vertebrae. The intertransverse and facet capsular ligaments are not shown in this figure. Adapted from Figure 3 of Ebraheim, Hassan, Lee, & Xu (2004).

2.3 General Neurophysiology

2.3.1 Neural Communication

Neurons are the signaling units of the nervous system. Their composition includes a region to sense incoming stimuli (often on a dendrite), a region to integrate incoming stimuli (an axon hillock), an axon to carry the signal to its target, and an axon terminal to communicate with its target (Kandel et al., 2013). Neurons can have any number of receptors on any number of dendrites (neuron inputs) and can connect to any number of other neurons or tissues (neuron outputs) (Llinás, 2003; Ristanović et al., 2006). The signal that travels from one end of a neuron to the other is an electrical signal called an action potential (Platkiewicz and Brette, 2010), while the communication between a neuron and its target is chemical in the form of various neurochemicals that diffuse between neurons in a narrow cytoplasmic gap called a synapse (van den Pol, 2012). The frequency of a neuron's action potentials are related to the amount and variety of neurochemicals that are released into the synapse (Zbili et al., 2016). Since action potentials have a main travel direction along the axon (the dromic direction) and neurochemicals are only released from one end of the neuron, communication between neurons only occurs in the dromic direction (Llinás, 2003). Therefore, the information carried by a neuron is primarily a function of which neurochemicals are released (De Biasi and Rustioni, 1988; Keller et al., 2001), the amounts of neurochemicals released (Zbili et al., 2016), and the neuron those neurochemicals are released from (Kandel et al., 2013).

An action potential is a transient spike in membrane voltage that begins at the axon hillock and travels down the axon to the axon terminal. The voltage inside an "inactive" neuron is roughly 65 to 75 mV less than the voltage outside the neuron (Hendrich et al., 2013; Lewis et al., 2011), thus a neuron is said to have a resting membrane potential of -65 to -75 mV. Neurochemicals binding to the receptors on the dendrites

of the post-synaptic neuron may increase (depolarizing) or decrease (hyperpolarizing) the membrane potential by allowing ions to flow in or out of the cell (Hodgkin and Huxley, 1952a; Kandel et al., 2013). The proximity of a given receptor to the axon hillock (Stuart et al., 1997), the geometry at the axon hillock (Sakatani and Hirose, 2003), and the local excitability of the membrane between the receptor and the axon hillock (Huang et al., 2017) affect the likelihood of action potential initiation. An action potential is more likely to occur at higher membrane potentials, with an increase of 10 to 20 mV at the axon hillock usually being sufficient to trigger an action potential (Platkiewicz and Brette, 2010; Wester and Contreras, 2013). An action potential involves greatly increasing the neuron's permeability to sodium ions, causing the membrane potential to depolarize to potentials of +40 mV (Stuart et al., 1997; Zbili et al., 2016). This transient sodium permeability propagates in the dromic direction of the axon travelling at a rate proportionate to the thickness of the axon and the presence of a myelin sheath, referred to as the neuron's conduction velocity (see Table 2-1) (Cragg and Thomas, 1961; Harper and Lawson, 1985; Hursh, 1939). The firing history and geometry of an axon can affect the shape and peak amplitude of an action potential (Rama et al., 2018), this in turn can signal what neurochemicals are released at the axon terminal (Zbili et al., 2016). The membrane potential hyperpolarizes following an action potential, and the neuron cannot be depolarized again for a short period (a few milliseconds); the time spent in this inactive state is a neuron's refractory period (Lowitzsch et al., 1977; Novak et al., 2004; Stuart et al., 1997).

These phenomena result in a few key behaviours regarding action potentials:

1. A larger input stimulus results in more frequent action potentials (Adriaensen et al., 1983; Xu et al., 2008b), defined as an increase in neural activity.
2. The type and number of receptors on the post-synaptic membrane indicate how sensitive a neuron's membrane potential is to a change in a given stimulus.
3. The frequency of a given neuron's action potentials can be saturated by a certain intensity of stimulus based on its refractory period (Maurer et al., 1977; Novak et al., 2004); the neuron's sensitivity dictates the stimulus intensity that saturates it.
4. The stochastic nature of triggering an action potential indicates that action potentials can be triggered by varying levels of depolarization, including "none"; some action potentials are spontaneous (Hodgkin and Huxley, 1952b; Martin et al., 2017).

Neurons may be classified by many characteristics, a non-exhaustive list includes grouping neurons by their axon diameter, the branching patterns of their dendrites and axon terminals, the stimuli they detect, their location in the nervous system, or the neurotransmitter they release. The terminology section describes a terse location-based classification that is useful for Chapter 6, however the axon diameter grouping described in Table 2-1 is more commonly used in the literature and relevant to Chapter 5.

Table 2-1: Classification of Afferent Neurons based on Axon Size and Myelination. Adapted from Tables 22-1 and 22-2 of (Kandel et al., 2013).

Fibre Group		Fibre diameter (µm)	Conduction Velocity (m/s)	Sample Primary Afferent Neuron
Myelinated	Aα	12 - 20	72 - 120	• Primary muscle spindle • Golgi tendon organ
	Aβ	6 - 12	36 - 72	• Non-noxious touch (skin) • Joint capsule mechanoreceptors
	Aδ	1 - 6	4 - 36	• Noxious hair pulling • Cooling (to 25°C)
Non-myelinated	C	0.2 – 1.5	0.4 - 2.0	• Most nociceptors • Warming (below 45°C)

2.3.2 Neural Plasticity

The interconnectivity of neurons is not fixed; the ability of neurons to change their connectivity is called neural plasticity (Morikawa and Paladini, 2011; Woolf and Salter, 2000). Plasticity involves the creation of new (or removal of existing) synapses or the adjusting the sensitivity of existing synapses (Woolf and Salter, 2000). Stimulus potentiation or depression, where a stimulus that elicits repeated action potentials increases or decreases the magnitude of excitatory membrane potential for a given stimulus respectively, can occur over shorter (Reeh et al., 1987) or longer time-scales (Paz et al., 2009). These changes can arise from the activation of previously inactive ion channels (Britton, 1996), or modulating the sensitivity of already active channels (Wang, 2008). Synaptogenesis, the formation of new synapses as a result of axon growth and the formation of axon terminals (Chen and Cheng, 2009), occurs in response to stimuli occurring over longer durations than required for potentiation or depression-based mechanisms (Coderre et al., 1993; Zito and Svoboda, 2002). Plasticity arising from neuron growth is also longer lasting than plasticity-related neural tuning changes such as potentiation (Woolf and Salter, 2000).

2.4 Mechanisms of Perceiving Mechanical Pain

The sensation of mechanical pain incorporates nociceptive processes in the periphery and spinal cord (Julius and Basbaum, 2001), as well as sub-cortical and cortical processing in the brain (Apkarian et al., 2005). These are framed with the currently accepted overview of pain involving a mix of neuron-specific and integrative theories.

2.4.1 Theoretical Overview

Two originally clashing theories have been amalgamated by current experts in order to reconcile the distinction between the objective nociceptive processes and the interpretive painful experiences (Perl, 2007). The labelled line theory made famous by Descartes (in Melzack & Wall, 1965) that may have originated with Aristotle (in Perl, 2007) posited that neurons intrinsically detected noxious or non-noxious stimuli through a direct pathway up to the brain. Contrarily, the Gate Control Theory (Melzack and Wall, 1965), which evolved into the Neuromatrix Theory (Melzack, 1999), posited that pain resulted from interpretations and modulations of peripheral stimuli by the cerebral cortex. Current evidence is in favour of sensory-specific peripheral units showing high specificity and diversity (Ghitani et al., 2017; Lu and Perl, 2005; Schmidt et al., 1995) that are fed into bi-directional serial and parallel circuitry in the spinal cord (Duan et al., 2014; Guo and Hu, 2014) and brain (Apkarian et al., 2005; Kucyi and Davis, 2017; Melzack, 1999). Circuitry and structures throughout the central nervous system are subject to heavy modulation from almost every other structure involved in this neuronal network (Andersen et al., 1995; Arntz and Claassens, 2004; Bushnell et al., 2013; François et al., 2017). The experience of pain is likely an integration of these signals in the context of the current state of brain activity (Kucyi and Davis, 2017).

2.4.2 Nociception in the Periphery and Spinal Cord

Noxious stimuli are first detected by nociceptors; receptors embedded in the membranes at the peripheral ends of nociceptive primary afferent neurons (Dubin and Patapoutian, 2010; Woolf and Ma, 2007). Mechanical stimuli are believed to be detected by a variety of receptors, since the removal of a single type of nociceptor has not been able to abolish mechanical nociception (Basbaum et al., 2009; Cordero-Erausquin et al., 2016; Park et al., 2011). Candidate receptors include acid-sensing ion channel 3 (ASIC3) (Chen et al., 2002; Osmakov et al., 2014; Price et al., 2001), transient receptor potential vanilloid 1 (TRPV1) (Caterina et al., 2000; Mense and Hoheisel, 2016), and 2 (TRPV2) (Lawson et al., 2008), and two-pore potassium channels (K2P) (Basbaum et al., 2009; Du and Gamper, 2013). The co-expression of specific receptors (Aoki et al., 2005; Greffrath et al., 2003) and diversity within a family of receptors (Brain, 2011; Du and Gamper, 2013; Osmakov et al., 2014) has hampered progress in uncovering roles for specific receptors related to detecting noxious mechanical stimuli. Additionally, each of the candidate receptors also respond to non-mechanical stimuli. ASIC3 responds to protons (Bianchi and Driscoll, 2002; Sherwood et al., 2012), TRPV1 responds to heat and capsaicin (chemical in chili peppers) (Caterina et al., 1997), TRPV2 responds very hot temperatures (Park et al., 2011), and K2P responds to hydroxy-α-sanshool (chemical in Szechuan peppers) and other chemical irritants (Bautista et al., 2008).

The nociceptive primary afferent neurons themselves are usually Aδ or C type neurons (Bessou and Perl, 1969; Julius and Basbaum, 2001; Schmidt et al., 1995), transmitting action potentials more slowly than non-nociceptive primary afferent fibres (Chalfie, 2009). The synapses of most primary afferent neurons are spatially organized in the dorsal horn of the spinal cord, with synapses occurring around the level of entry into the spinal column (Lu and Perl, 2005). Nociceptive primary afferent fibres of all types generally synapse in the outer lamina of the dorsal horn of the spinal cord (lamina I to III), with the

unmyelinated neurons tending to synapse in more superficial layers than the Aδ fibres (Cordero-Erausquin et al., 2016). Embedded within the axons of nociceptive primary afferent neurons is a specific type of voltage-gated sodium channel: Na_V 1.7 (Dib-Hajj et al., 2013), which when absent results in severe insensitivities to pain (Staud et al., 2011).

Once in the spinal cord, neurochemicals activate local interneurons and projection neurons, integrating information from non-nociceptive Aβ and Aδ primary afferent neurons (Braz et al., 2014). Glutamate is the primary excitatory neurotransmitter of nociceptive pathways (Ahern et al., 2005; De Biasi and Rustioni, 1988), with peptidergic C-type primary afferent neurons also releasing the neuropeptides substance P (Kallakuri et al., 1998; Saxler et al., 2008) and calcitonin gene-related peptide (CGRP) (Corey et al., 2011; Ikeuchi et al., 2012; Tesarz et al., 2011). Inhibitory interneurons in the spinal cord release GABA and glycine as neurotransmitters (Keller et al., 2001; Polgár et al., 2003), however, those inhibitory interneurons may also release ATP as a excitatory neurotransmitter onto a subset of their targets (Jo and Schlichter, 1999) indicating that a single interneuron can selectively excite and inhibit any of their targets.

Neurons within the spinal cord are highly interconnected: 90% of neurons within the dorsal horn synapse locally (Cordero-Erausquin et al., 2016), roughly 10% of neurons in lamina I and II share a connection (Lu and Perl, 2005, 2003), and up to 30% of neurons in lamina II through V share a connection (Cordero-Erausquin et al., 2016). These spinal cord circuits function as excitatory and inhibitory controls (Duan et al., 2014; Guo and Hu, 2014), with circuitry dedicated to controlling the ascending information relayed by noxious mechanical primary afferent nociceptors (Duan et al., 2014). Briefly, this control circuitry consists of excitatory somatostatin-derived interneurons and inhibitory dynorphin-derived interneurons, with non-noxious Aβ primary afferent neurons providing feed-forward inhibition and noxious small diameter (C and Aδ) primary afferent neurons (Duan et al., 2014). Within this polysynaptic circuitry, Aβ primary afferent neurons can transform from inhibitory to excitatory based on the presence or absence of inflammatory molecules (Kidd and Urban, 2001) or neuropeptides (Arcourt et al., 2017). The dynorphin-derived interneurons also inhibit the somatostatin interneurons when only non-noxious inputs are received by the spinal cord (Duan et al., 2014).

2.4.3 Interpreting Nociception in the Brain

Projections from the spinal cord into the brain are not limited to a single pathway (Braz et al., 2014; Craig, 2003), nor is there a primary "pain" region of the brain (Apkarian et al., 2005; Kucyi et al., 2014). The majority of projection neurons synapse in the thalamus after ascending the spinothalamic (Craig and Andrew, 2002; Wasner et al., 2008) or spinoreticular tracts (Braz et al., 2014). From the thalamus, nociceptive signals are sent to the primary and secondary somatosensory cortices (Apkarian et al., 2005), the rostroventral medulla (François et al., 2017; Heinricher et al., 2009), the anterior cingulate (Fuchs et al., 2014; Lieberman and Eisenberger, 2015) and insular cortices (Baliki and Apkarian, 2015; Kucyi and Davis, 2017), the prefrontal cortex (Kucyi et al., 2014), and potentially others (Apkarian et al., 2005). Evidence from different imaging and pain modalities appear to emphasize the dorsal anterior cingulate cortex as being a main contributor to painful experiences acting as a hub for integrating activity from other regions (Apkarian et al., 2005; Fuchs et al., 2014; Lieberman and Eisenberger, 2015; Wager et al., 2013). The rostroventral medulla (and potentially the periaqueductal gray) appears to contain a network of "On" and "Off" neurons which facilitate or suppress nociceptive information in the spinal cord (François et al., 2017; Goffaux et al., 2007; Heinricher et al., 2009). This pathway is strongly activated by endogenous and synthetic opioids (François et al., 2017). The somatosensory and insular cortices are likely involved in

stimulus localization since these regions are somatotopically organized (Apkarian et al., 2005). Prefrontal cortex activity is related to attention, and activity seen here is thought to reflect the high saliency of noxious stimuli (Kucyi et al., 2014). Also, a parallel pathway activated by non-peptidergic nociceptive neurons in the spinal cord activates the amygdala and hippocampus through the globus pallidus in rodents (Braz et al., 2005); a pathway related to emotional memory storage and retrieval (Mackiewicz et al., 2006). Most of these functions are assumed from other functions that the same regions perform in other contexts, however the current electrical state of the brain naturally fluctuates and can alter how a region may interpret information (Kucyi and Davis, 2017).

The features of cortical processing that lead to neural experiences are still unknown, however this processing involves conscious behaviours and moods. Telling participants that a very cold stimulus is hot can make them perceive that cold object to feel painfully hot and affect the intensity they perceive that stimulus to be (Arntz and Claassens, 2004). Mood and emotional affect are also well-known modulators of pain (Baliki and Apkarian, 2015; Bushnell et al., 2013), where more negative moods and affects increase the perceived unpleasantness of pain, but not its intensity (Villemure and Bushnell, 2009). These mood and affect-related changes may be linked to serotonin transport in the brain (Lindstedt et al., 2011). Attention directed away from any pain experienced can also reduce the perceived intensity of a painful stimulus (Kóbor et al., 2009; Villemure and Bushnell, 2009), however directing attention towards an image associated with a negative mood can exacerbate pain (Kenntner-Mabiala et al., 2007). Additional cross-modal influences that exacerbate painful experiences include unpleasant music, scents, and visual stimuli, with the strength of these associations moderated by temporal and spatial alignment of paired stimuli with the person's expectations (Senkowski et al., 2014). The brain regions active in these cognitive modulators of pain are variable, but can often involve the anterior cingulate cortex (Senkowski et al., 2014; Wager et al., 2013).

Those with chronic pain tend to have physical (Bushnell et al., 2013) and functional (Kucyi et al., 2014; Tatu et al., 2018) changes in their brains. People with chronic pain have been shown to have decreased gray matter in the prefrontal and anterior cingulate cortices (Bushnell et al., 2013; Seminowicz et al., 2011), as well as insular and somatosensory regions (Tatu et al., 2018). However those with chronic pain have similar total brain matter volumes as healthy controls (Mansour et al., 2017). The co-incidence of regions that lose gray matter are unlikely to have arisen from chance, with those authors inferring some functional connectivity between those regions (Tatu et al., 2018). Treatments successful in alleviating chronic pain also undo some of the plastic changes in regions of gray matter loss (Seminowicz et al., 2011). More positive moods can still decrease the unpleasantness of pain in those with chronic pain, indicating top-down inhibition remains intact despite gray matter loss and altered connectivity in the brain (Martucci, 2017).

2.4.4 Computational Models of Pain and Nociception

Computational models of pain are less common than models of other biological phenomena such as tissue loading (Arjmand and Shirazi-Adl, 2006; Cholewicki and McGill, 1994) or metabolic processes (Chalhoub et al., 2007; Roy and Finley, 2017), likely in part stemming from pain being a subjective experience (Argüello et al., 2015). The ability to accurately simulate pain following a noxious insult would be beneficial due to the limitations inherent in experimental procedures. Experimental studies on human participants are limited by the dependent variables that are able to be measured (Mogil et al., 2010), while the results from studies using animal homologues are limited by the inability to directly assess subjective experiences in addition to innate inter-species differences in anatomy and physiology (Langley et al., 2008).

Existing knowledge gained from both types of studies can be combined into mathematical simulations (Argüello et al., 2015; Britton and Skevington, 1996), which if validated can provide additional information on when an exposure becomes painful and which tissues are liable to be transmitting those noxious signals to the brain. However, many pain modelling attempts have narrowed their scope to exclude the brain, and instead label themselves as models of nociceptive signaling in order to avoid a computer-based representation of a subjective experience (Dennett, 1978).

There is an incredible diversity of peripheral receptors, one that is briefly surveyed in Section 6.1.1, but is frequently neglected in computational models. The most common simplification is to limit the type or class of nociceptor, and then homogenize all receptors in that "type" or "class" (Liu et al., 2015; Xu et al., 2008). This assumption in itself is reasonably accurate as the physical membrane channels themselves are similar within a receptor class (Lawson et al., 2008; Osmakov et al., 2014), however the choice of how many classes of receptor to model greatly influences other decisions. Models with high receptor diversity have often been restricted to a single post-synaptic potential (Song and Varner, 2009), with models attempting to extend their durations to a second or more either drastically reduce the receptor diversity to 3 or fewer (Britton and Skevington, 1989; Liu et al., 2015; Prince et al., 2005; Xu et al., 2008b).

Network connectivity is another aspect of nociceptive modelling often subject to simplification. There are billions of neurons within the brain and spinal cord, each with multiple inputs and outputs and connection-specific weightings. Although artificial neural networks can capture this architecture and the notion of relative weightings with high predictive accuracy (Haeri et al., 2003), they cannot elucidate mechanisms or provide insights into functional relevance since its connections are highly unlikely to reflect reality. Alternatively, probability distributions can be used to randomly generate neural connections. This representation is useful if the specific small-scale connections (individual synapses) are less important to functions than the overall large-scale connections (tract sections and functional brain regions), as is believed to be the case within the central nervous system (Kucyi and Davis, 2017; Mainero et al., 2007). This generation framework allows mechanisms to be investigated since connections are stored with each iteration and grounded in theory, but are allowed to vary between iterations, reflecting how the precise connections between humans can vary despite similar large-scale structures and connections (Bogduk et al., 1981; Higuchi and Sato, 2002; Tesarz et al., 2011). Distributions of connectivity will also be more robust than mapping a single set of connections from a single subject, allowing the eventual model outputs to be generalized to those whose neural architectures do not match the original subject's (Argüello et al., 2015). However, implementing these vast networks is often limiting since the number of computations scales nonlinearly with the number of connections ($\sim O(n^3)$ for n computations), which themselves can grow very quickly with the number of neurons (upper bound of (k-1)! for k neurons). Simplifications are necessary to these calculations to develop effective multi-scale models capable of simulating events on both electrophysiological timescales ($\sim 10^{-5}$ s) (Bagal et al., 2014; Colbert and Johnston, 1996; Harper and Lawson, 1985; Stuart et al., 1997; Zbili et al., 2016) and experiential or cognitive timescales (~1 s). This multi-timescale problem is perhaps one reason why models that include both mechanical and sensory processes are extremely rare.

The deterministic approach to address the neural connectivity problem is to vastly simplify the interconnectivity of these pathways (Britton and Skevington, 1989; Liu et al., 2015; Prince et al., 2005; Xu et al., 2008b), or focus on a single aspect of this pathway in great detail (Dezhdar et al., 2015; Song and

Varner, 2009; Yang et al., 2015).[1] While less biofidelic than stochastic approaches, these simplifications can often be more useful than a detailed procedurally generated architecture for making predictions (Almog and Korngreen, 2016). An early mathematical model demonstrated through a series of lemmas and proofs within a simple conceptual model of the Gate Theory of Pain that the time-varying inputs and multiple sites of inhibitory control can produce unintuitive emergent behaviour such as oscillatory "waves" of pain (Britton, 1996; Britton and Skevington, 1989). This somewhat unstable yet realistic behaviour can also be explained independently through an Ising model, where simultaneous alignment of local changes can produce large-scale changes of the model's state (Granan, 2016). Despite a clear lack of anatomical detail, these models are often designed with a targeted purpose in mind, that often dictates the model scope and list of assumptions (Almog and Korngreen, 2016; Britton and Skevington, 1996). Hypothesis-driven models such as these appear to be more useful than highly "accurate", purely predictive models of pain or nociception (Cecchi et al., 2012; Haeri et al., 2003), that lack the ability to determine mechanisms of pain signaling or nociception.

2.5 The Problem of Chronic Non-Specific Low Back Pain

The Introduction briefly outlined difficulties in diagnosing and treating those with low back pain arising from heterogeneity. This section intends to expand on those encapsulated under the umbrella term of non-specific low back pain—the largest group of those with low back pain (Balagué et al., 2012). The term non-specific refers to the inability to identify a known pain source through a combination of history, symptom presentation, and medical imaging.

The acute onset of non-specific low back pain is related to a history of mechanical loading (Cavanaugh et al., 1996; Hoogendoorn et al., 2000; Norman et al., 1998; Sterud et al., 2016), although there has been much disagreement as to causal factors relating mechanical exposures to low back pain (Balagué et al., 2012; Roffey et al., 2010b; Wai et al., 2010). Lost-time claims from workplace studies have indicated that longer exposures of static tasks (Lis et al., 2007; Tissot et al., 2009), and higher cumulative loads (Norman et al., 1998; Xu et al., 1997) are more likely to result in lost-time from work due to low back pain. Around 80% to 90% of those reporting low back pain had that pain resolved within six weeks (Costa et al., 2012) or three months (Andersson, 1999) of the onset of that pain. The burden of chronic low back pain arises from the others that do not recover and cannot return to work (Balagué et al., 2012; Wynne-Jones et al., 2014). A systematic review of randomized control trials investigating multiple, often unrelated treatments found that the severity of low back pain generally decreases sharply at first before stabilizing after three to six months (Artus et al., 2010). The intensity of chronic non-specific low back pain refers the intensity of pain after this stabilization point, with one of the major factors predicting the severity of chronic low back pain being the initial severity of acute low back pain (Dunn et al., 2006; Tamcan et al., 2010).

Mechanical factors alone seem to be insufficient at predicting who will develop chronic non-specific low back pain from those with acute non-specific low back pain (Balagué et al., 2012). The biggest risk factor for predicting low back pain is a history of low back pain, which is not a useful metric in predicting chronicity (Adams et al., 1999). Other risk factors for chronic low back pain such as inadequate rest time at work (Gallagher and Heberger, 2012; Waddell and Burton, 2001), high mental stress (Adams et al., 1999; Smeets et al., 2007), poor social interactions (Waddell and Burton, 2001), and a tendency to catastrophize

[1] In defense of Britton and Skevington (1989), their model was continuous, analytical, and implemented by hand.

(Airaksinen et al., 2006; Atlas and Wager, 2012) are common to other chronic pain disorders such as fibromyalgia (Van Houdenhove et al., 2005) or neck pain (Veiersted et al., 2013). It is believed that many of these psychological and sociological factors contributing to the chronicity of low back pain are related to the plastic changes in the brain and spinal cord that can perpetuate the experience of pain in the absence of external stimuli (Bushnell et al., 2013; Flor et al., 2006; Goubert et al., 2017; Tatu et al., 2018). Prolonged nociception can also upregulate transcription factors related to increasing the sensitivity of primary afferent nociceptive neurons, such as inflammatory cytokines and growth factors (Sperry et al., 2017). Other personal factors such as genetic history, a younger (< 40 years) age of symptom onset, and female sex have also been associated with an increased risk of developing chronic non-specific low back pain (Balagué et al., 2012; Müller-Schwefe et al., 2017). Despite a large number of known risk factors, the explained variability of existing factors (Adams et al., 1999) and ability to predict those likely to develop chronic low back pain (Carragee et al., 2005; Hill et al., 2016) are poor.

A proactive approach to prevent non-specific low back pain from becoming chronic has been to better assess and treat those with acute or persistent non-specific low back pain. This has been achieved by categorizing those with acute non-specific low back pain into more similar sub groups in order to better elucidate mechanisms of injury and pain (O'Sullivan, 2005; Stanton et al., 2011; Van Dillen et al., 2003). Implicitly assumed in sorting those with acute non-specific low back pain based on mechanical testing is that mechanical dysfunction causes their pain (Cholewicki and McGill, 1996; Panjabi, 2003; van Dieën et al., 2003). Although many different categorization systems exist (Karayannis et al., 2016), the intent is to best match treatments to patients based on symptom presentation and movements and tests that modify pain intensities (Dankaerts et al., 2009; Fairbank et al., 2011; Foster et al., 2011; Norton et al., 2016). There is evidence that these treatment approaches are more successful than general treatments for acute non-specific low back pain in terms of patient satisfaction and healthcare costs (Delitto et al., 1995; Fritz et al., 2003; Hebert et al., 2011; Stanton et al., 2011). However many prospective patients may not be adequately classified (Stanton et al., 2013), and most classification systems cannot adequately classify every patient (Foster et al., 2011). The repeatability of findings is questionable since those reporting the success of a given classification system are limited to a few isolated groups (Treatment-Based Classification: Delitto, Fritz et al.; Movement System Impairment: Sahrmann, Van Dillen et al.; O'Sullivan Classification: O'Sullivan, Dankaerts et al.). Additionally, these approaches have not been in widespread use for a long enough time to determine if treating acute and persistent non-specific low back pain using homogenous subgroups has effectively reduced the prevalence of chronic non-specific low back pain, as intended.

A reactive approach to help those who still develop chronic non-specific low back pain has been to integrate non-mechanical and mechanical treatments (Airaksinen et al., 2006; Moseley and Butler, 2015; Müller-Schwefe et al., 2017). Antidepressants and anticonvulsant drugs have some effectiveness at alleviating chronic non-specific low back pain provided there is evidence of nerve damage (Müller-Schwefe et al., 2017). Correcting deficits in spatial awareness of oneself has some effectiveness in reducing chronic pain (Moseley and Flor, 2012), however the relatively small symptom reductions suggest minor contributions from spatial awareness (Moseley, 2017). Chronic non-specific low back pain has also been treated by adjusting the patient's beliefs through stress-reduction (Cherkin et al., 2016), cognitive behavioural therapy (Cherkin et al., 2016), education (Moseley and Butler, 2015), and the placebo effect (Carvalho et al., 2016). Combining non-mechanical treatments has been shown to further enhance pain reductions than use of treatments in isolation provided some theoretical framework underpinning those combinations exists (Moseley, 2017; Müller-Schwefe et al., 2017).

Preventing and successfully treating chronic low back pain would alleviate a highly prevalent (Hoy et al., 2012) and costly burden on modern healthcare systems (Gore et al., 2012) that could mostly eliminate the worldwide leading source of years lived with a disabling disorder (Vos et al., 2012). Research has revealed that there is no "vaccine" (not even woolen underwear (Kiyak, 2012)), and that a limited viewpoint is insufficient for large-scale prevention and treatment (Balagué et al., 2012).

2.6 Viscoelastic Creep in the Low Back

Creep is reported as length change over time for a given load; assessments of creep are therefore under load-, not displacement-control (Fung, 1994). Both static and cyclic exposures can generate creep (Little and Khalsa, 2005; Solomonow, 2012), where a higher magnitude, longer duration, and more continuous exposure generates greater creep (Bazrgari et al., 2011; Muslim et al., 2013; Thornton et al., 2002; Toosizadeh et al., 2012). Tissue creep has been associated with increased tissue compliance (Barrett et al., 2016; Bazrgari et al., 2011; Busscher et al., 2011), altered neuromuscular reflexes (Claude et al., 2003; Gedalia et al., 1999; Rogers and Granata, 2006; Sánchez-Zuriaga et al., 2010), and structural damage (Gooyers et al., 2015; Parkinson and Callaghan, 2007; Viidik, 1972) in static and cyclic exposures.

Creep and creep-induced changes generally recover at a slower rate than they are generated, with the recovery times being somewhat proportionate to the magnitude of creep and time taken to generate creep (Table 2-2). A load must be applied in order to assess the recovery of creep, which may in turn alter the tissue properties of the specimen studied, therefore experimenters often use short (less than 2 seconds) static loads to intermittently assess creep recovery (Boucher et al., 2012; Busscher et al., 2011; McGill and Brown, 1992; Rogers and Granata, 2006).

2.6.1 *In-Vitro* and *In-Situ* Characterizations of Creep

Creep of tissues characterized *in-vitro* (Busscher et al., 2011; Little and Khalsa, 2005) or *in-situ* (Claude et al., 2003; Mow et al., 1989) often involve simultaneous measurements of loads and displacements (or stresses and strains) to determine intrinsic tissue properties. These methods allow for isolation of specific tissues (Gillespie and Dickey, 2004) or parts of specific tissues (Ayturk et al., 2010) to answer fundamental questions regarding the structure or function of the sections studied. Deriving material properties requires a theoretical framework in order to develop constituent equations relating stress and strain, and predicting the constants used in those equations by minimizing the error between experimental data and model predictions (Little and Khalsa, 2005; Provenzano et al., 2002; Toosizadeh and Nussbaum, 2013). The specific constituent equations can be grounded in continuum mechanics by representing tissues as a set of springs and dashpots (Hingorani et al., 2004), or be phenomenological using arbitrary mathematical functions (Solomonow et al., 2000). Implicit in these procedures is that the values of the constants returned give physical meaning to the tissues being studied such as stiffness (Busscher et al., 2011) or energy loss (Barrett et al., 2016). *In-vitro* testing has also examined injury mechanisms during creep-generating exposures. The failure of collagenous structures in these loading scenarios involves a separation or shearing of collagen fibres (Gooyers et al., 2015; Viidik, 1972), although weakening can occur at sub-failure loads, which can alter the outcomes (Parkinson and Callaghan, 2009; Thornton et al., 2002). *In-situ* testing can allow for simultaneous measurement of mechanical and neurological properties, with testing indicating that creep modifies both across different time scales, dependent on the exposure that generates creep (Claude et al., 2003; Solomonow et al., 2000).

Table 2-2: Sample Recovery Times for Creep and Creep-induced Changes in the Low Back from the Literature.

Source	Creep Exposure	Time for Variables to Recover
Bazrgari et al., (2011)	2, 4, or 10 minutes of static trunk flexion	Stiffness: 3, 20, and 50 minutes dependent on exposure time
Busscher et al., (2011)	30 minutes of static moment in flexion, extension, lateral bend or axial rotation	Creep: > 30 minutes Neutral Zone Range: > 30 minutes Neutral Zone Stiffness: 30 minutes
Claude et al., (2003)	20 minutes cyclical spine "flexion" at 0.1 Hz[A]	Creep: > 420 minutes Reflexes: 120 minutes
Hendershot et al., (2011)	2 or 16 minutes of static trunk flexion	Stiffness: 10 minutes Reflexes: > 60 minutes
King et al., (2009)	Six, 10 minute exposures of cyclical spine "flexion" over 110 minutes at 0.25 Hz[A]	Creep: > 420 minutes Cytokines: > 420 minutes
Little and Khalsa, (2005)	10 minutes static flexion	Creep: > 20 minutes Creep rate: 20 minutes
McGill and Brown, (1992)	20 minutes static trunk flexion	Creep (Males): > 30 minutes Creep (Females): ~20 minutes
Muslim et al., (2013)	16 or 24 minutes of static trunk flexion over 48 minutes	Stiffness: > 20 minutes Reflex Gain: > 20 minutes Reflex Force > 20 minutes
Rogers and Granata, (2006)	4 minutes of static trunk flexion	Creep: > 16 minutes Reflex Gain: > 16 minutes
Shin and Mirka, (2007)	10 minutes of static flexion	Creep: > 10 minutes EMG activity ratios: 10 minutes
Solomonow et al., (2000)	50 minutes of cyclical spine "flexion" at 0.5 Hz[A]	Creep: 420 minutes Reflexes: 60 to 240 minutes
Solomonow et al., (2003)	30 minutes of static lumbar "flexion" over 50 minutes[A]	Creep: > 420 minutes Reflexes: 420 minutes
Toosizadeh and Nussbaum, (2013)	6 minutes of static and repetitive (1/15 – 1/30 Hz) trunk flexion	Creep: > 12 minutes
Yang et al., (2011)	120 minutes of cyclical flexion (lifting) at 1/12 Hz	Cytokines: 1440 minutes (24 hours)

[A] "Flexion" appearing in quotation marks as a creep exposure refers to simulated flexion by applying posterior tension to spinal ligaments in-situ.

The invasive techniques and destructive testing procedures facilitates the use of animal homologues over human specimens. Human cadaveric tissue is most often harvested from older adults (Criscenti et al., 2015; Gallagher et al., 2005; Little and Khalsa, 2005) who have altered passive tissue properties compared to those likely undergoing exposures of interest (Twomey and Taylor, 1982). Porcine (Yingling et al., 1999), murine (Provenzano et al., 2002), ovine (Ambrosetti-Giudici et al., 2010), feline (Solomonow et al., 2000), and caprine models (Abramowitch and Woo, 2004) are commonly used due to ease of access and mechanical similarities to human tissue.

2.6.2 *In-Vivo* Characterizations of Creep

Characterizing creep *in-vivo* allows for testing on human populations relevant to the question of interest, however direct measurements of tissue loads are currently unfeasible. Loading is often controlled externally by using the mass of body segments (Abboud et al., 2016; McGill and Brown, 1992; Rogers and Granata, 2006; Shin et al., 2009; Toosizadeh and Nussbaum, 2013) and occasionally known external loads (Bazrgari et al., 2011; Parkinson et al., 2004; Yang et al., 2011). The flexion-relaxation phenomenon, where posterior trunk muscle activity is absent near full trunk flexion (Howarth et al., 2013a; Rogers and Granata, 2006), is often taken advantage of during static creep tests to isolate creep to passive tissues. Contrarily, repetitive flexion assessments of creep almost exclusively involve participants actively cycling through neutral and end-range postures (Howarth et al., 2013b; Muslim et al., 2013; Toosizadeh and Nussbaum, 2013; Yang et al., 2011), although assessments of creep and creep recovery may still occur in the absence of muscle activity (Howarth et al., 2013b). Eliciting creep responses in the lumbar spine *in-vivo* over shorter time frames (< 1 hour) requires near maximal trunk flexion range of motion, as minimal creep-induced changes have been observed after briefer exposures held at less than 70% range of motion in younger, healthy adults (Hendershot et al., 2011; Howarth et al., 2013a).

In-vivo testing allows for the incorporation of proprioceptive and neural responses, to determine how they change following a creep exposure. Muscle activity tends to increase for a given task following a static creep exposure (Abboud et al., 2018; Arjmand and Shirazi-Adl, 2006; Shin and Mirka, 2007), and this is framed as a method to compensate for a reduction in passive tissue stiffness (Panjabi, 2003). Trunk repositioning errors were also generally increased after a creep exposure, although not in a dose-response manner (Abboud et al., 2018). Repositioning errors may be related to changes in reflex gain, the magnitude of a myoelectric response for a given unexpected mechanical perturbation, which are suppressed following creep exposures (Granata et al., 2005; Rogers and Granata, 2006). Additionally, static creep in the low back can reduce the median power frequency in erector spinae musculature during isometric test contractions (Abboud et al., 2016; Shin et al., 2009), and there is some evidence that these changes are not a result of muscle fatigue (Sánchez-Zuriaga et al., 2010). It is not clear yet whether electrical signaling changes following low back creep arise solely due to changes in mechanical properties of the crept tissue, or if the nerves innervating those structures have altered sensitivities.

2.6.3 Creep and Low Back Pain

Exposures that generate creep in the low back are also related to the generation of acute low back pain. Jobs involving prolonged sitting (Lis et al., 2007), repetitive lifting (Cole and Grimshaw, 2003; Hoogendoorn et al., 2000), or working at floor height (Boschman et al., 2011; Labaj et al., 2016) have a high incidence of low back pain claims, believed to result from flexed trunk postures. Creep itself occurs in part because of micro-damage to the individual fibres in collagenous tissues and the interactions between them (Gooyers et al., 2015; Viidik, 1972), meaning that creep itself is a small-scale injury, albeit one that heals quickly

(Kumar, 2001; Solomonow, 2012). It is hypothesized that these microstructural changes may be inherently painful, and somewhat related to why chronic non-specific low back pain is very poorly related to findings on medical images (Balagué et al., 2012; Carragee et al., 2005; van Tulder et al., 1997). Static and repetitive trunk flexion exposures elevate inflammatory cytokines including interleukins 1β, 6 and 8, tumour necrosis factor α, and transforming growth factor β (King et al., 2009; Pinski et al., 2010; Yang et al., 2011). These inflammatory processes also sensitize peripheral nociceptive neurons in an attempt to mitigate injury to those tissues (Kidd and Urban, 2001; Zhang and An, 2007), but may also contribute to chronicity if inflammation persists (Latremoliere and Woolf, 2009). Repetitive trunk flexion can also damage the posterior annulus fibrosis and result in posterior disc herniation (Callaghan and McGill, 2001; Veres et al., 2009). Herniated nucleus pulposus material can then compress afferent nerves entering the spinal cord (Drake and Callaghan, 2009), which can further sensitize nociceptive neurons if compression persists (Sperry et al., 2017; Winkelstein and DeLeo, 2004).

2.7 Outstanding Problems

Chronic non-specific low back pain is a debilitating disorder (Gore et al., 2012; Vos et al., 2012; Woolf and Pfleger, 2003) that is difficult to predict and prevent (Adams et al., 1999). One approach to prevent chronic non-specific low back pain is to prevent acute non-specific low back pain, since chronic cases develop from acute cases. Those living with chronic non-specific low back pain also have interactions between mechanical and non-mechanical factors that perpetuate their pain (Bushnell et al., 2013; Müller-Schwefe et al., 2017; Waddell and Burton, 2001); understanding the painful aspects of their disorders therefore requires an integration of neurophysiological and biomechanical components. Exposures that are linked to low back pain such as prolonged trunk flexion (Boschman et al., 2011; Labaj et al., 2016) and repetitive lifting (Cole and Grimshaw, 2003; Hoogendoorn et al., 2000) can generate viscoelastic creep in the low back (McGill and Brown, 1992) and require extensive muscle activity (Mawston et al., 2007), both of which can influence nociceptive neural activity.

Some outstanding problems (and the chapters intended to address them) include:

- Does lumbar spine flexion alter the perception of pain? What facets of pain does it alter? (Chapters 3 and 4)
- Does the type of flexion exposure or features of that exposure affect the relationship (or lack thereof) between pain perception and lumbar spine flexion? (Chapters 3, 4, and 5)
- Are different tissues more susceptible to generating nociceptive afferent information? (Chapter 6)
- Can tissue loading profiles generate nociceptive activity that could feasibly be perceived as painful? How do factors related to trunk flexion influence that activity? (Chapters 5 and 7)

The overall route the thesis took to address this set of problems is visually depicted in Figure 2-5. The end-objective is presented in Chapter 7: predicting nociceptive neural activity in the brainstem that originated from lumbar spine tissues, the physiological precursor to low back pain, and estimating what role lumbar spine flexion has in modulating that nociceptive information. To make these predictions, data were firstly obtained and consolidated on how lumbar spine flexion affected lower back mechanical sensitivity and secondly on how different tissues might be differentially affected by mechanical exposures (Figure 2-5).

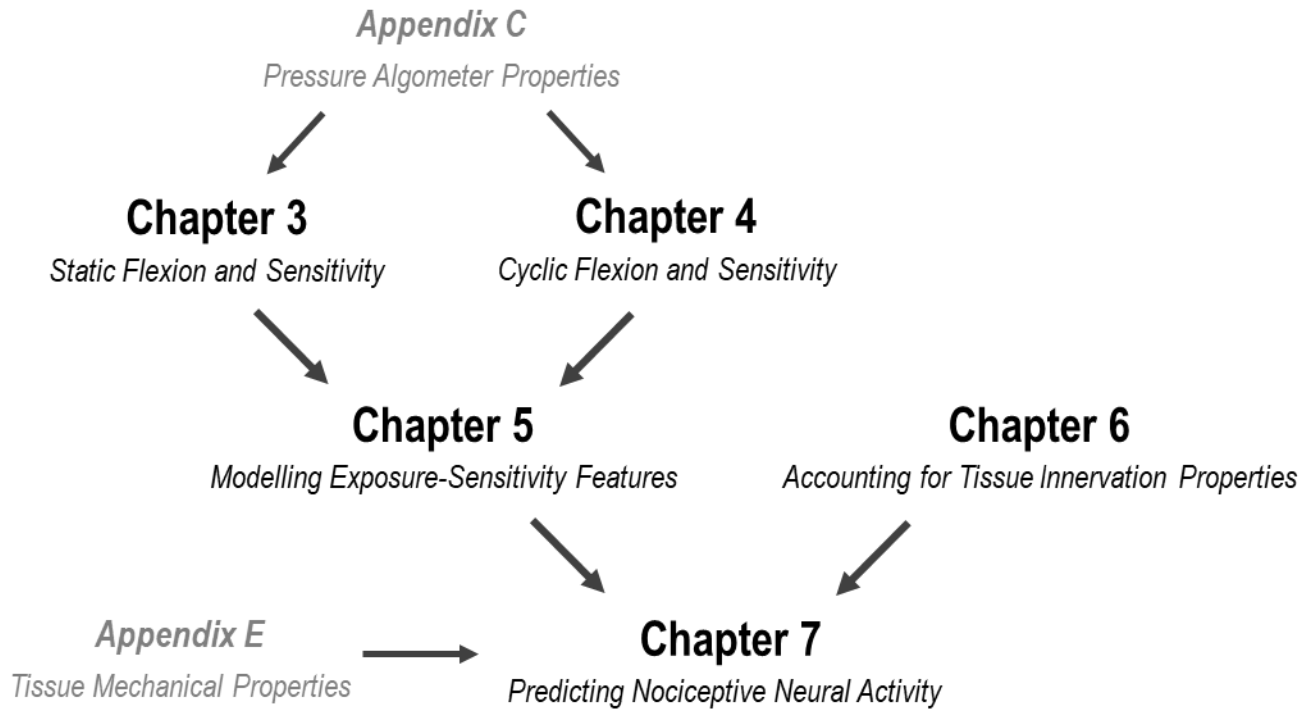

Figure 2-5: Visual Depiction of Thesis Design and Chapter Connectivity.

Chapter 3 - The Effects of Prolonged Trunk Flexion on Mechanical Pain Sensitivity in the Low Back

The findings in this chapter have been accepted as:

Viggiani, D. and Callaghan, J. P. (2021) The effects of an acute maximal seated lumbar spine flexion exposure on low back mechanical pain sensitivity. *Journal of Applied Biomechanics.*

3.1 Introduction

People working in prolonged, high-flexion postures such as sitting or stooped standing are at an increased risk for developing low back pain compared to other jobs (Boschman et al., 2011; Hoogendoorn et al., 2000; Lis et al., 2007; Zemp et al., 2016). There appears to be a dose-response relationship where longer exposures in flexed postures further increases the risk of low back pain development (Lis et al., 2007; Xu et al., 1997). From a mechanical perspective, there are two theoretical underpinnings to explain why this is the case. The first is that prolonged spine flexion generates creep in low back tissues, which can disrupt collagen connectivity and reduce the load-tolerance strength within ligaments (Thornton et al., 2002; Viidik, 1972). The second is that spine flexion reduces the moment arms of posterior spinal musculature (Jorgensen et al., 2003) and changes their line of action to produce larger shear forces (McGill et al., 2000). This change in loading profile that increases the total magnitude of loading and the proportion of shear loading both increase the likelihood of low back injuries (Norman et al., 1998; Thiede et al., 2014). Both of these mechanisms describe how tissues sustain damage under the assumption that tissue damage is perceived to be painful. Although this assumption is reasonable in a healthy, acute state (Loeser and Melzack, 1999), passive tissue creep from static high-flexion postures can introduce at least two confounders that can alter how someone perceives pain.

The first confounder is that tissue creep changes afferent neural responses originating from the affected tissue, and the specific changes in response to creep are highly variable. Stretch reflexes may be suppressed (Solomonow et al., 2003) or enhanced (Granata et al., 2005) following creep induced through passive, prolonged spine flexion. The laxity caused by muscle creep can affect muscular responses during isometric contractions (Abboud et al., 2016; Arjmand and Shirazi-Adl, 2006; Shin et al., 2009) or physical perturbations (Bazrgari et al., 2011; Hendershot et al., 2011), with a general trend of increased muscular co-activity after the creep exposure. Although these myoelectric changes are often discussed in relation to joint stability or proprioception, changes to reflexive or proprioceptive neural activity should also affect nociceptive afferents since both constitute non-nociceptive afferent information passing through the spinal cord (Braz et al., 2014; Britton and Skevington, 1996, 1989). Although not previously assessed, an increased reflex amplitude and the resulting increases in muscular activity should inhibit ascending nociceptive signals in the spinal cord and reduce the perception of pain (Basbaum et al., 2009; Braz et al., 2014).

The second confounder is that tissue creep is linked to local inflammatory responses. Higher levels of interleukins 1β, 6, 8 and 10, along with creatine kinase and tumor necrosis factor α have been measured within ligaments immediately and up to two hours post-creep compared to pre-creep levels in human and feline models (D'Ambrosia et al., 2010; Yang et al., 2011). Static creep can also upregulate RNA transcription of inflammatory cytokine producing genes where larger static loads increase total gene

expression more than lower static loads (D'Ambrosia et al., 2010). Inflammatory molecules themselves can sensitize the nervous system to pain by directly binding to nociceptors or indirectly by triggering the production of other sensitizing molecules such as bradykinin (Basbaum et al., 2009). The presence of prostaglandin E2 and low pH environments that result from local inflammation can also render what are normally mechanical-insensitive nociceptors as sensitive to mechanical stimuli, which intensifies the perception of mechanical pain (Namer et al., 2015). Furthermore, if inflammation persists and enough of the inflammatory molecules (and the neuropeptides released as a result of those inflammatory molecules) are able to reach the spinal cord, they can make primary non-nociceptive neurons activate secondary nociceptive neurons (Guo and Hu, 2014; Latremoliere and Woolf, 2009), which can make previously non-painful stimuli feel painful.

The net effect of the changes in neural discharge and the presence of inflammation are likely summative but may interact in the specific case of passive tissue creep in the low back. There is a need to determine if creep-induced changes occurring in passive tissues affect pain sensitivity.

3.2 Purpose and Hypotheses

Although the mechanics of passive tissue creep resulting from spine flexion have been successfully modelled using different approaches (Hingorani et al., 2004; Provenzano et al., 2002; Toosizadeh et al., 2012; Toosizadeh and Nussbaum, 2013), the effects of creep on pain sensitivity are not known. The purpose of this study was to determine if a sitting flexion exposure that produces passive tissue creep in the lumbar spine alters a person's sensitivity to mechanically induced pain. It was hypothesized that:

1a) Passive tissue creep will increase mechanical sensitivity assessed by pressure algometry: the pressure first detected as being painful will decrease and the perception of a fixed pressure will be greater.

1b) The amount of creep induced will be proportionate to the change in mechanical sensitivity, mechanical sensitivities will persist beyond partial creep recovery.

1c) A region of the body unaffected by the spine flexion exposure (tibial shaft) will not have its mechanical sensitivity altered.

3.3 Methods

This study exposed healthy human participants to 10 minutes of passive, end-range, seated spinal flexion; measures were taken before, immediately after, and up to 40 minutes after the spine flexion exposure. Pressure algometry and self-reported stimulus perceptions will assess mechanical pain thresholds of the L3/L4 intervertebral space and the mid-tibial shaft. Surface creep was quantified using accelerometers; electromyography confirmed a lack of active muscular involvement during maximum flexion exposures.

3.3.1 Participants

A convenience sample of 41 adults (20 males and 21 females) were recruited from a university population and the surrounding community. One male could not complete the prolonged exposure and one female's data was dropped due to technical problems, leaving a final sample size of 39 (physical characteristics in Table 3-1). A target sample size of at least 36 was estimated from a power analysis (`pwr` package (Champely, 2017); RStudio v1.0.143 RStudio Inc., Boston, MA) using sources provided in Table 3-2. These computations assumed six groups in a one-way ANOVA and should be able to detect differences with an effect size of at least 0.15 (Cohen's *f*). For all computations, a significance level of 0.05 and a power of 0.8

were used unless additional information was provided by the authors. Participants were between the ages of 18 and 35 years to mitigate any aging effects on the viscoelastic properties of the spine (Twomey and Taylor, 1982). Participants were excluded based on the following parameters, confirmed through a screening form given prior to data collection (Appendix A):

- Having sought medical care or missed time at school or work due to low back or lower limb pain within the past 12 months.
- Having a history of vasovagal syncope to limit fainting or dizziness as a result of experimental procedures.
- Having any diagnosed psychiatric, neurological, or chronic pain disorder due to potential influences on pain sensitivity (Melia et al., 2015; Petrini et al., 2015).
- Taking any analgesic or other pain medications at the time of participation.

Participants were instructed to avoid consuming caffeine, alcohol, high-fat or high-sugar foods, and vitamin C and E supplements for 24 hours prior to participating to control for immune system responses; confirmed through the screening form in Appendix A. All participants gave their written, informed consent to participate.

Table 3-1: Physical Characteristics of the Participants in Study 1.

	Males (n = 19)	**Females (n = 20)**
Age (years)	24.2 ± 4.4	22.9 ± 3.4
Height (m)	1.78 ± 0.07	1.66 ± 0.08
Mass (kg)	77.8 ± 12.5	66.8 ± 12.3
% Left Foot Dominant	15.8 %	0.0 %

Table 3-2: Sample size estimations from previous pressure-pain sensitivity testing. The ranges in estimated sample sizes come from different dependent variables used to determine effect sizes.

Source	**Intervention/Independent Variable**	**Estimated Sample Size**
Chesterton et al., (2003)	Gender	20 - 28
Hven et al., (2017)	Job Stress	60 - 86
Kosek et al., (1999)	Mild Skin Analgesic	24 - 34
Micalos and Arendt-Nielsen, (2016)	Exercise	11 - 23
Petrini et al., (2015)	Gender	10 - 20

3.3.2 Measurements and Instrumentation

Apart from the visual analog scales, all instrumentation consisted of analog voltages converted to digital format by a 16-bit conversion card with an excitation voltage of +/- 10 volts (First Principles, Northern Digital Inc., Waterloo, ON, Canada). This system has an internal clock allowing for automatic data synchronization for all sampling rates that are factors of 10,000,000.

Pressure Algometry

Pressure algometry determined pressure-pain thresholds (PPTs) and applied sub-threshold stimuli (STS) to the L3/L4 intervertebral space and a control location on the tibial shaft of the dominant leg (Figure 3-1). Two pressure algometers were constructed. Each algometer consisted of a rubber-tipped screw-head used as an applicator attached to a brushless servo-motor (12V DC linear Actuator, 10 cm stroke, 1200 N max load, Hydroworks, Clark, NJ, USA) with a load cell (MLP-300-CO, Transducer Technologies, Temecula, CA, USA) placed in series between the applicator and motor. The rubber tip of the applicator was slightly rounded to prevent local asperities and shaped to have a surface area of approximately 1 cm^2. The motor was set at a constant stroke displacement rate of 4 mm/s, which approximated a force rate application of 20 N/s (see Appendix C for rationale); forces were sampled from the load cell at 50 Hz. Algometers were mounted on separate adjustable rigid frames that allow forces to be applied normal to the participant's skin over both the low back and lower leg. Participants controlled both motors using a handheld switch. Pressure algometer parameters and reliability are detailed further in Appendix C. While pressure algometry measures are often presented in kilopascals (kPa) or kilograms-force (kgf), these data are computed in megapascals (MPa) to align with distribution parameters in Chapter 5.

For PPTs, participants were instructed to initiate motor stroke into the designated site, and then retract the motor at the instant the applied pressure is perceived as painful. Participants were given as much time to practice and familiarize themselves with this procedure using their non-dominant leg prior to the first measurement. The mean of three trials collected immediately following the familiarization procedure were used to set each participant's baseline PPT and derive STS. A single trial was used for all subsequent time points due to the time-sensitivity of the musculoskeletal responses and other concurrent measures being performed.

The pressure algometer described above also applied pressures corresponding to 70% of that participant's baseline PPT (Petrini et al., 2015). An experimenter receiving real-time force feedback from the load cell controlled the motor motion; the motor was immediately retracted once the target force was reached. Participants were asked to rate the stimulus intensity and unpleasantness of each stimulus immediately after their application on two separate 100 mm visual analog scales performed on a tablet using the app "E-Vas" that automatically records distances. The intensity visual analog scale was anchored with the descriptors "no sensation" (0 mm) and "worst pain imaginable" (100 mm); the unpleasantness visual analog scale anchor descriptors were "not unpleasant" (0 mm) and "the most unpleasant feeling imaginable" (100 mm) (Lindstedt et al., 2011). The intensity scale purposefully included non-painful and painful sensations to account for any changes in perception that may be perceived as not painful. Each pressure was applied once per assessment immediately following the PPT assessment. A depiction of PPT and STS is provided as Figure 3-2. The tibial pressure algometry measures were performed in upright standing, the L3/L4 measures were performed in maximal seated flexion (Figure 3-1).

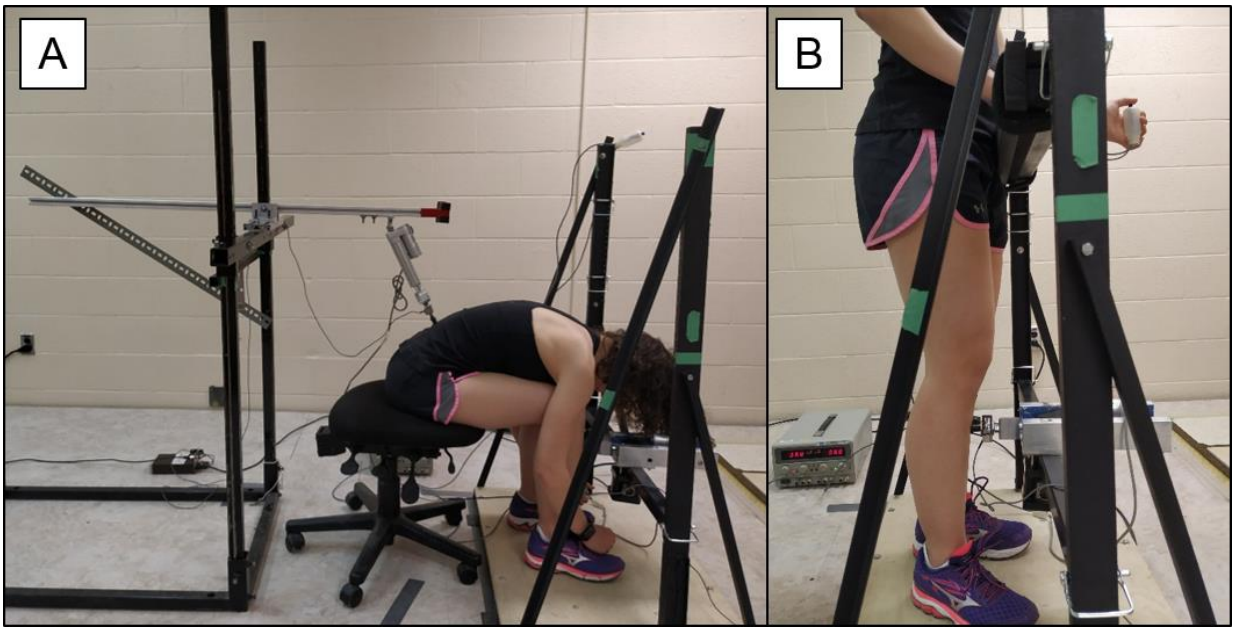

Figure 3-1: Pressure Algometry Interface. Motors mounted to rigid frames were adjusted to participant's anthropometry before applying pressures to the L3/L4 intervertebral space (Panel A) and the mid-tibial shaft (Panel B).

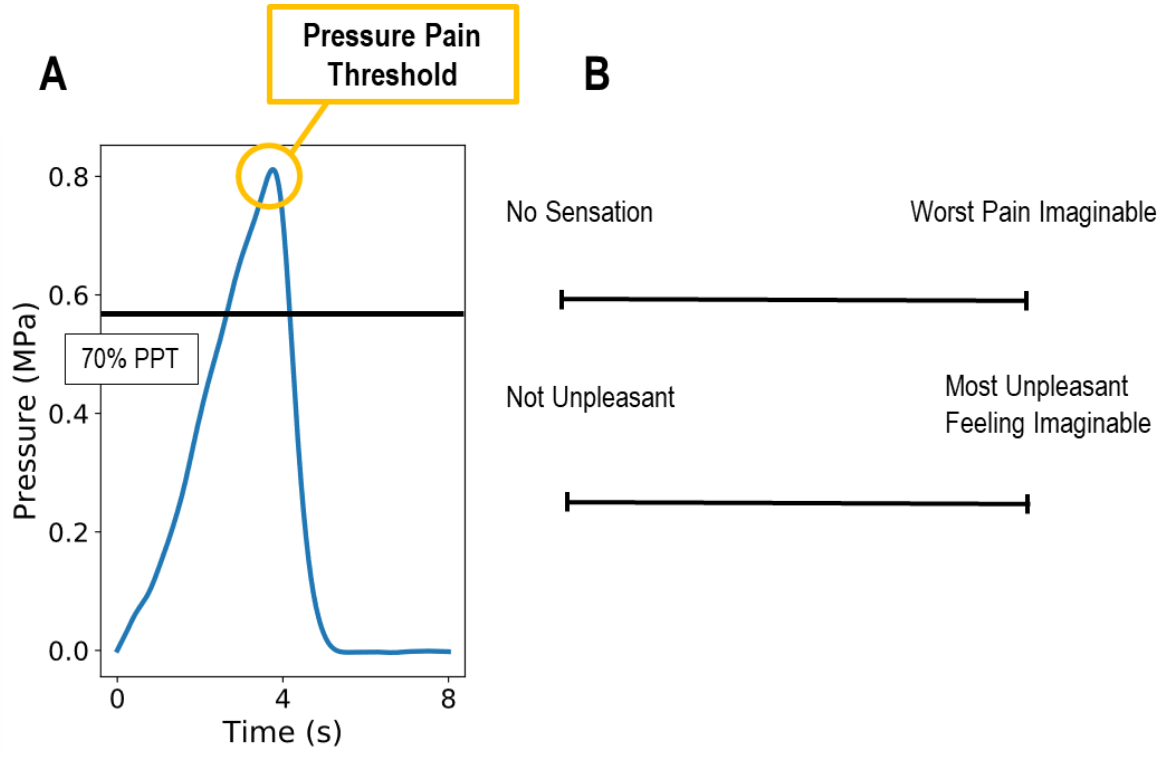

Figure 3-2: Pressure Algometry Measures. Sample filtered data from a baseline PPT assessment is depicted indicating the PPT value (global maximum) and the derivation of STS amplitude (Panel A). Participants would then rate the STS value using two 100 mm visual analog scales (Panel B).

Accelerometers

Tri-axial accelerometers (ADXL 345, SparkFun, Boulder, CO, USA) were affixed using medical fabric tape (Hypafix, BSN Medical, Hamburg, Germany) to the skin over the participant's T12 and S1 spinous processes while in neutral standing. Accelerometers were oriented on the participants with the x-axis aligned with the participant's medial lateral axis and the positive y-axis directed inferiorly. Raw accelerations were sampled at 50 Hz.

Electromyography

Surface electromyography of lumbar erector spinae was measured to determine muscle activity during and following the end-range spinal flexion. The placement protocol is documented in Appendix B. Signals were differentially amplified from a bipolar configuration with a common-mode rejection ratio or 115 dB (at 60 Hz; 10^{10} ohm input impedance), band-pass filtered from 10 to 1000 Hz, and gained by a factor of 500 to 5000 (AMT-8, Bortec, Calgary, AB, Canada). Gained signals were sampled at 2000 Hz.

3.3.3 Experimental Protocol

Data were collected in a single session taking place at least two hours after participants have awoken and at least two hours before participants went to sleep to limit the effects of diurnal variation on the spinal soft tissues (Adams et al., 1990). Figure 3-3 summarizes the experimental protocol for this study; not shown on Figure 3-3 is that accelerometers were calibrated by systematically exposing each axis to +/- 1 g, and pressure algometers were tested to ensure functionality prior to participant arrival.

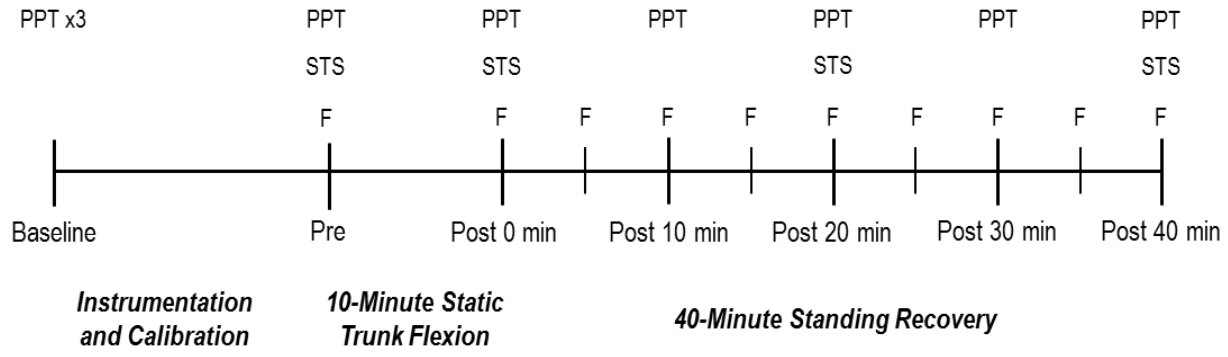

Figure 3-3: Overview of Chapter 3 Study Design. Measures taken before and after a 10 minute static trunk flexion intervention. The 10 minute static trunk flexion started immediately after all measures at the Pre time point. The unlabeled thinner vertical dashes in the Recovery phase indicate 5 minute intervals. PPT: Pressure-Pain Thresholds; STS: Sub-thrshold stimulus perception; F: Maximal Flexion Holds to assess creep recovery.

Upon obtaining informed consent, height, mass, age, and leg dominance (the leg selected to manipulate objects on the ground), participants had their baseline PPTs determined and STS intensity determined. After completing baseline measurements, participants were instrumented with surface electromyography, then performed a maximal voluntary isometric contraction and a quiet rest trial, with protocols for each detailed in Appendix B. Then accelerometers were positioned on participants and stood in a natural position for 5 seconds to establish a reference posture. A battery of pre-exposure measurements were taken following accelerometer placement and calibration consisting of both pressure algometry measures, and a maximal seated spine flexion trial. During these pre-exposure measures, participants were coached and given practice on how to round their spines while minimizing hip contributions to prevent hamstring tightness from impeding maximal flexion measures or confounding pressure algometry assessments.

The 10-minute seated spinal flexion exposure consisted of participants holding the previously coached flexed position. Two participants who reported light-headedness in the first two minutes of the exposure lay supine with their legs elevated on a table before being given the option to try again; one accepted and completed the study successfully while the other withdrew. Accelerometer and electromyographic data were recorded continuously during the 10 minute flexion exposure.

The Post 0 minute assessment started with a low back PPT and a low back STS assessment while participants remained in full seated flexion. After standing up and ensuring the participant did not have any symptoms precluding vasovagal syncope, the tibial pressure algometry measures were taken to complete the Post 0 minute assessment. Participants then stood on a 68.6 cm by 91.4 cm wooden platform continuously for 40 minutes, briefly interrupted to perform post-exposure measures performed at regular intervals according to Figure 3-3. Maximal flexion exposures to track creep recovery were performed every 5 minutes, PPTs assessments were taken every 10 minutes after completion, and STSs were rated for both sites every 20 minutes. Measures for these subsequent time points differed from the Post 0 minute testing order: all tibial algometry measures came first while standing, then participants sat down and flexed forward to allow low back algometry measures. This ordering minimized the total assessment time and total time spent in full flexion. Participants held maximum flexion for as short of a duration as possible while low back algometry assessments occurred; seated maximum spine flexion was held for 5 seconds in instances when no other assessments took place. Accelerometers and electromyography data were recorded whenever participants were fully flexed, load cell data were recorded any instance the algometers were in use. Participants were remunerated for their time and the collection session ended following the Post 40 minute assessment.

3.3.4 Data Processing

All data analyses were performed in Python (v3.5.1, Python Software Foundation, https://www.python.org/) using the `numpy` package unless otherwise specified.

Pressure Algometry

Load cell data were calibrated using a two-point calibration performed weekly, or whenever equipment was swapped. Time-varying forces were low-pass filtered using a 4th order, zero-lag Butterworth filter with a 2 Hz cut-off frequency to remove noise introduced by the natural frequency of the motor and frame. The maximum filtered forces measured by the load cell were converted to megapascals based on the indenter contact area (1/10,000 m^2) and recorded as the PPT from that trial. The three baseline trials were averaged to determine that participant's initial PPT.

Reports of intensity and unpleasantness were determined through direct measurement of the distance between the 0 mm anchor and the mark made by participants.

Accelerometers

The first (Pre) and last 10 seconds (Post 0 minute) of the 10-minute creep exposure were windowed and fed forward for analysis along with the remaining maximal flexion assessments. All accelerometer axes were re-expressed in gravitational accelerations by removing the 0 g voltage and dividing by the change in voltage between 0 and +1 g or -1 g dependent on whether signals are positive or negative. Gravitational accelerations were inputted into Equation 3-1 to estimate accelerometer orientation θ with respect to the vertical axis in the sagittal plane. Equation 3-1 is based on the orientation specified within section 3.3.2 and assuming that non-gravitational accelerations were negligible.

$$\theta = tan^{-1}\left(\frac{a_y}{a_z}\right) \quad (3\text{-}1)$$

Where a_y and a_z are the y and z components of a given tri-axial accelerometer in gravitational accelerations. This formulation on its own introduces multiple $\pi/2$ radian phase shifts occurring when the sign of a_z changes from positive to negative. Implementing this function using `atan2` functions native to most mathematical languages halves the number of phase shifts utilizing a conditional redistribution function to map outputs onto a more useful framework, θ_r shown in Equation 3-2.

$$\theta_r = \theta - \frac{3\pi}{2}\ if\ a_y > 0\ and\ a_z \leq 0; otherwise\ \theta_r = \theta + \frac{\pi}{2} \quad (3\text{-}2)$$

Here, θ_r is defined as 0 radians when the y-axis is pointing directly downwards and the z-axis is horizontal; an accelerometer can have orientations ranging from $+\pi$ to $-\pi$ radians. Thus, accelerometer orientations can occupy a continuous range centred about a position closely resembling an accelerometer orientation during upright stance.

The lumbar spine flexion angle was defined as the orientation (θ_r) of T12 accelerometer with respect to the S1 accelerometer. Lumbar spine flexion angles were expressed as a percentage of the participant's total range of motion by defining the neutral standing calibration trial as 0% and the maximal flexion angle achieved in the pre-flexion static calibration trial as 100% range of motion.

The percent change in lumbar spine flexion angle during the flexion exposure and recovery phases with respect to the 0 minute window in the 10 minute flexion exposure are the primary creep measure.

Electromyography

The processing steps in table 3-3 were performed on the entire 10 minute static flexion exposure and the 5-second creep assessments during the recovery phase to confirm that participants were at rest while in full spine flexion. The cumulative time spent above 5% maximal voluntary contraction was quantified for each participant, and participants were excluded if this time exceeded 10% of the total recording time. The dominant side was kept for statistical analysis unless contaminated, in which case the non-dominant side was kept instead; bilateral symmetry was assumed.

Table 3-3: Electromyography processing steps. All steps were applied in numerical order to the data indicated in the "Trials Applied to:" column. Steps 1 to 3 were applied to the resting trial, steps 1 to 4 were applied to the maximal voluntary contraction trial, and all steps were applied to the data recorded during static flexion (whether from the 10 minute continuous flexion exposure or the 5 second assessments during recovery from creep.

Electromyography Processing Step	Trials Applied to:
1) Raw signal conditioning: • 30 Hz high-pass Butterworth filter for bias-removal and reducing amplitude-based heart rate artifacts (Drake and Callaghan, 2006) • 60 Hz band-stop Butterworth filter for removal of electromagnetic hum (Mello et al., 2007)	• Static flexion • Resting • Maximal voluntary contraction
2) Convert voltages into absolute values	• Static flexion • Resting • Maximal voluntary contraction
3) 2.5 Hz low-pass Butterworth filter to represent time-varying activations (in volts) (Brereton and McGill, 1998)	• Static flexion • Resting • Maximal voluntary contraction
4) Removing the mean resting activations	• Static flexion • Maximal voluntary contraction
5) Expressing rest-removed muscle activations as a percentage of rest-removed maximal voluntary contraction activity	• Static flexion

3.3.5 Statistical Modelling

All statistical testing were performed in RStudio (v1.0.143 RStudio Inc., Boston, MA, USA) using significance levels of 0.05.

Statistical tests for hypotheses 1a and 1c aim to differentiate pain sensitivity as a function of time, which serves as a proxy for lumbar spine creep. For these hypotheses, the dependent variables were PPTs and ratings of STSs, with independent variables of Time (pre-flexion and five levels post-flexion: 0/10/20/30/40 minutes) and Site (Low Back/Tibia). Kolmogorov-Smirnov tests determined if data were normally distributed and Mauchly's tests determined if assumptions of sphericity were violated. two-way ANOVAs were performed on pressure algometry measures when normality was held; otherwise, Kruskal-Wallis tests were performed. Greenhouse-Geisser adjustments to p-values were made when sphericity assumptions were violated. Tukey's test was performed post-hoc in the case of significant findings to determine differences between time points.

Multiple linear regressions were performed between measures taken during static flexion and changes in mechanical sensitivity to determine if the two are related (hypothesis 1b). Fixed effects included

tissue creep (via lumbar spine flexion angle) and muscle activity (mean normalized EMG amplitudes), and one of two measures of tibial mechanical sensitivity (PPT and STSs); predicting the two measures of mechanical sensitivity in the low back at relevant time points. PPTs were normalized to pre-exposure values to prevent scaling effects from influencing predictions. Significant predictors were checked using Wald's χ^2 test.

3.4 Results

Features of the maximum flexion exposure are first presented in section 3.4.1, followed by pressure algometry outcomes in sections 3.4.2.

3.4.1 Characteristics of the Seated Flexion Exposure

There were main effects of Time on the maximal spine flexion angles ($F_{3.26,\ 120.7} = 8.30$; $p < 0.001$) during the static flexion assessments occurring before and every five minutes after the 10-minute maximal seated spine flexion exposure (Figure 3-4). All post-exposure time points were larger than the pre-exposure time point except the Post 10 ($p = 0.834$) and Post 30 minute ($p = 0.965$) time point. The magnitude of this creep response at each time point is shown in Table 3-4.

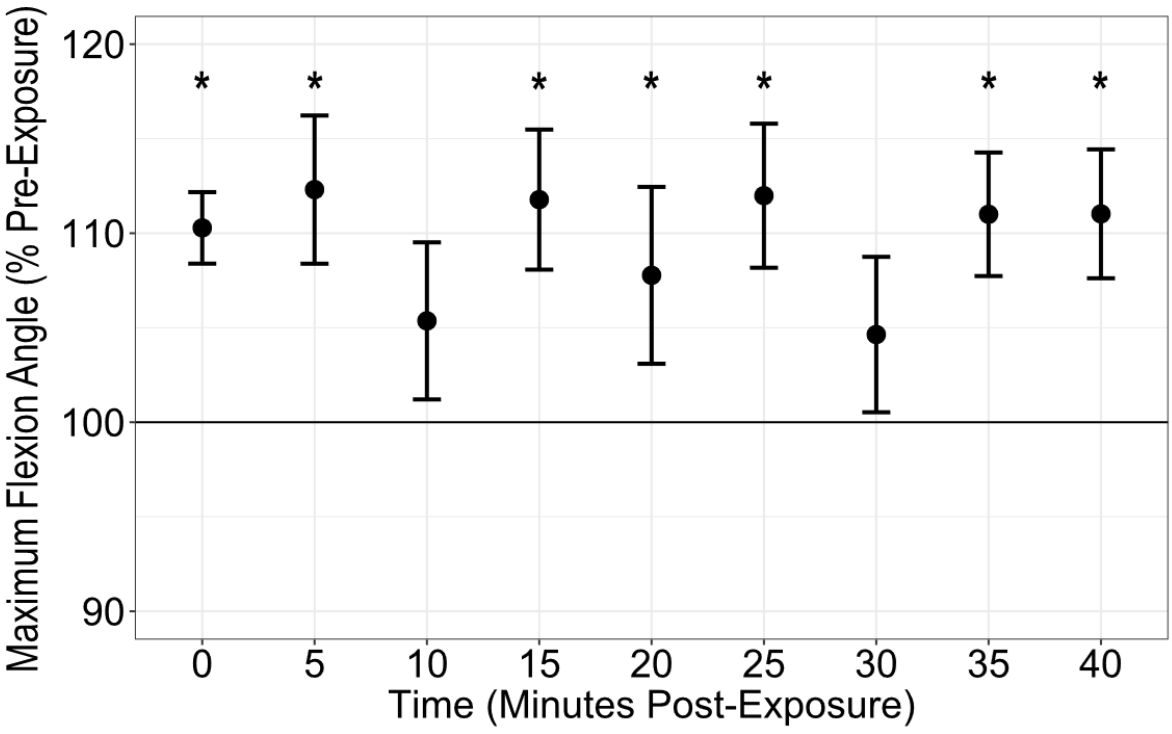

Figure 3-4: Maximal Spine Flexion Angles following the Prolonged Flexion Exposure. Data are normalized to the maximum flexion angles attained during the Pre-Exposure assessment (the horizontal line at 100%). Error bars show ±1 standard error. Time points that are significantly different ($p < 0.05$) than the Pre-Exposure time point are denoted by an asterisk.

Electromyography data collected during the prolonged flexion trial indicated that participants had activations above 5% maximal voluntary contraction for on average 0.27% of the 10 minute trial or approximately 1.62 seconds (range: 0 – 1.76%, 0 – 10.56 seconds). The mean activity levels during the static flexion creep-assessment trials were similar across all time points ($p = 0.315$) and were below 5% maximal voluntary contraction (Table 3-4).

Table 3-4: Creep Magnitude and Mean Muscle Activities during the Static Flexion Creep Assessments. Values are Mean ± 1SD; muscle activity units are % maximal voluntary contraction.

Time Point	Creep Magnitude	Mean Muscle Activity
Pre	0.0 ± 0.0°	2.5 ± 3.3%
Post 0	4.4 ± 2.7°	3.0 ± 3.1%
Post 5	4.9 ± 5.6°	3.4 ± 4.4%
Post 10	1.4 ± 7.6°	3.2 ± 4.5%
Post 15	4.6 ± 5.7°	3.6 ± 4.1%
Post 20	2.9 ± 9.2°	4.5 ± 3.6%
Post 25	4.6 ± 5.7°	4.1 ± 3.9%
Post 30	1.1 ± 7.8°	3.3 ± 5.4%
Post 35	4.3 ± 5.3°	3.5 ± 3.9%
Post 40	4.2 ± 5.3°	3.3 ± 3.4%

3.4.2 Mechanical Pain Sensitivity Measures

PPTs were higher in the low back compared to the tibia ($F_{1,37} = 9.72$; $p = 0.004$), but were similar across all time points ($p = 0.833$; Figure 3-5). There was a Time*Site interaction in the perceived unpleasantness ($F_{2.1, 74.7} = 5.25$; $p = 0.007$) but not intensity ($p = 0.102$) of the STSs (Figure 3-6). Specifically, participants perceived the low back stimulus as more unpleasant than the tibial stimulus at the Post 0 minute time point ($p = 0.001$); the Post 0 minute low back point was also perceived as more unpleasant than the Pre ($p = 0.047$) and the Post 40 minute time point ($p = 0.023$).

Multiple linear regressions indicated that the magnitude of creep and higher interactions between creep magnitude, muscle activation level and tibial PPTs could predict lower back PPT magnitudes (Table 3-5). The only predictors of either the unpleasantness or intensity of the lower back STSs were the corresponding measure at the tibia (Table 3-5).

Table 3-5: Outcomes of Multiple Linear Regressions to Predict Lower Back Pain Sensitivity. The Measure column indicates the lower back measure that the regression was predicting. The Predictors column indicates the significant ($p < 0.05$) predictor terms from the regression; interaction terms are denoted as A*B. The marginal and conditional R^2 refer to the explained variance of the significant predictors without and with the inclusion of random effects in the regression respectively. PPT: Pressure-Pain Threshold; EMG: Mean muscle activity from electromyography.

Measure	Predictors	Marginal R^2	Conditional R^2
Pressure-Pain Threshold	• Creep • Creep*Tibial PPT • Creep*EMG*Tibial PPT	0.100	0.305
Unpleasantness	• Tibial Unpleasantness	0.105	0.784
Intensity	• Tibial Intensity	0.155	0.689

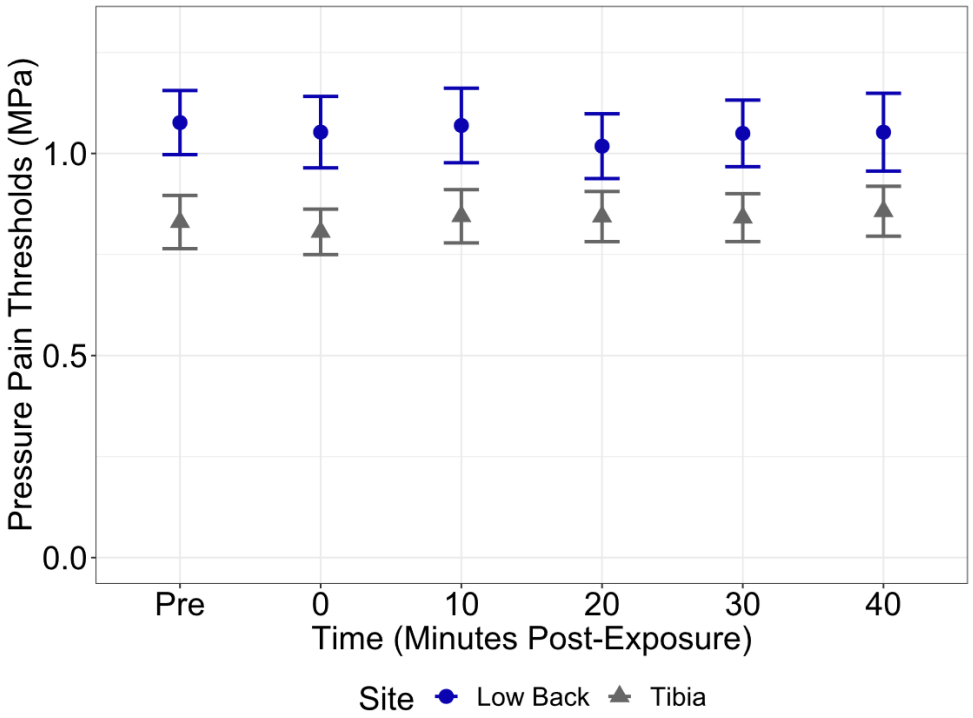

Figure 3-5: Pressure-Pain Thresholds Before and After 10 Minutes of Static Flexion. The L3/L4 intervertebral space (low back, blue circles) had significantly larger ($p < 0.05$) threshold than the mid-tibial shaft (tibia, gray triangles). Error bars show ± 1 standard error.

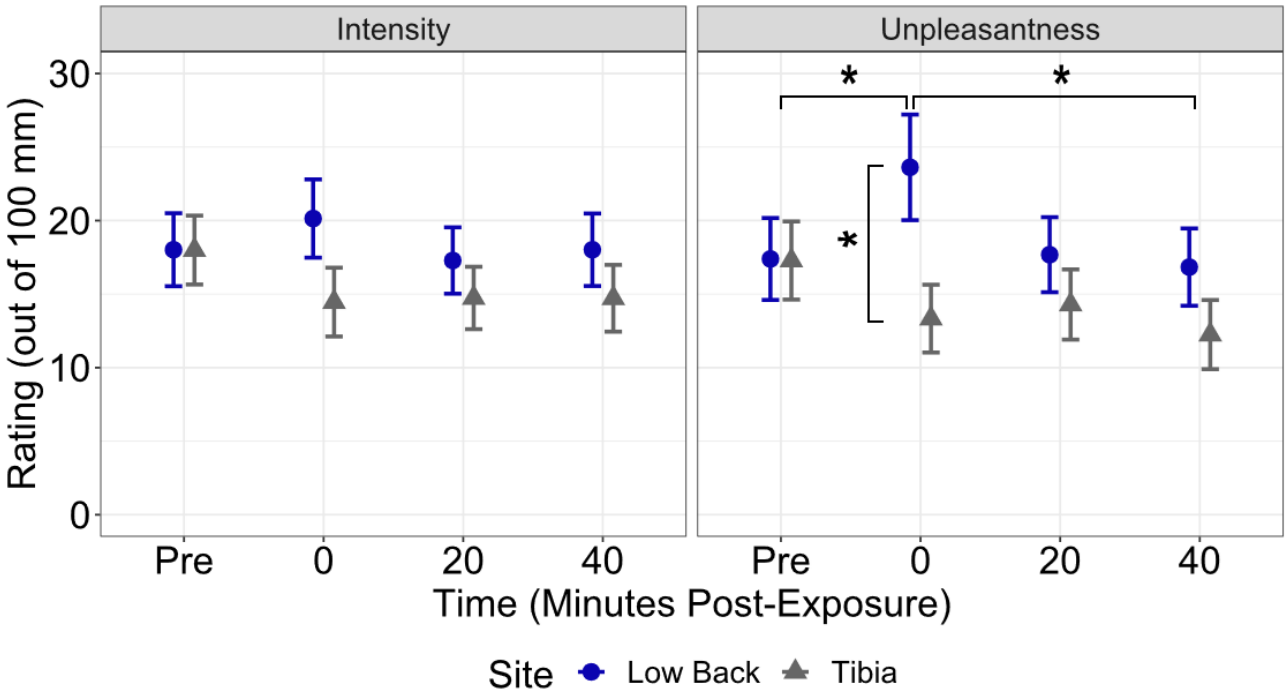

Figure 3-6: Perceptions of Sub-Threshold Stimulus Intensity (left) and Unpleasantness (right). L3/L4 intervertebral space data are the blue circles; mid-tibial shaft data are the gray triangles. Error bars show ± 1 standard error. Significant differences ($p < 0.05$) are indicated by asterisks.

3.5 Discussion

A 10-minute seated maximal spine flexion exposure increased flexion range of motion by 10.3%, with changes persisting for at least 40 minutes. This exposure increased the level of unpleasantness participants experienced during a fixed pressure application to the L3/L4 intervertebral space, but PPTs and perception of stimulus intensity were not affected by prolonged trunk flexion. The amount of creep, muscle activity, and tibial pain sensitivity measures in varying combinations could predict the L3/L4 pain sensitivity measures over time, but the strength of these predictions was weak. Myoelectric activity confirmed that the exposure and subsequent assessments of creep were predominantly indicative of passive tissue properties. Reconciling these findings points towards a central process altering participant's perception of external pressures following static lumbar spine flexion (Fuchs et al., 2014; Villemure and Bushnell, 2009).

Hypothesis 1a, stating that the prolonged flexion exposure should increase mechanical pain sensitivity in the low back was partially accepted since STS unpleasantness increased, however the other too measures of mechanical sensitivity were unchanged throughout the study. Hypothesis 1b, stating that the magnitude of creep could predict pain sensitivity measures was partially accepted; PPTs were the only measure where this was true. Hypothesis 1c, stating that tibial mechanical sensitivity would not be altered by the exposure was accepted.

The inconsistency of perceived unpleasantness solely changing with low back creep while PPTs being the only measure creep could predict may point towards a variable response of pain sensitivity to passive tissue creep. However, these two measures of pain sensitivity converge in cortical activity whether generated by viscoelastic changes, or external factors. Our perception of stimulus unpleasantness is highly linked to our current mood (Villemure and Bushnell, 2009) and may also be linked to activity in the dorsal anterior cingulate cortex (Fuchs et al., 2014). Contrarily, identifying a PPT from blunt pressure is thought to relate to C-fibre afferent sensitivity (Treede et al., 2002), which may be a function of peripheral innervation (Schmidt et al., 1995), or a lack of descending inhibition from structures in the brain and brainstem such as the anterior cingulate cortex (Duan et al., 2014; Goffaux et al., 2007; Guo and Hu, 2014). It can be hypothesized that prolonged passive flexion could stimulate anterior cingulate cortex activity, however this is still conjecture since there was no measurement of brain activity in this study. Alternatively, participants simply may not have liked the flexion exposure, which in turn influenced their perception of the STSs (Martucci, 2017; Villemure and Bushnell, 2009). This mood effect also explains the transient change in perceived unpleasantness immediately following the exposure (Figure 3-6) despite creep not recovering after the 40-minute standing period (Figure 3-4).

It is likely that the exposure did not generate a sufficient inflammatory response or increase neural afferent activity enough to unambiguously sway mechanical pain sensitivity into a purely sensitized or desensitized state relative to before the exposure. Afferent neural activity was assessed indirectly through muscle activity (Table 3-4) and did appear to increase slightly with creep, but this was not significant, nor were muscle activities on their own predictive of any pain sensitivity measure. Although other authors have reported upregulation of inflammatory molecules following prolonged flexion (D'Ambrosia et al., 2010; Yang et al., 2011), the duration of these exposures (1-2 hours with rest breaks) covered a much longer time period than the exposure used here (10 minutes continuously). Our exposure, although capable of generating creep, may not have persisted long enough for the effects of any inflammatory pathways to be observed through pressure algometry (Ackermann et al., 2005). Changes in concentrations of circulating biomarkers of inflammation (Parks et al., 2004; Yang et al., 2011), which were not believed to be necessary

initially, are likely required to determine if inflammatory pathways are involved in pain sensitivity changes following prolonged flexion exposures. However, there may have been individual changes favouring either pathway between participants that can be explained by the significant prediction of lower back PPTs by interactions between creep magnitude and tibial PPTs. The consistent finding that tibial pain sensitivity measures could predict lower back sensitivity measures may speak to individual differences in PPTs being greater than creep-induced changes, or that any changes occurring may occur in both regions, contrary to exercise-induced hypoalgesia models of pain (Micalos and Arendt-Nielsen, 2016). More directed investigations should discern if any features of pain processing are affected by viscoelastic changes to passive tissues.

Different tissues may be differently affected by static flexion. Ten minutes of seated full spine flexion can alter the internal fibre arrangement without any changes in muscle thickness or activation while controlling for muscle length (Pinto et al., 2021). Our assessment of creep here relied solely on skin-based measures, intended to represent a combination of skin and presumably posterior ligament stretch, however muscle properties are also affected by the creep exposure, coinciding with one of the multiple linear regressions producing a significant interaction term of creep magnitude, tibial pain sensitivity, and muscle activation, despite muscle activity in not being affected directly by the creep exposure (Table 3-3). The fibre flattening in muscles from Pinto et al., (2021) could increase the risk of shear-related injuries, since fibre obliquity in the lumbar erector spinae allows that muscle to oppose and protect the spine from anterior shear forces (Gallagher and Marras, 2012). While the main purpose of this chapter was to isolate pain sensitivity rather than address injury risk, this provides some explanation as to why prolonged flexion exposures are related to low back pain (Lis et al., 2007; Xu et al., 1997; Zemp et al., 2016), independent of changes in pain sensitivity.

The methods used to generate creep have been shown to determine the end effects of that creep exposure and may influence pain sensitivities. Presently, we used a 10-minute seated maximum flexion exposure, similar to other authors (McGill and Brown, 1992; Rogers and Granata, 2006), however other authors have used different postures (Shin and Mirka, 2007; Toosizadeh and Nussbaum, 2013). The magnitude of creep reported here (4.4 ± 2.7°) is slightly less than other authors using seated protocols (5.5° (McGill and Brown, 1992) and 5.3 ± 4.5° (Rogers and Granata, 2006)), however our exposure duration was half as long, and exposure time is another known mediator of creep effects (Bazrgari et al., 2011). Also, the creep our participants experienced did not recover following 40 minutes of standing, which is consistent with the time constants from some groups (Busscher et al., 2011; Rogers and Granata, 2006; Solomonow et al., 2003) but not others (McGill and Brown, 1992; Shin and Mirka, 2007) using prolonged spine flexion. A seated posture was chosen after piloting with a 10-minute standing full-flexion exposure revealed a 50% participant completion rate (due to leg pain); sitting participants down increased the success rate to 98%. However, it was more difficult to reduce hip motion in our seated setup compared to the strapping used by other groups during standing (Muslim et al., 2013; Shin and Mirka, 2007) while still being able to reliably assess PPTs. Although our seated flexion exposure seemed representative of other seated flexion exposures, the changes seen here may be specific to seated flexion.

While flexion range of motion generally remained elevated throughout the 40-minute standing recovery period, there were two time points when range of motion was temporarily reduced: the Post 10 and Post 30 time points (Figure 3-4). These two time points were unique in that they assessed PPTs, but not STSs (Figure 3-3). Participants spent the longest time in flexion during the Pre, Post 0, Post 20, and Post 40 assessments that measured both PPTs and STSs (15 – 25 seconds), and the least time in flexion

during the Post 5, 15, 25, and 35 time points when only flexion range of motion was measured (5 seconds). Based on viscoelasticity predicting that a longer time in flexion allows for greater tissue elongation, it would be expected that transient reversions to Pre-exposure values would occur at the time points with shorter flexion assessments (Fung, 1994; Provenzano et al., 2001). However, since PPTs were consistently assessed before STSs, and the flexion range of motion assessments were taken during the PPT assessments when applicable, participants should have experienced similar levels of transient flexion in the time points that only assessed PPTs (Post 10 and Post 30) as they did during the time points assessing both PPTs and STSs (Pre; Post 0, 20, and 40). Other potential concerns include heterogeneity in creep recovery or inconsistencies in reaching maximal seated flexion range of motion. While it is likely that some participants did return to Pre-Exposure flexion ranges of motion, they were not identifiable by participant gender, the only between-participant factor this study was designed to accommodate. The variance in creep recovery could also account for the ability for flexion range of motion to weakly predict low back PPTs (Table 3-5) despite there being no effects of Time in either measure. While it is possible that the experimental design could have influenced these flexion range of motion measures, there was not a systematic element unique to the Post 10 and Post 30 assessments that should reduce flexion range of motion.

This study introduced a novel pressure algometer to assess PPTs and STSs, which was determined to have a between-day root-mean-square error of 0.2 MPa in determining PPTs in Appendix C. This root-mean-square error magnitude was approximately the magnitude of the differences between the tibial and low back PPTs, which could cast doubt onto how meaningful those differences could be. Additionally, tibial PPTs have previously been assessed over the tibialis anterior muscle belly instead of the tibial shaft as were done presently (Hven et al., 2017; O'Neill et al., 2007). While both factors could increase the variability relative to non-motorized methods (Melia et al., 2015), the purpose of including a distal site was to control for changes over time rather than compare for main effect of site. Also, the current sample size was predicted to have an 80% chance to detect smaller effect sizes then had been reported by most authors for pressure algometry measures (Chesterton et al., 2003; Melia et al., 2015; Micalos and Arendt-Nielsen, 2016; Petrini et al., 2015; Stefanik et al., 2020). While being far from comprehensive, there is reasonable confidence in the current measures that a 10-minute seated flexion exposure did not alter lower limb sensitivity.

Lumbar spine flexion range of motion could predict local pain sensitivity; however, these predictions were relatively weak. Additionally, increases in perceived stimulus unpleasantness could be related to changes in descending information from the cortex, potentially instigated through mood. There did not appear to be any changes in mechanical sensitivity following seated lumbar spine flexion related to altered neural feedback or inflammatory pathways.

Chapter 4 - Effects of Repetitive Trunk Flexion on Mechanical Pain Sensitivity in the Low Back

The findings in this chapter have been published as:

Viggiani, D. and Callaghan, J. P. (2021) Interrelated hypoalgesia, creep, and muscle fatigue following a repetitive trunk flexion exposure. *Journal of Electromyography and Kinesiology.* 57, 102531.

4.1 Introduction

Repetitive trunk flexion is commonly observed in construction (Boschman et al., 2011), manual materials handling (Murtezani et al., 2011), and childcare workers (Labaj et al., 2016), and is thought to be contribute to their high incidence of low back pain (Dempsey and Hashemi, 1999; Grant et al., 1995). Intervertebral disc injuries (Callaghan and McGill, 2001; Veres et al., 2009) and vertebral fractures (Gallagher et al., 2005; Gooyers et al., 2015) have both been documented to occur following compression combined with repetitive spinal flexion, with vertebral fractures more commonly occurring under higher loads (Parkinson and Callaghan, 2009). Repeated spine flexion can also induce creep in posterior spinal elements (Little and Khalsa, 2005; Solomonow et al., 2000; Toosizadeh and Nussbaum, 2013), which can increase passive tissue laxity (Provenzano et al., 2002; Solomonow et al., 2000; Thornton et al., 2002) through the disruption of collagenous networks (Gooyers et al., 2015; Viidik, 1972). Although evidence exists for repetitive sagittal plane motion to cause injury (Kumar, 2001), it may also affect mechanical pain sensitivity through a combination of creep-based and active motion-based pathways.

Repetitive trunk motions could alter pain sensitivity through exercise-induced hypoalgesia—the phenomenon that continuous or interval exercise reduces pain sensitivity (Kodesh and Weissman-Fogel, 2014; Koltyn, 2000). The exercise performed needs to be at or above 50% of heart rate reserve (Naugle et al., 2014) and performed for at least ten minutes (Hoffman et al., 2004) in order to increase pain thresholds near the active musculature (Micalos and Arendt-Nielsen, 2016). The effects of this reduction in pain sensitivity do not persist long after the exercise is terminated, suggesting that transient changes associated with exercise are responsible for this phenomenon (Koltyn, 2000). The effects of exercise-induced hypoalgesia may also be more potent on chemical or thermal pain than on mechanical pain (Kodesh and Weissman-Fogel, 2014). This phenomenon appears to be a subset of conditioned pain modulation pathways (Gajsar et al., 2018; Lemley et al., 2015) related to endogenous opioid release after oxidative stress (Koltyn et al., 2014) or direct inhibition from cognitive centres in the cerebral cortex (Jones et al., 2017).

Repetitive trunk flexion can also affect pain sensitivity through muscle fatigue in addition to the hormonal or cognitive pathways outline above, mainly through central fatigue mechanisms (Gandevia, 2001). Central fatigue, a decline in muscle power resulting from signals from the central nervous system, is believed to be initiated by an increase in non-nociceptive C-fibre activity (Hill, 2000; Taylor et al., 2016). This C-fibre afferent activity specific to fatigue is believed to inhibit motor centres within the brain (Kennedy et al., 2015), but may also contribute to peripheral neuron hyper-excitability (Andersen et al., 1995; Taylor et al., 2000). The effects of this neuronal hyper-excitability may be seen in part through reductions in proprioception (Boucher et al., 2012; Lee et al., 2003) and compromised postural control (Larson and Brown, 2018; Vuillerme and Pinsault, 2007), but these observations may stem from other modifications in afferent or efferent signaling. Although the increase C-fibre activity itself is not predicted

to alter nociceptive afferents in the Gate Control or Neuromatrix frameworks (Braz et al., 2014; Melzack, 1999), reduced peripheral neuron thresholds may affect the other large diameter afferent information converging at the spinal cord, affecting pain perception (Basbaum et al., 2009; Braz et al., 2014). Conversely, the acidic environment that occurs with muscle fatigue can activate ASIC3 membrane channels (Gregory et al., 2016)—proteins that are abundant on nociceptive neurons (Osmakov et al., 2014)—which can increase rather than decrease mechanical pain sensitivity. A direct assessment indicated that pain sensitivity was reduced following isometric brachioradialis fatigue (Hoeger Bement et al., 2009). However, muscle fatigue caused by repeated dynamic contractions may produce a different net effect on pain sensitivity since specific changes following muscle fatigue are highly task-dependent (Enoka and Duchateau, 2008; Taylor et al., 2000).

The creep-specific alterations to afferent feedback may also differ between static and repetitive loading in the absence of muscle activity. Using an *in-situ* animal model, Solomonow and colleagues (2000) determined that passive cyclical ligament loading produced an initial reflex suppression that was followed by a period of extended hyper-excitability three to four hours after loading had finished. This hyper-excitability is not seen in the same animal model during static loading (Solomonow et al., 2003) and does not appear to be influenced by loading magnitude (Claude et al., 2003). In humans, repetitive trunk flexion can increase the onset angle of the flexion-relaxation phenomenon (Howarth et al., 2013b), however this shift is similar to that induced by static trunk flexion (Howarth et al., 2013a). Mechanical changes following repetitive trunk flexion in humans have also been more transient than in static flexion, with changes in lumped passive stiffness (Parkinson et al., 2004) and movement repeatability (Howarth et al., 2013b) being similar between the start and end of repeated motions despite decreases in both measures in the middle of these protocols. Since mechanical (Toosizadeh and Nussbaum, 2013) and inflammatory (Beharriell et al., 2020; Pinski et al., 2010) changes during viscoelastic creep increase with higher movement frequencies, the aforementioned transient creep effects may have resulted from the low loading frequencies in those studies (1/15 to 1/30 Hz).

Changes to mechanical pain sensitivity following repetitive trunk flexion may differ from sensitivity changes following prolonged passive trunk flexion. Potential mechanisms for these differences may relate to muscle fatigue, cognitive or hormonal alterations from exercise, or differences in loading history.

4.2 Purpose and Hypotheses

The purpose of this study was to determine how repetitive trunk flexion/extension, which can induce muscle fatigue and lumbar spine creep, affects mechanical sensitivity to pain at local and distal locations. It was hypothesized that:

2a) Mechanical sensitivity in the low back and lower leg will be decreased immediately after completing repetitive trunk flexion/extension; pressure-pain thresholds (PPTs) will increase, and the unpleasantness and intensity ratings of sub-threshold stimuli (STSs) will decrease.

2b) Mechanical sensitivity in the low back and lower leg will match the findings in Chapter 3 after 40 minutes of standing recovery following repetitive trunk flexion/extension. This assumes that any fatigue effects of mechanical sensitivity will have dissipated by the end of the 40 minute recovery period.

2c) The magnitude of fatigue (reductions in static moment-generating capacity) or creep (changes in maximal flexion range of motion) alone will not be related to changes in mechanical sensitivity immediately after repetitive trunk flexion/extension.

4.3 Methods

This study had participants perform repetitive unloaded trunk flexion and extension for up to 10 minutes followed by 40 minutes of standing recovery. Intermittent isometric contractions and ratings of perceived exertion assessed muscle fatigue in the lumbar spine extensors and anterior leg during and after the repetitive exercise. Pressure algometry determined PPTs and perceptions to STSs in the low back and lower leg. Accelerometers placed on the low back tracked the generation and recovery of lumbar spine creep.

The methods of this study were those in Chapter 3. The major differences involve modifying the creep assessments and measuring indicators of muscle fatigue. The reader will be referred to the relevant sections of Chapter 3 where applicable.

4.3.1 Participants

A convenience sample of 37 adults (18 males and 19 females) were recruited from a university population and the surrounding community (Table 4-1). All participants performed the study detailed in Chapter 3 (passive flexion) and met similar inclusion criteria which also controlled for are age-dependent effects of muscle fatigue (Avin and Frey Law, 2011; Dalton et al., 2010). At least 48 hours occurred between testing sessions to prevent any residual effects from one exposure during the other collection. The first 19 participants in the passive flexion study detailed in Chapter 3 performed that study first, while the remaining 18 participants performed this study first. Equipment construction and modifications necessary to perform the strength testing in this study did not occur until the first nineteen participants were collected in the passive flexion study, hence the staggered recruitment.

Table 4-1: Physical Characteristic of the Participants in Study 2

	Males (n = 18)	**Females (n = 19)**
Age (years)	23.8 ± 4.4	23.2 ± 3.4
Height (m)	1.77 ± 0.07	1.66 ± 0.08
Mass (kg)	75.1 ± 9.9	65.9 ± 12.1
% Left Foot Dominant	16.7 %	0.0 %

4.3.2 Measurements and Instrumentation

Accelerometers, electromyography, and force data were sampled using a 16-bit conversion card and an excitation voltage of +/- 10 volts (First Principles, Northern Digital Inc., Waterloo, ON, Canada). Sampling rates of all analog data were factors of 10,000,000 for automatic data synchronization.

Pressure Algometry

Measurements of pressure algometry were identical to those documented in section 3.3.2 of Chapter 3. The same pressure algometer in that study (Appendix C) determined PPTs, perceptions of 70% of a participant's PPT (Petrini et al., 2015). Also like in Chapter 3, assessments were performed in between the L3 and L4 spinous processes and on the mid-tibial shaft. Both measures were taken while participants were standing,

participants held full lumbar spine flexion during the lower back assessments but remained standing upright for the tibial assessments.

Visual analog scales identical to those documented in section 3.3.2 of Chapter 3 were given to participants to report their perception of stimulus intensity and unpleasantness to pressures matching 70% of their PPTs.

Accelerometers

Accelerometers were used to track lumbar spine motion identically to the methods reported in Sections 3.3.2 of Chapter 3.

Electromyography

Surface electromyography of the L3 erector spinae and tibialis anterior determined if evidence of fatigue was present in either muscle. Erector spinae electromyography were measured bilaterally while tibialis anterior electromyography was measured only on the dominant limb. Electrode placement and preparation are documented in Appendix B. Signals were differentially amplified from a bipolar configuration with a common-mode rejection ratio or 115 dB (at 60 Hz; 10^{10} ohm input impedance), band-pass filtered from 10 to 1000 Hz, and gained by a factor of 500 to 5000 (AMT-8, Bortec, Calgary, AB, Canada). Gained signals were sampled at 2000 Hz.

Isometric Joint Strength

Trunk extension and ankle dorsiflexion isometric strength were evaluated while participants stood at a height-adjustable external fixation device designed to constrain pelvis motion. For trunk extension isometric strength, participants had padded cabling wrapped around their back at the level of T6 passed under their axillae and connected to a uniaxial load cell (MLP-300-CO, Transducer Technologies, Temecula, CA, USA) tethered to a wall. The length of the tether was adjusted to provide resistance to extension when participants were in a neutral standing posture. Participants were instructed to maximally extend against the padded cables with their pelvis supported by the fixation device; the peak tension was recorded as their trunk extension strength. For ankle dorsiflexion, participants were instructed to maximally dorsiflex their ankles against resistance provided by a 6-degree of freedom force cube (MC3-6-500, AMTI, Watertown, MA, USA) bolted to the underside of the frame supporting the tibial pressure algometer in series with 100 mm steel tube and a scalloped piece of pine; positioned above their dominant foot. The additional serial materials and use of a force cube over a uniaxial load cell provided a better, more stable fit to participant's feet during tibialis anterior strength trials. The height of the force cube was adjusted so participants met resistance at a neutral ankle angle (Tabard-Fougère et al., 2018). Voltage outputs from the force transducers were sampled at 50 Hz.

Ratings of Perceived Exertion

Participants were asked to report their overall perceived exertion using a 10-point Borg scale (Borg, 1982) every two minutes during the active trunk flexion-extension exercise.

4.3.3 Experimental Protocol

Data were collected in a single session taking place within one hour of the start of the first data collection session, and at least two hours after participants awoke to limit the effects of diurnal variation on the soft tissues about the spine (Adams et al., 1990). The pressure algometer controllers and strength interface stability were tested to ensure functionality prior to the start of each session. Figure 4-1 summarizes the protocol of this study.

Upon obtaining informed consent, height, mass, age, and leg dominance (the leg selected to manipulate objects on the ground) if necessary, participants stood in the pelvis external-fixation device to have the pressure algometry and isometric strength testing components adjusted to fit their anthropometry. Once adjustments were completed, participants had their baseline PPTs determined, and STS pressure derived. Participants stood in full spinal flexion during low back pressure algometry (Figure 4-2; Panel D).

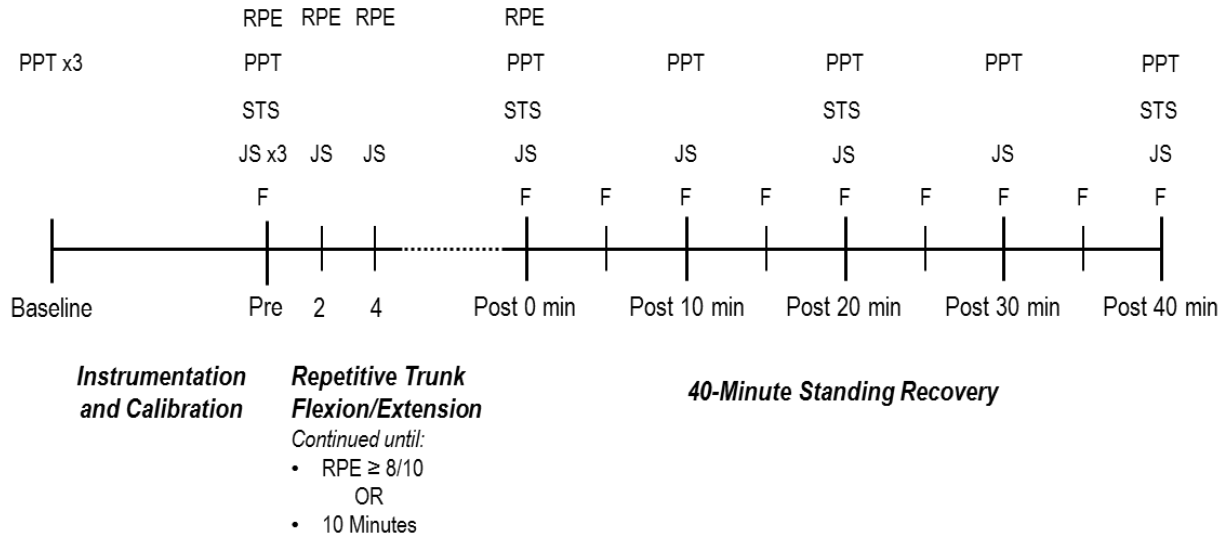

Figure 4-1: Overview of Chapter 4 Study Design. The overall design is similar to the study documented in Chapter 3, with the dependent measures and intervention task differing between studies. The Repetitive Trunk Flexion/Extension Task will cease once the participant reports an exertion level of 8/10 or higher, or once 10 minutes have elapsed. Assessments of isometric joint strength and perceived exertion will be conducted every two minutes during this task. PPT: Pressure-Pain Thresholds at both sites; STS: Sub-Threshold Stimulus applications and associated perception ratings at both sites; RPE: Borg 10-point Rating of Perceived Exertion; JS: Isometric Joint Strength assessed within the external fixation device, including both trunk extension and ankle dorsiflexion tests; F: Maximal Flexion Holds to assess creep recovery.

After baseline sensitivity measures, participants were instrumented with surface electromyography, performed two maximal voluntary contractions (one per muscle), and a single resting trial. Protocols for these normalization procedures are described in Appendix B. After electromyography preparations were completed, participants were instrumented with accelerometers. A neutral standing calibration trial and maximal standing range of motion trials were collected, similar to the passive flexion study in Chapter 3.

Baseline isometric joint strength testing began once participants completed with three attempts alternating between trunk extension and dominant ankle dorsiflexion (Figure 4-2; Panels A and C). Participants were instructed to steadily build force during strength testing and be given at least two minutes rest between tests. Once strength testing was completed, participants completed all pressure-pain algometry testing before the 10-minute flexion-extension exercise. Starting from neutral standing, a single cycle of the task consisted of two seconds of flexion, four seconds of maintaining maximal flexion, and two seconds of extension back to neutral standing in time to a metronome. Participants performed cycles once every ten seconds. Instructions given to participants were as follows:

- "For this exercise, you will bend your trunk forward towards your toes, briefly holding yourself at the bottom, and then returning back up to your natural standing posture."
- "Using this metronome as a guide, take two seconds to bend forward, hold yourself at the bottom for four seconds, and then take two seconds to stand back up."

- "Lean into the bar positioned at your pelvis and let your trunk, neck and head bend over in front of you."

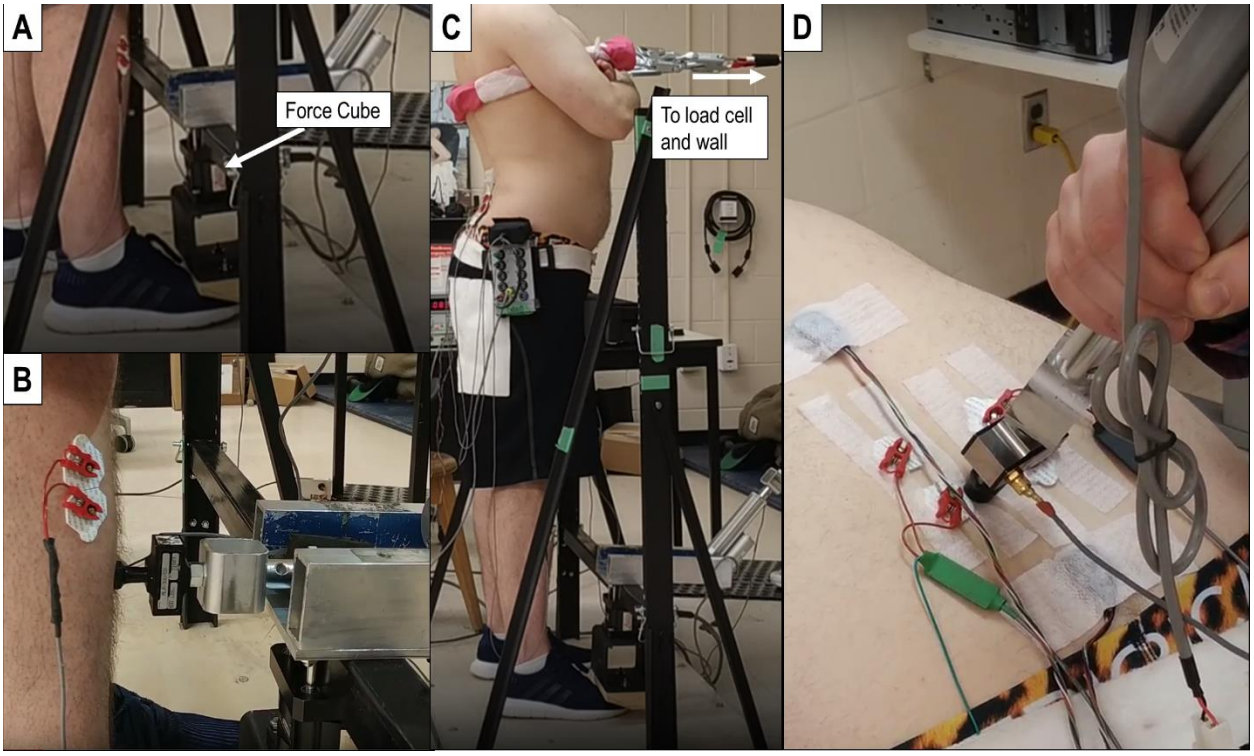

Figure 4-2: Testing Procedures for Chapter 4 Study. Ankle dorsiflexion strength was measured using a force cube mounted to the underside of the tibial pressure algometry frame, a wooden block and steel tube ensured neutral ankle angles against resistance (Panel A). Tibial pressure algometry was identical to Chapter 3 (Panel B). Low back extension strength was measured using a tether wrapped under participant's axillae, adjusted to provide resistance at a comfortable, near-neutral posture (Panel C). Low back pressure algometry was similar to Chapter 3, only participants stood in full flexion instead of sat in full flexion (Panel D).

Sample angular kinematics for the repetitive trunk flexion/extension task are shown in Figure 4-3 to illustrate timing.

Every two minutes (12 cycles), the trunk flexion/extension task was briefly interrupted for a rating of perceived exertion and assessments of trunk extension and ankle dorsiflexion isometric strength. Like the pre-task assessments, participants gradually ramped up force to hold a maximal effort for joint strength testing, unlike the pre-task assessments, a single test of each joint was conducted rather than three tests. Ratings of perceived exertion preceded isometric joint strength testing when taken. The repetitive flexion/extension task continued until participants gave a rating of perceived exertion of at least 8/10 or once 10 minutes (60 cycles) elapsed.

After completing the trunk flexion/extension task, participants held a fully flexed spinal posture (rounded spine instructions) for five seconds to assess spinal range of motion. Participants then stood upright on a platform in front of the fixation device for 40 minutes. During this 40 minute recovery phase, assessments of spinal flexion range of motion were completed every 5 minutes; PPTs and isometric strength measures were completed every 10 minutes; and perception of STSs were conducted every 20 minutes (Figure 4-1). After 40 minutes elapsed, participants were remunerated, and the session ended.

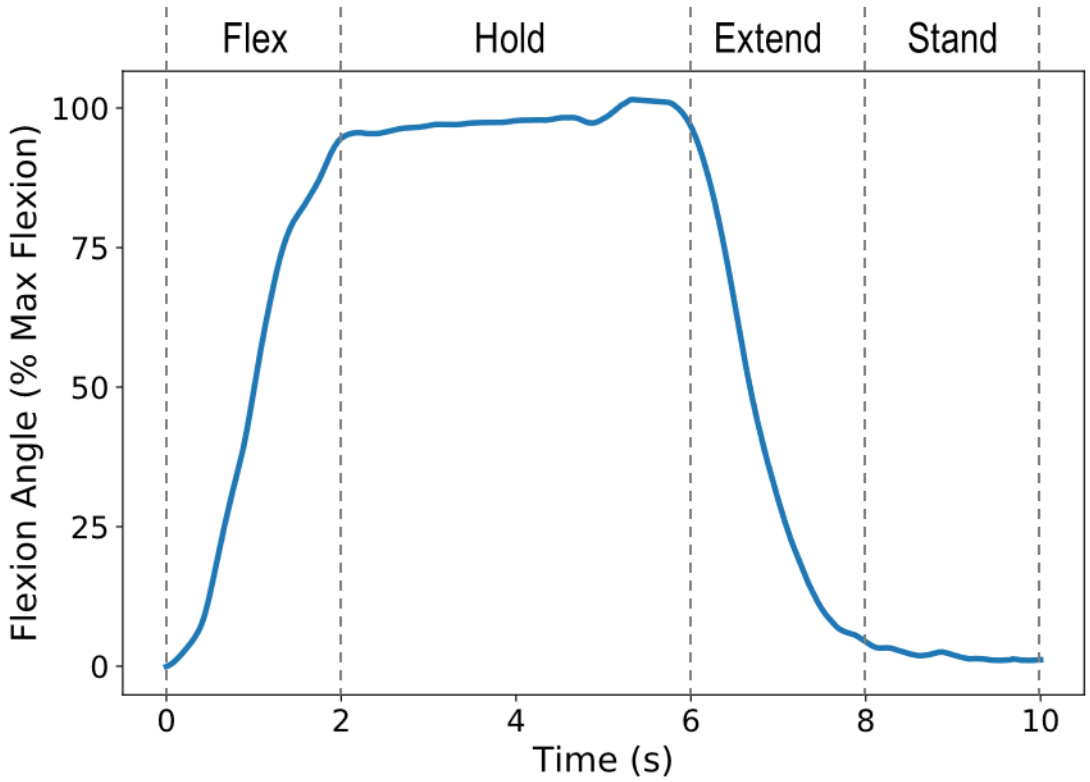

Figure 4-3: Sample Sagittal Plane Angular Kinematics during the Repetitive Trunk Flexion/Extension Task. The vertical axis is a percentage of the range of motion from the pre-task static flexion trial normalized so 0% is upright standing and 100% is the angle measured from the pre-task static flexion trial. This figure is included to illustrate the duty-rest cycle for the repetitive flexion-extension exposure used in this study.

4.3.4 Data Processing

All data analyses were performed in Python (v3.5.1, Python Software Foundation, https://www.python.org/) using the `numpy` package unless otherwise specified.

Pressure Algometry

Data processing was identical to those described under the "Pressure Algometry" subheading of section 3.3.4 in Chapter 3. Measures are intended to represent mechanical sensitivity in the low back and lower leg.

Accelerometers

Accelerometer data processing was identical to what was documented in Section 3.3.4 under the "Accelerometers" subheading. Data used for analysis were the first and every 12th cycle of the repetitive flexion-extension exercise, and the static flexion holds used to assess creep immediately and every 5 minutes after the exercise was completed. As done for Chapter 3, lumbar spine flexion angles were expressed as a percentage of the participant's total range of motion by defining the neutral standing calibration trial as 0% and the maximal flexion angle achieved in the pre-flexion static calibration trial as 100% range of motion.

Electromyography

Electromyography data was used as an indicator of muscle fatigue. Myoelectric signals from the intermittent maximal contractions had a 60 Hz band-stop filter applied to remove electromagnetic interference (Mello et al., 2007). Cleaned signals from the maximal exertions were split into half-second

windows, and each window underwent a Fourier transformation (MacIsaac et al., 2001). The mean power frequency was computed on each half-second window using equation 4-1, and the average of all the windowed mean power frequencies were taken as the mean power frequency from that trial.

$$MnPF = \frac{\sum_{i=0}^{F} f_i p_i}{\sum_{i=0}^{F} p_i} \quad (4\text{-}1)$$

In equation 4-1, $MnPF$ is the mean power frequency, F is the maximum measurable frequency, f_i is the ith frequency and p_i is the power at that frequency. Mean power frequencies were expressed as a percentage of the average of the three baseline maximal contractions immediately preceding the repetitive flexion/extension task.

Isometric Joint Strength

Data from the load cells representing isometric trunk extension and ankle dorsiflexion strength was used along with electromyography to track the development and recovery from muscle fatigue. Raw force data was calibrated using a 2-point static calibration, and filtered using a 6 Hz cut-off, 4th order, dual-pass, low pass Butterworth filter (Viggiani and Callaghan, 2018). The maximal filtered force from each trial was taken as the strength from that trial. Like mean power frequencies, strengths were expressed as a percentage of the average strength from the three pre-flexion/extension maximal contractions.

4.3.5 Statistical Modelling

All statistical testing was performed in RStudio (v1.0.143 RStudio Inc., Boston, MA) using significance levels of 0.05.

Hypotheses 2a and 2b were concerned with differentiating measures of pain sensitivity with respect to the repetitive trunk flexion/extension exposure. For these tests, the dependent variables were PPTs and ratings of STSs, with independent variables of Time (pre-flexion/extension and five levels post-flexion/extension: 0/10/20/30/40 minutes) and Site (low back/tibia). The specific time points compared differentiate hypothesis 2a (0 minutes post-flexion/extension) from hypothesis 2b (40 minutes post-flexion/extension. Two-way ANOVAs were performed on PPTs and perceptions of fixed-pressure stimuli, using Greenhouse-Geisser adjustments to the degrees of freedom were made when Mauchly's test indicated that assumptions of sphericity were violated. Tukey's test was performed post-hoc in the case of significant findings.

In regard to hypothesis 2c, multiple linear regressions were performed to determine how creep and muscle fatigue indicators were related to each measure of low back pain sensitivity. Non-normalized terms (creep magnitude and PPTs) were normalized to pre-exposure values prior to conducting multiple linear regressions. Significant predictors were checked using Wald's χ^2 test.

Aside from the three hypotheses, statistical testing was also performed to confirm that the ankle dorsiflexors were not fatigued following the repetitive trunk flexion/extension protocol. This involved two additional two-way repeated measures ANOVAs with factors of Time (pre-flexion/extension, four during flexion/extension, and five post-flexion/extension) and Site (low back/ankle). Dependent variables were mean power frequencies and isometric joint strengths. Similar tests for and contingencies for violations of

sphericity were performed as was described in relation to hypotheses 2a and 2b. Tukey's test was performed post-hoc in the case of significant findings.

4.4 Results

Data related to identifying creep and fatigue effects of the flexion exercise are presented first in section 4.4.1; findings concerning hypothesis 2a and 2b are presented next in section 4.4.2; lastly, findings concerning hypothesis 2c are presented in section 4.4.3.

4.4.1 Creep- and Fatigue-Related Variables

The peak rating of perceived exertion during the flexion/extension exercise reported by any participant was 7/10, meaning all participants performed the exercise for the full ten minutes. Average ratings of perceived exertions were 2.9 ± 1.7 out of 10 for females and 4.5 ± 1.1 out of 10 for males; this difference was significant as determined by a Student's t-test ($p = 0.003$). Sex was then included as a between-subject factor on all subsequent data presented.

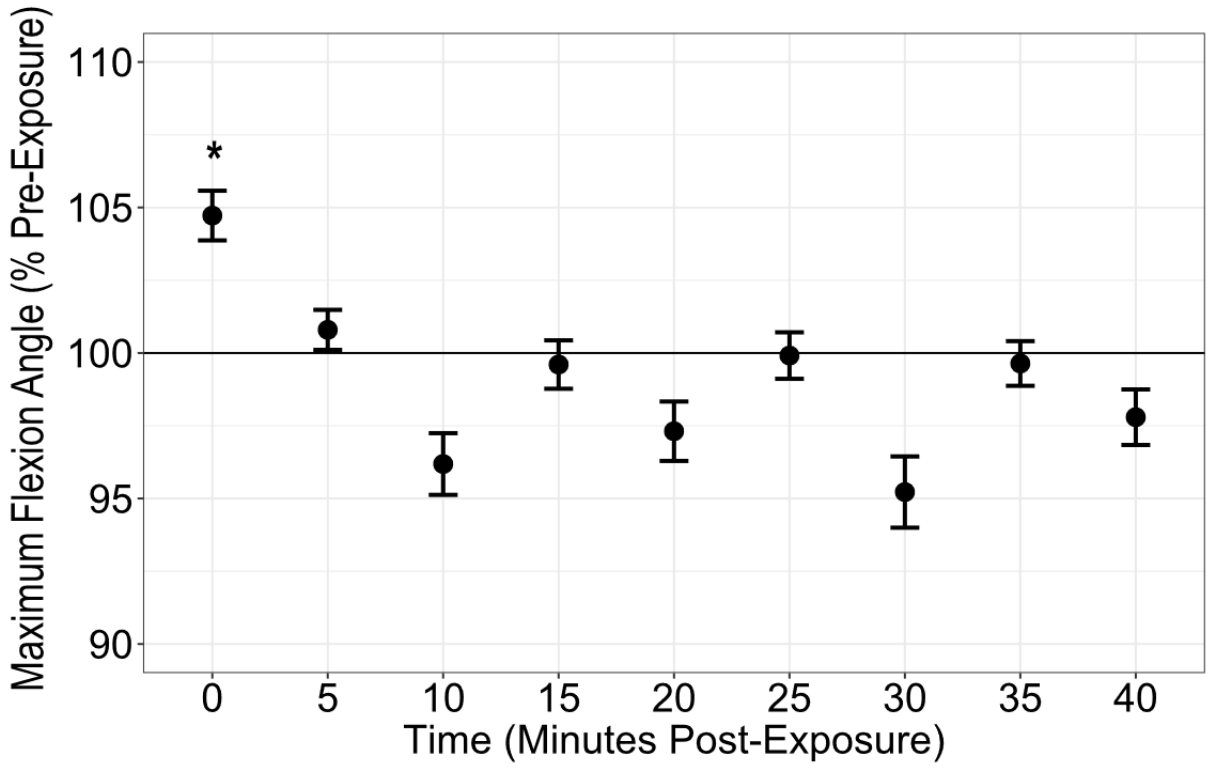

Figure 4-4: Maximal Spine Flexion Angles following the Repetitive Flexion/Extension Exercise. Data are normalized to the maximum flexion angles attained during the Pre-Exposure assessment (the horizontal line at 100%). Error bars show ±1 standard error. Time points that are significantly greater ($p < 0.05$) than the Pre-Exposure time point are denoted by an asterisk.

The repetitive flexion/extension exercise had a main effect of Time on maximum spine flexion angles ($F_{4.2,\ 147.4} = 13.80$; $p < 0.001$; Figure 4-4). Maximum spine flexion was increased by 2.7 ± 1.4° at Post 0 minutes compared to Pre-exposure ($p < 0.001$). The Post 0 minute time point had larger maximum flexion angles than all other time points, ($p < 0.01$), and all other time points had similar maximum flexion angles

as the Pre-exposure ($p > 0.175$). There were no effects of Sex ($p = 0.976$), nor were there any Sex*Time interactions ($p = 0.656$) on spine flexion angles.

There were Time*Site interactions on both isometric joint strengths ($F_{5.5, 194.3} = 5.68$; $p < 0.001$; Figure 4-5) and mean power frequencies ($F_{4.0, 141.3} = 3.88$; $p = 0.007$; Figure 4-6). Reductions were found in both variables at the low back site, but not the lower limb sites. For joint strengths, reductions were found at minutes six and eight of the exercise, as well as at post 0 minutes compared to pre-exposure values ($p < 0.01$). For mean power frequencies, all exercise time points and the Post 0 minute time point were lower than the Pre-exposure and Post 10 minute time points ($p < 0.038$); the eight minute time point of the exercise was also lower than the Post 20, Post 30 and Post 40 minute time points ($p < 0.036$). There were no other effects ($p > 0.540$) or interactions ($p > 0.065$) on isometric joint strengths of mean power frequencies.

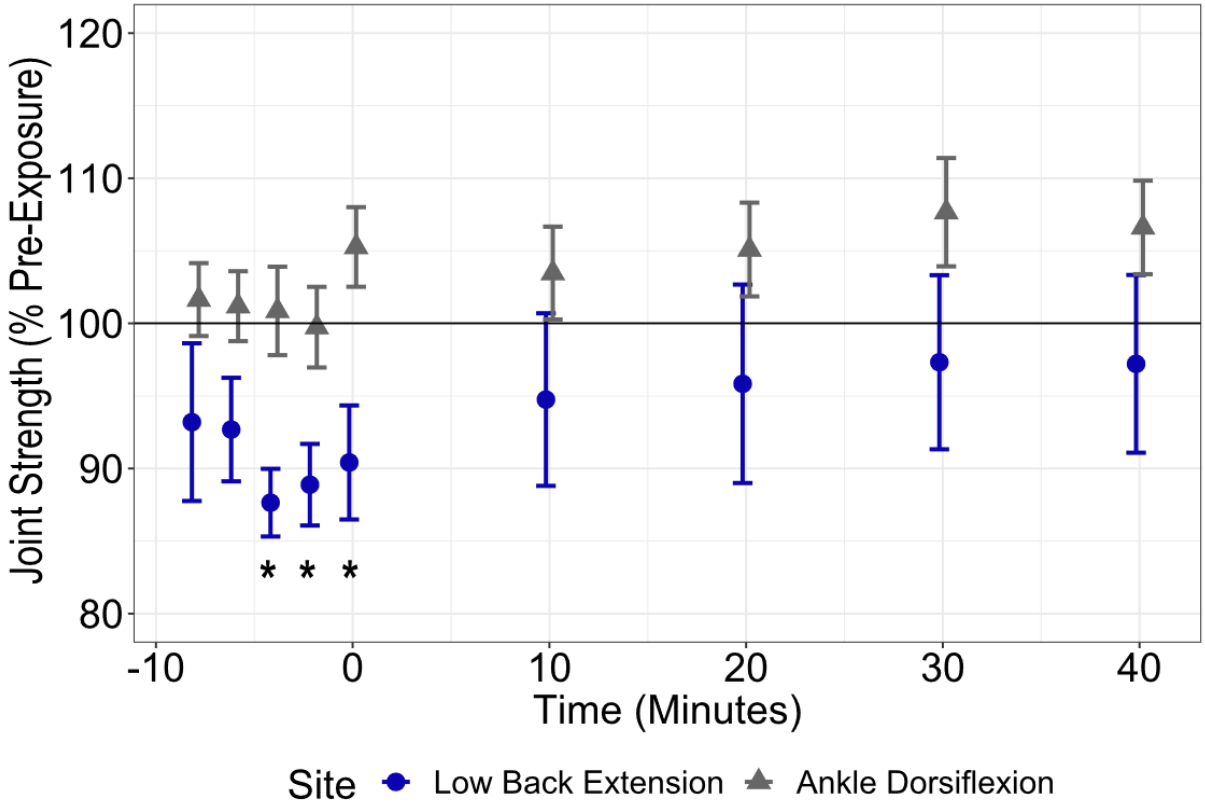

Figure 4-5: Isometric Joint Strengths during and following the Repetitive Flexion/Extension Exercise. L3/L4 intervertebral space data are the blue circles; mid-tibial shaft data are the gray triangles. Data are normalized to Pre-exposure values; time 0 indicates the end of the exercise. Error bars show ± 1 standard error. Significant reductions ($p < 0.05$) compared to Pre-exposure values are denoted with an asterisk.

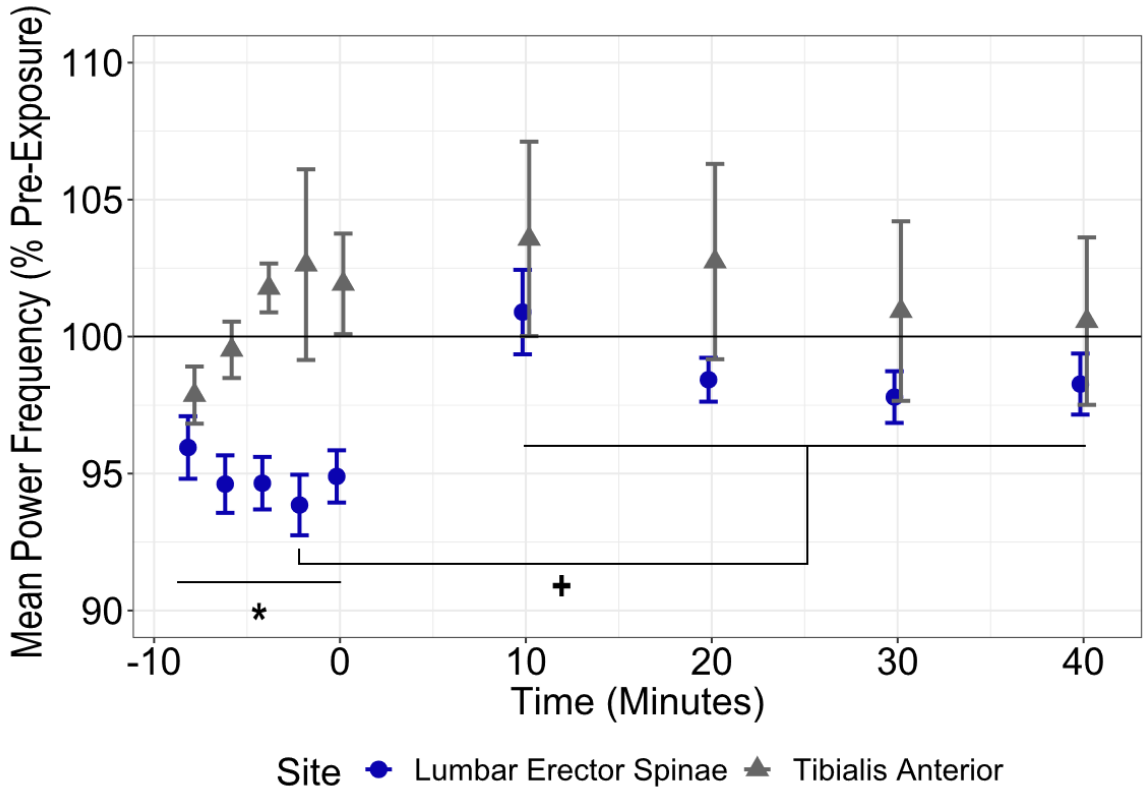

Figure 4-6: Mean Power Frequencies during and following the Repetitive Flexion/Extension Exercise. L3/L4 intervertebral space data are the blue circles; mid-tibial shaft data are the gray triangles. Data are normalized to Pre-exposure values; time 0 indicates the end of the exercise. Error bars show ± 1 standard error. Significant reductions ($p < 0.05$) compared to Pre-exposure values are denoted with an asterisk; Post-exposure time points that significantly differ ($p < 0.05$) from the 8-minute time mark are denoted by the plus symbol.

4.4.2 Changes in Pain Sensitivity Measures

There was a Time*Site interaction ($F_{3.8, 133.0} = 2.56$; $p = 0.044$) where lower back PPTs responded differently than the tibial PPTs. While tibial PPTs did not vary over time ($p > 0.396$; Figure 4-7), PPTs were elevated in the lower back at the Post 10 minute time point compared to the lower back Pre-Exposure measure ($p = 0.033$; Figure 4-7). The lower back Post 40 minute time point was not greater than the lower back Pre-Exposure time point despite similar a similar mean and distribution to the lower back Post 10 minute time point ($p = 0.051$). PPTs were greater above the L3/L4 intervertebral space than on the tibial shaft, similar to Chapter 3 ($F_{1, 35} = 16.96$; $p < 0.001$). There were no other main effects or interactions on PPTs.

Additionally, there were no statistical effects found for the STS ratings of perceived unpleasantness ($p > 0.166$) or intensity ($p > 0.102$; Figure 4-8).

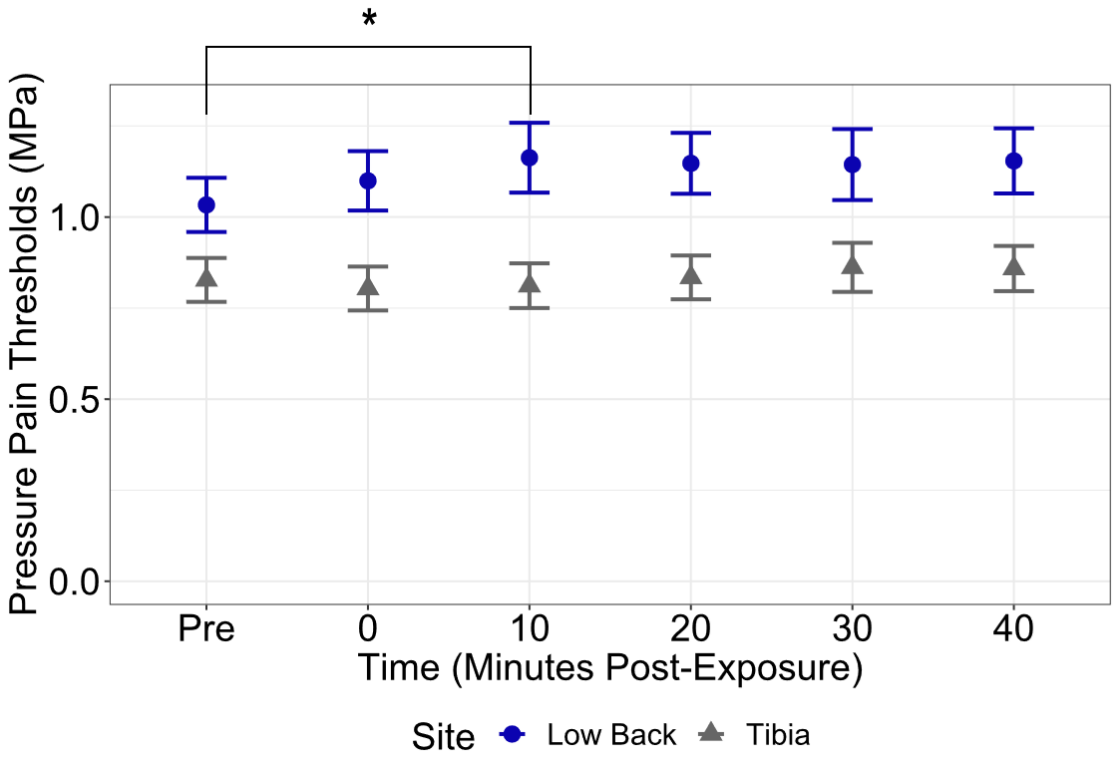

Figure 4-7: Pressure-Pain Thresholds before and after the Repetitive Flexion/Extension Exercise. L3/L4 intervertebral space data are the blue circles; mid-tibial shaft data are the gray triangles. Error bars show ± 1 standard error. Significant differences ($p < 0.05$) in the low back following the exercise compared to Pre-exposure values are denoted with an asterisk.

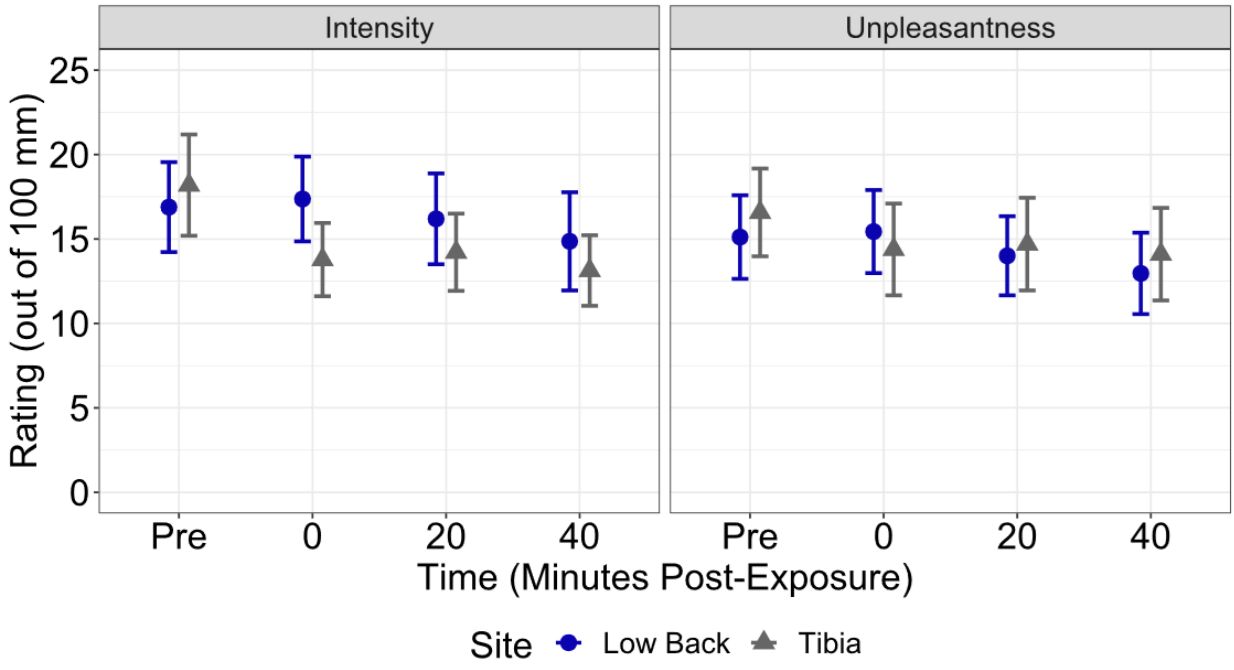

Figure 4-8: Ratings of Intensity and Unpleasantness to Sub-Threshold Stimuli before and after the Repetitive Flexion/Extension Exercise. L3/L4 intervertebral space data are the blue circles; mid-tibial shaft data are the gray triangles. Error bars show ± 1 standard error.

4.4.3 Regressions

Significant predictors of lower back PPTs and perceptions of STSs are listed in Table 4-2 along with the explained variance the significant predictors provide. All measures of pain sensitivity (PPTs, sub-threshold stimulus unpleasantness and intensity) significantly correlated with each other ($p < 0.023$). Additionally, measures taken at the low back significantly correlated with tibial measures for all pain sensitivity measures ($p < 0.001$).

Table 4-2: Outcomes from Multiple Linear Regressions. The Measure column indicates the lower back measure that the regression was predicting. The Predictors column indicates the significant ($p < 0.05$) predictor terms from the regression; interaction terms are denoted as A*B. The marginal and conditional R^2 refer to the explained variance of the significant predictors without and with the inclusion of random effects in the regression respectively. PPT: Pressure-Pain Threshold; MnPF: Mean Power Frequency.

Measure	Predictors	Marginal R^2	Conditional R^2
Pressure-Pain Threshold	• Tibial PPT • Creep*Strength • Creep*MnPF	0.046	0.808
Unpleasantness	• Tibial Unpleasantness • Strength*Tibial Unpleasantness • MnPF*Tibial Unpleasantness	0.370	0.643
Intensity	• Tibial Intensity • MnPF*Tibial Intensity	0.131	0.749

4.5 Discussion

A 10-minute cyclic trunk flexion-extension exercise resulted in a 5% increase in lumbar spine range of motion, a 10-12% decrease in lumbar spine extension moment, and a 5-6% decrease in lumbar erector spinae mean power frequencies. Local PPTs were elevated 10 minutes after the exercise however there was no change in the perception of STSs. Also, all measures related to the lower limb were unaffected by this exercise. Like Chapter 3, lower back pain sensitivity measures could be predicted by their tibial counterparts, and the interactions between creep, tibial measures and fatigue indicators. Contrary to Chapter 3, the incorporation of muscular activity and replacing a sustained load with a cyclic load of the same duration points towards exercise- and fatigue-related changes shaping the pain sensitivity responses beyond the cognitive or mood-related factors more prevalent in the static exposure.

Hypothesis 2a, stating that lower back and lower limb pain sensitivity would decrease immediately after the exercise was rejected. Lower limb pain sensitivity was unaffected by the repetitive flexion-extension exercise while lower back pain sensitivity was only elevated in one of three variables 10 minutes after the exercise was completed, not immediately following. Rejecting this hypothesis likely indicates that exercise-induced hypoalgesia was not the only mechanism responsible for the observed lower back desensitization since changes would be expected at the Post 0 minute time point (Naugle et al., 2014). Hypothesis 2b, stating that the pain sensitivity changes would match those in Chapter 3 at the end of the 40-minute recovery period was accepted since all Post 40 minute measures of pain sensitivity were similar to Pre-Exposure values. While accepting hypothesis 2b seems to indicate that a 40-minute recovery window

is sufficient to alleviate any lasting effects of a 10-minute repetitive trunk flexion exposure, the lower back PPT values being on the cusp of statistical significance at the end of the recovery period (Figure 4-7) and the apparent decrease in STS ratings over time (Figure 4-8) may indicate less stability in these measures over time than the statistical analysis would imply on its own. A longer recovery period may be useful in to develop a more definitive answer than this present work. Hypothesis 2c, stating that neither creep nor fatigue alone could predict changes in pain sensitivity, was accepted. Both measures required an interaction term to be a significant predictor in all three regressions. However, lower limb measures of pain sensitivity were highly influential in predicting low back pain sensitivity, similar to the observation in Chapter 3 regarding the interpersonal variability in these measures.

Our data also suggests a participant-specific component to the exposures. First, the conditional R^2 values were substantially greater than the marginal R^2 values of the regression equation (Table 4-2). Conditional R^2 values allow each participant to have their own intercept, while marginal R^2 values assume all participants have the same intercept. Furthermore, the recurring finding across variables where tibial sensitivity could predict L3/L4 measures also support an individualized response to the repetitive trunk flexion exposure (Figure 4-7). There was a bit of a disconnect between the regression indicating that tibial sensitivity changes could predict L3/L4 differences, despite there being a Time*Site interaction in PPTs. One explanation for this disparity is the scale of PPT changes; both tibial and L3/L4 measures show similar contours of changes over time (lowest initially with increases at 10 and 40 minutes post exposure) however the magnitude of these changes are larger and statistically meaningful in only the L3/L4 measures. Other groups have similarly only been able to determine meaningful relationships between PPTs and occupationally (Hven et al., 2017) or clinically relevant outcomes (Knapstad et al., 2019) after accounting for inter-participant variability in their analyses. Taken together, the exercise-based phenomena of exercise-induced hypoalgesia and facilitation of descending inhibition through central fatigue appear to have manifested as group-wide effects in PPTs (Figure 4-7), while creep effects were perhaps seen through the regression outcomes.

Additionally, any of the above mechanisms could be combined with potentially hyperalgesic effects of creep to produce the time course of pain sensitivity changes. One potential avenue for this change would be through inflammatory pathways, which should generate longer-lasting hyperalgesia to counter the relatively transient hypoalgesic effects related to exercise or muscle fatigue. Although the low frequency of the exercise (0.1 Hz) compared to *in-situ* models of creep (0.25 to 0.5 Hz) (King et al., 2009; Pinski et al., 2010) renders inflammatory responses less prominent in the current work, it may have sufficiently decreased the Post 20 through 40 minute PPTs to be statistically similar to the Pre-Exposure time point. Another potential avenue would be an attention-related decrease in descending inhibition due to the exposure itself, parallel to the mood-related changes discussed in Chapter 3. Participants were required to move every 5 seconds while attending to a metronome, and perform two maximal exertions every 2 minutes, which would require that participants attend to their posture and the external cues guiding the task. Directing attention towards a painful region can produce local hyperalgesic effects (Kóbor et al., 2009) with preferential increases in affective pain over sensory pain (Kenntner-Mabiala et al., 2007). However, there was no increase in the perceived unpleasantness of a sub-threshold stimulus currently, unlike Chapter 3. Independent effects of creep from this repetitive exercise are currently difficult to discern beyond the changes specific to exercise, and a passive vs active paradigm would be more useful in future work looking to elaborate on this question in order to remove confounding effects of exercise and muscle fatigue (Olson, 2014).

The exercise performed was primarily designed to induce creep, however muscle fatigue was an expected by-product. Alterations including extending the duration of the exercise or adding load to the hands could have both increased the magnitude of creep (Bazrgari et al., 2011; Toosizadeh and Nussbaum, 2013) and muscle fatigue (Xia and Frey Law, 2008; Yung et al., 2012). The magnitude of creep seen presently (2.7 ± 1.4°) was similar to other similar protocols using a 6-12 minute repetitive flexion exposure (2.7° (Abboud et al., 2018); ~2° (Voglar et al., 2016); 1.6° - 2.0° (Toosizadeh and Nussbaum, 2013)). However, the recovery from creep was much quicker compared to these authors (> 12 minutes) and the relative recovery of others using alternative methods of creep induction (current: < 50% exposure time; others: 100 – 700% exposure time; Table 2-2 has references). Comparing this study to Chapter 3, disparities in the duration of creep recovery, the pain sensitivity measures affected and the significant predictors in the regression equations further illustrate the point that the type of exposure is pivotal in determining the effects of creep (Little and Khalsa, 2005; Toosizadeh and Nussbaum, 2013).

Some limitations of the study are as follows. While participants had a bar to lean into to limit flexion from non-spine structures, there were no physical constraints on motion from other joints, and some hip flexion coupling would be expected during the exercise (Thomas and Gibson, 2007). As a result, hip extensor creep or fatigue may have influenced pain sensitivity changes, despite the implicit assumption that changes not seen in the lower back could be represented by the lower limb. Also, the inclusion of multiple tests at some time points but not others may have generated bias in those measures. Specifically having maximal spine flexion follow a maximal low back extension contraction may have caused some participants to adopt a less extreme "recovery" posture during the flexion range of motion assessments when those measures overlapped, evidenced in Figure 4-4. However, the intervening time points would not suffer from this limitation, and those measures did not contradict the multi-measure time points in terms of determining when creep recovery occurred. All pain sensitivity measures inherently have some aspect of self-reporting, and tend to be highly variable, partially mitigated by the larger sample size used presently than other studies assessing creep-related changes (Bazrgari et al., 2011; Rogers and Granata, 2006; Shin and Mirka, 2007).

In conclusion, creep generated from repetitive flexion-extension produced a delayed reduction in mechanical pain sensitivity that represents the net effect of exercise-induced hypoalgesia, attentional demands, and altered afferent neural feedback. This change was only manifested in PPTs, not STSs, indicating that these changes are relatively unique to higher magnitude stimuli. The resulting delayed desensitization could make it more difficult for people to identify potentially dangerous internal loads, creating a situation where the risk of low back injuries could be elevated following repetitive trunk flexion.

Chapter 5 – Linking *In-Vivo* Mechanical Sensitivities to Model Development

This chapter's purpose is to consolidate the *in-vivo* findings in Chapter 3 and 4 to components of the model presented in Chapter 7. First, a distribution of pressure-pain thresholds (PPTs) to be used to generate the stochastic portion of the model are produced and fit to a distribution. Second, a discussion on how to incorporate viscoelastic changes is presented to frame the modelling decisions and provide a rationale for the compromises made.

5.1 On Low Back Mechanical Sensitivity Distributions

The first two studies involved four PPT assessments occurring before any mechanical exposure; three of which were averaged together to dictate the sub-threshold stimuli, and the fourth used as the Pre-Exposure measure. These data were taken from all 39 participants across both studies and used to develop a "base" distribution of low back mechanical sensitivity for use in Chapter 7. Data were sorted from smallest to largest to generate empirical cumulative distribution functions which were then fit to Normal, Gumbel, and Gamma distributions ($\Phi(x)$) using a two-stage fitting method. First the Method of Moments was used to derive estimates for distribution parameters (Munkhammar et al., 2017; Wooldridge, 2001), those estimates were then used as initial estimates to Least-Squares fit distributions to the data.

5.1.1 Distribution Functions

The Normal Distribution is a commonly assumed symmetrical distribution with convenient mathematical properties, defined using the cumulative distribution function in Equation 5-1.

$$\Phi_N(x) = \frac{1}{2}\left[1 + \operatorname{erf}\left(\frac{x - \mu_N}{\eta\sqrt{2}}\right)\right] \tag{5-1}$$

Where x is the dependent variable (in this case PPTs), μ_N is a location parameter indicating where the distribution centre lies and η is a scaling parameter dictating the width of the distribution.

The Gumbel distribution is an asymmetric distribution used to represent the occurrence of local maxima, originally developed to predict extreme weather events (Gumbel, 1941). The cumulative distribution function is defined by two parameters: μ_G a location parameter and β a scaling parameter (Equation 5-2)

$$\Phi_G(x) = \exp\left(-\exp\left(\frac{x - \mu_G}{\beta}\right)\right) \tag{5-2}$$

The parameters μ_G and β perform the same roles as μ_N and η do in the Normal distribution, only the Gumbel distribution has a different shape arising from the double-exponentiation.

The Gamma distribution is another asymmetric distribution representing a class of shapes using the gamma family of functions; its cumulative distribution function is defined using Equations 5-3 through 5-5.

$$\Phi_\Gamma(x) = \frac{\gamma\left(k, \frac{x}{\theta}\right)}{\Gamma(k)} \tag{5-3}$$

$$\Gamma(k) = \int_0^\infty t^{k-1} \exp(-k)\, dt \tag{5-4}$$

$$\gamma\left(k, \frac{x}{\theta}\right) = \int_0^{\frac{x}{\theta}} t^{k-1} \exp(-t)\, dt \tag{5-5}$$

In Equation 5-3, the distribution parameters k and θ reflect the distribution's shape and scale respectively; and t is a dummy variable of integration in Equations 5-4 and 5-5. Equation 5-4 is the Gamma Function, and Equation 5-5 is the Lower Incomplete Gamma Function. Unlike the Normal and Gumbel distributions, there is no explicit location parameter, instead the product $k\theta$ dictates the location of the distribution, with the shape converging on the Normal distribution for large values of k.

5.1.2 Method of Moments

The Method of Moments is a technique to estimate distribution parameters using different statistical moments of the population of interest the distribution is intended to represent (Munkhammar et al., 2017; Wooldridge, 2001). The first statistical moment is the estimated population mean, $\bar{x}$, and the second statistical moment is the estimated population variance, s^2. Both terms can be characterized from a variable x with n samples using Equations 5-6 and 5-7.

$$\bar{x} = \frac{1}{n}\sum_{i=1}^{n} x_i \tag{5-6}$$

$$s^2 = \frac{1}{n}\sum_{i=1}^{n} (x_i - \bar{x})^2 \tag{5-7}$$

All three distributions have established formulae relating their distribution parameters to these two statistical moments. For the Normal Distribution:

$$\bar{x} = \mu_N \tag{5-8}$$

$$s^2 = \eta^2 \tag{5-9}$$

For the Gumbel Distribution:

$$\bar{x} = \mu_G + \beta\gamma_{EM} \tag{5-10}$$

$$s^2 = \frac{\pi^2}{6}\beta^2 \tag{5-11}$$

Where γ_{EM} is the Euler-Mascheroni constant ~ 0.5772156649015… and π ~ 3.14159265359…

For the Gamma Distribution:

$$\bar{x} = k\theta \tag{5-12}$$

$$s^2 = k\theta^2 \tag{5-13}$$

After the initial estimates of each of the distribution parameters were determined from the first two moments of the PPTs (Equations 5-6 and 5-7), they were used as initial estimates to fit each of the respective cumulative distribution functions, $\Phi(x)$, to the ordered PPTs using the `curve_fit` function in the `scipy` package in Python. The root-mean-square errors between the fit $\Phi(x)$ functions and the raw data were computed to determine which distribution would be most appropriate to use. Although data fitting and errors were computed with respect to the cumulative distribution functions, the probability distribution functions of all three distributions were also determined by computing $d\Phi/dx$.

5.1.3 Distribution Fitting Results

The distribution coefficients and root-mean-square errors are presented in Table 5-1, with depictions of the cumulative distribution functions and probability distribution functions in Figure 5-1.

Table 5-1: Low Back Pressure-Pain Threshold Distribution Fitting Results.

Distribution	**Coefficients (MPa)**		**Root-Mean-Square Error**
Normal	μ_N: 0.96620	η: 0.32669	0.1360
Gumbel	μ_G: 0.84269	β: 0.28237	0.0421
Gamma	k: 8.63524	θ: 0.11478	0.0573

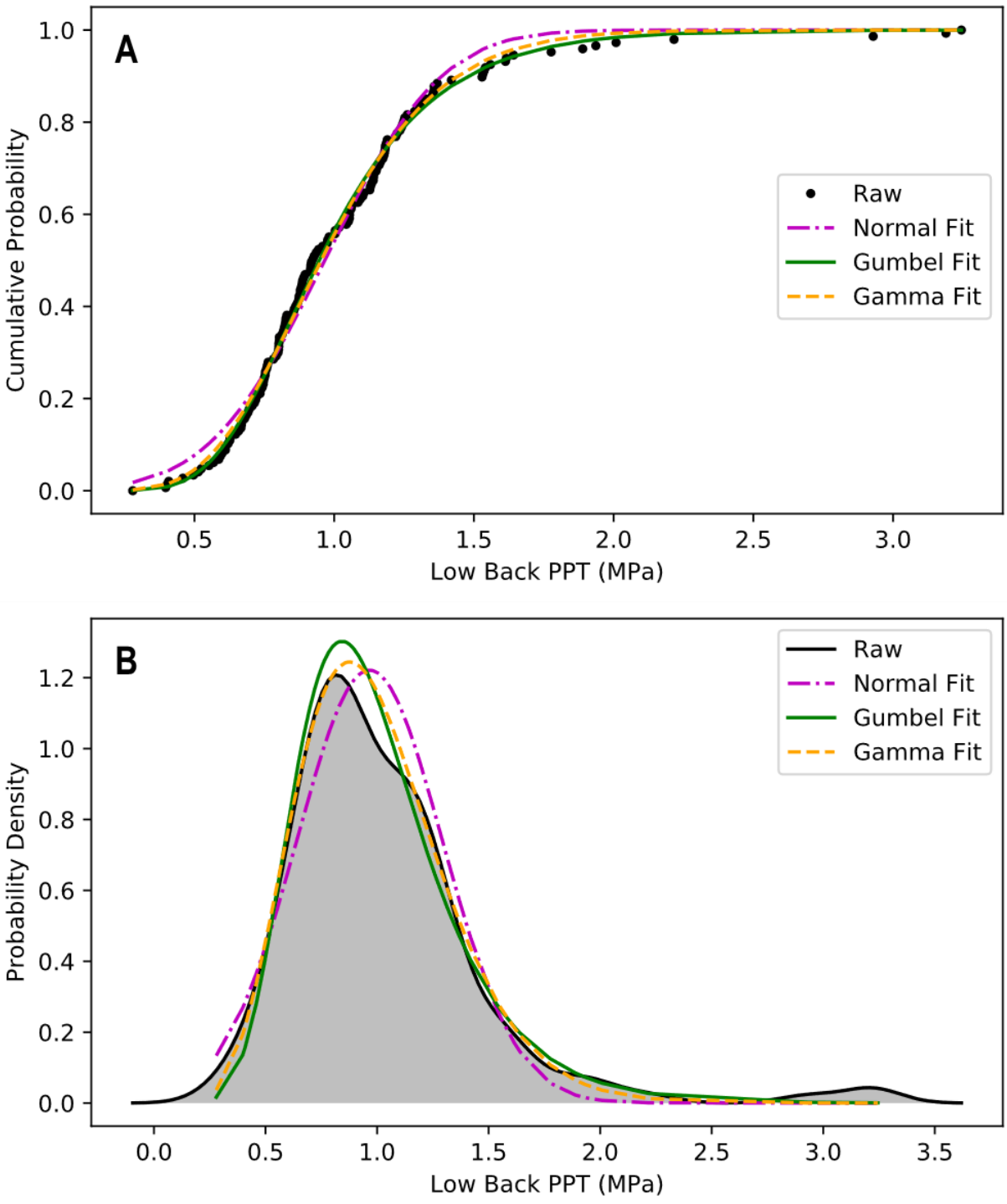

Figure 5-1: Fit Visualizations of a Normal (magenta dot-dash), Gumbel (green solid), and Gamma (orange dash) Distributions to Raw Pressure-Pain Thresholds (black). Fitting was performed on the Cumulative Distribution Functions (Panel A) which were mapped to Probabiltiy Distribution Functions of each distribution (Panel B).

5.1.4 Implementing Pressure-Pain Threshold Distributions

The Normal distribution fit was less accurate than either the Gumbel or Gamma distributions. While the Gumbel and Gamma distributions appeared to fit the PPT data similarly, the Gumbel distribution is much

easier to manipulate. Since the output of $\Phi(x)$ is a percentile relating to a given PPT input, this function needs to be inverted, $\Phi^{-1}(x)$, to predict a PPT associated with a percentile. Deriving this for the Gumbel distribution is straightforward and easy to implement (Equation 5-14).

$$\Phi_G^{-1}(x) = -\beta \ln(-\ln(x)) + \mu_G \tag{5-14}$$

Inverting the Gamma cumulative distribution function is non-trivial due to the improper integrals in its definition; the Gamma distribution was only intended to be used as a last-resort option if the Normal and Gumbel distributions proved inadequate. Since the Gumbel and Gamma distributions fit the data similarly, the PPT generator function will be defined by substituting the coefficients in Table 5-1 into $\Phi_G^{-1}(x)$ (Equation 5-15).

$$PPT(x) = -0.28237 \ln(-\ln(x)) + 0.84269 \tag{5-15}$$

5.2 On Incorporating Viscoelasticity into a Model of Mechanical Nociception

A global objective of this thesis as stated in the Introduction was to predict whether mechanical exposures that involve viscoelastic creep could generate nociceptive neural activity. Accomplishing this objective necessitated a predictive model of nociceptive neural activity that could respond to a mechanical exposure while incorporating the viscoelastic changes that mechanical exposure would also generate. Modelling the effects of viscoelasticity on mechanical low back nociception requires a function to define how viscoelasticity affects mechanical sensitivity, referred to here as $\zeta(t)$. $\zeta(t)$ would interface with a model of nociceptive neural activity that converts tissue loading into neural activity by modifying either the conversion of physical loads into neural activity, or by modifying the neural activity after its conversion. The intention was to use Chapter 3 to derive $\zeta(t)$ and then use Chapter 4 to determine how a moderating factor (exercise) would influence $\zeta(t)$ to improve model external validity. However, Chapter 3 appears to indicate that the necessary viscoelasticity-sensitivity relationship is non-existent: viscoelastic creep did not appear to affect mechanical sensitivity making $\zeta(t) = 0$. Although stimulus unpleasantness was increased immediately following the exposure, this was likely a cortical effect (Villemure and Bushnell, 2009), and not within the scope of nociceptive neural activity in the periphery and spinal cord. The data in Chapter 4 does indicate that viscoelasticity could interact with a well-known exercise-based desensitizing effect (Ellingson et al., 2014; Kodesh and Weissman-Fogel, 2014; Koltyn et al., 2014; Lemley et al., 2015; Naugle et al., 2012), despite not having any real influence on mechanical sensitivity on its own. This raises the question: "What does this mean for a model of mechanical nociception?".

Viscoelastic effects are time-dependent (Fung, 1994; Provenzano et al., 2002), and the physiological changes related to these viscoelastic effects are also time-dependent (Busscher et al., 2011; Claude et al., 2003; D'Ambrosia et al., 2010; Muslim et al., 2013; Rogers and Granata, 2006; Shin and Mirka, 2007; Toosizadeh et al., 2012); both would need to be modelled as functions of time. While Chapter 3 supports an invariant viscoelastic function, Chapter 4 supports a nuanced viscoelasticity interaction with muscle fatigue or exercise, represented with the time-varying function $\phi(t)$. The regression approach in Chapter 4 was intended to lend insight to both the derivation of $\phi(t)$ and determining how it interacted with $\zeta(t)$.

While the regression approach did identify three factors related to low back PPTs: tibial PPTs, the product of creep magnitude and strength, and the product of creep magnitude and mean power frequency; the rest of the data in Table 4-2 are less promising for developing this relationship. First, removing tibial PPTs from that regression decreased the explained variance more dramatically than the removal of both creep-fatigue interaction terms (Table 5-2), showing its relative dominance. Second, even including the tibial PPT left the entire regression able to explain less than 5% of the total variance, and thus only able to represent less than 5% of the distribution needed for the model. The impressive "Conditional R^2" cannot be used for predictive purposes since the amount of explained variance entirely depends on an *a-posteriori* fit where all inputs and outputs are known before the prediction is made. Lastly, muscle fatigue and viscoelastic creep recovered simultaneously, which taken in tandem with no significant non-interaction terms and the lack of effect from Chapter 3, makes the problem of defining $\zeta(t)$ and $\phi(t)$ an indeterminate one. However, $\phi(t)$ does have a basis in the exercise-induced hypoalgesia literature (Ellingson et al., 2014; Kodesh and Weissman-Fogel, 2014; Koltyn et al., 2014; Lemley et al., 2015; Naugle et al., 2012), but the timing does not appear to line up with the time course of changes in Chapter 4. To re-iterate the Chapter 4 Discussion: the exercise-based effects do not appear to have occurred in isolation; the creep effects may have delayed the exercise-induced hypoalgesia mechanism from occurring until after creep recovered. There is some evidence for a creep-fatigue interaction during trunk flexion (Dickey et al., 2003; Sánchez-Zuriaga et al., 2010; Shin et al., 2009), but there are no proposed pathways or specific mechanisms for this interaction to occur: modelling this interaction for predictive purposes would be arbitrary without understanding what other factors are needed to explain more of the variance in mechanical sensitivity. As a result, the information that Chapter 4 provides is insufficient to determine how $\zeta(t)$ should respond or interact with $\phi(t)$ without some additional simplification.

Table 5-2: Contributions to Repetitive Flexion Pressure-Pain Threshold Regression. The predictor variables are listed under Sub-Components, the Marginal R^2 values are computed using a common intercept, the Conditional R^2 values are computed with each participant receiving their own intercept.

Model Sub-Components	Marginal R^2	Conditional R^2
Tibial PPT, Creep*Strength, and Creep*MnPF	0.046	0.808
Tibial PPT	0.045	0.810
Creep*Strength and Creep*MnPF	0.0009	0.835

This raises the practical question: "How can viscoelastic creep be incorporated into a model of mechanical nociception if it is unclear how it affects mechanical pain sensitivity?". Three potential answers to this question are posed here. Each option is posed with the goal of adding some component of Chapters 3 and 4 into a mechanism-driven model of mechanical nociception in low back tissues.

5.2.1 Option 1: Ignore Viscoelastic Effects

The most conservative approach would be to ignore all viscoelastic effects entirely: the term $\zeta(t)$ would not exist. This is the most straightforward to implement but would compromise the scope of the model. In choosing this option, the mechanical desensitization reported in Chapter 4 would be entirely attributed to exercise or muscle fatigue using $\phi(t)$, which while not unplausible (Ellingson et al., 2014; Koltyn et al.,

2014), is a simplification this thesis has already touched on (Section 4.5). This approach would reframe the entire thesis to be more centred on a relationship between muscle fatigue and mechanical nociception. While this relationship is certainly deserving of a thesis, it is one that Chapters 3 and 4 are unsuited to address since the exposures were designed to avoid muscle fatigue as much as feasibly possible, and the assessments prioritized assessing creep over muscle fatigue. This is a possible but poorly realized option and will not be considered further.

5.2.2 Option 2: Combine the Flexion Exposures into a Single Generalized Exposure

This option involves combining data from both Chapters 3 and 4 into a single dataset; effectively ignoring any effects of muscle fatigue and generates a novel relationship for an arbitrary "generalized flexion exposure": Any effects from this exposure would inform $\zeta(t)$; $\phi(t)$ would not exist. To generate this novel exposure, the 37 participants common to both existing exposures had their Static and Repetitive exposure maximal flexion angle, PPT, and sub-threshold stimulus data averaged together. To determine changes within the low back relative to the tibial control site, PPT and sub-threshold stimulus data had the tibial values subtracted from the low back magnitudes. The only remaining independent variable was time, and these amalgamated data were entered into one-way repeated-measure ANOVAs using the same procedures described in Sections 3.3.5 and 4.3.5. Additionally, a regression for this generalized exposure was performed to predict low back sensitivity measures from the level of creep and related tibial measure, again with identical methods to the regressions in Sections 3.3.5 and 4.3.5, only dropping the predictor variables that were not consistent across exposures and thus could not be averaged together.

Generalized Flexion Exposure Results

Maximal flexion angles were significantly affected by Time ($F_{3.83,\ 134.0} = 13.74$, $p < 0.001$) where the Post 0, Post 5, Post 15, Post 25, and Post 35 time points were greater than the Pre-exposure time point (Figure 5-2). The magnitude of angular creep at the Post 0 time point was 3.5 ± 1.9°.

Relative PPTs were unaffected by Time ($F_{2.94,\ 102.90} = 0.563$, $p = 0.728$; Figure 5-3), but relative sub-threshold stimulus intensity ($F_{2.87,\ 97.45} = 3.25$, $p = 0.025$) and unpleasantness ($F_{2.73,\ 92.95} = 4.32$, $p = 0.007$) changed over time. The Post 0 time point had higher ratings than the Pre-exposure time point for both dimensions (Figure 5-4) with no other time points being different from each other.

Multivariate regressions determined that creep magnitude and tibial analogs could weakly predict low back mechanical sensitivity (Table 5-3). First, there were two significant predictors of low back PPTs: tibial PPTs ($\chi^2 = 6.04$, $p = 0.014$) and the interaction between tibial PPTs and creep magnitude ($\chi^2 = 9.37$, $p = 0.002$). Second, there were two significant predictors of low back sub-threshold stimulus intensity: tibial sub-threshold stimulus intensity ($\chi^2 = 8.52$, $p = 0.004$) and creep magnitude ($\chi^2 = 8.84$, $p = 0.003$). Lastly, the only significant predictor of low back sub-threshold stimulus unpleasantness was creep magnitude ($\chi^2 = 8.47$, $p = 0.004$).

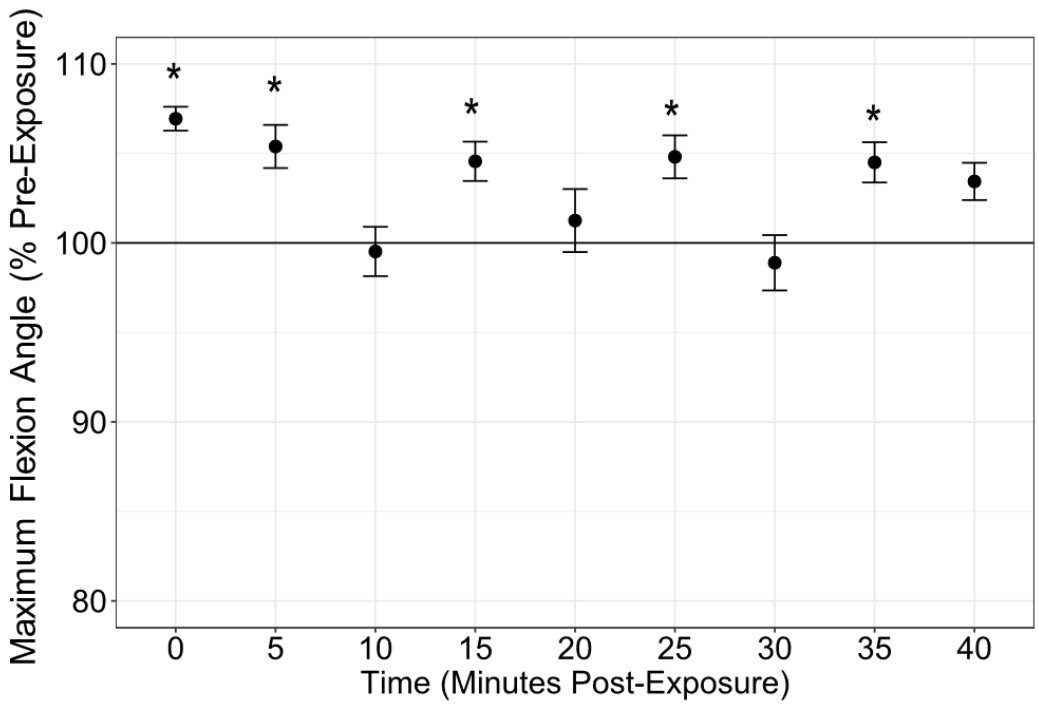

Figure 5-2: Maximal Flexion Angles Following the Generalized Flexion Exposure as a Percentage of the Pre-Exposure Values. Asterisks indicate time points that are significantly different from Pre-Exposure ($p < 0.05$). Data are Mean ± 1 SE.

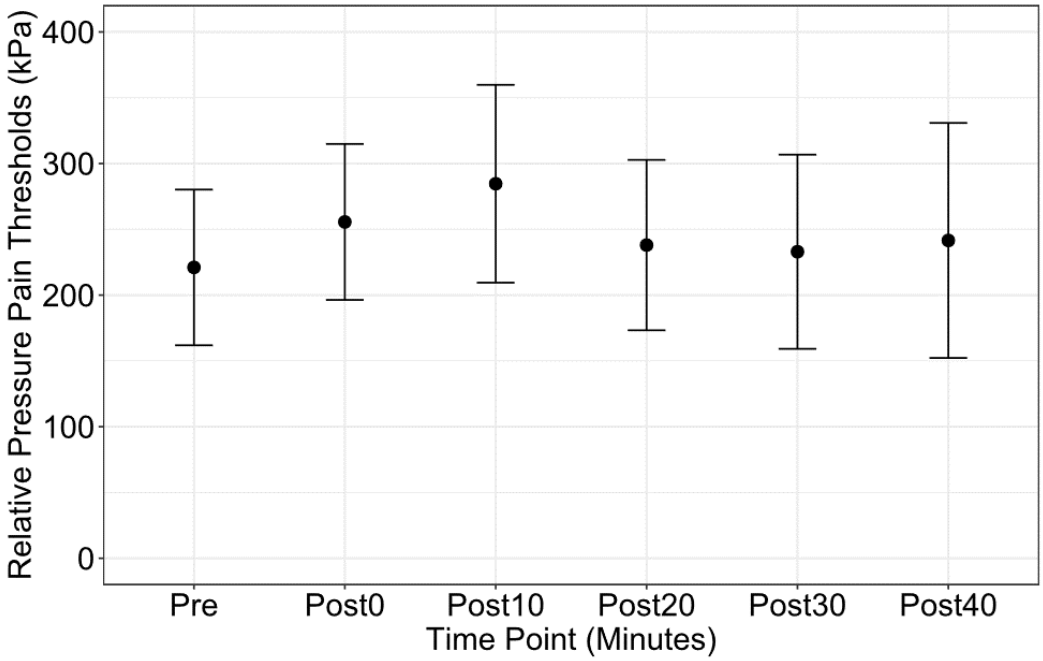

Figure 5-3: The Low Back Pressure-Pain Thresholds Relative to the Tibial Pressure-Pain Thresholds Before and After the Generalized Flexion Exposure. Data consist of the threshold for the low back minus the threshold for the tibia at that given time point and are displayed are Mean ± 1 SE.

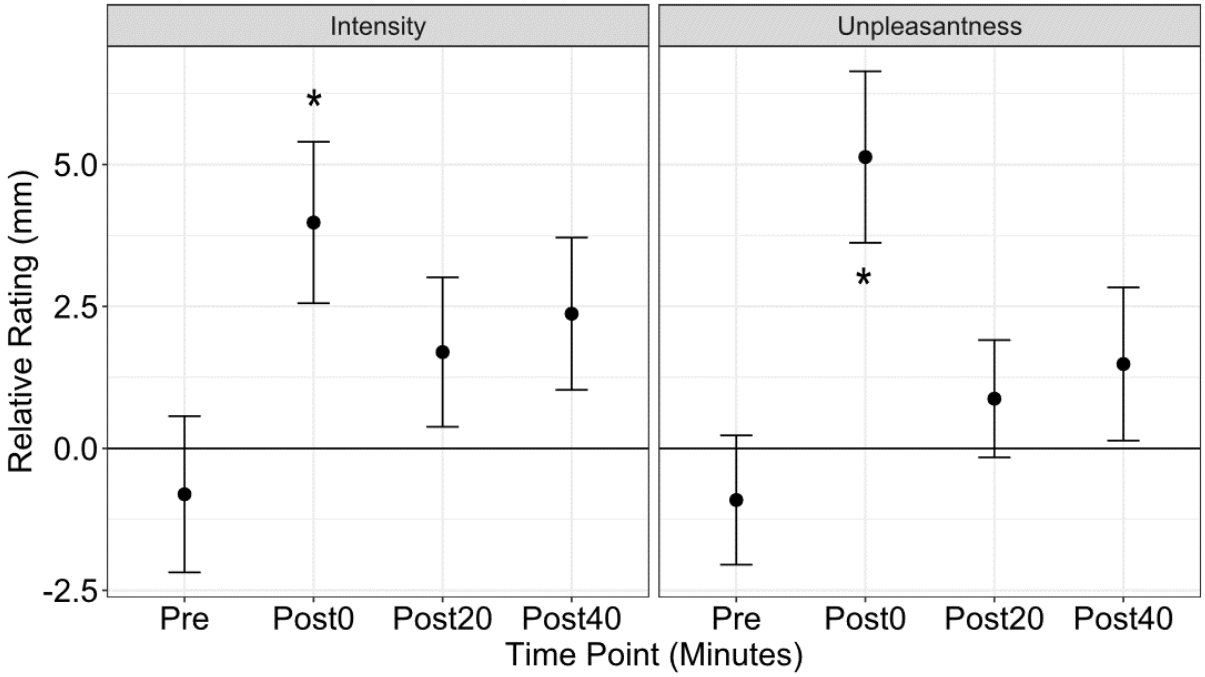

Figure 5-4: Relative Sub-Threshold Stimulus Ratings of Intensity (Left) and Unpleasantness (Right) Before and After the Generalized Flexion Exposure. Data consist of the rating for the low back minus the rating for the tibia at that given time point and are displayed as Mean ± 1 SE.

Table 5-3: Regression Outcomes for the Generalized Flexion Exposure. The predictors in the second column predict the Dependent variable in the low back with the explained variance in the Marginal R^2 column when using a fixed intercept, or with the explained variance in the Conditional R^2 column when letting each participant have its own intercept.

Dependent Variable	Significant Predictors	Marginal R^2	Conditional R^2
Pressure-Pain Threshold	• Tibial PPT • Creep*Tibial PPT	0.045	0.241
STS Intensity	• Creep • Tibial STS Intensity	0.050	0.252
STS Unpleasantness	• Creep	0.105	0.334

Generalized Flexion Exposure Discussion

The generalized flexion exposure would have the following characteristics to be considered for modeling:

- The flexion exposure would generate 3.5 ± 1.9° of creep that persisted for 35 minutes using the criteria in Chapter 3
- PPTs would be unaffected by the exposure, but sub-threshold stimulus intensity and unpleasantness would both be elevated immediately after the exposure before returning to baseline levels within 20 minutes

- Creep magnitude and distal sensitivity analogs would be weak but significant predictors for all three mechanical sensitivity measures.

To implement these findings, the exposure type, and thus muscle fatigue, would be ignored. Instead, the time spent in the flexion exposure, t_{flex}, would be used to generate a temporal constant, τ_{STS}, representing the time before neural activity recovers (Equation 5-16), where $t = 0$ indicates when the flexion exposure started.

$$t_{flex} < \tau_{STS} \leq 3t_{flex} \tag{5-16}$$

The viscoelastic function $\zeta(t)$ would be biphasic consisting of a scaled creep portion and a smoothed step down based on τ_{STS} (Equations 5-17 to 5-19).

$$\zeta(t) = \zeta_0 \, f_{rise}(t) \, f_{fall}(t) \tag{5-17}$$

$$f_{rise}(t) = \exp\left(-\frac{t_{flex}}{(t+1)^{\zeta_1}}\right) \tag{5-18}$$

$$f_{fall}(t) = \frac{1 - \tanh\big(\zeta_2(t - \tau_{STS})\big)}{2} \tag{5-19}$$

Where ζ_0 scales the magnitude of the effect from the time the flexion exposure started to the time the flexion exposure ended at t_{flex}, ζ_1 determines the creep rate, and ζ_2 determines the rate that $\zeta(t)$ returns down to zero centred around τ_{STS} (Figure 5-5). $\zeta(t)$ would activate a viscoelastic-state neuron that would modify ascending information, but not affect the sensitivity of that ascending information to tissue stresses.

The main strength of this approach is that there is an unambiguous description of "creep" to be incorporated into the model. This could be done through a viscoelastic-sensitive neuron that would modify ascending neural information without altering the overall mechanical sensitivity. The time course of these changes is plausible both in terms of recovery time relative to exposure length (Shin and Mirka, 2007; Solomonow et al., 2000) and changes in neural feedback relative to recovery (Howarth et al., 2013b; Shin and Mirka, 2007; Solomonow et al., 2000). However, there are other conflicting works, both concerning the relative creep recovery time (Howarth et al., 2013a; Little and Khalsa, 2005; McGill and Brown, 1992) and window of neural changes (Hendershot et al., 2011; Rogers and Granata, 2006; Solomonow et al., 2003). One main drawback is that the modelled exposure does not exist; these data are a numerical average of two distinct exposures. Another drawback is that the parameters ζ_0, ζ_1, and ζ_2 are essentially meaningless since the sub-threshold stimuli do not translate to nociception. Stimulus perception is more closely related with the experience of pain rather than nociceptive neural activity (Petrini et al., 2015; Villemure and Bushnell, 2009), meaning that the specific values would not be relevant to the data from Chapters 3 and 4 needed to validate the model. There are also separate moderating factors and mechanisms involved to modify mechanical sensitivity with each exposure type that are ignored. One notable example of this is the delayed desensitization unique to the repetitive exposure (Chapter 4), likely related to exercise (Koltyn et al., 2014; Naugle et al., 2014) or muscle fatigue (Taylor et al., 2000), that was washed out by

averaging two exposures together. There is also a novel sub-threshold stimulus intensity increase at the Post 0 time point not present in either exposure that could also be an artifact of the exposure averaging since some evidence of this difference is present in both Figures 3-6 and 4-8. While intensity and unpleasantness perception are believed to be rooted in distinct processing pathways (Ellingson et al., 2014; Lindstedt et al., 2011; Petrini et al., 2015), both rely extensively on cortical inputs and would incur similar implementation concerns.

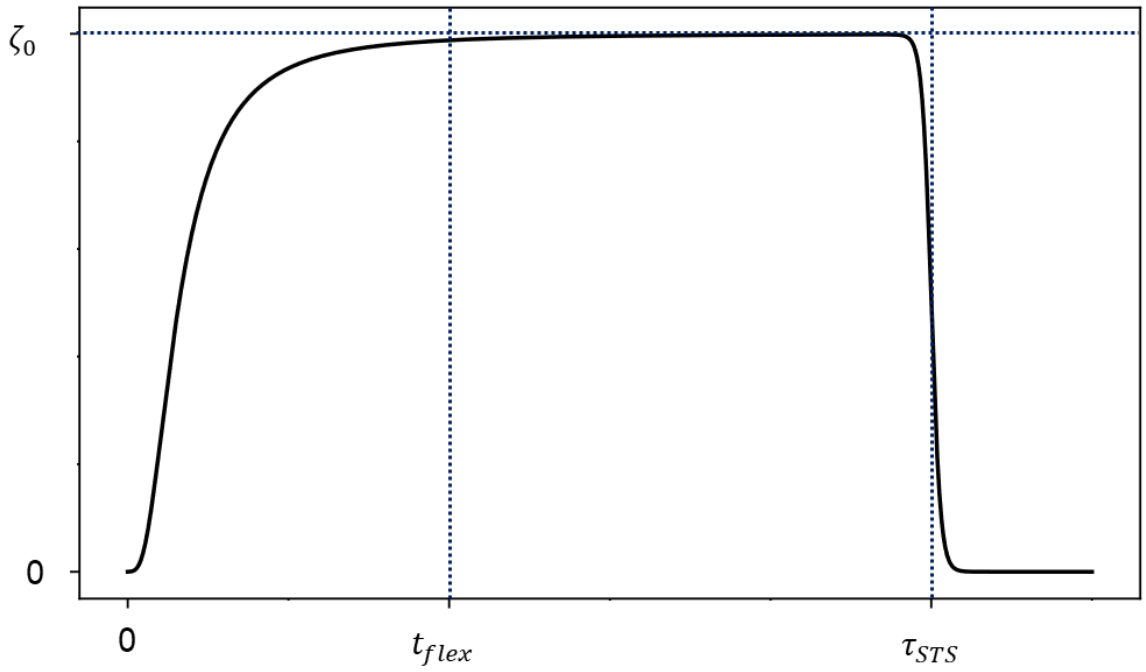

Figure 5-5: A Sample Plot of $\zeta(t)$ based on Equation 5-17. The value of $\zeta(t)$ approaches ζ_0 as $t \to \infty$, but careful selection of ζ_1 allows $\zeta(t) \cong \zeta_0$ at t_{flex}; τ_{STS} indicates the midpoint of the descending function $f_{fall}(t)$.

This option is feasible to implement, though not without substantial drawbacks that hinder the model's external validity.

5.2.3 Option 3: Represent Viscoelasticity as a Discrete State

Many of the problems arise from implementing viscoelasticity as a function of time; one that has been previously adopted (Liu et al., 2015; Toosizadeh and Nussbaum, 2013) and proposed in Equation 5-18 in $f_{rise}(t)$. An alternative to modelling these time changes would be to identify a finite number of states to act as "snapshots" to model. Predictions would not be concerned with how mechanical sensitivity evolved over time in response to a viscoelastic exposure but would rather predict short-term behaviour in pre-determined states. The model would make predictions in four extreme scenarios:

1. No viscoelastic or fatigue-related changes present (Pre-Exposure Chapters 3 and 4)
2. Only viscoelastic changes present (Chapter 3)
3. Only muscle fatigue present (External References)
4. Both viscoelastic changes and muscle fatigue present (Chapter 4)

This option would be implemented by making $\zeta(t)$ and $\phi(t)$ constants over a much shorter time frame (~10 seconds) instead of the longer timescales needed for Equation 5-17 (~1 hour). $\zeta(t)$ would

function as an activation constant for a viscoelastic-sensitive neuron, one whose net effect would be to modify the fatigue neuron's activity, which would be activated by $\phi(t)$.

One advantage of this approach is the ability to short-circuit the arbitrary creep-fatigue interaction: by ignoring how the viscoelasticity and fatigue interact over time to generate a delayed desensitization, the extreme case of the interaction could be represented in isolation. Similar snapshots could be taken to assess viscoelastic creep in isolation based on Chapter 3, and to assess muscle fatigue in isolation using prior data on exercise-induced hypoalgesia (Koltyn et al., 2014; Lemley et al., 2015; Naugle et al., 2012). An additional advantage of using this state-representation is the ability to save computation time. The timescale for viscoelastic- and fatigue-related changes is in minutes, while the neurological simulations need to occur at the sub-millisecond level. By ignoring the time taken to enter each state, simulations could focus on the smaller timescale needed to model neuron-neuron interactions without needing an excessive number of frames to track the relatively slow changes related to creep or exercise. The major disadvantage to this approach would be that the model's scope is dramatically reduced to predicting a limited number of predetermined scenarios. While less versatile, the reduction in scope permits a more robust model within simulated states. Additionally, the dichotomization does accommodate real-world exposures, including those from Chapters 3 and 4; an advantage over the generalized exposure generated for Option 2. The benefits offered by this simplification warrants its consideration moving forward.

5.2.4 Moving Forward?

The two feasible choices involve a) simplifying the data in Chapters 3 and 4 into a single dataset with unambiguous parameters or b) reducing the model scope to focus on extreme cases without concern for how they were achieved. The generalized flexion exposure (a) is an attractive option since it allows a holistic model to combine mechanical and neurological timescales in a continuous workflow. While representing four states (b) improves the model's external validity but limits the exposure features to a predetermined list. Referring to the introduction, the purpose of including a nociceptive model incorporating viscoelastic creep in this thesis was to provide an estimate for whether mechanical exposures involving trunk flexion can elicit nociceptive activity in certain tissues, and if that activity was influenced by viscoelastic changes that occur simultaneously during those exposures. This purpose seems better suited towards Option 3 (choice b). Option 2's (choice a's) benefits are more "nice-to-have" features, but unnecessary for predictive purposes. Pursuing Option 2 for the sake of a holistic model seems ill-advised without i) having a specific exposure linked to a dataset tracking viscoelastic and sensitivity changes and ii) additional data to meaningfully parametrize $\zeta(t)$ in terms of nociceptive neural activity. Option 3's benefits are more directly related to the scenarios where viscoelastic changes would occur, and although it takes shortcuts to reach them, those shortcuts will allow the model to focus on simulating relevant states that have data to support them.

Chapter 6 - Nociceptive Innervation of Passive Collagenous Structures in the Lumbar Spine

6.1 Introduction

The passive tissues of the low back include facet joint capsules, the intervertebral disc, ligaments, tendons, subcutaneous tissue, and skin; all of which contain nociceptive afferent neurons that respond to mechanical disruption (Bogduk et al., 1981; Higuchi and Sato, 2002; Hirsch et al., 1963). While analyses of tissue loads can predict injury across tissue types (ligament, intervertebral disc, skin etc.) (Gedalia et al., 1999; Gooyers et al., 2015; Howarth and Callaghan, 2012), pain can occur at sub-failure loads in healthy (Arendt-Nielsen et al., 2011), inflamed (Kidd and Urban, 2001; Zhang and An, 2007), or otherwise sensitized states (Latremoliere and Woolf, 2009). In healthy tissues, the relative neural density and activation thresholds will influence that tissue's sensitivity to stimuli, noxious or otherwise (Julius and Basbaum, 2001). Variability in innervation densities and neural diversity can arise as a result of tissue type (Biedert et al., 2000), region of a given tissue (Kiter et al., 2010), location of a tissue within the body (Frahm et al., 2013; Kawakami et al., 2001), genetic factors (Koskinen et al., 2005; Liu et al., 2014), and medical history (Ikeuchi et al., 2012; Wetzel et al., 2017). The receptors on the sensory nerves innervating a tissue will also influence how sensitive tissues are to a stimulus intensity (Chen et al., 2006; Slugg et al., 2000), and their sensitivity across stimulus modalities (Brain, 2011; Chen et al., 2002). This variability makes it difficult to predict which structures are likely to be perceived as painful when there are multiple load-bearing tissues. Determining the nociceptive neuronal features and characteristics within the different passive tissues of the low back will provide greater understanding and allow for more quantitative analysis regarding the onset and persistence of low back pain.

There are two common approaches to quantify the stimuli a neuron responds to: electrophysiological (Namer et al., 2015; Schmidt et al., 1995) and histological (Kiter et al., 2010; Liu et al., 2014). Electrophysiological methods involve stimulating the receptive field of a given neuron while recording action potentials propagating along that neuron to determine characteristics about the types of stimuli that neuron encodes. While common in animal models because of the direct input-output quantification (Barrot, 2012; Mogil et al., 2010), its use in humans is infrequent and confined to nerves of the distal limbs due to the invasiveness of the procedures (Langley et al., 2008). This approach also limits the number of neurons that are characterized, which prevents accurate innervation density calculations and increases the likelihood of obtaining a non-representative sample of neurons. Histological approaches involve molecular markers that bind to a specific protein of a neuron that can be visualized in response to fluorescence or chemiluminescence (Lichtman and Conchello, 2005; Mahmood and Yang, 2012); that neuron's responsiveness is inferred from the markers bound to it instead of being directly measured. Although histology must be performed on excised tissue samples and does not allow receptor field characterization, these techniques are better suited to determining the neuronal population characteristics, such as innervation density (Koskinen et al., 2005; Liu et al., 2014; Saxler et al., 2008). Histology techniques are also viable on humans since cadaveric tissues can be used with these methods (Kiter et al., 2010). Western Blotting, a robust, semi-quantitative histological approach affording high sensitivity was used to determine relative concentrations of the neuronal proteins of interest to acquire human data (Mahmood and Yang, 2012).

6.1.1 Nociceptive Neuron Diversity

Histology methods have previously characterized the variety of neurons that innervate passive tissues, with the dermal and epidermal skin layers in rats being those most frequently studied. The receptors and neuronal markers that are relevant for nociception are discussed with respect to five major categories.

First, nociceptive neurons can vary in terms of their size; often quantified as axonal fibre diameter. Nociceptive neurons have smaller diameters (Aδ and C fibre classes) relative to other sensory afferent neurons (Aβ fibre) (Julius and Basbaum, 2001); however, some larger diameter Aβ fibres may function as nociceptors in pathological states such as chronic inflammation (Arcourt et al., 2017; Zhang and An, 2007). The different sizes of nociceptors are believed to transmit different sensations: the (relatively) larger myelinated Aδ fibres are believed to conduct a fast, sharper "first pain" while the smaller unmyelinated C fibres transmit a slower "second pain" that is both slower to build in intensity and longer lasting (Beissner et al., 2010; Julius and Basbaum, 2001). Stimuli that evoke responses from Aδ fibres are often described as "pricking" or "sharp", while stimuli evoking C fibre responses are described as "dull" or "pressing" (Beissner et al., 2010); however the language used to describe pain is beyond the scope of this work (Duncan, 2017). These two distinct sensations of pain are based on larger-diameter neurons having a faster conduction velocity (Cragg and Thomas, 1961; Hursh, 1939) facilitating shorter refractory periods and high firing frequencies (Garell et al., 1996). Aδ fibres are better able to discriminate the intensity of a noxious stimulus than C fibres and have more regular stimulus-response firing characteristics (Garell et al., 1996; Slugg et al., 2000) while also tending to have higher mechanical activation thresholds (Chen et al., 2006; Handwerker et al., 1987). The sparser distribution and larger receptive fields of C fiber branches also renders stimuli as harder to localize relative to Aδ fibres (Dubin and Patapoutian, 2010). The pressure-pain threshold methods employed in Chapters 3 and 4 using blunt pressure are believed to preferentially activate C fibres over Aδ fibres (Beissner et al., 2010; Treede et al., 2002). Additionally, C fibres are believed to play a more prominent role in both peripheral and central sensitization than Aδ fibres (Latremoliere and Woolf, 2009; Woolf and Salter, 2000). Although neuron size is an established parameter with regards to neuron function (Henneman et al., 1965; Hursh, 1939), much of the focus on understanding nociception and pain has focused on the unmyelinated C fibres in the periphery (Basbaum et al., 2009; Braz et al., 2014; Britton and Skevington, 1996; Loeser and Melzack, 1999).

Second, nociceptive neurons can be classified as being peptidergic or non-peptidergic. Peptidergic neurons contain short polypeptides that function as accessory neurotransmitters called neuropeptides (Ackermann et al., 2005; Basbaum et al., 2009; Kashiba et al., 2001). These two broad classes of neurons overlap in terms of size and pain modality, however non-peptidergic have slightly shorter action potential durations and higher action potential thresholds than peptidergic neurons when controlling for neuron size (Stucky and Lewin, 1999). This difference in electrical activation appears to arise from a specific voltage gated sodium channel (Na_V 1.8) that inactivates more slowly in non-peptidergic neurons (Choi et al., 2007). Peptidergic and non-peptidergic primary afferent neurons synapse in different regions of the spinal cord (Fang et al., 2006), further suggesting different functional roles in addition to different electrophysiological characteristics. Neuropeptides have a slow rate of reuptake relative to neurotransmitters, making these additional signals from peptidergic neurons longer lasting (Basbaum et al., 2009) and more susceptible to sensitization through temporal summation (Woolf and Salter, 2000). This temporal summation-based sensitization process involves prolonged peptidergic activity unblocking NMDA receptors on projection neurons in the spinal cord that can dramatically increase the excitability of these secondary nociceptive neurons (Britton, 1996; Latremoliere and Woolf, 2009). In contrast, non-peptidergic neurons are involved

in inflammation-based sensitization pathways which may involve protein kinase C ε signaling in the spinal cord (Joseph and Levine, 2010) or increased glutamate transporter activity in the thalamus (Weisshaar et al., 2017). Both classes of neurons can be identified with different immunoreactive antigens: Calcitonin Gene-Related Peptide (CGRP) is a neuropeptide, and is therefore selective to peptidergic neurons (Corey et al., 2011; Tesarz et al., 2011) with Isolectin-B_4 (IB_4) often used to identify non-peptidergic neurons (Stucky and Lewin, 1999; Vydyanathan et al., 2005; Weisshaar et al., 2017), with both widely present in the dorsal root ganglion. The ability of IB_4 to identify non-peptidergic neurons appears to be limited to primary afferent neurons; up to 40% of all projection neurons that are immunoreactive to IB_4 also contain neuropeptides in rat spinal cords (Fang et al., 2006; Kashiba et al., 2001). Although there are other neuropeptides that are targeted for characterizing peptidergic nociceptive neurons such as substance P or tropomyosin receptor kinase A (Kallakuri et al., 1998; Kashiba et al., 2001; Tesarz et al., 2011), IB_4 is the sole selective target used to label non-peptidergic neurons despite its common co-expression with the purinergic $P2X_3$ receptors (Saeed and Ribeiro-da-Silva, 2012). It is not known how the proportion of peptidergic and non-peptidergic neurons varies between different passive tissues of the spine.

Third, some neurons (nociceptive and non-nociceptive) can respond to inflammation. Inflammation can cause normally innocuous stimuli to feel painful, achieved in part by inflammatory molecules altering the sensitivity of pathways within the neuron to sodium (Gould et al., 2004; Joshi et al., 2006) and calcium ion channel activity (Murakami et al., 2002; Sluka, 1998). Sodium channel production is increased in an inflamed state (Gould et al., 2004), and calcium channels will trigger a greater release of neurotransmitter for a given history of action potentials following inflammation (Kidd and Urban, 2001). In addition to increasing the activity of existing nociceptors, inflammatory molecules may also directly activate previously sensitized nociceptors (Rukwied et al., 2013), change primary afferent neurons from inhibiting to exciting projection nociceptive neurons in the spinal cord (Zhang and An, 2007), or cause previously inactive nociceptors to respond to thermal or mechanical stimuli (Namer et al., 2015). The inflammation response associated with tissue damage begins with the release of K^+ and H^+ ions, histamine, bradykinin, nitric oxide, and ATP from the damaged cells (Kidd and Urban, 2001). These initial molecules signal the production of pro-inflammatory cytokines (including tumour necrosis factor α, nerve growth factor, and interleukins 1β, 6, 8, and 10) and prostaglandins, which interact with local tissues to induce swelling, increase blood flow through vasodilation, and sensitize the area to pain through the mechanisms outlined above (Medzhitov, 2008; Zhang and An, 2007). Of the many factors involved with inflammation, activity of the bradykinin B1 receptor (B1R) has specifically been associated with mechanical hyperalgesia in skin and muscle following mechanical disruptions (Santos et al., 2017; Schuelert et al., 2015). The signaling cascade initiated by activating this receptor results in white blood cell migration to the receptor location and the production of prostaglandins through cyclooxygenases to mediate other pro-inflammatory changes (Santos et al., 2017). B1R can also be inhibited by the sympathetic nervous system (Poole et al., 1999), which may also be responsible for decreased sensitivity to pain arising from sympathetic activity (Julius and Basbaum, 2001). Prostaglandins and other cytokines have also been shown to be elevated following repetitive tensile loading in posterior lumbar ligaments where higher magnitude and frequencies of loading caused greater increases in inflammatory activity (D'Ambrosia et al., 2010; King et al., 2009; Pinski et al., 2010). The presence of an inflammatory mediator such as B1R would be a useful distinction in determining which tissues might have altered pain sensitivity following mechanical exposures. As alluded to above, inflammatory responses to pain may be preferential to non-peptidergic nociceptors (Joseph and Levine, 2010; Weisshaar et al., 2017), but there are no direct comparisons in the literature to date.

Fourth, there are certain strains of voltage-gated sodium (Na_V) channels that are unique to nociceptors: Na_V 1.7, 1.8, 1.9, and potentially Na_V 1.1. Na_V 1.7 and 1.8 both line the axon of the nociceptor and transmit action potentials, Na_V 1.9 aids in determining the nociceptor's resting membrane potential and excitability (Bagal et al., 2014). These different functions have been determined through gain-of-function and loss-of-function mutations to the genes encoding these membrane proteins: SCN9A (Na_V 1.7), SCN10A (Na_V 1.8), and SCN11A (Na_V 1.9) (Bagal et al., 2014). Gain-of-function mutations to both SCN9A and SCN10A increase sensitivity to pain, while gain-of-function mutations to SCN11A may reduce (Huang et al., 2017) or enhance sensitivity to pain (Huang et al., 2014) dependent on the specific mutation. While a removal SCN9A from sensory neurons results in a partial insensitivity to pain (Staud et al., 2011), removing SCN9A from both sensory and sympathetic neurons results in a complete insensitivity to pain (Minett et al., 2012). Na_V 1.7 specifically has been shown to produce a current that activates and inactivates quickly with a long refractory period suited to lower frequency firing (Dib-Hajj et al., 2013). Na_V 1.7 is also more selective for, but not exclusive to C nociceptors (Cummins et al., 2007). The inactivation rates and activation thresholds of Na_V 1.8 depend on the presence of IB_4, with faster inactivation and lower activation thresholds in IB_4-negative neurons (Choi et al., 2007). Na_V 1.7 is also implicated as being specific to mechanical pain sensations in a rat model (Minett et al., 2012), however this finding has not been replicated across rodent species (Cai et al., 2016; Hockley et al., 2017) or humans (Staud et al., 2011). Recent work has uncovered an antagonist derived from a spider (*Heteroscodra maculata*) toxin can selectively inhibit only the Na_V 1.1 channels on Aδ nociceptors responsible for sensing acute mechanical pain (Osteen et al., 2016). Very little is known about these Aδ nociceptors, however their apparent modality-specificity is noteworthy. The contralateral effects of the selective inhibition of these fibres suggests a central, more modulatory role rather than a peripheral, transmission-related role regarding mechanical pain (Pitcher and Henry, 2004). However the Na_V 1.1 channels themselves are located within the periphery, which is distinct from the other commonly studied Na_V channels located in the dorsal root ganglion (Bagal et al., 2014), and peripheral inhibition supports these Aδ fibres as being transmitters instead of modulators of mechanical pain (Osteen et al., 2016). It is also not clear if the isolated toxin affects all Na_V 1.1 channels, or just those specific to Aδ mechanical nociceptors due to the large heterogeneity within classes of a given Na_V channel (Bagal et al., 2014; Choi et al., 2007; Cummins et al., 2007).

Fifth and lastly, although its utility has been questioned (Handwerker, 2010), nociceptors may be discriminated based on the modality of stimuli they sense: mechanical, heat, chemical, cold, or a combination (termed polymodal (Bessou and Perl, 1969)). Unlike other sensory neurons, nociceptors do not have specialized receptor endings—they are described as having "free nerve endings" in that their axon terminates in the target tissue (Biedert et al., 2000; Mense and Hoheisel, 2016; Yahia et al., 1988). The modality of noxious stimulus a nociceptor detects is mainly based on the membrane protein channels embedded within the peripheral ends of that nociceptor (Dubin and Patapoutian, 2010; Toda et al., 2004). One exception to this observation has been found in rats related specifically to hair-pulling where the nociceptor ending has been shown to wrap around the hair cell (Ghitani et al., 2017). There is great redundancy in that there is not a single channel, nor single family of channels that is responsible for detecting a specific modality of pain; however, some specific channels have been studied in detail. Acid-sensing ion channel 3 (ASIC3; there are 6 in total: 1a, 1b, 2a, 2b, 3, and 4), is involved in detecting noxious mechanical stimuli (Borzan et al., 2010; Osmakov et al., 2014). As its name suggests, ASIC3 detects high concentrations of H^+ ions (Gregory et al., 2016; Price et al., 2001), however ASIC3s are found in high concentrations on the specialized endings of non-nociceptive mechanical sensory neurons including Meissner corpuscles and Merkel discs (Price et al., 2001). The receptor itself consists of a large extracellular

"hand" region that is mechanically linked to the ion channel embedded in the axonal membrane, and deflection of this extracellular hand region opens the ion channel (Osmakov et al., 2014). The absence of a structural membrane protein called stomatin-like protein 3 decouples the ASIC3 hand from the ion channel, preventing this channel from responding to mechanical stimuli (Qi et al., 2015; Wetzel et al., 2017). Removal or inactivation of ASIC3 impairs but does not prevent mechanical sensation, noxious or otherwise (Bianchi and Driscoll, 2002; Chen et al., 2002; Geffeney and Goodman, 2012). Transient receptor potential vanilloid 1 receptors (TRPV1) are responsive primarily to noxious heat (Cordero-Erausquin et al., 2016; Dubin and Patapoutian, 2010), but repeated activation of these channels can cause mechanical allodynia (light touch perceived as painful) (Wang, 2008). The mechanical allodynia can be induced either through inflammation (Ahern et al., 2005; Brain, 2011) or by capsaicin (Caterina et al., 1997; Cordero-Erausquin et al., 2016; Wang, 2008). Removal of the TRPV1 receptor severely attenuates thermal pain but does not affect mechanical pain in rodents (Caterina et al., 2000), suggesting that the mechanical allodynia induced by TRPV1 is induced through circuits within the central nervous system. Polymodal nociceptors are thought to have a combination of modality-specific channels (Braz et al., 2014), although some recent modelling approaches have determined that it is feasible that many thermal receptors are simply mechanical receptors with higher thermal expansion coefficients (Liu et al., 2015; Xu et al., 2008b, 2008a). This may explain the high incidence of thermal-mechanical polymodality among nociceptors (Bessou and Perl, 1969; Lawson et al., 2008; Toda et al., 2004).

The variety of receptors and other molecules within nociceptive neurons creates a functionally diverse population of primary afferent neurons that contribute to the perception of pain. Documenting this functional diversity will allow for systems-level approaches to understanding nociceptive transmission to investigate new perspectives and studies relating stimulus properties to the perception of pain (Brodal, 2017). Comparisons across tissue types within a subject are also lacking and may be useful in guiding pain-related treatments or interventions.

6.2 Purpose and Hypotheses

The purpose of this study was to document the diversity in nociception-relevant innervation in human passive tissues in the low back, specifically the interspinous and supraspinous ligament complex, the annulus fibrosus from a lumbar intervertebral disc, and the skin over the low back. It was hypothesized that:

3a) Skin tissue will have the highest innervation density; annulus and ligament tissue will have similar innervation densities.

3b) The proportion of each antigen relative to the total innervation will be similar across tissue types.

6.3 Methods

This study determined the relative concentration of four neuronal membrane proteins within samples of human cadaveric passive tissues using Western Blotting. Skin, annulus, and ligament samples from five donors were labelled for four different proteins with protein concentrations expressed relative to the concentrations found in skin.

Capitalized chemical, antibody, and other solution details/suppliers are provided in Appendix D.

6.3.1 Tissue Samples

Four fresh-frozen human cadaveric donors (1 Male, 3 Female; Ages 67 – 100) were acquired from the University of Waterloo School of Anatomy between January and March 2020 (Table E-1, Appendix E). Cadavers were sectioned while still frozen from the lower-thoracic region (estimated T11) to the mid femoral shaft using a reciprocating saw. This lower trunk section was thawed over the course of 72 hours in a 4°C fridge. Upon thawing, the abdominal viscera and anterior musculature were dissected away from the lumbar spine, leaving the posterior skin, subcutaneous tissue, posterior lumbodorsal fascia, paraspinal musculature, and vertebral column intact. The iliolumbar and sacroiliac joints were sawed through, and this posterior lumbar spine section was frozen at -20°C until the mechanical testing occurred as described in Appendix E (for the purposes of Chapter 7) at which point samples were thawed for a second time. After this second thawing but before mechanical testing, skin samples were removed and re-frozen at -20°C; the outer third of the posterior annulus fibrosus (AF) and supraspinous-Interspinous ligament complex (SILC) from the tested levels were isolated and refrozen after completing mechanical testing. Isolated samples from all three tissues were further dissected on ice to remove excess blood and subcutaneous tissue to obtain the samples described in Table 6-1 before starting the Western Blotting protocol.

Table 6-1: Characteristics of Tissue Samples Extracted from Donors

Sample	Location	Physical Characteristics of Harvested Sample
Supraspinous - Interspinous Ligament Complex	L3/L4	Whole ligament excluding bony attachments
Lumbar Annulus Fibrosus	Posterior aspect of the L3/L4 intervertebral disc	Full width and height of outer third of annulus, 5-10 linear mm between facet joints on posterior aspect
Skin	Over the midline between the L3 and L4 spinous processes	Full thickness of dermis including residual subdermal tissue, 2 cm^2 rectangular area

6.3.2 Western Blotting

The Western Blot involved taking the cleaned and isolated samples on ice through an eight-stage process: Homogenization, Bicinchoninic Acid (BCA) Assay, Sample Preparation, Gel Preparation, Antibody Preparation, Western Blot Protocol, Chemiluminescence, and Ponceau Visualization. This process occurred over the course of four days. All three tissue types were treated identically, unless otherwise specified samples were placed on ice in between steps.

Days 1 and 2 – Homogenization, BCA Assay, Sample, Gel and Antibody Preparation

Homogenization involved cutting the isolated tissue into 250 – 500 mg sections with a straight razor while still on ice. Cut tissues soaked overnight in 200 µL Muscle Lysis Buffer and 20 µL of Protease Inhibitor in a 4°C fridge. On Day 2, an additional 400µL of Muscle Lysis Buffer was added before undergoing three 30-second sonication bursts of 100 W separated by 10 minutes of rest to destroy cell membranes (Vibracell VC600, Soncis & Materials Inc. Danbury, CT, USA). Sonicated tissues were homogenized in a glass-glass

mortar and pestle for 3 – 5 minutes with an additional 380 µL of Muscle Lysis Buffer added into the glass mortar, for a total liquid content of 1 mL. Homogenized tissues were centrifuged at 1000 rpm at 4°C (Model 5804, Eppendorf Canada Ltd, Mississauga, ON, Canada) for 5 minutes before the supernatant was extracted.

The BCA assay started by diluting 50 µL the supernatant 1:10 in distilled water. 10 µL of diluted samples were loaded into a 96-well plate along with 10 µL of six evenly spaced calibration concentrations of Bovine Serum Albumin (BSA) (0.0 µg/µL to 1.0 µg/µL); both the calibration and samples were loaded in triplicate. BCA stock solutions were mixed and 200 µL of the mixed BCA solution were loaded into each well. Wells were covered with paraffin wax and incubated at 37°C for 30 minutes (Incubating Mini Shaker, VWR International, Mississauga, ON, Canada). Incubated samples had their absorption spectra quantified (Cytation 5, BioTek Instruments Inc. Winooski VT, USA) to estimate the sample's protein concentration in µg/µL.

Samples were then prepared for Western Blotting to have a total protein concentration of 1 µg/µL. For a total prepared sample volume of v µL (thus containing a total of v µg of protein) and a sample protein concentration of c, Equations 6-1 through 6-3 were used to determine the volumes of supernatant, v_s, Sample Buffer, v_B, and Muscle Lysis Buffer, v_M, to be mixed for each prepared sample.

$$v_s = \frac{v}{c} \tag{6-1}$$

$$v_B = 0.25v \tag{6-2}$$

$$v_M = v - (v_s + v_B) \tag{6-3}$$

Prepared samples and unused supernatant were stored at -80°C until needed.

Twelve percent acrylamide gels consisting of a denser Running Gel below a Stacking Gel were prepared in 4-gel batches. After assembling a glass-plate sandwich, 12.6 mL of distilled water was combined with 9 mL of a 4x Running Gel Stock and 14.4 mL of 30% Acrylamide and then degassed for 5 minutes at room temperature to make the Running Gel solution. 150 µL of 1:10 Ammonium Persulfate and 15 µL of TEMED were mixed into the de-gassed Running Gel before being transferred into the glass sandwiches, filling each sandwich to approximately 80% of capacity. The top of the Running Gel was lined with distilled water and let to sit for 30 minutes at room temperature. The Stacking Gel consisted of 9.2 mL distilled water mixed with 3.8 mL of 4x Stacking Gel Stock and 2 mL of 30% Acrylamide, which were combined and de-gassed for 5 minutes at room temperature. The de-gassed Stacking Gel was mixed with 76 µL of 1:10 Ammonium Persulfate and 15µL of TEMED before applying the Stacking Gel on top of the settled Running Gel in the glass sandwiches. 15-channel well combs were carefully inserted into the freshly applied Stacking Gel to minimize air bubble formation and let to rest for at least 30 minutes at room temperature. Finished gels were wrapped in a wet cloth and stored in a sealed plastic bag in a 4°C fridge for no more than a week until needed.

Primary antibodies were diluted 1:1000 in a mixture of 250 mg BSA and 10 mL of Tris Buffer Solution with Tween (TBS-T) and stored at -20°C until needed. Secondary antibodies were prepared in an identical BSA-TBS-T solution at a dilution of 1:2000 (PGP9.5, CGRP, B1R) or 1:10,000 (ASIC3). Primary

antibodies were prepared well in advance and re-frozen after use, discarded after the fifth use. Secondary antibodies were prepared on the day they were used (Day 4) and discarded after use.

Table 6-2: Antibodies for Immunofluorescence. All primary antibodies will be reactive to humans, the secondary antibody column indicates the host animal of the primary antibody.

Primary Antibody	Target Function
Protein Gene Product 9.5 (PGP9.5)	Membrane protein common to all neurons (Ikeuchi et al., 2012; Koskinen et al., 2005)
Calcitonin Gene-related Peptide (CGRP)	Neuropeptide within unmyelinated, nociceptive, peptidergic sensory neurons (Ikeuchi et al., 2012; Saxler et al., 2008; Tesarz et al., 2011)
Bradykinin B1 receptor (B1R) agonist	Membrane receptor that sensitizes neurons to noxious stimuli in the presence of bradykinin (Santos et al., 2017; Schuelert et al., 2015; Toda et al., 2004)
Acid-Sensing Ion Channel 3 (ASIC3) agonist	Membrane receptor involved in painful and non-painful mechanical sensation (Chen et al., 2002; Osmakov et al., 2014), prominent specialized touch organs

Days 3 and 4 – Western Blot Protocol, Chemiluminescence, and Ponceau Visualization

The Western Blot Protocol consisted of sample denaturing, gel electrophoresis, and membrane transfer followed by immunohistology. Prepared samples were denatured at 95°C for 5 minutes (Eppendorf Thermomixer R 5355, Mississauga ON, Canada) then spun down for 3 to 5 seconds in a mini centrifuge (Galaxy MiniStar, VWR International, Mississauga, ON, Canada) before being put back on ice. Gels were set up in a Gel Electrophoresis tub, the comb was carefully removed from each gel, and 12 of the 15 wells were loaded with 20 µL of prepared samples (4 donors with 3 tissues each). An additional well was loaded with 2.2 µL of a Ladder solution to track molecular weights. Gel Electrophoresis was run under voltage-control at 135 V for 90 minutes (PowerPac, Bio-Rad Laboratories, Montreal, QC, Canada), after which gels were removed from the glass sandwich and cut at approximately 42 kDa, 30 kDa, and 17 kDa to separate primary antigens based on their molecular weights (ASIC3 ~ 57 kDa, B1R ~ 37 kDa, PGP9.5 ~ 26 kDa, and CGRP ~ 10 kDa).

Cut gels were immediately transferred to membranes (Immun-Blot PVDF Membrane, Bio-Rad Laboratories, Montreal, QC, Canada) where all cut gels of a specific molecular weight band were transferred to the same membrane. Before transfer, membranes were rinsed in methanol and soaked in Transfer Buffer. A Transfer Stack was prepared from the bottom up consisting of a damp cloth pad, rinsed membrane, cut gels, and a second damp cloth pad; each layer was lightly covered with Transfer buffer and rolled out to remove air pockets between layers. The Transfer Stack was sealed after removing the excess

Transfer Buffer and underwent a Dry Transfer under voltage-control at 25 V for 30 minutes (TransBlot Turbo, Bio-Rad Laboratories, Montreal, QC, Canada).

Transferred Membranes were removed from the Transfer Stack and incubated in a dry container for 5 minutes at 37°C. Dried membranes were blocked with BSA diluted 1:20 in TBS-T for one hour at room temperature on a rocker table (~0.25 Hz). Blocking solution was washed off once with TBS-T for 5 minutes at room temperature before applying the prepared primary antibody. Membranes were put in a 4°C fridge overnight on a shaker table (100 rpm) to allow primary antibodies to incubate. Primary antibodies were removed from membranes the following day and washed three times with TBS-T for 5 minutes each at room temperature before applying the prepared secondary antibodies. Membranes soaked in secondary antibodies for 1 hour on a rocker table at room temperature before being washed off three time with TBS-T for 5 minutes each.

Chemiluminescence involved mixing a 1:1 ECL solution, running the 250 µL of the ECL solution over each membrane for up to a minute using a pipette, and imaging the membranes (ChemiDoc MP, Bio-Rad Laboratories, Montreal, QC, Canada). Imaging parameters were adjusted for optimal resolution and images were saved as "raw .tiff" files for processing.

Membranes had the ECL solution washed two times with TBS-T for 5 minutes each, before being soaked in a Ponceau Solution for 45 minutes at room temperature. The Ponceau Solution was washed off three times for 5 minutes each with distilled water, and then imaged to confirm protein loading.

6.3.3 Image Processing

All image-related processing was performed in ImageJ (v 1.49, National Institutes of Health, Bethesda, MD, USA). A rectangle of fixed dimensions was drawn on each image tailored to the size of the largest blot. The mean pixel intensity of that rectangle centred over each blot was quantified and subtracted from the background pixel intensity at a blank molecular weight immediately above or below the blot. The background-removed intensities for all tissues were divided by the background-removed skin intensity from that donor, on that gel.

This process was repeated for four gels across two membranes for each antigen to get four skin-normalized measures of protein concentrations per tissue per donor. The three most similar skin normalized concentrations of each protein from a single donor were averaged together to get a single measure per donor. Additionally, the skin-normalized values of the non-PGP9.5 antigens (CGRP, B1R and ASIC3) were also divided by the amount of PGP9.5 in that tissue (Antigen/PGP9.5).

6.3.4 Statistical Modelling

Testing for hypotheses 3a and 3b aims to determine if different tissue types have similar patterns of innervation; hypothesis 3a is concerned with PGP9.5, and hypothesis 3b is concerned the other three antigens. The small sample size (n = 4) limits the interpretability of statistical testing. For hypothesis 3a, all values for skin tissues had a value of one, and the hypothesis will be assessed by computing 99% confidence intervals for AF and SILC tissues and determining where those confidence intervals lie with respect to the skin measures for each antigen. A confidence interval that does not contain 1.0 was said to be different than skin. Hypothesis 3b is concerned with the relative amount of the remaining three antigens within a tissue and would be accepted if the ratio of each protein as a proportion of PGP9.5 is consistent across tissues.

6.4 Results

BCA results are presented in Table 6-3, with the homogenization methods appearing to give similar total protein content across tissue types. Western blotting did not reveal any consistently measurable protein levels for B1R or CGRP antibodies in any of the tissues and those antigens were removed from analyses (Figure 6-1). Based on the 99% confidence interval bounds, AF tissues had substantially lower concentrations of PGP9.5 and ASIC than skin, with SILC tissues having similar levels of PGP9.5 but slightly less ASIC3 than skin. The concentration of ASIC3 relative to PGP9.5 was much higher in AF tissues than SILC tissues.

The individual values in Table 6-5 as well as the images in Figure 6-1 indicate one donor (20130) having substantially higher SILC PGP9.5 content than the other donors despite controlling for total protein content through the BCA and confirming through Ponceau staining.

Table 6-3: Individual Results of the Bicinchoninic Acid Assay. Values for each donor are the mean of triplicate readings, the Mean ± SD includes all individual data points from each donor (12 readings).

Tissue	Donor	Total Protein Concentration (µg/µL)
AF	20129	2.515
	20130	3.041
	20131	2.687
	20132	2.295
	Mean ± SD	***2.635 ± 0.290***
SILC	20129	2.474
	20130	3.009
	20131	2.233
	20132	1.888
	Mean ± SD	***2.448 ± 0.408***
Skin	20129	2.496
	20130	2.171
	20131	2.954
	20132	2.221
	Mean ± SD	***2.487 ± 0.327***

Table 6-4: Mean and 99% Confidence Intervals of Lumbar Annulus and Ligament Protein Concentrations Relative to Skin. All skin samples were set of have protein concentrations of 1.

Antigen		PGP9.5	ASIC3	ASIC3/PGP9.5
AF	*Mean* *(99% CI)*	0.071 (0.000 – 0.153)	0.337 (0.132 – 0.542)	8.299 (1.277 – 15.321)
SILC	*Mean* *(99% CI)*	1.019 (0.153 – 1.885)	0.688 (0.377 – 0.999)	0.798 (0.289 – 1.307)

Table 6-5: Individual Protein Concentrations from Donors. All skin samples were set of have protein concentrations of 1.

Tissue	**AF**				**SILC**			
Donor	***20129***	***20130***	***20131***	***20132***	***20129***	***20130***	***20131***	***20132***
PGP9.5	0.0122	0.0208	0.1334	0.1167	0.8781	1.9960	0.5282	0.6736
ASIC3	0.1769	0.2309	0.4362	0.5037	0.7165	0.9553	0.7097	0.3725
ASIC3/PGP9.5	14.5260	11.0824	3.2703	4.3171	0.8159	0.4786	1.3437	0.5530

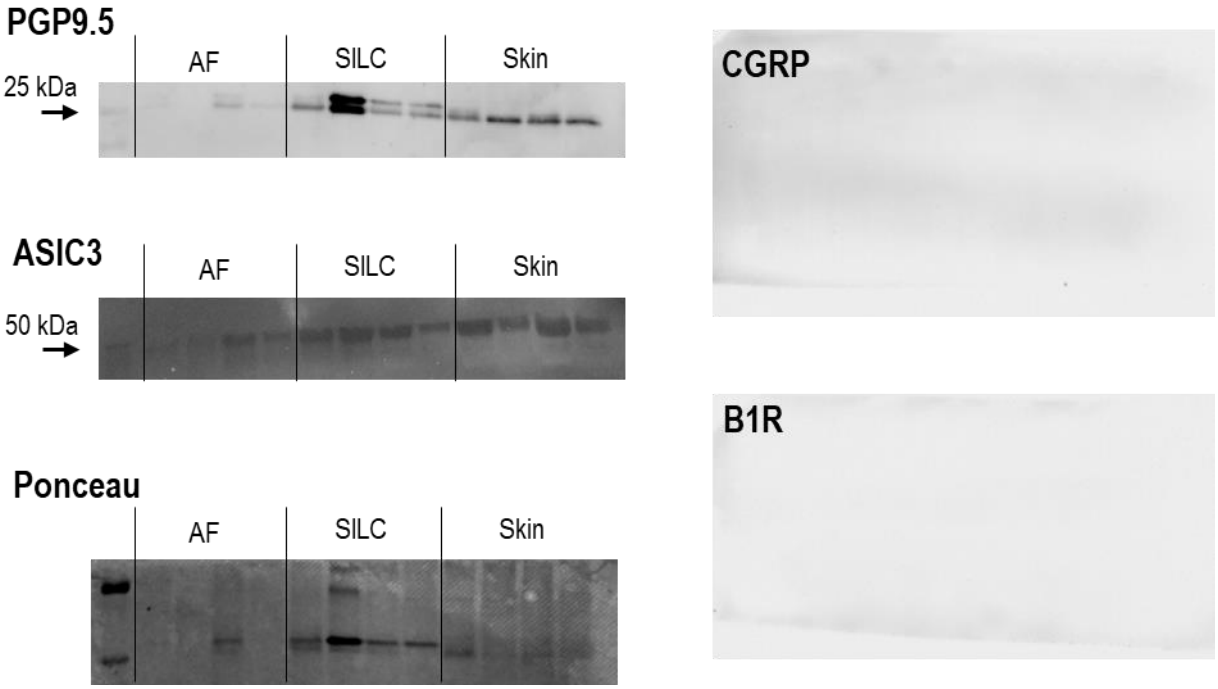

Figure 6-1: Representative Images from Western Blotting. Darker, larger blots indicate greater protein concentrations. Data was available for PGP9.5 and ASIC3 (left), however CGRP and B1R (right – each showing a full gel on a membrane) did not display immunoreactivity. The Ponceau image was taken from the same membrane used to generate the PGP9.5 image; the heavy blot from participant 20130 in the SILC range remains visible.

6.5 Discussion

Western blots were run on three types of human cadaveric tissues to determine the relative protein concentration of four neuron membrane proteins. This semi-quantitative procedure indicated that SILC and skin have similar total neuronal densities indicated by PGP9.5 concentrations, both of which larger than in AF tissues by about a factor of 10. ASIC3 concentrations showed a gradient from Skin having the highest concentration to the AF having the lowest concentration, but the AF had the highest relative concentration of ASIC3. CGRP and B1R were not detected in any of the tissues.

Hypothesis 3a, stating that skin would have the highest innervation density and the SILC and AF tissues would have similar innervation densities, was rejected. The data supports Skin and SILC tissues having similar innervation densities based on the concentrations of PGP9.5 being similar. However, the small sample size and single outlier data point that was included makes the apparent equivalence of skin

and SILC tissues tenuous. All four antigens (PGP9.5, CGRP, B1R, and ASIC3) have been demonstrated in human skin (Aoki et al., 2005; Frahm et al., 2013; Ikeuchi et al., 2012; Osmakov et al., 2014; Russell et al., 2014; Santos et al., 2017; Schuelert et al., 2015) and AF tissues (Bailey et al., 2011; Dimitroulias et al., 2010; Gruber et al., 2012; Roberts et al., 1995), but there is a lack of data for SILC tissues. Additionally, most of the published work has not related the relative concentrations of these proteins with respect to some standard, making it difficult to estimate what the expected relative concentrations of each antigen would be even in those previously reporting those data. The one consistency has been a relative lack of innervation in the AF tissues compared to skin (Bailey et al., 2011; Groh et al., 2021; Roberts et al., 1995; Roofe, 1940). While the SILC has relatively little data the innervation of the cervical and lumbar facet capsular ligaments can provide some insight into what could be expected in spinal ligaments. Facet capsular ligaments throughout the spine have a high concentration of specialized nerve endings featuring ASIC3 receptors (Cavanaugh et al., 1996; Chen et al., 2006; Kallakuri et al., 1998). Additionally, the cervical facet joint capsular nerves have contained CGRP, but this neuropeptide and others (like substance P) were found in higher concentrations when tracing these nerves to their cell bodies in the dorsal root ganglion than in the tissues themselves (Kallakuri et al., 2004; Ohtori et al., 2003). These data on an adjacent ligamentous structure support the SILC being highly and diversly innervated, which agrees with the available relative concentrations of PGP9.5 and ASIC3. Hypothesis 3b is concerned primarily with the ASIC3/PGP9.5 column in Table 6-4, stating that the relative amount antigen relative to PGP9.5 concentrations would be consistent across tissue types. This hypothesis was also rejected since there was a much larger proportion of ASIC3 in AF tissues compared to SILC and Skin tissues. Since ASIC3 is primarily concerned with detecting either protons or mechanical stimuli (Osmakov et al., 2014; Sherwood et al., 2012), this could indicate that AF tissues are relatively less capable at sensing other modalities such as heat (Kameda et al., 2019), relative to ligament or skin tissues. Despite Western blotting being a semi-quantitative measure and the limited sample, the stark contrast between the AF and other two tissues indicate at least an ordinal scale of innervation density where the AF has fewer total nerves, but a higher proportion of mechanically sensitive receptors than SILC or skin tissues.

The failure to demonstrate B1R or CGRP in either skin or AF tissues may be a result of the donor sources, multiple freeze-thaw cycles, or the homogenization process. Although there were no explicit positive controls, both proteins were present to varying extents in the existing tissues, just not a consistent level for the current analysis. Prior work identifying CGRP in human lumbar tissues has focused on finding "any evidence" of CGRP in those with prior disc pathology (Aoki et al., 2005; Dimitroulias et al., 2010; Roberts et al., 1995), with 50% to 60% of samples studied not showing any evidence of CGRP-positive fibres. B1R is prevalent in rat skin and muscle tissues (Santos et al., 2017), and the genes responsible for B1R production have been shown to be upregulated in those with at least grade III disc degeneration (Gruber et al., 2012), the authors do not provide a reference to interpret that upregulation with respect to. Without a relevant denominator, the absolute occurrence of B1R-positive fibres could be rare, all that can be inferred is that B1R is more common in those with more severe disc degeneration. Additionally, the three freeze-thaw cycles needed to isolate the tissues, bring them through mechanical testing, and then perform the Western blots on may have destroyed these proteins (Hochman et al., 2014). Multiple freeze-thaw cycles can destroy cells and reduce the bioactivity of proteins (Arsiccio et al., 2020; Cao et al., 2003), limiting this study's ability to detect antigens. Tissues were harvested from January to February 2020, with mechanical testing conducted between September and October 2020, and Western blotting conducted between May and July 2021. This less-than-ideal timeline was forced by external circumstances, but nonetheless warranted the three freeze-thaw cycles. The aggressive homogenization procedures required to

extract proteins from skin tissues may have also denatured these proteins (Roseboom et al., 2020). Indeed, the homogenization process was the sixth iteration of increasingly aggressive protocols. The commonly employed solvent SDS-Page to homogenize skin tissues (Roseboom et al., 2020) destroyed peptide bonds in the AF and SILC tissues based on pilot BCA assays. The multi-part MLB-sonication homogenization process, while time-consuming, seemed to sufficiently extract some proteins from all three tissues with some degree of similarity. Due to the small sample size, this data should not be used to claim that CGRP or B1R does not exist in any of the tissues studied, merely that the current processes prevented reliable and repeatable measures of those two antigens.

An alternative to expressing pixel intensity with respect to skin, would be to mix a standard sample containing all three tissue types together and express protein concentrations relative to that standard. While this additional level of control would have been helpful to compare between tissues, this expression relative to skin was chosen for its direct utility in the model (Chapter 7). Traditional house-keeping proteins, including GAP-DH, Actin, Type-I Collagen, and α-Tubulin were assessed in the present Western blots to show protein migration and transfer (Mahmood and Yang, 2012), however these showed inconsistent and non-repeatable results, with only Type-I collagen and Actin showing any immunoreactivity in AF and SILC tissues. The post-chemiluminescence Ponceau was the most consistent indicator of protein content on the membrane, and while not equivalent across the three tissues, (Figure 6-1) it demonstrated that all three proteins showed a mostly similar protein transfer, albeit one there the AF had approximately 10% less transfer than SILC or Skin. An additional analysis where a Ponceau-based correction factor was applied to all samples demonstrated similar findings to what was presented in the Results (Table 6-6). There is likely regional variability in innervation densities within tissues, the data presented reflects the full thickness of the dermis, the full transverse cross-section of the SILC, and the full posterior aspect of the outer-third of the AF. Although not a complete picture, this approach is appropriate for a first step to approximate innervation density and characteristics on a tissue-level scale.

Table 6-6: Relative Protein Concentration after Introducing a Multiplication Correction Factor Based on Ponceau Staining. All skin samples were set of have protein concentrations of 1.

Antigen		**PGP9.5**	**ASIC3**	**ASIC3/PGP9.5**
AF	*Mean*	0.075	0.360	8.299
	(99% CI)	(0.000 – 0.162)	(0.145 – 0.575)	(1.277 – 15.321)
SILC	*Mean*	1.039	0.707	0.798
	(99% CI)	(0.188 – 1.891)	(0.399 – 1.014)	(0.289 – 1.307)

This study sought to determine the relative concentration of four neuronal membrane proteins in three lumbar spine passive tissues. While there was a lack of data for two of the target proteins (CGRP and B1R), there is evidence that the posterior annulus has a little less than 1/10 the innervation density of posterior ligaments or lumbar skin. However, that annular innervation has a higher proportion of ASIC3-sensitive nerves than the other two tissues, a membrane protein highly linked to mechanical sensitivity.

Chapter 7 - Prediction of Nociceptive Spinal Cord Afferent Information from Tissue Loads

7.1 Overview

This chapter documents a model that predicts the percentage of people who would experience nociceptive activity in their brainstem in response to a one-dimensional loading profile. Tissue stresses, levels of muscle fatigue, and viscoelastic state were inputted into the model to describe loading history and muscular contributions. A Sensitivity Module (Section 7.4) converted incoming tissues stresses neural activity in three classes of peripheral neurons (Aβ non-nociceptive, Aδ nociceptive, and C nociceptive), this neural activity was then transmitted through simplified circuitry in the spinal cord in the Neurological Module (Section 7.5) to predict neural activity in the brainstem that would go on to inform the experience of pain. A given loading profile was simulated 100 times, with each iteration using a different pressure-pain threshold (PPT) informing a tissue-specific mechanical sensitivity. The percentage of these iterations containing sufficient neural activity in the brainstem was then taken as the likelihood of that exposure generating nociceptive activity that could be the foundation of a painful experience. This process is depicted in Figure 7-1.

The Sensitivity Module was adapted from (Gerling et al., 2018), which convolved a three-part exponential decay function over the time-derivative of tissue stresses. Two additional linear scaling factors were incorporated based on stress magnitudes and sensitivity to mechanical stimuli respectively to allow sensitivity not only to the rate of stress change, but also the magnitude of tissue stresses, and for sensitivity to be varied across individuals/iterations. The parameters from (Gerling et al., 2018) were assumed for skin, however to account for variation between tissues, the kernel function and scaling factors were adjusted based on the protein contents found in annulus and ligament tissues relative to skin, as well as the intended primary afferent neuron. This scaled convolution converted a tissue stress into a current, which was then fed into the Neurological Module.

The Neurological Module was a network of ten Hodgkin-Huxley type neurons (Hodgkin and Huxley, 1952a) that predicted membrane potentials based on the electrical current and ion channel activity of a given neuron, governed by a set of four ordinary differential equations. The solutions to these equations for each of the ten neurons were solved in 0.2 millisecond time-steps to keep track of when action potentials were triggered to allow neurons to activate or inactivate each other, with timings incorporating conduction velocities and axon lengths. This required modifying the original Hodgkin-Huxley formulation to allow for an external neuron to alter a given neuron's ion channel states. Connectivity between neurons was established using prior electrophysiological data assessing these circuits directly (Cordero-Erausquin et al., 2016; Guo and Hu, 2014; Lu and Perl, 2005, 2003; Taylor et al., 2016), and indirectly (Granata et al., 2005; Sánchez-Zuriaga et al., 2010; Solomonow, 2012), and were affected using sign-specific post-synaptic potential functions. These membrane potentials are followed to the completion of the stress application, with the primary output being these membrane potentials, specifically the membrane potential of the "Brainstem Neuron" (Table 7-7).

A single iteration of the model involves selecting a single stress profile and a mechanical sensitivity, generating feasible neuronal properties, and following that stress from the periphery to the brainstem through the Sensitivity and Neurological Modules. If the membrane potential of the Brainstem Neuron in

the Neurological Module satisfied a minimum action potential frequency and duration, that iteration was deemed to have nociceptive activity. The same stress profile was then re-simulated 99 more times, each with a different mechanical sensitivity and neuronal properties to determine the likelihood of that stress profile generating nociceptive activity.

The remainder of this chapter details the implementation and representation of the two modules and other components in this overview.

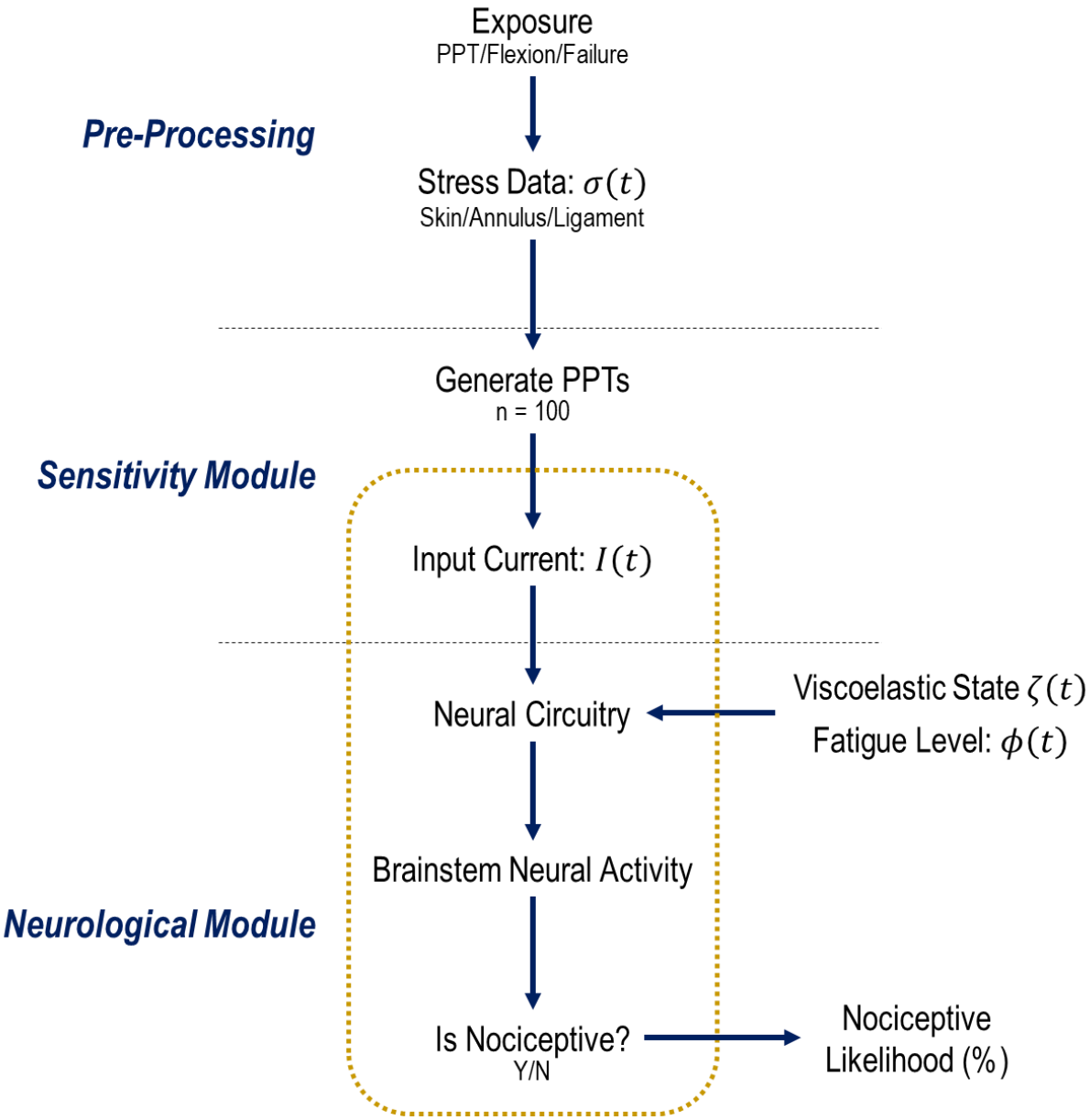

Figure 7-1: Overview of Model and Data Flow. The model predicts the likelihood that a given exposure will generate nociceptive activity in the brainstem for one of three tissues. It achieves this through a mechanistic simulation of neural activity based on empirical relations between stress and skin sensitivity, which are transferred to other tissues based on immunoblotting data. The item within the gold dashed box are simulated 100 times, each time with a different Pressure-Pain Threshold (PPT), items outside the box are consistent throughout simulations.

7.1.1 A Note on Model Scope

This is a model of nociceptive neural activity, not painful experiences. While the model decides if a stress profile is nociceptive based on the number and timing of action potentials in the brainstem, it makes no effort to contextualize that activity. It is assumed that the nociceptive activity *could* activate those circuits in the absence of any extraneous inputs not accounted for, including but not limited to cortical pathways involving attentional (Kóbor et al., 2009) or mood (Martucci, 2017), or descending pathways commonly targeted by pharmacological agents (François et al., 2017). In that vein, pain disorders or other abnormalities that have caused plastic changes to any of the structures involved, whether modeled directly (periphery or spinal cord) or part of a downstream pathway (cortex), are assumed to be absent. This follows from the PPTs being derived in healthy participants in a relatively neutral laboratory environment. This model is thus limited to those same restrictions and scope.

7.1.2 Computational Framework

The model was coded into Python (v 3.6.3) relying on the `numpy`, `pandas`, `scipy`, `matplotlib`, `random`, and `time` libraries. Computations between modules occurred in the following order:

1. Stress data, $\sigma(t)$, were either derived or pre-processed for input in the Sensitivity Module.
2. The Neurological Module generated neurons with predetermined properties for the given iteration, including their mechanical sensitivity, physical, and electrical properties.
3. The entire time-course of the stress data $\sigma(t)$ were converted to an input electrical current, $I(t)$, in three peripheral neurons by the Sensitivity Module.
4. The Neurological Module then simulated all neuron-neuron interactions in 0.2 millisecond time-steps based on the input current $I(t)$ and pre-established neural circuitry.
5. A decision was made based on the membrane potentials computed by the Neurological Module as to whether the stress profile $\sigma(t)$ was nociceptive for that iteration.
6. Steps 2 through 5 were repeated for each subsequent iteration.

While the stress data pre-processing and Sensitivity Module used functional programming, the Neurological Module used object-oriented programming. The two approaches can be interlaced and melded together in Python, this process does not alter the underlying mathematics, however it will alter how that mathematics will be communicated in this chapter. The main distinction is that the Neurological Module contained specific neuron "objects" referred to by name (Table 7-7); this feature is not possible in describing the other facets of this model.

7.2 Purpose and Hypotheses

The purpose of this model is to determine the likelihood that a person could generate nociceptive activity in their central nervous system, $\Lambda_{\%}$, from one of three mechanical exposures. The tissues studied are the same isolated in Chapter 6: the annulus fibrosus, the supraspinous-interspinous ligament complex, and skin from the mid-lumbar spine. These tissues were chosen as they are often implicated in mechanical low back pain. The three exposures chosen are: PPT testing, full lumbar spine flexion, and tissue failure; using PPT testing as a starting point to generate predictive nociceptive activity during the Flexion and Failure Exposures. It is hypothesized that:

4a) There will be no nociceptive activity generated by the Flexion Exposure in any tissue; $\Lambda_{\%}$ will equal 0.

4b) The Failure Exposure will generate nociceptive activity in a larger proportion of ligament tissues than annulus tissues; Ligament $\Lambda_{\%}$ > Annulus $\Lambda_{\%}$

4c) The presence of muscle fatigue will decrease $\Lambda_{\%}$

4d) The presence of viscoelastic creep will not affect $\Lambda_{\%}$, but will affect the firing characteristics of the circuits involved for the subset of people who do experience nociceptive activity.

These hypotheses appear trivial given that the model is built from prior data presented in this thesis that support all four hypotheses. The general approach is to base all modelling on existing physiological processes, with the intention of using these hypotheses to tune and check the model's behaviour, all of which are grounded in the earlier chapters. The goal of this chapter is to satisfy these four criteria while minimally compromising biofidelity before investigating interactions between them, reflective of a more real-world mechanical exposure.

7.3 Obtaining Stress Data

The first step in the model involved generating tissue-specific one-dimensional stresses based on one of three exposures: PPT, Full Flexion, and Tissue Failure (Table 7-1). All stress data pertained to structures about the L3/L4 joint.

Table 7-1: Summary of Exposures and Tissues Relevant to those Exposures.

Exposure	Description	Tissue(s) Simulated
Pressure-Pain Threshold (PPT)	Tent-function of stress with ascending and descending slopes of 0.2 MPa/s	Skin
Full Flexion	Moving from a neutral posture to 10° of intervertebral flexion over two seconds, holding that flexed posture for four seconds, then returning a neutral posture over two seconds	Annulus, Ligament
Tissue Failure	Loading the tissues under displacement-control to failure under the conditions used for mechanical testing in Appendix E	Annulus, Ligament

The purpose of the PPT exposure was to validate the Sensitivity and Neurological Modules. The Full Flexion exposure was intended to be used as a demonstration of a non-nociceptive exposure, but one with the potential to generate nociceptive activity if sensitized. Full flexion is also relevant for inducing viscoelastic changes to lower back tissues (Dickey et al., 2003; Howarth et al., 2013b; McGill and Brown, 1992; Pinto et al., 2021; Solomonow, 2012). The Failure exposure was chosen as an indicator of the largest stress possible in a tissue, to determine what the greatest amount of nociceptive activity coming from a

tissue could be. In that vein, the PPT exposures were distributed over a wide range of values to ensure stability and adequate range of the sensitivity and neurological components, while the Flexion and Failure exposures represented sample stress profiles to apply the model to predict the nociceptive activity during those exposures.

Simulated data were used over experimental data to remove any effects of measurement noise on predictions while having an effectively infinite resolution to limit interpolation over the very small timescales needed for the Neurological Module. The Sensitivity Module developed in Section 7.4 depends on the time-derivative of stress to generate a current (Gerling et al., 2018), and smooth mathematical approximations of experimental data were favoured over the noisy source data to reflect representative stress profiles for each exposure that would not be influenced by high-frequency artifacts in the data. One advantage of this method over traditional filtering techniques to reduce high-frequency noise is that low-pass filtering attenuates peaks in time-varying data (Drake and Callaghan, 2006; Howarth and Callaghan, 2009; Winter, 2009). Additionally, using mathematical functions allowed specific time-points to be specified explicitly, reduced computation time from reading in experimental data from external files, and can facilitate analytical solutions to parts of the model in the future to simplify computations without any loss of data (Dvoretzky, 1956).

7.3.1 Pressure-Pain Threshold Exposure

PPT stress data were generated using a smoothed tent function of the form:

$$\sigma_{PPT}(t, p_0) = f_{inc}(t) + l(t, p_0)[f_{dec}(t, p_0) - f_{inc}(t)] \tag{7-1}$$

Where:

$$f_{inc}(t) = 0.2t \tag{7-2}$$

$$f_{dec}(t) = -0.2t + 2p_0 \tag{7-3}$$

$$l_{PPT}(t) = \frac{1 + \tanh\left(l_0\left(t - \frac{p_0}{0.2}\right)\right)}{2} \tag{7-4}$$

The functions $f_{inc}(t)$ and $f_{dec}(t)$ are linear increasing and decreasing functions used to construct the tent, and the interpolation function $l_{PPT}(t)$ is used to connect the two linear functions at the point of intersection. The input t indicates time in seconds and p_0 indicates the target PPT in MPa, l_0 is a constant that dictates how "tight" the fit is, which was set at 5.0 for this model as it caused minimal distortion without greatly affecting the time-derivative of $\sigma_{PPT}(t)$; Figure 7-2 shows how varying l_0 affects $\sigma_{PPT}(t)$. The 0.2's indicate a rate of stress application of 0.2 MPa/s. Appendix F presents a general form for this interpolation technique.

These smoothed tent-functions were intended to represent ideal PPT applications, as they are often described in the literature: linearly increasing at a pre-determined rate to a peak before a decrease down to baseline (Chesterton et al., 2003; Gajsar et al., 2018; Hven et al., 2017; Lacourt et al., 2012; Melia et al., 2015; Petrini et al., 2015; Rolke et al., 2006).

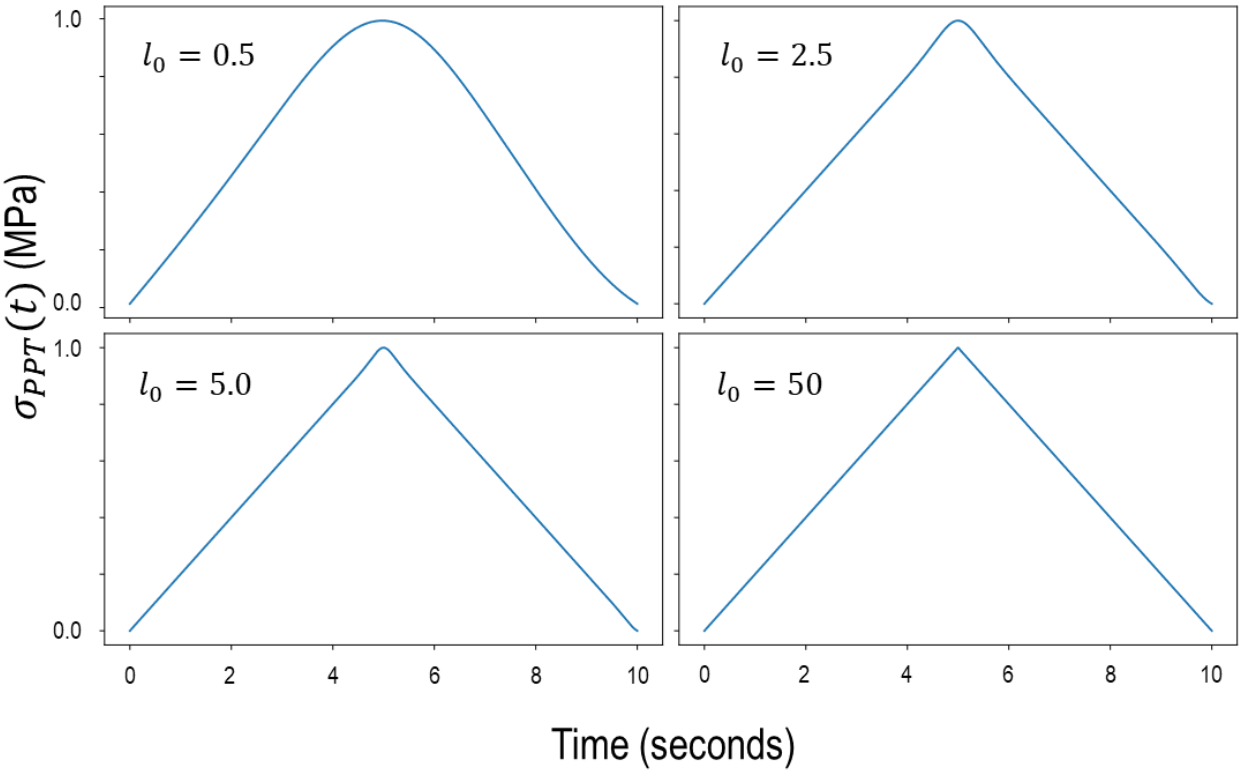

Figure 7-2: Variation in l_0 and its Effects on the Smoothed-Tent Function used to Simulate Pressure-Pain Threshold Data.

7.3.2 Full Flexion Exposure

Full flexion was assumed to consist of an L3/L4 joint angle of 10°, which represents an upper limit of radiographic and fluoroscopic studies investigating L3/L4 intervertebral range of motion in a maximal standing flexed posture (Been and Kalichman, 2014; Breen et al., 2019; De Carvalho et al., 2010; Galbusera et al., 2021; Harvey et al., 2016; Mellor et al., 2014; Oxland et al., 1991; Viggiani et al., 2017; White III and Panjabi, 1990). The specific full-flexion task investigated was a 4-second maximal trunk flexion hold preceded by a 2-second flexion motion to move into the posture from upright standing, followed by a 2-second extension motion described by Equations 7-5 to 7-7 and shown in Figure 7-6.

$$\theta_{IVA}(t) = 10\, g_{inc}(t) g_{dec}(t) \tag{7-5}$$

Where:

$$g_{inc}(t) = \frac{1}{2}\left[1 + \tanh\left(2\sqrt{2}(t-1)\right)\right] \tag{7-6}$$

$$g_{dec}(t) = \frac{1}{2}\left[1 + \tanh\left(-2\sqrt{2}(t-7)\right)\right] \tag{7-7}$$

In Equations 7-5 through 7-7, t is the time in seconds, the 10 in Equation 7-5 indicates an end range of motion of 10°, the "-1" and "-7" indicate the number of seconds (1 and 7 respectively) where the

$\theta_{IVA}(t)$ function is halfway through moving into and out of the flexed posture. This angle was then used to predict one-dimensional tissue strain using a trapezoidal approach: By assuming tissues' resting length occurred at θ_{IVA} = 0°, the displacements could be modelled using a trapezoid (Figure 7-3). In this formulation, the tissues' current length due to flexion, $x_{Flex}(t)$, could be computed given the intervertebral angle, θ_{IVA} and the moment arm of that tissue relative to the joint centre of rotation, r, using Equation 7-8.

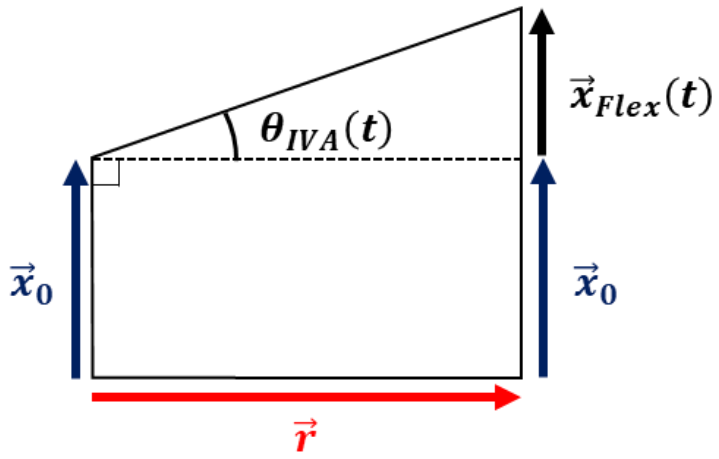

Figure 7-3: Trapezoidal Approximation to Determine Tissue Lengths as a Function of Intervertebral Angle for the Annulus Fibrosus and Supraspinous-Interspinous Ligament Complex. x_0 is the resting tissue length, which increases by $x_{Flex}(t)$ as a function of the intervertebral angle, $\theta_{IVA}(t)$, and the perpendicular distance or moment arm of that tissue, r.

$$x_{Flex}(t) = r \cdot \tan\left(\theta_{IVA}(t)\right) \tag{7-8}$$

While x_0 is not required for computing $x_{Flex}(t)$, it is necessary to determine the moment arm r when an empirical measurement of r is unavailable. A moment arm for the AF, r_{AF}, was taken from the literature to equal 20.2 mm (Dao, 2016) for an adult human L3/L4 joint based on MRI data. However, an indirect computation was required to derive the values for the SILC (Figure 7-4). The disc height at the centre of rotation, h_0, and the horizontal distances between the centre of rotation and the posterior aspect of both the superior and inferior vertebral bodies, d_{sup} and d_{inf}, were taken from digitized CT images to determine the relative positions of posterior surfaces of the intervertebral joint (Galbusera et al., 2021; Zhou et al., 2000). The angles between those surfaces and the posterior ends of the spinous processes for L3, α_{sup}, and L4, α_{inf}, were taken from a second data source (Lin et al., 2018), which also provided the lengths of those spinous processes, s_{sup} and s_{inf}. Combing these terms together into Equation 7-9 allows for an estimation of x_{SILC_0}; note that h_0 points vertically, d_{sup} and d_{inf} point horizontally (posteriorly), and the directions of s_{sup} and s_{inf} are indicated by α_{sup} and α_{inf}, which are defined relative to the anterior-horizontal. Lastly, deriving r_{SILC} required finding a vector perpendicular to x_{SILC} and determining the distance between the centre of rotation and the line extending from x_{SILC}. All values are given in Table 7-3.

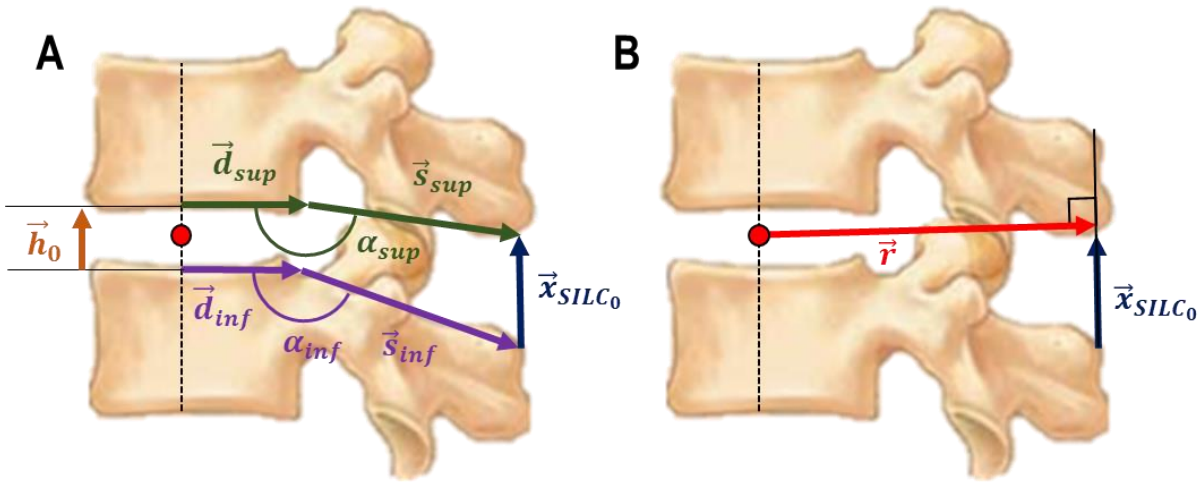

Figure 7-4: Estimating the Supraspinous-Interspinous Ligament Complex Moment Arm. Variables explained in text with numerical values given Table 7-3. Panel A: determining x_{SILC_0}; Panel B: determining r_{SILC} from x_{SILC_0}.

$$\vec{x}_{SILC_0} = \vec{h}_0 + \vec{d}_{sup} + \vec{s}_{sup} - (\vec{d}_{inf} + \vec{s}_{inf}) \tag{7-9}$$

Table 7-2: Distances and Orientations of L3/L4 Geometry taken from the Literature. Sources indicated in text; see Figure 7-4 for intermediate terms.

Tissue	Term	Value
AF	r	20.2 mm
SILC	h_0	11.6 mm
	d_{sup}	17.6 mm
	d_{inf}	17.6 mm
	α_{sup}	135.5°
	α_{inf}	133.8°
	s_{sup}	23.8 mm
	s_{inf}	22.6 mm
	x_0	14.0 mm
	r	32.3 mm

While Equation 7-8 should satisfy any value of θ_{IVA} where -90° < θ_{IVA} < 90°, the physiological bound on θ_{IVA} is much stricter. These posterior tissues develop tension in flexion, putting a lower bound of

0°, and the previously described upper bound of 10° (Harvey et al., 2016; Viggiani et al., 2017), confining Equation 7-8 to a highly linear region of the $\tan(x)$ function (Figure 7-5). Thus, linear approximations were developed to these bounds (Table 7-4).

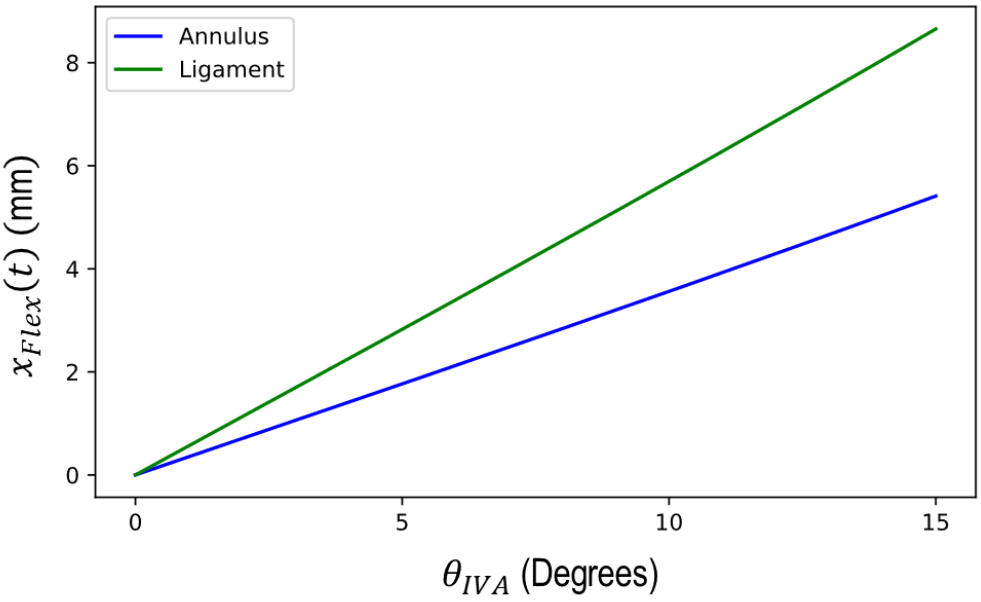

Figure 7-5: Estimated Tissue Lengths for the Annulus and Ligament Tissues using Equation 7-8 and Table 7-3.

Table 7-3: Linear Approximations to the Intervertebral Angle-Tissue Length Relationship.

Tissue	$\tan(x)$ Fit	Linear Fit	R^2
AF	$x_{Flex}(t) = 20.2\tan(\theta_{IVA}(t))$	$x_{Flex}(t) = 0.3575\ \theta_{IVA}(t)$	> 0.999
SILC	$x_{Flex}(t) = 32.3\tan(\theta_{IVA}(t))$	$x_{Flex}(t) = 0.5717\ \theta_{IVA}(t)$	> 0.999

The outputs of the Equations in Table 7-3 are displacements in mm, requiring two additional steps to be converted into a tissue stress. First, the stiffnesses, variation in resting length, and mean resting length derived from failure and sub-failure testing informed a constituency model (Barrett and Callaghan, 2018) that can predict Forces from displacements using Equations 7-10 through 7-13.

$$F(z_{Flex}(t)) = k\eta\left[\Phi'\left(z_{Flex}(t)\right) + z_{Flex}(t)\Phi\left(z_{Flex}(t)\right)\right] \tag{7-10}$$

$$z_{Flex}(t) = \frac{x_{Flex}(t) + \mu}{\eta} \tag{7-11}$$

$$\Phi\left(z_{Flex}(t)\right) = \frac{1}{2}\left[\text{erf}\left(\frac{z_{Flex}(t)}{\sqrt{2}}\right) + 1\right] \tag{7-12}$$

$$\Phi'\left(z_{Flex}(t)\right) = \frac{1}{\sqrt{2\pi}}\exp\left(-\frac{z_{Flex}(t)^2}{2}\right) \tag{7-13}$$

In which $F\left(z_{Flex}(t)\right)$ describes the tensile force in a tissue as a function of tissue displacement z-score during flexion, $z_{Flex}(t)$, which is defined by the appropriate Equations in Table 7-3 to convert a displacement in mm to a unitless z-score of collagen length over time. The tissue-specific constants k, η, and μ represent the tissue stiffness, the standard deviation of fibre resting length, and the mean resting length, respectively; and were determined in Appendix E through curve-fitting force-displacement tissue failure profiles (Table 7-4). The functions $\Phi\left(z_{Flex}(t)\right)$ and $\Phi'\left(z_{Flex}(t)\right)$ represent the cumulative distribution function and probability distribution function for a normal distribution, where $\text{erf}(x)$ is the Error-Function and $\exp(x)$ is the natural exponent function.

After being converted to a tensile force, the outputs from the function $F\left(z_{Flex}(t)\right)$ in Equation 7-10 were divided by the representative tissue cross-sectional areas derived in Appendix E (Table 7-4) to obtain the tissue stresses during this task.

$$\sigma_{Flex}(t) = \frac{F\left(z_{Flex}(t)\right)}{A} \tag{7-14}$$

Where A is the cross-sectional areas in Table 7-4 in mm^2. Dividing a Force in Newtons by an area in mm^2 results in the units of MPa, making it consistent with the units of $\sigma_{PPT}(t)$. The resulting $\sigma_{Flex}(t)$ profiles with respect to both time and the flexion angle generated through Equation 7-5 are depicted in Figure 7-6.

Table 7-4: Representative Tissue Properties Taken from Appendix E.

Tissue	A (mm^2)	k (N/mm)	η (mm)	μ (mm)
AF	109.9	25.692	0.401	-1.962
SILC	49.6	21.072	0.860	-5.570

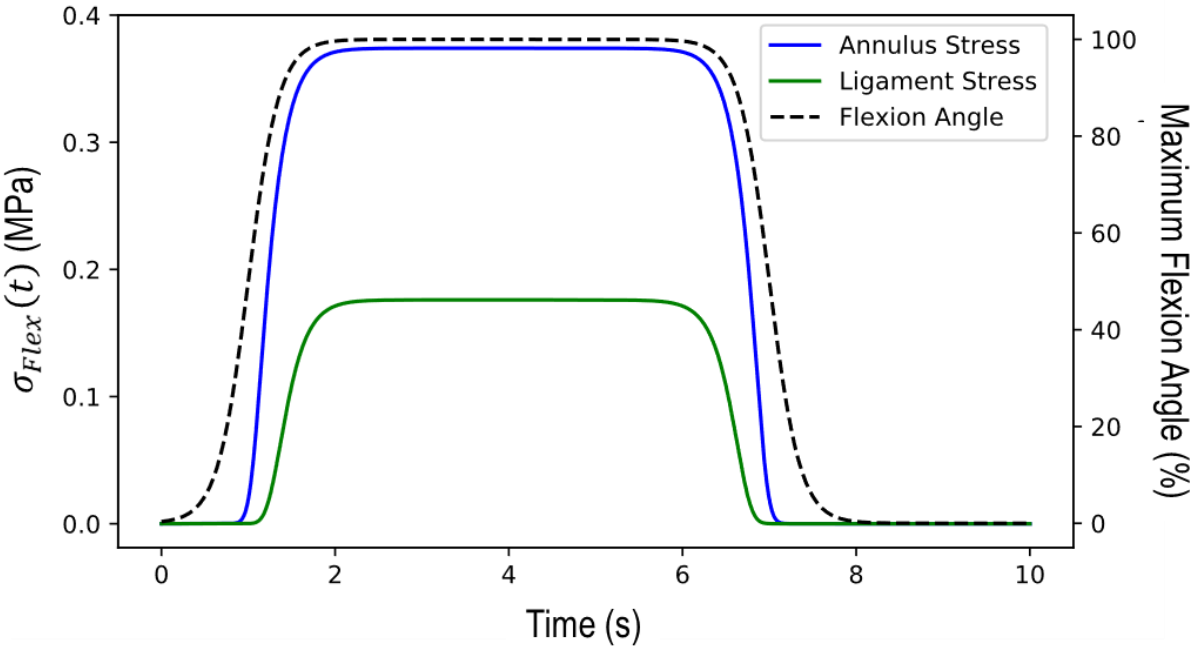

Figure 7-6: Tissue Stresses and Flexion Angle during the Flexion Exposure. The stress functions $\sigma_{Flex}(t)$ for both the annulus (blue) and ligament (green) tissues are in solid lines with respect to the left axis; the dashed black line is the flexion angle as a percentage of maximum flexion angle with respect to the right axis.

7.3.3 Failure Exposure

The failure exposure, $\sigma_{Fail}(t)$, consisted of joining a pre-failure function smoothly connected to a post-failure function using the same interpolation framework as in $\sigma_{PPT}(t)$ (Equation 7-15). The pre-failure function, $\sigma_{Pre}(t)$, used Equations 7-10 to 7-13, involving linearly increasing tissue displacement at 5% strain per second using the representative tissue properties in Table 7-4 (Equation 7-16). These displacements were continued until tissue reached a force corresponding to the maximum stress observed in all mechanical testing for each tissue (Table 7-5) and was termed $x_{Fail}(t)$. The time when each tissue reached its failure stress was termed t_{Fail}. The post-failure region of the curve, $\sigma_{Post}(t)$, was simplified using an exponential function (Equation 7-17), under the constraint that the shape constants β_0, β_1, and β_2 not only fit experimental data, but also be within 1.0 MPa to the failure stress at t_{Fail} to facilitate a smooth interpolation between the pre-failure and post-failure functions using Equation 7-18. As with Equation 7-4 in Section 7.3.1, a value of 5.0 was used for l_0 in Equation 7-18 as a tightness-of-fit constant.

$$\sigma_{Fail}(t) = \sigma_{Pre}(t) + l_{Fail}(t)[\sigma_{Post}(t) - \sigma_{Pre}(t)] \tag{7-15}$$

$$\sigma_{Pre}(t) = \frac{F\left(z_{Fail}(t)\right)}{A} \qquad z_{Fail}(t) = \frac{x_{Fail}(t) + \mu}{\eta} \tag{7-16}$$

$$\sigma_{Post}(t) = \exp\left(-\beta_1(t - \beta_2)\right) + \beta_0 \tag{7-17}$$

$$l_{Fail}(t) = \frac{1 + \tanh\left(l_0(t - t_{Fail})\right)}{2} \tag{7-18}$$

Table 7-5: Properties of the Simulated Failure Exposure for Ligament and Annulus.

Tissue	Failure Stress	Peak Displacement: $x_{Fail}(t_{Fail})$	β_0	β_1	β_2	t_{Fail}
AF	0.694 MPa	4.925 mm	0.0132	1.164	1.4786	1.73 s
SILC	2.206 MPa	10.700 mm	0.0089	1.677	4.9487	4.50 s

The resulting curves for Equation 7-15 are compared to the experimental data of the most-tolerant samples for both ligament and annulus in Figure 7-7. In this figure, the mechanical properties of the "representative" tissues from Table 7-4 are used for the $\sigma_{Pre}(t)$ part of the curve, while the $\sigma_{Post}(t)$ part of the curve uses the shown experimental data as a basis for curve-fitting the β terms in Equation 7-17.

The peak stresses for both tissues were substantially smaller than other sources in the literature (Ebara et al., 1996; Isaacs et al., 2014; Pintar et al., 1992; Robertson et al., 2013b; Skaggs et al., 1994; Stemper et al., 2014), with annulus longitudinal failure stresses ranging from 2.0 – 10.0 MPa, and supraspinous-interspinous ligament tensile failure stresses ranging from 6.0 – 50.0 MPa. An additional failure waveform: $\sigma_{Fail10}(t)$ was implemented by multiplying $\sigma_{Fail}(t)$ by 10, positioning the peak failure stresses in the middle of these ranges: Annulus = 6.94 MPa, Ligament = 22.06 MPa.

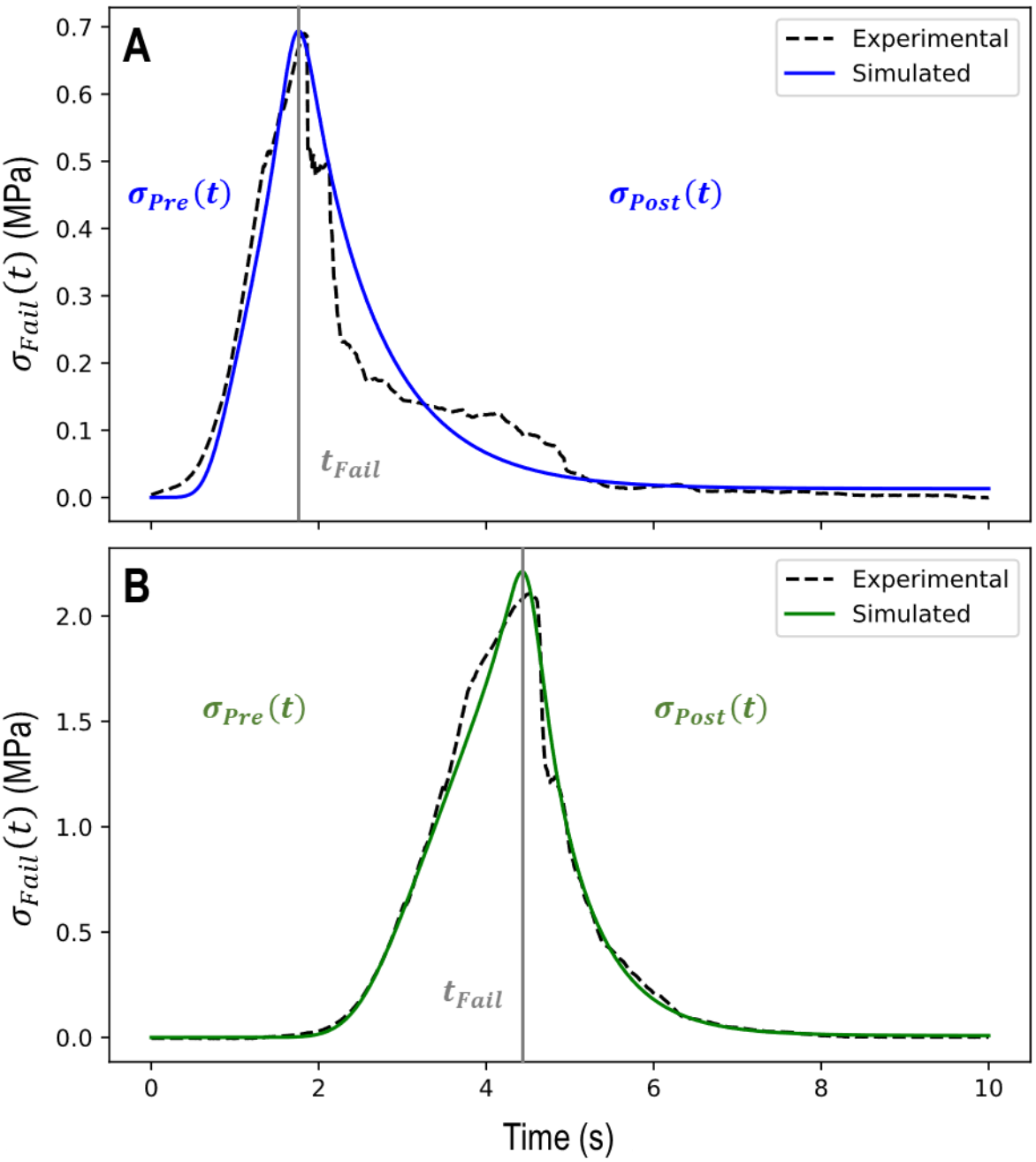

Figure 7-7: Simulated Failure Stresses for Annulus (Panel A) and Ligament (Panel B). The experimental data in the dashed black lines come from the failure test that produced the largest failure stresses, and the tissue moduli do not reflect the "representative" moduli depicted in the solid lines that arose from dividing the stiffnesses in Table 7-4 by the cross-sectional areas of the corresponding tissue. The $\sigma_{Fail10}(t)$ waveforms were identical in shape, but scaled up by a factor of 10, effectively mimicking a tissue with the same failure force-displacement properties, but with a cross-sectional area 1/10th of those used to generate $\sigma_{Fail}(t)$.

7.4 Sensitivity Module

The Sensitivity Module converted the time-varying tissue stresses from each exposure, $\sigma(t)$, into time-varying electrical currents, $I(t)$ that are fed into the Neurological Module. The general framework was adapted from (Gerling et al., 2018) (Equations 7-19 to 7-21).

$$I(t) = \frac{\psi_{TN} s(\sigma_m)}{p_i} (\gamma * \sigma')(t) \tag{7-19}$$

$$\gamma(t) = \gamma_r \exp\left(-\frac{t}{\tau_r}\right) + \gamma_s \left(k_{peak} \exp\left(-\frac{t}{\tau_s}\right) + k_{steady}\right) + \gamma_u \exp\left(-\frac{t}{\tau_u}\right) \tag{7-20}$$

$$s(\sigma_m) = s_0 \ln(\sigma_m - s_1) + s_2 \tag{7-21}$$

Most of the Sensitivity Module is summarized in these three equations. Equation 7-19 is the main overview of the module: the convolution between a neural activation function $\gamma(t)$, and the first time-derivative of tissue stress, $\sigma'(t)$. This convolution is scaled by the product of a peak tissue stress scaling function, $s(\sigma_m)$, and the neuron and tissue-specific mechanical sensitivity scaling parameter ψ_{TN}, divided by the iteration-specific PPT generated from the distribution in Chapter 5 using Equation 5-15, p_i. The kernel $\gamma(t)$ (Equation 7-20) is a triphasic exponential decay function with three time-constants: τ_r, τ_s, and τ_u, representing time-constants of rapid, slow, and ultra-slow receptors respectively, embedded in the receptor end of the peripheral neural membranes. Each of these individual responses are scaled up by three phase-scaling parameters: γ_r, γ_s, and γ_u, the sum of which was set to 1 to avoid any gain in $\gamma(t)$. There are two additional shape parameters governing the slow (subscript s) portion of Equation 7-20: k_{peak} and k_{steady}. Equation 7-21 is the logarithmic scaling function to scale the input current based on the peak tissue stress, σ_m, with two constants: s_0, s_1, and s_2. The specific values of the parameters for each instance are presented in Table 7-6, the next subsection describes how each of the values were obtained.

7.4.1 Deriving Constants for the Sensitivity Module

The Sensitivity Module was developed after a draft of the Neurological Module was programmed, as such it is difficult to describe the derivation of the Sensitivity Module parameters without referring to the Neurological Module. This subsection is set up such that no knowledge of the specifics of the Neurological Module is required, but the reader should be aware that a functioning precursor to the Neurological Module was necessary to develop the Sensitivity Module.

Table 7-6: Sensitivity Module Parameters. An Explanation for where each was derived from is in the text of this section.

Parameter	Aδ			C		
	Skin	*Annulus*	*Ligament*	*Skin*	*Annulus*	*Ligament*
ψ_{NT}	1.042	0.074	1.062	1.000	0.071	1.019
τ_r	0.008					
τ_s	0.2					
τ_u	1.7446					
γ_r	0.7084			0.60		
γ_s	0.2286			0.25		
γ_u	0.0666			0.15		
k_{peak}	0.87					
k_{steady}	0.13					
s_0	17.743			27.530		
s_1	-0.533			-2.014		
s_2	29.201			-4.831		

Equations 7-19 and 7-20 were originally developed to model the currents generated in non-nociceptive touch-receptors in skin based on Merkel-disc activity stimulating large-diameter, myelinated, Aβ primary afferent neurons (Gerling et al., 2018). However, nociceptive information is carried primarily through smaller diameter myelinated Aδ and unmyelinated C primary afferent neurons (Braz et al., 2014; Chen et al., 2006; Dubin and Patapoutian, 2010; Julius and Basbaum, 2001; Kandel et al., 2013; Schmidt et al., 1995; Woolf and Ma, 2007; Xu et al., 2008b), and this is reflected in the Neurological Module. However, the Neurological Module does also include Aβ primary afferent neurons, since they affect nociceptive inhibition in the spinal cord (Cordero-Erausquin et al., 2016; Guo and Hu, 2014). Additionally, the C-fibres have peptidergic and non-peptidergic sub-categories with their own distinct structural and activation properties (Saeed and Ribeiro-da-Silva, 2012; Stucky and Lewin, 1999). There are also three different tissues simulated, and the composition of peripheral neuronal membrane proteins is not consistent between tissues as indicated in Chapter 6. This would require twelve distinct sets of twelve parameters (ψ_{tissue}, τ_r, τ_s, τ_u, k_{peak}, k_{steady}, γ_r, γ_s, γ_u, s_0, s_1, and s_2) to input into Equations 7-19 through 7-21, however obtaining the data required to tailor parameters to all tissue types was beyond the scope of this thesis, thus some simplifications were made to reduce 144 parameters down to 23.

First, the triphasic kernel function $\gamma(t)$ was developed to fit a specialized sensory receptor, the Merkel Disc, with the rapid and slow phases based on physiological processes, and the ultra-slow response included to improve the fit to experimental electrical activity at the axon hillock (Gerling et al., 2018), meaning there is no guarantee that a triphasic shape would be ideal for the free-nerve endings that transmit

nociceptive information (Braz et al., 2014; Dubin and Patapoutian, 2010; Mense and Hoheisel, 2016; Xu et al., 2008b). It is difficult to determine the number of phases present in the raw data from other published recordings of free-nerve endings (Hoheisel et al., 2011; Lu and Perl, 2005, 2003; Mense and Hoheisel, 2016) without being able to test or compare those data to fitted responses since these parameter pertain to a kernel function, not the current-time plots. Additionally, the time constants associated with these phases (τ_r, τ_s, and τ_u) are specific to the Merkel disc and may not be representative of nociceptive neurons. The specific values of the phase constants would also influence the shape constants k_{peak} and k_{steady} pertaining to the slow phase. *In-situ* conductive testing would be required to obtain appropriate values in each of the three tissues, which would be impossible on the cadaveric donors available. As a result, the three time-constants and two shape-constants were not altered across tissue types or neuronal classes, and the values obtained by Gerling et al. were used in the model (Table 7-6).

Markers identifying non-peptidergic and peptidergic neurons, such as IB_4 or CGRP, exist in the dorsal root ganglion post-mortem, not in the periphery. As a result, all attempts to distinguish the electrical properties of these classes of nociceptive C-type neurons requires recording a neuron in the dorsal root ganglion while a stimulus is applied, and then retroactively using an immunotagging procedure to determine whether that neuron was peptidergic or not. This step is necessary since there is non-negligible overlap in the distributions of the physical and conductive properties of these two neuronal populations (Stucky and Lewin, 1999). However, previous work has found a lack of non-peptidergic neurons in the annulus (1.0% of all neurons) relative to skin (19.5% of all neurons) in rats (Aoki et al., 2005), while no data was available for any spinal ligament relative to other tissues. While nearly a twenty-fold increase between these tissues, the net effect in accounting for these between-tissue differences on the Sensitivity Module would be minor. Based off the data of Stucky and Lewin comparing the conductive properties of non-peptidergic and peptidergic neurons (Stucky and Lewin, 1999), those authors determined that the peptidergic neurons fired their action potentials roughly 3 milliseconds sooner than non-peptidergic counterparts after controlling for input sensitivity and action potential shape. Controlling for the ratio of peptidergic to non-peptidergic neurons in skin from (Aoki et al., 2005) (41.1% peptidergic to 19.5% non-peptidergic), the extreme weighting of the annular tissue (54.4% peptidergic to 1.0% non-peptidergic) would at most shift the some facet of $\gamma(t)$ by slightly less than 3 milliseconds. It is unclear which parameter this should be applied to; however, the most likely candidate would be to slightly increase the weighting constant γ_r in Equation 7-20 to cause the resulting action potential to occur appropriately sooner. However, the net effects on the ensuing responses of the Neurological Module were not affected in any detectable way other than a shift all responses by 3 milliseconds, which was deemed negligible compared to the much longer delays afforded by myelination (100 – 500 ms). Thus, peptidergic and non-peptidergic C-neurons were combined into a single class of C-type neurons for the purposes of the Sensitivity Module (three right-most columns in Table 7-6).

Including the non-nociceptive Aβ primary afferent neuron in the existing formulation proved problematic due to the mechanical sensitivity term, p_i, in the denominator of Equation 7-19. The reader may note there are no columns for Aβ neurons in Table 7-6 for this reason. The mechanical sensitivity of non-nociceptive Aβ neurons (< 0.00001 MPa) (Abraira and Ginty, 2013), defined as the minimum stress or pressure required to stimulate an action potential, is far below that of the nociceptive neuron's mechanical sensitivities (> 0.2 MPa). Scaling the input currents up so dramatically through a very small value of p_i caused unnatural behaviours of the Aβ primary afferent neuron (Figure 7-8). Since the Aβ neuron activity needed to saturate at very low pressures relative to the other two neurons, a makeshift logarithmic function

was used in place of the convolution approach outlined above (Equation 7-22). Equation 7-22 generates a shape that immediately exceeds the minimum input current of 1.26 pA (Section 7.5.1) for very small positive values of $\sigma(t)$ that quickly saturate (Figure 7-8). The constants were derived to facilitate a useful interaction of the second- and third-order neurons in the Neurological Module.

$$I_{A\beta}(t) = 2.45 \ln(59.2\, \sigma(t) + 1) + 1.25 \tag{7-22}$$

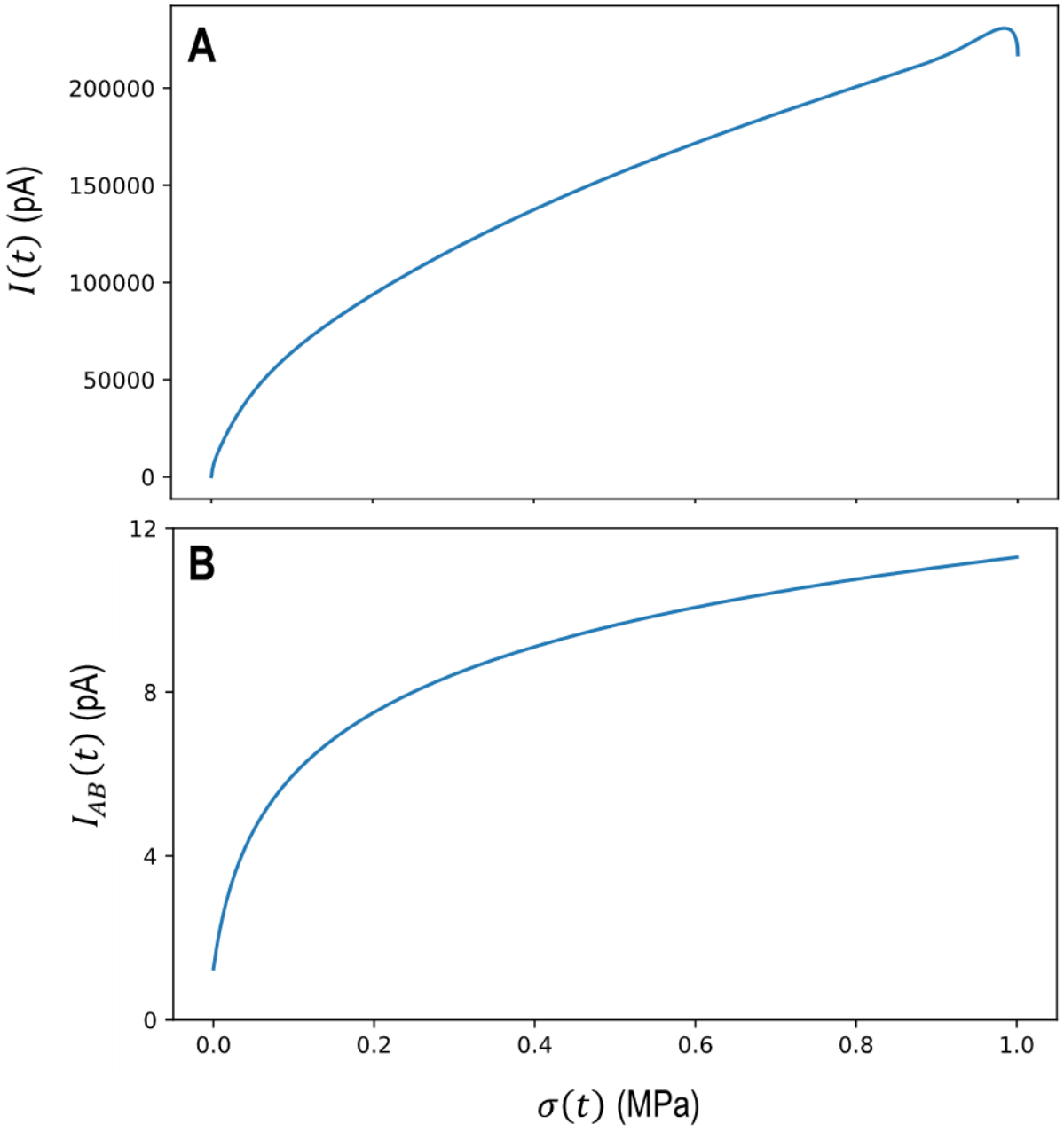

Figure 7-8: Input Currents for the Aβ Primary Afferent Neuron as a function of Tissue Stress for a 1.0 MPa Pressure-Pain Threshold Application. Panel A is the plot generated using Equations 7-19 to 7-21, Panel B is the correction using Equation 7-22. Note that Hodgkin-Huxley Neuron models become unstable at currents greater than 30 pA.

Aδ and C nociceptive neurons were distinguished by modulating the weightings of the phase-scaling parameters γ_r, γ_s, and γ_u in Equation 7-20. While it is understood to be a simplification (Handwerker, 2010; Nagi et al., 2019; Perl, 2007), Aδ nociceptive neurons transmit "fast" pain while C nociceptive neurons transmit "slow" pain (Basbaum et al., 2009; Braz et al., 2014; Ghitani et al., 2017). Initially, the planned distinction between these neuron types was to be isolated to their conduction velocities, however, adjusting conduction velocity alone could not sufficiently account for the persistence of "slow" pain following direct stimulation of C nociceptive fibres (Schmidt et al., 1995). The Aδ nociceptive neurons used the values of γ_r, γ_s, and γ_u that held the same relative weighting as the Aβ primary afferent neurons in Gerling et al (Gerling et al., 2018), normalized to limit gain (Table 7-6). The ultra-slow phase-scaling constant γ_u was increased by a factor of 2.5 for the C nociceptive fibres, and the other two phase-scaling constants were reduced to prevent gain, the rapid phase-scaling constant disproportionately so to exaggerate this effect. The resulting kernel function using the constants in the C-fibre columns of Table 7-6 showed an elongated, flatter decline than the corresponding values from the Aδ columns (Figure 7-9). This change caused a longer train of action potentials for the same input stimulus in C nociceptive neurons compared to the Aδ nociceptive neurons, as would be expected (Basbaum et al., 2009; Pitcher and Henry, 2004; Schmidt et al., 1995).

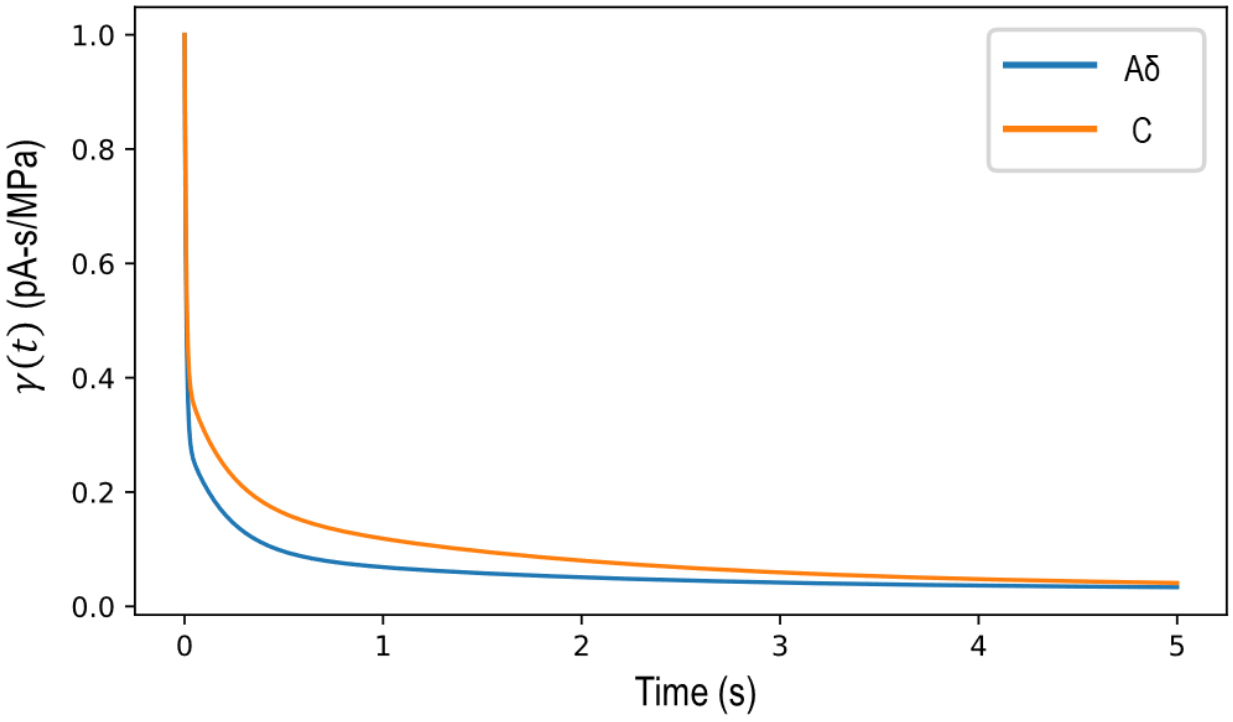

Figure 7-9: Comparison of Kernel Functions $\gamma(t)$ for Aδ (blue) and C (orange) Primary Afferent Neurons. The units of $\gamma(t)$ are such to make the Equation 7-19 output a current in pA.

The greater area under the C-fibre $\gamma(t)$ would also make it more sensitive to stresses. To correct this, both kernel functions were simulated over the full range of possible $\sigma_{PPT}(t)$ curves to adjust their overall sensitivity using the logarithmic scaling function in Equation 7-21. Initially, the shape of $s(x)$ was not assumed but was to be fit to PPT data under the following scenario: for a neuron of sensitivity p_i, a PPT whose peak pressure equals σ_m generated by Equation 7-1 should generate an input current $I(t)$ that can

elicit a peak firing rate of 21 Hz. In other words, Equation 7-21 was developed to answer the question: "What is the minimum linear scaling factor needed to cause a neuron to fire at its minimum firing rate when applying a stress equal to that neuron's mechanical threshold?". This additional scaling factor was needed since without it, the Sensitivity Module would only be sensitive to the rate-of-change of stress, not stress magnitudes, which would be incompatible with the variation in PPT data observed under a constant rate of stress application (Chesterton et al., 2003; Lacourt et al., 2012; Melia et al., 2015).

Simulations were run using seven evenly spaced peak stress from 0.4 MPa to 1.6 MPa, representing the 5th to 95th %ile of PPT data from Chapters 3 and 4. A range of values of $s(\sigma_m)$ in increments of 0.1 were simulated to determine the ensuing peak firing rate of the primary afferent neuron. The minimum value of $s(\sigma_m)$ required to evoke a 21 Hz peak firing rate or higher was then tracked and fit to peak stress, which represents the peak stress applied, using a least-squares approach. The data and logarithmic fits are shown in Figure 7-10. Quadratic fits were initially considered and did have better fit coefficients to the data ($R^2 > 0.9985$ for quadratic compared to $R^2 > 0.9675$ for logarithmic), however the logarithmic fits were preferred since they increase monotonically, and large stresses (> 3.0 MPa) could generate negative values of $s(\sigma_m)$ using the quadratic fit. The values for s_1 presented in Table 7-6, corresponding to the parameters the Sensitivity Module used, were 1.0 larger than the fit values depicted in Figure 7-10. This additional buffer was included to ensure neuron responsiveness in instances where the logarithmic fit underpredicted the empirically derived value.

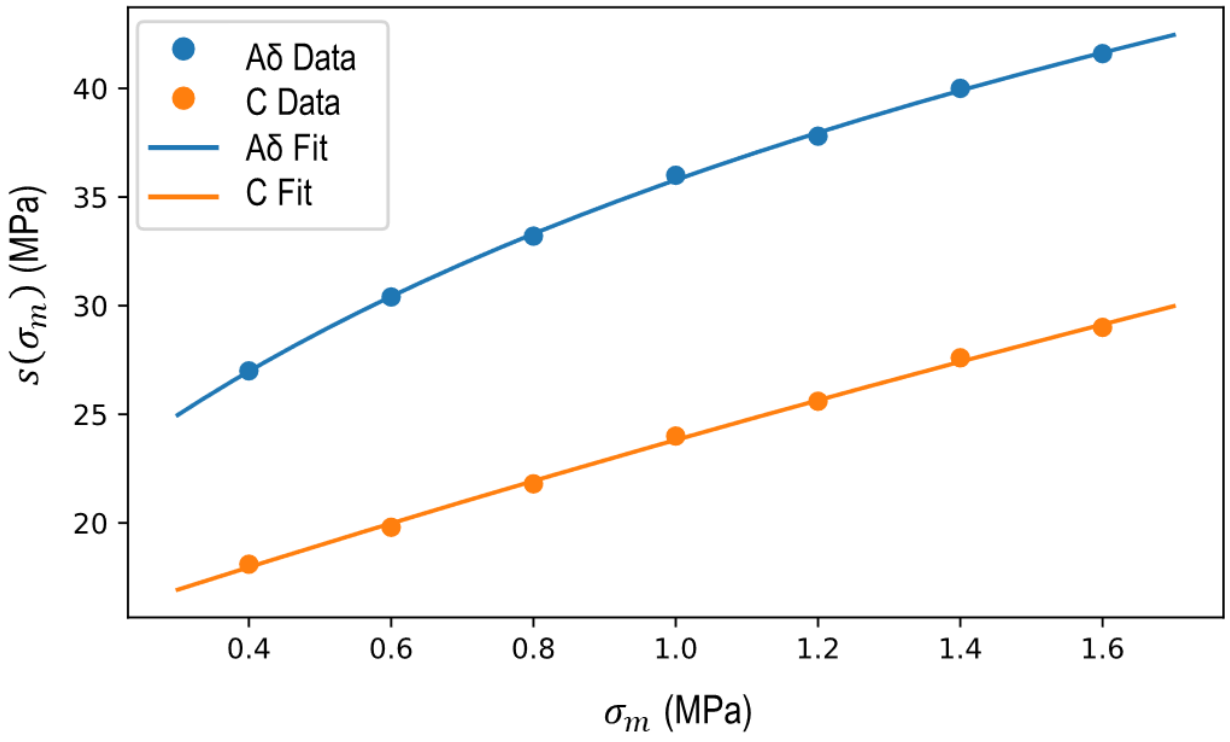

Figure 7-10: The Relation Between Peak Stress, σ_m, and a scaling function of peak stress, $s(\sigma_m)$ using the Smoothly Interpolated Linear PPT Function. Dots indicate the simulated minimum values of $s(\sigma_m)$ while the solid lines indicate quadratic functions fit to the simulated data; The data and fit for the Aδ kernel function are in pale blue, while those for the C kernel function are in orange. Note that $\sigma_m = p$ for these data.

The term ψ_{NT} varied based on the specific neuron type: Aδ or C; and tissue: skin, annulus, or ligament (Table 7-6). The first step involved linearly scaling ψ_{NT} based on the relative concentration of PGP9.5 across the three tissues as reported in Chapter 6 (Table 6-4). A second multiplicative factor of 1.042 was then applied to all Aδ thresholds, to approximate the distributions reported by authors comparing Aδ and C fibre thresholds within a subject (Adriaensen et al., 1983; Koltzenburg et al., 1997).

7.4.2 Synopsis of the Sensitivity Module

The Sensitivity Module generated three distinct time-varying currents from a single time-varying stress input $\sigma(t)$ that were applied to the Neurological Module:

1. A nociceptive current $I_{A\delta}(t)$ using Equations 7-19 to 7-21 to the Aδ primary afferent neuron
2. A nociceptive current $I_C(t)$ using Equations 7-19 to 7-21 to the C primary afferent neuron
3. A non-nociceptive current $I_{A\beta}(t)$ using Equation 7-22 to the Aβ primary afferent neuron

7.5 Neurological Module

The Neurological Module received the time-varying input currents, $I(t)$, and used them to propagate action potentials through a simplified spinal cord circuit to reach the brainstem. In addition to the stress-derived currents from the Sensitivity Module, two additional inputs were converted into currents, each received by dedicated neurons: one for the current viscoelastic state of the tissue, represented by the function $\zeta(t)$, and another for the current level of muscle fatigue, represented by the function $\phi(t)$. The first draft of the Neurological Module, the one used to develop the Sensitivity Module, did not include the viscoelastic state nor the muscle fatigue neuron, but retained all other components and features.

Tables 7-7 and 7-8 contain the connectivity and physical properties of each neuron in the model. The values were generated for each iteration of the model and used during Equations 7-23 and 7-24 were used to govern the relationship between axon diameter, d, in Table 7-8 and conduction velocity, v, where Equation 7-23 was used for myelinated neurons (Hursh, 1939), and Equation 7-24 was used for unmyelinated neurons (Kandel et al., 2013). The connectivity between the primary afferent neurons and interneurons in Table 7-7 is based on consolidating common features from Figure 1 in Guo and Hu, (2014), Figure 1 in Cordero-Erausquin et al., (2016), and Figure 4 in Braz et al., (2014). The connectivity of the VS neuron is inferred from Solomonow, (2012) and the data in Chapter 3, while the connectivity of the FL neuron is based on the analgesic pathways outlined in Lima et al., (2017).

$$v = 6d \tag{7-23}$$

$$v = \frac{16d + 20}{13} \tag{7-24}$$

Table 7-7: Neuron Object Labels and Connectivity. Plus signs in parentheses (+) indicate excitatory connections, minus signs indicate inhibitory connections (-). Inputs listed as a function of time, t, are considered excitatory but do not function through the same mechanism as another named neuron object. The Brainstem neuron output is a decision algorithm described in Section 7.5.4.

Neuron	Acronym	Inputs	Outputs
Aβ Primary Afferent	Aβ	• $I_{A\beta}(t)$	• VC (+) • II (+)
Aδ Primary Afferent	Aδ	• $I_{A\delta}(t)$	• PN (+) • II (-)
C Primary Afferent	C	• $I_C(t)$	• PN (+) • II [A] (-) • TI (-)
Projection Neuron	PN	• Aδ (+) • C (+) • VC (+) • II (-)	• BN (+)
Vertical Cell	VC	• Aβ (+) • II (-) • TI (-) • VS (+)	• PN (+)
Inhibitory Interneuron	II	• Aβ (+) • Aδ (-) • C (-) • FS (+)	• PN (-) • VC (-)
Tonic Inhibitor	TI	• $I_{TI}(t)$ • C (-)	• VC (-)
Viscoelastic State Neuron	VS	• $\zeta(t)$	• VC (+)
Fatigue Level Neuron	FL	• $\phi(t)$	• PN [B] (-) • II (+)
Brainstem Neuron	BN	• PN (+)	• Λ_i

[A]This output could also be inhibited by the FL neuron

[B]This output used a slightly altered inhibitory connection, see Section 7.5.2.

Table 7-8: Additional Neuron Properties. Numbers in square brackets indicate an inclusive uniform distribution with the numbers given as the lower and upper bounds, respectively. Numbers given with a μ and η indicate the mean and standard deviation of a normal distribution, respectively. Axon lengths and refractory periods are derived from Gerstner et al., (2014); axon diameters and activation thresholds are derived from Kandel et al., (2013); see text for input current and conduction velocity derivation.

Property	**Aβ**	**Aδ**	**C**	**PN**	**VC**	**II**	**TI**	**VS**	**FS**	**BN**
Location	Periphery			Spinal Cord				Periphery	Brainstem	
Myelinated	Yes		No	Yes				No	Yes	
Axon Length	[0.095, 0.102] m			[0.95, 1.02] m	[0.005, 0.040] m			[0.095, 0.102] m	[0.005, 0.040] m	
Axon Diameter	μ: 9.0 μm, η: 1.5 μm	μ: 3.5 μm, η: 1.0 μm	μ: 0.3 μm, η: 0.1 μm	μ: 9.0 μm, η: 0.5 μm	μ: 7.0 μm, η: 1.5 μm			μ: 0.3 μm, η: 0.1 μm	μ: 7.0 μm, η: 1.5 μm	
Refractory Period	[5, 7] ms	[7, 12] ms		[5, 10] ms				[7, 12] ms	[5, 10] ms	
Activation Threshold	μ: 30 mV, η: 2.5 mV									
Input Current	$I_{A\beta}(t)$	$I_{A\delta}(t)$	$I_C(t)$	0.0 pA			1.8 pA	$\zeta(t)$	$\phi(t)$	0.0 pA
Conduction Velocity Equation	7-23		7-24	7-23				7-24	7-23	

7.5.1 Hodgkin-Huxley Neuron Formulation

Neuron objects were implemented using the Hodgkin-Huxley neuron model (Hodgkin and Huxley, 1952a). This model describes the change in membrane voltage based on five parameters:

1. The existing membrane voltage, $V(t)$ in mV.
2. The activation constant of the potassium ion channels, n, bounded between 0 and 1.
3. The activation constant of the sodium ion channels, m, bounded between 0 and 1.
4. The inactivation constant of the sodium ion channels, h, bounded between 0 and 1.
5. The external electrical current applied to the neuronal membrane, or input current $I(t)$, in pA.

The model consists of a series of four ordinary differential equations that govern how $V(t)$, n, m, and h change with respect to each other over time.

$$\frac{dV(t)}{dt} = \frac{1}{C_m}\left[I(t) - \left(I_K(t) + I_{Na}(t) + I_L(t)\right)\right] \tag{7-25}$$

$$\frac{dn}{dt} = \alpha_n\big(V(t)\big)(1-n) - \beta_n\big(V(t)\big)\,n \tag{7-26}$$

$$\frac{dm}{dt} = \alpha_m\big(V(t)\big)(1-m) - \beta_m\big(V(t)\big)\,m \tag{7-27}$$

$$\frac{dh}{dt} = \alpha_h\big(V(t)\big)(1-h) - \beta_h\big(V(t)\big)\,h \tag{7-28}$$

In Equation 7-25, the change in membrane voltage $V(t)$ equals the input current $I(t)$ minus the sum of the currents arising from potassium, sodium, and leaky ion channels in the membrane ($I_K(t)$, $I_{Na}(t)$, and $I_L(t)$), divided by the membrane capacitance, C_m. Equations 7-26 through 7-27 all have the same form, taking the difference between the product of an "open state" function of the membrane voltage, $\alpha\big(V(t)\big)$, and one minus the appropriate ion channel constant, and the product of a "closed state" function of the membrane voltage, $\beta\big(V(t)\big)$, and the appropriate ion channel constant.

The formula to describe each of the membrane channel currents in Equation 7-25 are shown in Equations 7-29 through 7-31.

$$I_K(t) = g_K\, n^4\, (V(t) - V_K) \tag{7-29}$$

$$I_{Na}(t) = g_{Na}\, m^3 h\, (V(t) - V_{Na}) \tag{7-30}$$

$$I_L(t) = g_L(V(t) - V_L) \tag{7-31}$$

Where g_K, g_{Na}, and g_L are the membrane conductances in mS/cm^2 of the potassium, sodium, and leaky ion channels; the terms V_K, V_{Na}, and V_L are the equilibrium voltages for each channel in mV. Each of these currents increases as the membrane voltage $V(t)$ gets further away from the equilibrium voltages, or when each of n, m, or h increase as the membrane conductances are assumed to be constant.

Unlike the previous equations in this section, the open and closed state functions $\alpha\big(V(t)\big)$ and $\beta\big(V(t)\big)$ in Equations 7-32 through 7-37 do not have a standard form or represent physiology but rather are fit to conductance and equilibrium voltage data for a given population of neurons. The specific form of these functions as listed below describes mammalian pyramidal neurons, adapted to define the resting membrane potential as 0 mV instead of the original -65 mV as published (Gerstner et al., 2014).

$$\alpha_n\big(V(t)\big) = \frac{0.02\ (V(t) - 40)}{1 - \exp\left(-\frac{V(t) - 40}{9}\right)} \tag{7-32}$$

$$\beta_n\big(V(t)\big) = \frac{-0.002\ (V(t) - 40)}{1 - \exp\left(\frac{V(t) - 40}{9}\right)} \tag{7-33}$$

$$\alpha_m\big(V(t)\big) = \frac{0.182\ (V(t) - 30)}{1 - \exp\left(-\frac{V(t) - 30}{9}\right)} \tag{7-34}$$

$$\beta_m\big(V(t)\big) = \frac{-0.124\ (V(t) - 30)}{1 - \exp\left(\frac{V(t) - 30}{9}\right)} \tag{7-35}$$

$$\alpha_h\big(V(t)\big) = 0.25\ \exp\left(-\frac{V(t) + 25}{12}\right) \tag{7-36}$$

$$\beta_h\big(V(t)\big) = \frac{0.25 \exp\left(\frac{V(t) - 3}{6}\right)}{\exp\left(\frac{V(t) + 25}{12}\right)} \tag{7-37}$$

Where $\exp(x)$ denotes the natural exponent of x.

Table 7-9 lists the initial states of $V(t)$, n, m, and h, while Table 7-10 lists the values and units of the membrane conductances and equilibrium voltages. C_m was set to 1.0 µF/cm, which effectively removes it from Equation 7-25.

Table 7-9: Initial States for $V(t)$, n, m, and h.

Parameter	Initial Value
V_0	0.0
n_0	0.10509
m_0	0.04975
h_0	0.62246

Table 7-10: Conductances and Equilibrium Voltages for Each Ion Channel. Conductances taken from Table 2.1 in (Gerstner et al., 2014). Original equilibrium voltages V_K and V_{Na} were shifted by +65 mV to allow a resting membrane potential of 0 mV, then V_L was determined analytically to set Equation 7-25 to equal zero given a membrane voltage $V(t)$ of 0 mV and removing the input current term, $I(t)$.

Channel	Conductance	Equilibrium Voltage
Potassium	$g_K = 35.0$ mS/cm^2	$V_K = -12.0$ mV
Sodium	$g_{Na} = 40.0$ mS/cm^2	$V_{Na} = 120.0$ mV
Leaky	$g_L = 0.3$ mS/cm^2	$V_L = -1.056$ mV

There are two notes regarding the constants in this section. The first is that they have been derived using the millisecond as the base unit of time instead of the second. While the channel conductances can be scaled accordingly, the α and β functions should not undergo this unit transformation without being re-fit. Since the present model operates in seconds, this computationally involved converting times from seconds into milliseconds to determine the electrical properties before converting back into seconds for the rest of the module. The other note is that a dimension analysis will reveal that the solution to Equation 7-25 has the units mV/cm instead of mV. This appears to derive from channel conductances in Table 7-10 being expressed per unit area (cm^2) while the capacitance term C_m is expressed per unit length (cm). Electrical capacitance is frequently expressed per unit area of the capacitor, in this case, the cross-sectional area of the channel. The numerical value of C_m being 1.0 allows a convenient workaround since raising 1.0 to any power, including 0.5 which would be needed to rectify the unit misalignment, equals 1.0, and indeed may have been a typographical error that never needed to be rectified form the original work (Hodgkin and Huxley, 1952a).

Input Currents

Input currents to each of the ten neurons are listed in Table 7-8. The primary afferent neurons, Ab, Ad and C all had their own unique terms from the Sensitivity Module: $I_{A\beta}(t)$, $I_{A\delta}(t)$, and $I_C(t)$. The TI neuron, activated by $I_{TI}(t)$, had a constant input current of 1.8 pA ($I_{TI}(t)$ = 1.8 pA) in order to maintain a constant firing rate of 32 Hz (Yasaka et al., 2010). The VS and FL neurons had their own dedicated input currents $\zeta(t)$ and $\phi(t)$ respectively to reflect the different states discussed in Chapter 5. The remaining neurons had their $I(t)$ set to 0 pA.

The relationship between firing rate and a tonic value of $I(t)$ was empirically determined by simulating firing rates to a range of currents from 1 pA to 8 pA (Figure 7-11). The minimum current required to generate any tonic firing was 1.26 pA, corresponding to a firing rate of 21 Hz; values of $I_{ext}(t)$ greater than this threshold were logarithmically related to tonic firing rates, F_{Tonic} (Equation 7-38).

$$F_{Tonic} = 20.220 \ln(I(t) - 0.4091) + 25.502 \quad (7\text{-}38)$$

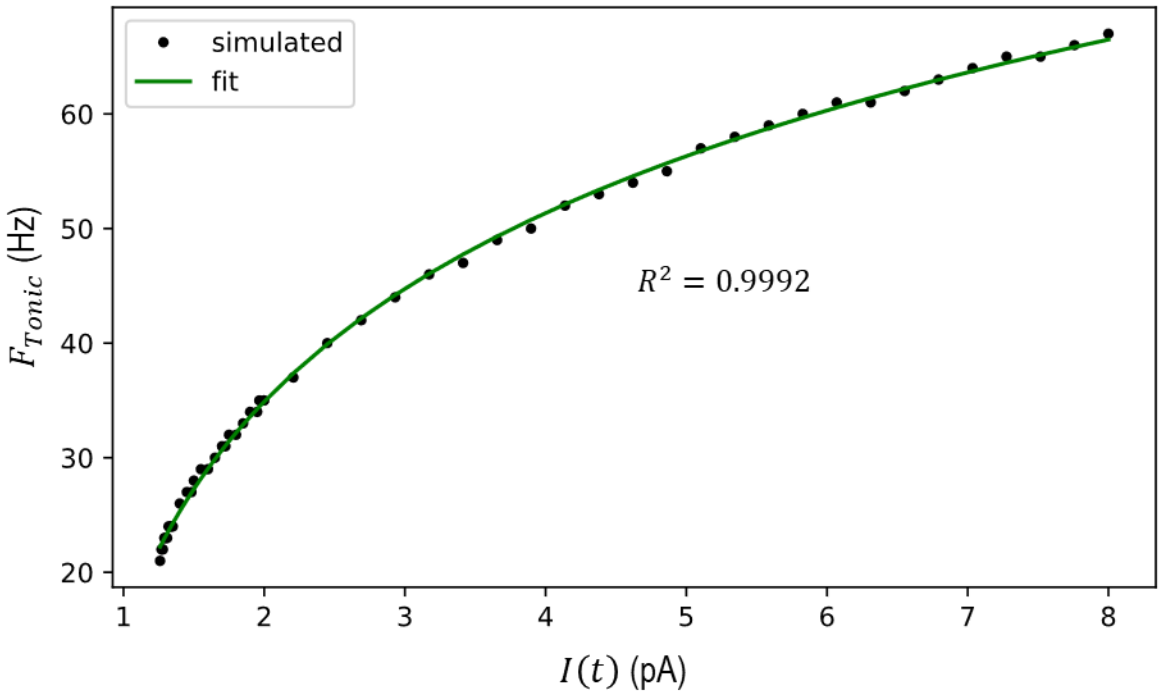

Figure 7-11: Simulated and Fit Tonic Firing Rates versus External Current for the Given Parameters. The black dots indicate individual tonic firing rate simulations using the given current applied continuously for one second, the green solid line shows data fit using Equation 7-38.

Both $\zeta(t)$ and $\phi(t)$ were constant $I(t)$ functions informed by Equation 7-38, however both functions caused additional effects. The mean collagen fibre length term from Table 7-4, μ, was multiplied by 1.1 when $\zeta(t)$ was greater than 1.26 pA, which roughly corresponds to a 10% increase in allowable flexion range of motion as measured in Chapter 3. The inhibitory connection between the C and II neurons was removed when the mean value of $\phi(t)$ exceeded 1.26 pA, representing pre-synaptic inhibition of this connection during exercise-induced hypoalgesia (Koltyn et al., 2014; Lemley et al., 2015).

7.5.2 Neuron-Neuron Interactions

Equation 7-25 describes how the membrane voltages, $V(t)$, of the neurons in Table 7-7 change over time. Whenever any neuron's membrane voltage would exceed its activation threshold (Table 7-8), it would activate all its outputs (Table 7-7). This entailed waiting a set amount of time based on that neuron's conduction velocity, v, (Equation 7-23 or 7-24) and its axon length, l_{axon} (Table 7-8), termed the post-synaptic potential delay time, or t_{PSPd} (Equation 7-39).

$$t_{PSPd} = \frac{l_{axon}}{v} \tag{7-39}$$

The net result of the fired action potential would be to open the sodium ion channels if excitatory (plus sign in Table 7-7) or the potassium ion channels if inhibitory (minus signs in Table 7-7) (Hodgkin and Huxley, 1952b). To affect the downstream neurons, a post-synaptic potential equation, $k(t)$ (Equation 7-40), was applied to either the sodium activation equation (Equation 7-27) or the potassium activation (Equation 7-26) and shifted by the time taken for the action potential to reach its target, t_{PSPd}.

$$k(t) = k_0 \frac{\exp(k_1(t - t_{PSPd}) + k_2)}{(1 + \exp(k_3(t - t_{PSPd}) + k_4))} \tag{7-40}$$

The specific dynamics of $k(t)$ are dependent on the neurotransmitter the neuron releases (De Biasi and Rustioni, 1988; Lu and Perl, 2005, 2003; McCormick, 1989; Yoshimura and Jessell, 1990; Yoshimura and Nishi, 1995). The model used glutamate as the excitatory neurotransmitter (El Mestikawy et al., 2011; Lu and Perl, 2005; Yasaka et al., 2010; Yoshimura and Jessell, 1990), and GABA (gamma-aminobutyric acid) as the inhibitory neurotransmitter (Lu and Perl, 2003; McCormick, 1989; Yasaka et al., 2010; Yoshimura and Nishi, 1995). The constants in Table 7-11 were used to generate $k_+(t)$, the excitatory post-synaptic potential function, and $k_-(t)$, the inhibitory post-synaptic potential function, with the resulting waveforms. The constants in Table 7-11 were generated by least-squares fitting $k(t)$ to the "representative" waveforms presented in Figure 1Ab of (Yoshimura and Jessell, 1990) ($k_+(t)$) and Figure 1C of (McCormick, 1989) scaled to have a peak amplitude of 1.0, and are depicted in Figure 7-12.

Table 7-11: Post-Synaptic Potential Function, $k(t)$, Constants.

Term	k_0	k_1	k_2	k_3	k_4
Excitatory $k_+(t)$	0.9158	-43	0.65	-820	6.8
Inhibitory $k_-(t)$	0.8306	-7.5	0.47	-300	6.7

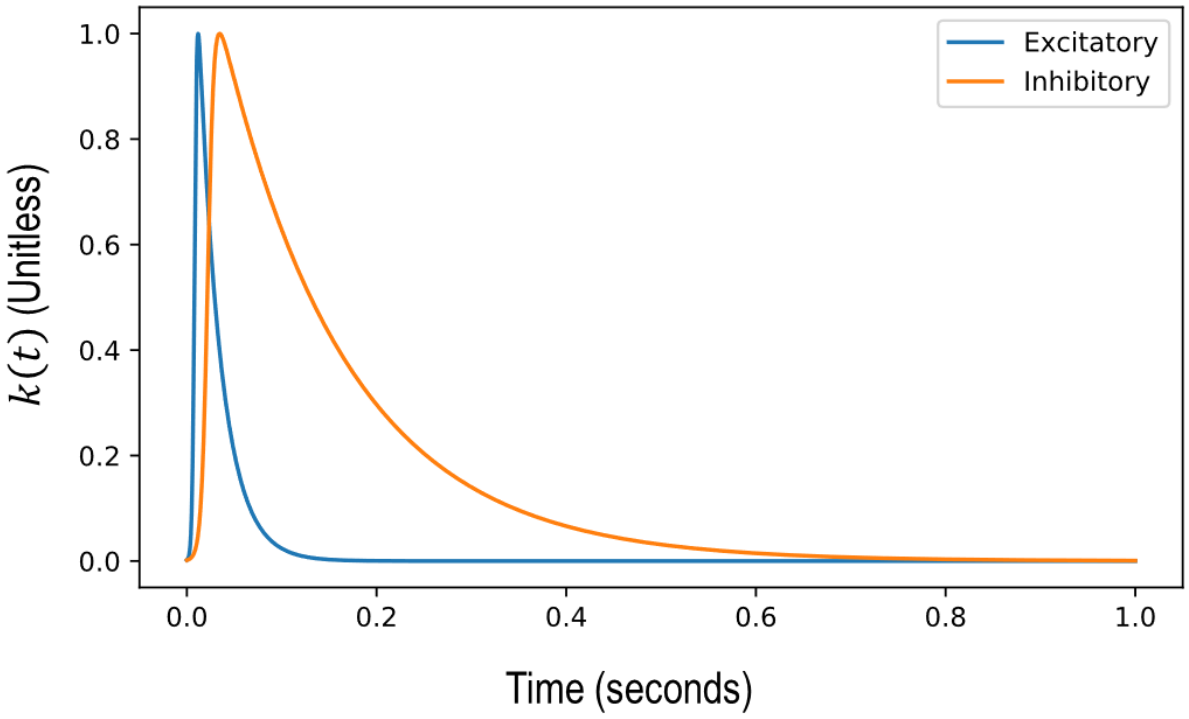

Figure 7-12: The Shapes of the Two Post-Synaptic Potential Functions. The Excitatory shape, $k_+(t)$, is in blue, and the inhibitory shape, $k_-(t)$, is in orange. Both waveforms use a delay, t_{PSPd}, of 0.0 seconds in this figure.

The implementation of $k_+(t)$ and $k_-(t)$ in the Hodgkin-Huxley Neuron formulation is presented in Equations 7-41 and 7-42, which replaced Equations 7-26 and 7-27 respectively. Equation 7-28 was not altered.

$$\frac{dn}{dt} = \left[\alpha_n\big(V(t)\big) + s_{inhibit}k_-(t)\right](1-n) - \beta_n\big(V(t)\big)\,n \tag{7-41}$$

$$\frac{dm}{dt} = \left[\alpha_m\big(V(t)\big) + s_{excite}k_+(t)\right](1-m) - \beta_m\big(V(t)\big)\,m \tag{7-42}$$

The linear scaling factors $s_{inhibit}$ and s_{excite} in Equations 7-41 and 7-42 respectively were set to 0.01 and 0.08 respectively for all output connections in Table 7-7 except for the FL neuron's inhibitory output to the PN neuron, this used a value of 0.00357. The values for $s_{inhibit}$ and s_{excite} were determined in tandem with each other using an iterative trial-and-error approach to ensure the following conditions:

1. In the absence of any inhibitory inputs from $k_-(t)$, an excitatory firing rate of 21 Hz in one pre-synaptic neuron would trigger a firing rate of 21 Hz in the post-synaptic neuron
2. In the presence of an inhibitory firing rate of 21 Hz from $k_-(t)$, excitatory firing rate of 21 Hz in one pre-synaptic neuron would not trigger any excitatory activity in the post-synaptic neuron
3. In the presence of an inhibitory firing rate of 21 Hz from $k_-(t)$, an excitatory firing rate of 21 Hz in two pre-synaptic neurons would trigger a firing rate of 21 Hz in the post-synaptic neuron

In other words, one pre-synaptic excitatory signal will excite its targets, but one pre-synaptic inhibitory signal will stop one pre-synaptic excitatory signal from exciting its targets. Given the connectivity network in Table 7-7, satisfying these three criteria allowed for the following Neurological Module behaviours.

Scenario 1: For low stresses where only the Aβ neuron will fire action potentials

- The Aβ neuron will send excitatory signals to the VC and II neurons.
- The VC is under steady inhibition from the TI neuron and will not respond to the Aβ neuron's excitatory inputs.
- The II neuron will get excited, which will inhibit the VC and PN neurons. The VC now has two pre-synaptic inhibitory signals, meaning a second excitatory signal beyond the one already provided by the Aβ neuron will still not activate the VC. The PN neuron has one inhibitory input, which will cancel out one excitatory input if one existed, effectively "closing the gate" in the Gate Control/Neuromatrix framework (Braz et al., 2014; Melzack, 1999).

Scenario 2: For stresses applied at a high rate such that the Aβ and Aδ neurons are activated at the same frequency, but the C neuron is not activated

- The Aβ neuron will excite the VC and II neurons as above, but the Aδ neuron will also excite the PN and inhibit the II neuron.
- The slower Aδ neuron signals will first hit an inhibited PN neuron, initially sending no signal to the BN neuron, however, since the Aδ neuron will also inhibit the II neuron, the II will not be able to inhibit the PN, allowing the Aδ neuron to activate the PN neuron.

Scenario 3: For stresses applied at a low rate such that the Aβ and C neurons are activated at the same frequency, but the Aδ neuron is not activated

- The Aβ neuron will excite the VC and II neurons as above, and C neuron will excite the PN and by inhibiting the II neuron as the Aδ neuron did, but the C neuron will also inhibit the TI neuron.
- Inhibiting both the TI and II neurons means the Aβ neuron can excite the VC neuron, leading to the PN and BN neurons being further excited.
- The slower decaying but smaller amplitude $I(t)$ function means the C neuron's firing rate will persist for longer but be at a lower peak frequency than when just the Aβ and Aδ neurons were activated, causing a "slow pain" sensation relative to the Aδ neuron's "fast[er] pain" (Basbaum et al., 2009; Julius and Basbaum, 2001).

Scenario 4: For stresses activating all three primary afferent neurons

- The Aβ neuron will excite the VC and II neurons, then the Aδ neuron will excite the PN and inhibit the II neuron, and lastly the C neuron will excite the PN and inhibit the II and TI neurons.
- The Aδ-neuron mechanism of removing the II inhibition on PN occurs first, but the PN's activity is then compounded by the C-neuron mechanism of removing TI inhibition from the VC, giving the PN three effective excitatory signals: one from the Aδ neuron, one from the C neuron, and one from the VC neuron.

Scenario 5: When the VS neuron is active

- Low stresses will not generate any activity in the BN neuron despite the additional excitatory input on the VC neuron from the VS neuron since the VC neuron will have two inhibitory signals, one from the II and one from the TI.

- The Aδ or C neuron mechanisms will occur at similar thresholds but will elicit greater PN activity since the VC has an additional excitatory input.

Scenario 6: When the FL neuron is active

- An additional layer of inhibition is applied to the PN and VC from the II, and a second layer of inhibition is directly applied to the PN neuron.
- The Aδ and C neurons must both be highly active and the Aβ neuron's firing rate must be saturated due to its $I_{A\beta}(t)$ function for the PN neuron to excite the BN neuron.

While these scenarios were derived assuming all inputs fired at a frequency of 21 Hz for a fixed duration, the ability for a neuron to activate another neuron is firing-rate dependent. Although one inhibitory input cancels out one excitatory input when both occur at 21 Hz, the excitatory input can still "break through" the inhibitory input if the excitatory input has a sufficiently high frequency. The inhibitory function $k_{-}(t)$ also sums more quickly than $k_{+}(t)$ at higher rates due to its slower decay even after applying the correction factor s. This means that an inhibitory input may still cancel an excitatory input even if the excitatory input has a higher frequency.

7.5.3 Implementation of the Neurological Module over Time

The neurons in the Neurological Module excite or inhibit other neurons using the connectivity in Table 7-7 and the properties in Table 7-8. Each neuron's membrane potential $V(t)$ was governed by Equations 7-25, 7-28, 7-41, and 7-42, as well as the input functions $I_{A\beta}(t)$, $I_{A\delta}(t)$, $I_C(t)$, $\zeta(t)$, and $\phi(t)$. Each of these time-varying inputs were 10 seconds in length and were divided into 50001 time-steps. The subscript q is used to count time-steps.

When a neuron's membrane potential exceeded its activation thresholds in Table 7-8, Equation 7-40 was used to update Equations 7-41 and 7-42, which then fed back into Equation 7-25. This system of equations was iterated through with each time-step of the model and solved using a Forward Newton-Euler Approximation (Equation 7-43). This approach was chosen over a more accurate solving method, like a Runge-Kutta 45 solver, in favour of the Forward Newton-Euler's computation speed. Additionally, optimized solvers such as the `odeint` function in the `scipy` package in Python were avoided since Equations 7-41 and 7-42 needed to respond to the post-synaptic potential function (Equation 7-40) before a full solution could be implanted. Using these optimized solvers would have required too many function calls to warrant any computational savings, or would have necessitated re-running the entire Neurological Module after each action potential was fired.

$$y_{q+1}(t) = y_q(t) + y'_q(t)\Delta t \tag{7-43}$$

For any time-varying function, $y(t)$, with a known first derivative with respect to time, $y'(t)$, the next instance of $y(t)$, y_{q+1} will equal the sum of the current instance of $y(t)$, $y_q(t)$, with the product of the derivative at the qth time point $y'_q(t)$ and the time between the qth and $q+1$ time point, Δt. Although the Neurological Module's time-resolution was reasonably high, Δt = 0.0002 s, an additional intermediate step was taken to ensure the numerical stability of Equation 7-25.

$$y_{q^+}(t) = y_q(t) + \frac{y'_q(t)\Delta t}{2} \tag{7-44}$$

$$y_{q+1}(t) = y_{q^+}(t) + \frac{y'_{q^+}(t)\Delta t}{2} \tag{7-45}$$

The intermediate step in Equations 7-44 and 7-45 is indicated with the subscript q^+. While no values at these intermediate time points were used to fire action potentials using Equation 7-40, the values of $V(t)$, n, m, and h, and their derivatives (Equations 7-25, 7-28, 7-41, and 7-42) were computed at these times.

The computation done for the qth time-step of the Neurological Module were as follows:

1. The refractory period counter for each neuron was decreased by Δt if it was non-zero.
2. The Hodgkin-Huxley series of ordinary differential equations, 7-25, 7-28, 7-41, and 7-42 were solved using the two-part Newton-Euler Approximation in Equations 7-44 and 7-45.
3. Each neuron was checked to see if it had fired an action potential: The neuron's current membrane voltage, $V_q(t)$ needed to exceed its activation threshold generated from Table 7-8 and its refractory period counter needed to equal zero.
    a. If both requirements were met, an action potential was sent to each of that neuron's targets, as indicated in the "Outputs" column of Table 7-7, and that neuron's refractory counter was set to equal its refractory period.
    b. To send an action potential, the post-synaptic potential function (7-40), was called as $k(t - t_q)$, to be scaled by the appropriate scaling constant based on whether that output was excitatory (s_{excite}) or inhibitory ($s_{inhibit}$).
4. The above steps were repeated for the $q + 1$ time point until reaching the end of the inputted $I(t)$ data.

As an additional note on step 3b. The function $k(t)$ already contains a built-in time-shifting term: t_{PSPd}, however t_{PSPd} only represents the delay that arises from action potentials having a finite conduction velocity. Including the second shifting term, t_q, is necessary to represent the time at which the action potential was triggered.

7.5.4 Brainstem Decision Algorithm

The following criteria were evaluated to determine whether a stress profile $\sigma(t)$ elicited nociceptive neural activity:

- Did an action potential train lasting at least 500 milliseconds occur in the BN neuron?
- Was the peak firing rate of that action potential train greater than 21 Hz?

An action potential train was defined as a set of consecutive action potentials whose peaks are no further than 200 milliseconds apart from each other. A peak firing rate of at least 21 Hz for at least 500 milliseconds was required as the minimum neural activity required to register an Exposure and its associated stress profile as being nociceptive. Twenty-one was chosen since it was the minimum firing frequency that could be generated via external current (Figure 7-11), and 500 milliseconds being a conservative estimate of the time needed to translate sensory information into a perception (Libet et al., 1991).

This decision process was implemented for each of the 100 iterations. The output was a Boolean list of length 100, Λ, where the iteration-specific PPT, p_i, had its own specific decision, Λ_i. The percentage of Λ that was `True` was considered the percentage of people who would generate nociceptive activity from that Exposure, this was labelled using $\Lambda_{\%}$.

7.6 Running the Model

This section lists the major steps and sequence of events taken when the model was run and is intended to give a post-description synopsis. The sequence of events is also graphically depicted in Figure 7-1.

1. The user selects an Exposure from Table 7-1, then indicates a viable tissue corresponding to that Exposure. Values for $\zeta(t)$ and $\phi(t)$ are selected to indicate the current viscoelastic and fatigue states respectively of the person experiencing that Exposure.
2. A $\sigma(t)$ profile for the specific Exposure-Tissue combination was generated from t = 0s to t = 10s with a time step, Δt, of 0.0002 s using one of Equations 7-1, 7-14, or 7-15; other fixed values necessary to generate $\sigma(t)$, such as p_0, were selected or drawn from the appropriate table (Table 7-4, or 7-5).
3. One hundred PPT values were generated using Equation 5-15 from Chapter 5.
4. The Sensitivity Module relied on Equations 7-19 and 7-22, using the constants in Table 7-6. This process was computationally inexpensive, taking approximately 0.5 seconds to convert a $\sigma(t)$ into three $I(t)$ functions for each iteration.
5. Specific neuron object properties were generated using the values and distributions in Table 7-8 and computed using Equations 7-23 and 7-24.
6. The Neurological Module computed the time-varying membrane voltages, $V(t)$, for each neuron iterating through all values of t (Section 7.5.3).
7. The decision algorithm determined the value of Λ_i to either be `True` or `False`.
8. All iterations of p_i were then evaluated by repeating Steps 4 through 7 to compute $\Lambda_{\%}$.

The model was run in two stages. First, PPT exposures were used to determine the effects of $\zeta(t)$ and $\phi(t)$, since the model was built under the assumption that all PPT exposures would elicit nociceptive activity in the absence of these two inputs: $\Lambda_{\%} \equiv 100\%$ in those instances (Section 7.6.1). Second, four scenarios were run for each of the six remaining Tissue-Exposure combinations ($\sigma_{Flex}(t)$, $\sigma_{Fail}(t)$, and $\sigma_{Fail10}(t)$; each for Annulus and Ligament tissues) using representative $\zeta(t)$ and $\phi(t)$ values from the first stage:

1. No input from $\zeta(t)$ or $\phi(t)$, reflecting no prior exposure. (Base)
2. Input from $\zeta(t)$ but not $\phi(t)$, which would follow a non-fatiguing task that generated viscoelastic creep such as prolonged lumbar spine flexion (Howarth et al., 2013a; Shin and Mirka, 2007; Toosizadeh and Nussbaum, 2013). (Viscoelastic)
3. Input from $\phi(t)$ but not $\zeta(t)$, which would follow a fatiguing task that did not generate lumbar spine viscoelastic creep such as moderate to high intensity exercise (Kennedy et al., 2015; Taylor et al., 2000). (Muscle Use)
4. Input from both $\zeta(t)$ and $\phi(t)$, which would follow a task that generate muscle fatigue and lumbar spine creep such as repetitive lifting (Claude et al., 2003; Toosizadeh and Nussbaum, 2013; Yang et al., 2011). (Combined)

7.6.1 Deriving $\zeta(t)$ and $\phi(t)$

The viscoelastic input $\zeta(t)$ was first derived by finding the maximum tonic current that would not alter the peak stress needed to elicit a PPT response during the PPT exposure. This criterion reflects the prolonged flexion exposure from Chapter 3 that did not change PPTs. Implementation-wise, this was done by iterating through values of $\zeta(t)$ by increments of 0.1 pA until a $\sigma_{PPT}(t)$ waveform set to a peak stress of 90% of the generated sensitivity p, generated a $\Lambda_{\%}$ that exceeded 0.05. This should reflect a value of $\zeta(t)$ that could change up to 5% of PPTs by at least 10%, reflecting some individual variation but not a consistent enough effect to modify population-wide characteristics.

Once a value of $\zeta(t)$ was determined, the value for $\phi(t)$ was derived first by taking the mean percentage increase in PPTs between the Pre and Post 10 time points in Chapter 4, 13.6%, and iterating through values of $\phi(t)$ until it effectively increased simulated PPTs by this amount. This involved iterating through values of $\phi(t)$ in increments of 0.1 pA, and determining the minimum percentage increase in applied stress, needed to keep $\Lambda_{\%}$ at 1 for that value of $\phi(t)$. The value of $\phi(t)$ that kept the percentage increase closest to 13.6% was selected for other simulations. This was conducted while holding $\zeta(t)$ at the previously determined value since Chapter 4 reflects an exposure where both $\zeta(t)$ (viscoelastic) and $\phi(t)$ (exercise/fatigue) would be in effect.

7.7 Model Results

A single iteration of the model, the time taken to generate a single value of Λ_i for a 10 second trial, took between 78 and 137 seconds, with an average runtime of 10,107 seconds (2 hours, 48 minutes, and 27 seconds) needed to generate a single value of $\Lambda_{\%}$ on a personal computer with a 2.1 GHz processor with 8.0 GB of RAM. Most of this time was spent evaluating the Hodgkin-Huxley system of ordinary differential equations in Sections 7.5.1 and 7.5.2, and longer runtimes were correlated with a larger total number of action potentials. Sample membrane voltages for PPT exposures are shown in Figures 7-13 through 7-15.

The values for $\zeta(t)$ and $\phi(t)$ were derived to be 12.1 and 9.8 pA respectively, corresponding to tonic firing rates of 75.2 and 70.8 Hz. Incorporating $\zeta(t)$ increased the peak firing rates of BN neurons for which Λ_i was `True` by 4.2 Hz but did not alter BN activity in instances when Λ_i was `False`. No stable value of $\phi(t)$ was found that could afford a 13.6% increase in PPTs across the entire distribution, the desensitizing effects of $\phi(t)$ became asymptotic starting at values of 9.8 pA for a $\zeta(t)$ of 12.1 pA; which effectively increased PPTs by 12.1% across the entire distribution. While $\zeta(t)$had uniform effects across mechanical sensitivities, p, $\phi(t)$ disproportionately affected smaller values of p_i, a trend not seen experimentally (Figure 7-16).

The model predicted a $\Lambda_{\%}$ of either 0% or 100% for all baseline exposures except for the $\sigma_{Fail10}(t)$ exposure in AF tissues (Table 7-12). Incorporating $\zeta(t)$ only resulted in minor changes to $\Lambda_{\%}$, and only if $\Lambda_{\%}$ did not equal zero or one. Incorporating $\phi(t)$ had a dramatic effect on $\Lambda_{\%}$ for the $\sigma_{PPT}(t)$ exposure in skin and the $\sigma_{Fail10}(t)$ exposure in AF tissues, decreasing the value of $\Lambda_{\%}$ by 70% or more for these exposures; $\phi(t)$ did slightly reduce $\Lambda_{\%}$ in the SILC's $\sigma_{Fail}(t)$ condition, but did not alter $\Lambda_{\%}$ for any other tissue-exposure combinations. There were no observable interaction effects when $\zeta(t)$ and $\phi(t)$ were both in effect beyond the changes occurring when only $\phi(t)$ was in effect.

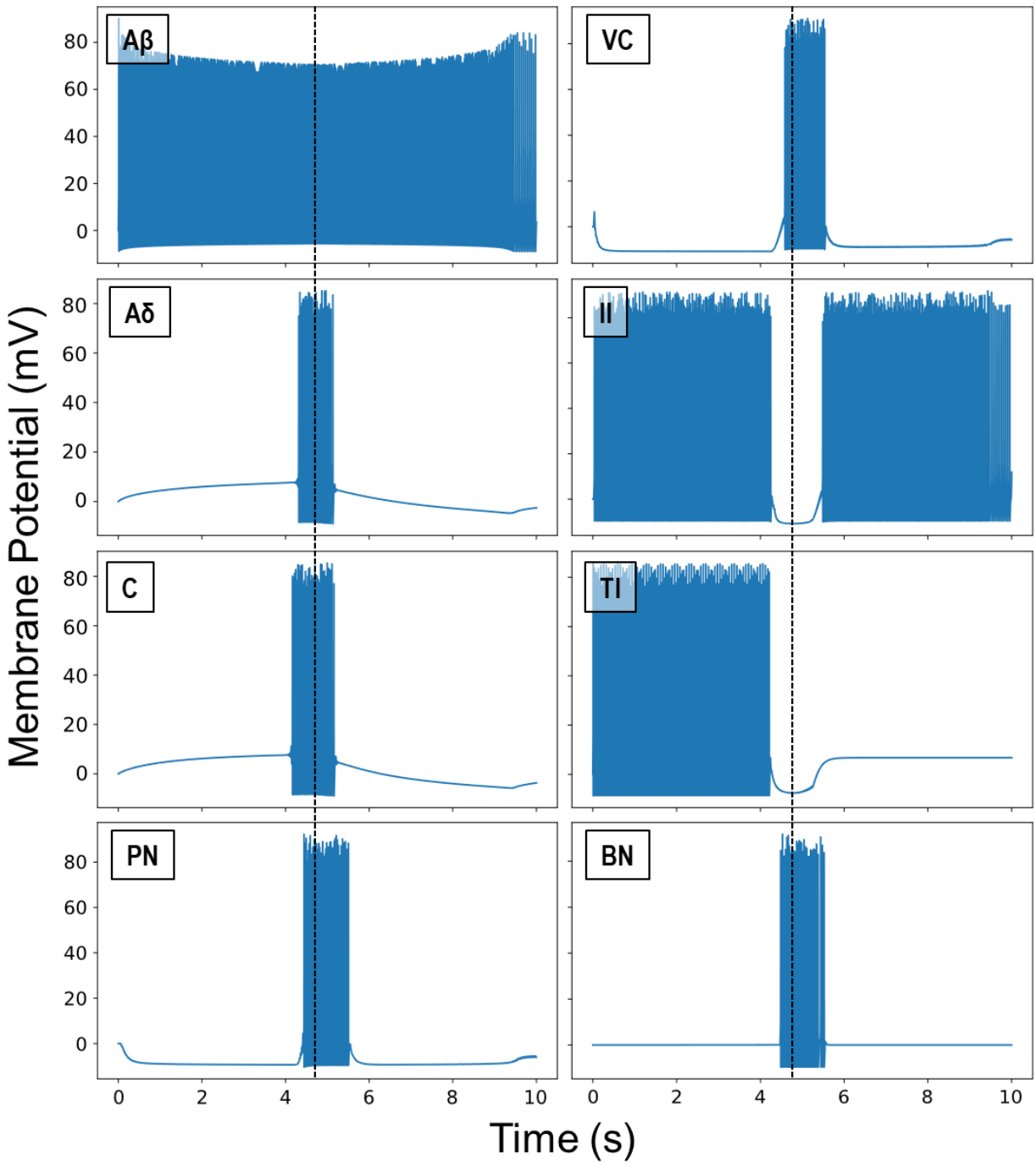

Figure 7-13: Neuron Membrane Voltages during a Base PPT Exposure. The vertical dashed black lines indicate the time of peak stress in $\sigma(t)$. The Viscoelastic and Fatigue Neurons are not pictured since both $\zeta(t)$ and $\phi(t)$ were set to zero. See Table 7-7 for Abbreviations. This Exposure had a Λ_i of `True` since the BN Neuron had an action potential train lasting for at least 500 ms that had a peak firing rate that exceeded 21 Hz.

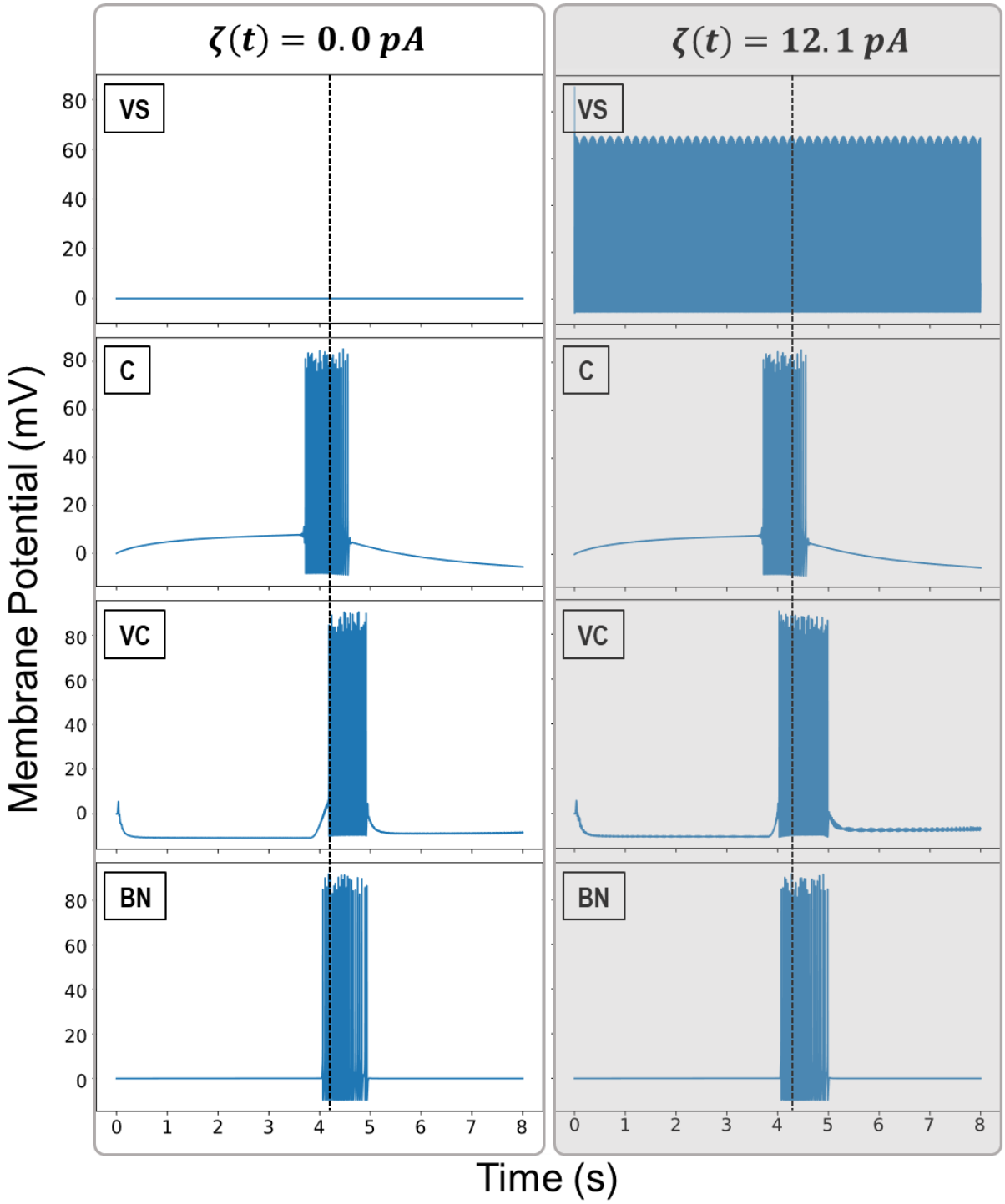

Figure 7-14: Neuron Membrane Voltages Being Influenced by $\zeta(t)$. The vertical dashed black lines indicate the time of peak stress in $\sigma(t)$; see Table 7-7 for abbreviations. The unshaded plots on the left use no input for $\zeta(t)$, while the shaded plots on the right use the default $\zeta(t)$ of 12.1 pA. The main effect of the VS neuron can be seen in the earlier onset and longer duration of the VC neuron's action potential train. This did not appreciably change when the BN action potential train starts or finishes but did increase the BN neuron's peak firing rate. Both stacks returned a Λ_i of `True`.

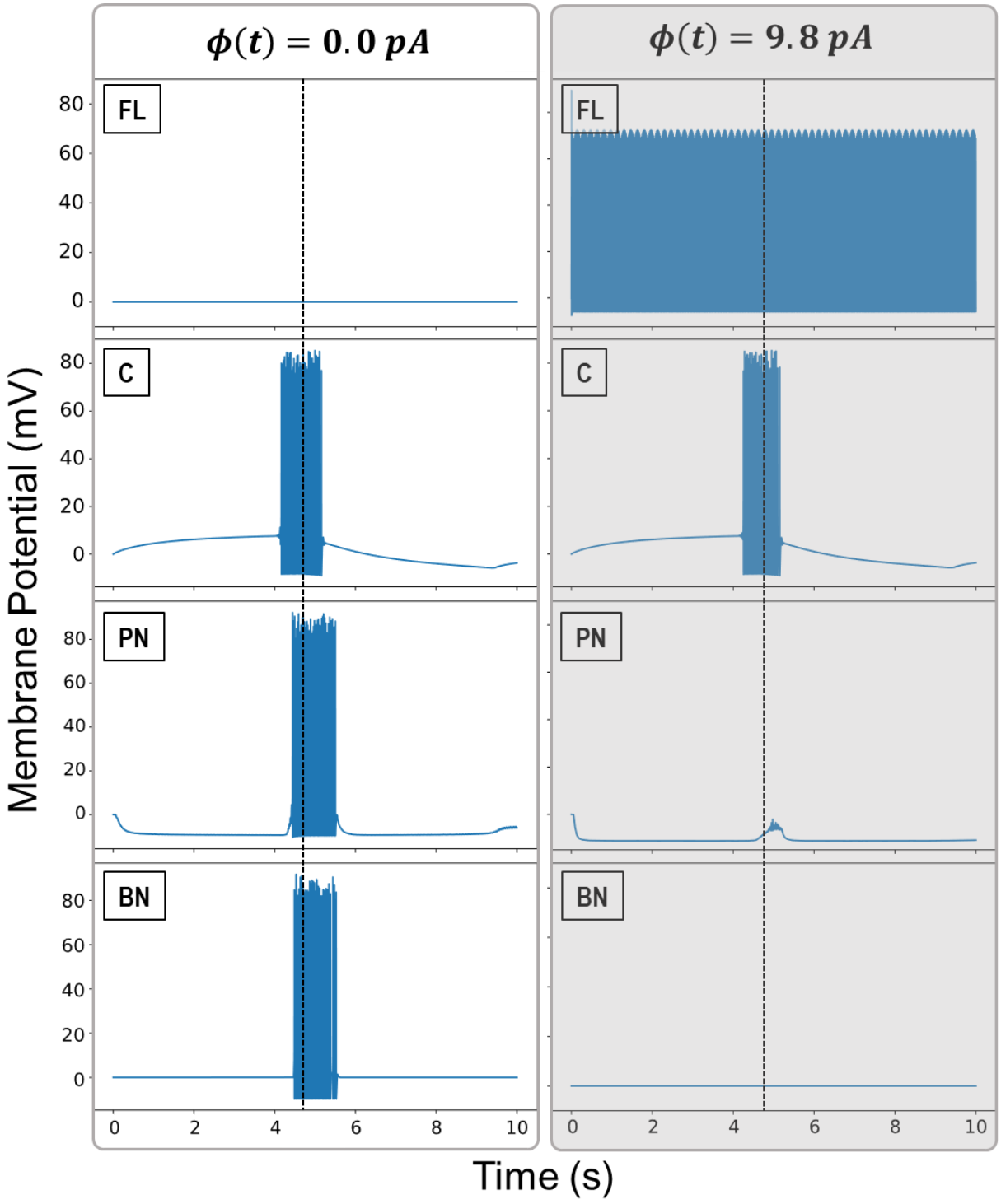

Figure 7-15: Neuron Membrane Voltages Being Influenced by $\phi(t)$. The vertical dashed black lines indicate the time of peak stress in $\sigma(t)$; see Table 7-7 for abbreviations. The unshaded plots on the left use no input for $\phi(t)$, while the shaded plots on the right use the default $\phi(t)$ of 9.8 pA. The main effect of the FL neuron can be seen by inhibiting the PN neuron through direct and indirect mechanisms. The left, unshaded stack returned a Λ_i of `True`; the right shaded stack returned a Λ_i of `False` since the activity in the BN neuron did not generate an action potential train.

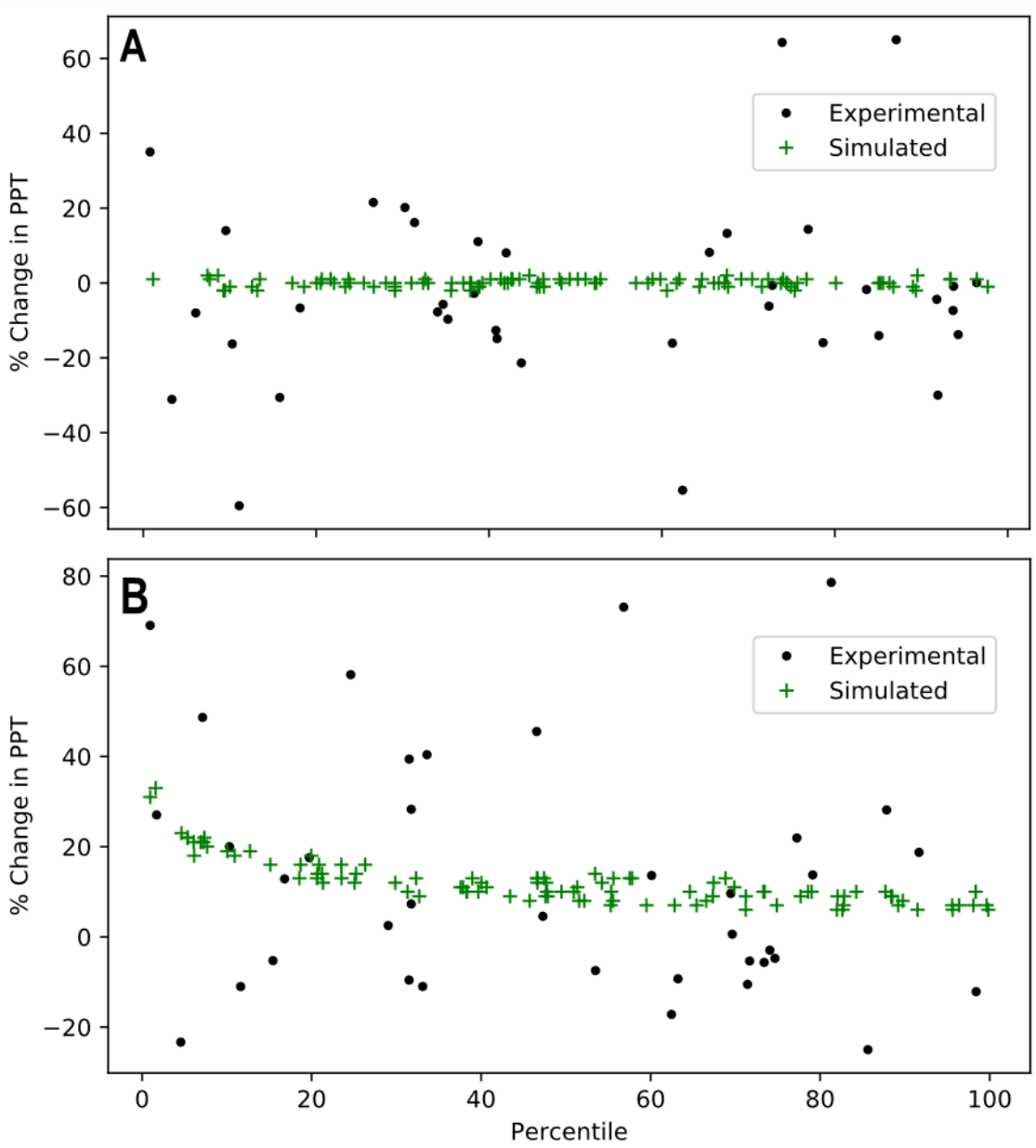

Figure 7-16: The Relationship between Mechanical Sensitivity Percentile and the Percent Change in PPTs following the Exposures in Chapters 3 and 4. In simulating Chapter 3 data (Panel A: $\zeta(t) = 12.1$ pA; $\phi(t) = 0.0$ pA), neither the experimental (black dots) nor simulated data (green plus symbols) show any relation between the change in PPT and the mechanical sensitivity percentile ($R^2 < 0.015$). In simulating Chapter 4 data (Panel B: $\zeta(t) = 12.1$ pA; $\phi(t) = 9.8$ pA), the experimental data does not show a relationship between mechanical sensitivity percentile and change in PPT ($R^2 = 0.038$), but the simulated data indicate the percent change is a logarithmic function of mechanical sensitivity ($R^2 = 0.902$).

Table 7-12: Predicted Nociceptive Likelihoods, $\Lambda_{\%}$, for each Tissue-Exposure Combination. Base refers to both $\zeta(t)$ and $\phi(t)$ being set to zero; Viscoelastic used $\zeta(t) = 12.1$ pA and $\phi(t) = 0$ pA; Muscle Use used $\zeta(t) = 0$ pA and $\phi(t) = 9.8$ pA; and Combined used $\zeta(t) = 12.1$ pA and $\phi(t) = 9.8$ pA.

Tissue	Exposure	Base	Viscoelastic	Muscle Use	Combined
Skin	$\sigma_{PPT}(t)$	100%	100%	0%	0%
AF	$\sigma_{Flex}(t)$	0%	0%	0%	0%
	$\sigma_{Fail}(t)$	0%	0%	0%	0%
	$\sigma_{Fail10}(t)$	88%	81%	9%	10%
SILC	$\sigma_{Flex}(t)$	0%	0%	0%	0%
	$\sigma_{Fail}(t)$	100%	100%	98%	98%
	$\sigma_{Fail10}(t)$	100%	100%	100%	100%

7.8 Discussion

A model was developed that predicts the likelihood a given tissue stress profile would generate nociceptive neural activity in the central nervous system and was tested for three different exposures: a PPT assessment, a flexion range of motion test, and tissue failure. The model included potential effects of viscoelasticity and physical activity, and while the former had little functional outcome on the model's predictions, the latter was influential for exposures with peak stresses falling close to or within the range of mechanical sensitivities. The data appears to support all our hypotheses: there were no instances of nociceptive activity generated in any flexion exposures (4a), the nociceptive likelihoods, $\Lambda_{\%}$, were higher for SILC failure than AF failure (4b), the presence of $\phi(t)$ did reduce $\Lambda_{\%}$, albeit potentially not as substantially as the data in Chapter 4 suggests it should (4c), and the presence of $\zeta(t)$ did alter peak firing rates without influencing $\Lambda_{\%}$ (4d).

One of the major predictions from the model is that dependent on the peak stresses achieved, between 12% (Fail10 condition) and 99.9% (Fail condition) of participants would not generate any nociceptive neural activity in their brainstems under AF failure. While this appears to counter-indicate the high prevalence of discogenic low back pain (Andersson, 1999; Balagué et al., 2012; Hoy et al., 2012; Verrills et al., 2015), it may offer an initially unintuitive explanation for it. The current practice to confirm disc damage or disease as a source of low back pain is to image the disc for evidence of physical disruption (Braithwaite et al., 1998; Carragee et al., 2005; Verrills et al., 2015). If the AF can rupture without generating any nociceptive neural activity, it would increase the percentage of cases that do generate nociceptive neural activity that show tissue damage on medical images. The phenomenon of discogenic low back pain often being referred to the lower limb is believed to be a result of disc materials compressing the spinal cord (Deyo and Mirza, 2016), which can only occur is the AF has already failed (Newell et al., 2017). One meta-analysis predicted that approximately 11.1% of individuals with annular fissures were asymptomatic for low back pain, which aligns with the $\Lambda_{\%}$ of 88% (representing ~12% asymptomatic) in the AF-$\sigma_{Fail10}(t)$ condition (Brinjikji et al., 2015). The failure stress profile used represents an acute loading scenario, while the etiology of most discogenic low back pain involves more chronic injury

mechanisms, which frequently fail AF tissues at lower peak stresses than acute loading scenarios (Callaghan and McGill, 2001; Deyo and Mirza, 2016; Gooyers et al., 2015; Parkinson and Callaghan, 2009); it is probable that $\Lambda_{\%}$ would be reduced further in simulating chronic AF failure. Most of this is predicated on the very low innervation ratios for AF tissues, as indicated by ψ_{NT} in Table 7-6, which derives from a small sample of cadaveric tissues (Chapter 6). The stark effects of ψ_{NT} can be seen in comparing the SILC Fail condition with the AF Fail10 condition. The peak stress of the SILC Fail condition is one-third that of the AF Fail10 condition, with comparable rates of stress development. However, the highly innervated SILC tissues cause $\Lambda_{\%}$ to consistently be close to one in the lower stress Fail scenario while the AF Fail10 $\Lambda_{\%}$ is less than one. It is possible that the data in Chapter 6 provide an underestimate of an appropriate value of ψ_{NT} for AF tissues, or that ψ_{NT} does not scale linearly with total nerve density, both of which could either increase or decrease the predicted $\Lambda_{\%}$. Besides ψ_{NT}, another potential source of error is the derivation of Equation 5-15, used to generate mechanical sensitivities. Other datasets of low back mechanical sensitivity testing have values that are approximately one-half of the sensitivities used to inform this model (Imamura et al., 2013; Lacourt et al., 2012). Decreasing the mechanical sensitivity, p_i, by a factor of 2 to match these distributions would double $I(t)$ based on equation 7-19. This change would likely increase the AF Fail10 $\Lambda_{\%}$ to 1.0 but would still likely keep the $\Lambda_{\%}$ for the Fail scenario below 1.0. The difference between the peak stresses of the AF Fail and Fail10 scenarios are a factor of 10, which would keep the AF Fail $\Lambda_{\%}$ in a hypothetically shifted mechanical sensitivity distribution above the AF Fail10 $\Lambda_{\%}$ with the unshifted distribution since the scaling function $s(\sigma_M)$ is a natural logarithmic function and $\ln(10) \sim 2.5$. All this assumes an acute loading scenario, which has much larger peak stresses than chronic loading scenarios as discussed above. In taking both the potential error in estimating ψ_{NT} and the potential overestimation of mechanical sensitivities, the sparse innervation and relatively low failure stresses compared to ligamentous tissues render the AF less likely to generate nociceptive neural activity than other tissues in the low back.

There could be improvements in implementing both $\zeta(t)$ and $\phi(t)$. While the overall shift in PPTs were similar between the simulated (+12.1%) and experimental data (+13.6%), the simulated effects of $\phi(t)$ showed a sensitivity dependency that did not match the experimental data. Specifically, the relative effects of $\phi(t)$ were underestimated at larger applied stresses, and the variability of both $\phi(t)$ and $\zeta(t)$ effects were substantially less than indicated by the raw data (Figure 7-16). A potential avenue to alter this sensitivity-dependency of $\phi(t)$ would be to increase the value of s_{excite} in Equation 7-42 for the FL-II interaction and adjust the FL-PN inhibition accordingly. However, the high firing rates of the FL neuron (> 70 Hz) and the time course of the excitatory post-synaptic potential function, $k_+(t)$, causes the sodium activation constant, m, to stay at its maximum value of 1.0 with the existing value of s_{excite} (0.08) for firing rates at around 70 Hz. This was likely the reason no additional effects were seen by increasing $\phi(t)$ beyond 9.8 pA. A similar rationale could be applied to $\zeta(t)$, only the saturation point of the sodium inactivation constant, n, occurs at a higher firing rate than 70 Hz since the value of $s_{inhibit}$ was much lower (0.01) than s_{excite} (0.08). The limiting factor for a maximum value of $\zeta(t)$ would be the VS neuron's $I(t)$ function rather than its ability to activate its target, the VC neuron, also because of this difference in s_{excite} and $s_{inhibit}$. A solution to address the lack of variability would be to introduce a stochastic element to s_{excite} and $s_{inhibit}$ exclusive to the VS and FL outputs. This change would be feasible in later iterations; however, it was not necessary for the scope of the current model which focused on the overall effects on $\Lambda_{\%}$. Although $\zeta(t)$ did alter the mechanical properties through μ to match creep effects in Chapter 3, the stress-relaxation test from Appendix E did not appear to cause any appreciable change in any of the three load-displacement constants ($k, \eta,$ and μ). Any expected change to these constants following a creep- or stress relaxation-

generating exposure should decrease the stress for a given strain by decreasing k or increasing μ (Fung, 1994; Provenzano et al., 2001). Thus, with $\zeta(t)$ presently coupled to μ decreased $\Lambda_{\%}$ relative to a simplified model that would ignore these effects, which may have resulted in more liberal estimates of the effects of $\zeta(t)$. Despite the potential overestimation, $\zeta(t)$ had minimal effects on most predictions of $\Lambda_{\%}$. The most noticeable effects of $\zeta(t)$ were a 9% decrease for the AF $\sigma_{Fail10}(t)$ "Viscoelastic" state relative to the "Base" state, which was roughly one-seventh of the effects of $\phi(t)$ for that same tissue-exposure combination. Although the effects of $\phi(t)$ were potentially underestimated and the effects of $\zeta(t)$ were potentially overestimated, this model provides a first step in quantifying the magnitude of these two considerations following lumbar spine flexion exposures.

The usefulness of model predictions are highly dependent on model validity (Lewandowski, 1982). The current validation process involved either taking components that have been previously shown to be valid in their respective domains, such as those used to predict membrane voltages (Gerstner et al., 2014; Hodgkin and Huxley, 1952a) and generate $\sigma(t)$ profiles (Barrett and Callaghan, 2018). However, the major process implemented here that required validation was the Sensitivity Module, specifically Equation 7-19. While the authors who initially derived Equation 7-20 had a mechanistic basis for doing so, allowing it to be applied more liberally than a purely predictive approach, it was grounded in non-nociceptive neural activity, not nociceptive neural activity (Gerling et al., 2018). The validation process used presently was to take the PPT data from Chapters 3 and 4 that reflected a base state ($\zeta(t) = \phi(t) = 0$) and derive a scaling factor, $s(\sigma_M)$, to have the model predict PPT data with 100% accuracy. Whether this procedure was the most appropriate or not, the peak stresses applied during this derivation procedure were around 2.0 MPa, while the peak stresses the model intended to evaluate were up to 10 times greater in the Fail10 condition. The estimates of the Fail10 condition, where stresses exceeded those the Sensitivity Module was tested against should be interpreted with caution. While a logarithmic relationship was assumed for $s(\sigma_M)$ (Equation 7-21), the shape may be sigmoidal, asymptotic (like Equation 5-17), linear, or some other shape, all with the potential to affect $\Lambda_{\%}$ through $I(t)$. Perhaps the mechanical sensitivity-dependence on $\phi(t)$ illustrated in Figure 7-16 could be evidence that a logarithmic relationship was too steep, or that peak stress (σ_M) was not the optimal variable to input into this function. Another facet of the Sensitivity Module that influenced model predictions was the shape of the kernel function, $\gamma(t)$. While the weighting of the three phases in the decay function were arbitrarily chosen to give C-fibres differential sensitivity to the time-derivative of tissue stress (Treede et al., 2002), they were done so before validating the Sensitivity Module against PPT data and could be accounted for in an ideal scaling function $s(\sigma_M)$. Even for exposures with stress profiles within the validation range of the PPT exposures, a major concern for the Sensitivity Module was the rate of stress application. The PPTs exposures had controlled, fixed stress-derivatives, while the Flex and Fail exposures had more variable rates of stress increase and decrease. One method to generate these data would have been to collect PPT data at more variable stress (pressure) rates, although this effect may be minimal relative to the existing variability of PPTs since studies with high (~0.5 MPa/s) and low rates (~0.05 MPa/s) of pressure application have similar PPT values for similar sites in similar populations to each other (Chesterton et al., 2003; Finocchietti et al., 2011; Petrini et al., 2015).

While there were stochastic elements in generating mechanical sensitivities and the Neurological Module, the remainder of the model was deterministic. The main purpose of including any stochastic elements was to account for interpersonal variability; while this was explicitly done through PPT distributions, the variation in neuron properties may have also accomplished this goal. The variation in neuron properties in Table 7-8 was likely primarily responsible for the variation seen in the simulated data

points in Figure 7-16 and could obscure how $\zeta(t)$ affected $\Lambda_{\%}$ since the viscoelastic effects were developed to have a more subtle effect on model outputs. Including neuron property variability was intended to make the model more biofidelic, since classes of neurons do not have homogenous properties (Gerstner et al., 2014; Kandel et al., 2013). While this variation may be able to be ignored in the future, there are minimal benefits to doing so since it would be a minor simplification with minimal computational savings. The mechanical side of the model was kept deterministic for two reasons: one being that there was a limited sample to generate distributions from, and the other to only model extreme exposures. The exposures were selected to represent exposures that are known to not generate nociceptive activity (normal range of motion) and exposures with the maximum likelihood of generating nociceptive activity (tissue failure) to provide face validity to the model (Lewandowski, 1982). While the data exist to model this distribution, including that additional variability greatly expands the solution space and would necessitate more iterations to arrive on a value of $\Lambda_{\%}$ arising from more possible combinations. Including variability in mechanical properties would likely make the predictions more relevant since there is substantial variability in tissue properties (Howarth and Callaghan, 2012; Mattucci et al., 2013; Troyer et al., 2012), intervertebral flexion angles (Breen et al., 2019; De Carvalho et al., 2010; Fairbank et al., 2011; Galbusera et al., 2021; Harvey et al., 2016; Mellor et al., 2014; Viggiani et al., 2017), and tissue failure tolerances (Bass et al., 2007; Gooyers et al., 2015; Gregory and Callaghan, 2011; Isaacs et al., 2014; Weidenbaum et al., 1995) among others. However, this model primarily aimed to evaluate the effects of sensitivity, and the additional inclusion of variation in stiffness, failure tolerance, and other properties would cloud any effects through the increased randomness at a very steep computational penalty.

A multiscale model that predicts nociceptive neural activity in the brainstem from a one-dimensional stress profile was presented in this chapter. The model was developed using PPT distributions, immunohistology data, and mechanical testing in conjunction with variants on existing models of neurological sensitivity and electrophysiology. One major prediction is that it would be unlikely for nociceptive signals to originate from AF tissues. This is a combination of the relatively low failure stresses and low innervation density of the AF relative to the surrounding tissues.

Chapter 8 – Conclusions

The overall purpose of this thesis was to develop a more complete understanding of how lumbar spine flexion can influence the development of low back pain. The path taken to achieve this purpose was to first determine how flexion altered mechanical sensitivity, and then to simulate what those alterations could do to exposures often associated with low back pain. Chapters 1 and 2 provided a perspective on the scope of this problem and relevant literature, ending with a set of four outstanding problems. Chapters 3 and 4 provided data on how mechanical sensitivity was altered by in two types of flexion exposures, summarized in Chapter 5 as the interaction of two systems: one specifically related to creep effects and a second that reflects the muscular activity required to move a person into and out of flexed postures. Chapter 6 presents anatomical data measured to inform the model presented in Chapter 7 capable of simulating extreme exposures and determining the nociceptive neural activity that could shape low back pain.

At the start of the thesis, the theoretical understanding was that some facet of lumbar spine flexion altered ascending neural activity which was used in a modulatory circuit to either facilitate or inhibit nociceptive information. The goal of the thesis was then to quantify which direction and how strong this modulatory effect was. The source of this modulation was assumed to come either from creep itself (Claude et al., 2003; Granata et al., 2005; Howarth et al., 2013a; Muslim et al., 2013; Solomonow et al., 2003; Toosizadeh and Nussbaum, 2013), inflammation (Kidd and Urban, 2001; Pinski et al., 2010; Yang et al., 2011), muscle fatigue (Søgaard et al., 2006; Taylor et al., 2000), or physical activity (Ellingson et al., 2014; Gajsar et al., 2018; Koltyn et al., 2014; Naugle et al., 2014). The data in this thesis determined that the effects of creep in isolation were minimal but could interact with muscle fatigue or physical activity to produce a delayed desensitization effect. The lack of a conclusive mechanism or interaction is one failing of the study design and practical implementation of these chapters: mechanisms were assumed based on time-profiles rather than measured directly. The solution to address this ambiguity was to identify extreme cases to effectively define the bounds of this problem: what exposure scenarios would be the most and least likely to have lumbar spine flexion and the influence the resulting viscoelastic creep could have on low back pain development. Ultimately, this resulted in identifying two (and a half) exposures in two different tissues under four conditions (defined through $\zeta(t)$ and $\phi(t)$) that should represent mechanical exposures with the most (failure) and least chance (normal range of motion) of generating nociceptive activity in a highly innervated (ligament) and minimally innervated (outer annulus) tissue. Simulating the sixteen corners of this solution space determined that the tissue and exposure have a more prominent and consistent effect than creep or fatigue effects that could follow lumbar spine flexion. However, these exposure-specific features did influence exposures that were already close to a nociceptive boundary, such as pressure-pain thresholds. This thesis' answer to the first question: which direction was the modulatory effect of lumbar spine flexion? It inhibited nociceptive information, but only for exposures involving extensive muscle activity. Otherwise, it influenced the perception of mechanical stimuli, but not the overall sensitivity. This thesis' answer to the second question: how strong was this effect? The model predicted a strong effect for a few specific conditions, though there were limitations in implementing this in the model simulations which could underestimate its effect in higher stress exposures.

How does the data in this thesis influence our theoretical understanding of low back pain development, viscoelastic creep, or mechanical nociception? Repetitive lumbar spine flexion is commonly believed to damage tissues and that damage is supposedly the thing that makes your lower back hurt. The thesis defines a scenario where that damage-pain linkage is disrupted in the absence of any pain disorder:

a repetitive load involving extensive muscle use that precedes annulus fibrosus failure; where it was estimated that up to 90% of people would not perceive this exposure as painful. This likelihood could theoretically decrease to 0% when lower magnitude, repetitive loads are responsible for tissue failure as is common for annular tissues (Callaghan and McGill, 2001; Gallagher and Heberger, 2012; Gooyers et al., 2015; Newell et al., 2017). How can this exposure then lead to low back pain in those who would not generate a nociceptive signal? One scenario is that the annulus damage could trigger an inflammatory response that sensitizes the injury site; however this pathway could take as long as weeks or months to result in low back pain (Kidd and Urban, 2001). Another scenario arises from the observation that physiological loading is not only applied to a single tissue: an exposure that causes the annulus to fail may bring other tissues close to failure. Those neighbouring tissues could generate a nociceptive signal either from the exposure that caused the annulus to fail, or from an altered loading scenario that arose because the annulus failed. The nociceptive signal related to an annular injury may not come from the annulus, but the whole exposure could generate at least one nociceptive signal from a more innervated tissue such as the supraspinous-interspinous ligament complex. While this thesis provides a semi-quantitative estimation of the relative innervation of the annulus and posterior ligaments, it was already known that ligaments were highly innervated and postulated that they could be the source of many nociceptive signals in those with non-specific low back pain (Cavanaugh et al., 1996; Roberts et al., 1995; Sperry et al., 2017). It is possible that the highly sensitive ligament and capsular tissues could inadvertently signal annulus damage. The mechanism for such an interaction would be as follows: an exposure generates tissue stresses in both tissues that can: a) elicit nociceptive activity in a ligament without damaging it and b) damage the annulus fibrosus without eliciting nociceptive activity in it. The ability for one tissue to signal damage in another would fit into the theory that our pain system is a highly sensitive non-specific warning system (Basbaum et al., 2009; Brodal, 2017), with the data from this thesis suggesting the scenario could be plausible in at least 90% of asymptomatic people.

This thesis presents several novel contributions. First, it documents the construction and reliability of a motorized displacement-control pressure algometer for evaluating pressure-pain thresholds and the perception of sub-threshold stimuli. The algometer can be applied to other locations than those studied, as well as additional sensitivity metrics such as supra-threshold stimulus perception (Micalos and Arendt-Nielsen, 2016) or voluntary mechanical pain tolerance (Petrini et al., 2015). Second, it describes the asymmetric distribution of lower back mechanical sensitivity using the Gumbel distribution—a distribution developed to predict the occurrence of local maxima (Gumbel, 1941). This approach aligns with the idea that experiencing pain is the result of the brain interpreting extreme neural inputs with more weight than less-extreme inputs (Perl, 2007). Third, while multiple peripheral cadaveric tissues were probed for PGP9.5, CGRP, B1R, and ASIC3; only PGP9.5 and ASIC3 were consistently detected throughout technical replicates. Previously, CGRP and B1R were consistently found in the dorsal horn of human cadaver samples (Gruber et al., 2012; Saeed and Ribeiro-da-Silva, 2012), and it is suggested that authors investigate these proteins in the central nervous system instead of the periphery. Lastly, a model that interfaces between mechanical stress and neural activity was developed. While many features were adapted directly, three novel contributions include: i) a geometric simplification to convert flexion angles into one-dimensional tensile strains, ii) a coefficient to adapt inputted neural currents to a distribution of mechanical sensitivities, and iii) modifications to Hodgkin-Huxley neurons to facilitate simplified inter-neuron communication demonstrated in a small neural circuit.

Epidemiology links lumbar spine flexion and low back pain and this thesis explored features influencing that connection. Of the two relevant features, creep and muscle use, muscle use has a larger influence on how tissue damage is perceived, with the potential to influence how a sizeable percentage of the population perceives annular tissue failure.

References

Abboud, J., Nougarou, F., Descarreaux, M., 2016. Muscle activity adaptations to spinal tissue creep in the presence of muscle fatigue. PLoS One 11, 1–14. https://doi.org/10.1371/journal.pone.0149076

Abboud, J., Rousseau, B., Descarreaux, M., 2018. Trunk proprioception adaptations to creep deformation. Eur. J. Appl. Physiol. 118, 133–142. https://doi.org/10.1007/s00421-017-3754-2

Abraira, V.E., Ginty, D.D., 2013. The sensory neurons of touch. Neuron 79, 618–639. https://doi.org/10.1016/j.neuron.2013.07.051

Abramowitch, S.D., Woo, S.L.Y., 2004. An improved method to analyze the stress relaxation of ligaments following a finite ramp time based on the quasi-linear viscoelastic theory. J. Biomech. Eng. 126, 92. https://doi.org/10.1115/1.1645528

Ackermann, P.W., Bring, D.K.I., Renström, P., 2005. Tendon innervation and neuronal response after injury, in: Tendon Injuries: Basic Science and Clinical Medicine. pp. 287–297. https://doi.org/10.1007/1-84628-050-8_9

Adams, M.A., Dolan, P., Hutton, W.C., Porter, R.W., 1990. Diurnal changes in spinal mechanics and their clinical significance. J. Bone Jt. Surg. 72, 266–270.

Adams, M.A., Mannion, A.F., Dolan, P., 1999. Personal risk factors for first-time low back pain. Spine (Phila. Pa. 1976). 24, 2497–505.

Adriaensen, H., Gybels, J., Handwerker, H.O., Van Hees, J., 1983. Response properties of thin myelinated (A-delta) fibers in human skin nerves. J. Neurophysiol. 49, 111–22.

Ahern, G.P., Brooks, I.M., Miyares, R.L., Wang, X., 2005. Extracellular Cations Sensitize and Gate Capsaicin Receptor TRPV1 Modulating Pain Signaling. J. Neurosci. 25, 5109–5116. https://doi.org/10.1523/JNEUROSCI.0237-05.2005

Airaksinen, O., Brox, J.I., Cedraschi, C., Hildebrandt, J., Klaber-Moffett, J., Kovacs, F., Mannion, A.F., Reis, S., Staal, J.B., Ursin, H., Zanoli, G., 2006. Chapter 4: European guidelines for the management of chronic nonspecific low back pain. Eur. Spine J. 15, 192–300. https://doi.org/10.1007/s00586-006-1072-1

Almog, M., Korngreen, A., 2016. Is realistic neuronal modeling realistic? J. Neurophysiol. 116, 2180–2209. https://doi.org/10.1152/jn.00360.2016

Ambrosetti-Giudici, S., Gédet, P., Ferguson, S.J., Chegini, S., Burger, J., 2010. Viscoelastic properties of the ovine posterior spinal ligaments are strain dependent. Clin. Biomech. 25, 97–102. https://doi.org/10.1016/j.clinbiomech.2009.10.017

Andersen, O.K., Jensen, L.M., Brennum, J., Arendt-Nielsen, L., 1995. Modulation of the human nociceptive reflex by cyclic movements. Eur. J. Appl. Physiol. Occup. Physiol. 70, 311–321. https://doi.org/10.1007/BF00865028

Andersson, G.B.J., 1999. Epidemiological features of chronic low-back pain. Lancet 354, 581–585. https://doi.org/http://dx.doi.org/10.1016/S0140-6736(99)01312-4

Aoki, Y., Ohtori, S., Takahashi, K., Ino, H., Douya, H., Ozawa, T., Saito, T., Moriya, H., 2005. Expression and co-expression of VR1, CGRP, and IB4-binding glycoprotein in dorsal root ganglion neurons in rats: Differences between the disc afferents and the cutaneous afferents. Spine (Phila. Pa. 1976). 30, 1496–1500. https://doi.org/10.1097/01.brs.0000167532.96540.31

Apkarian, A.V., Bushnell, M.C., Treede, R.D., Zubieta, J.K., 2005. Human brain mechanisms of pain perception and regulation in health and disease. Eur. J. Pain 9, 463–484. https://doi.org/10.1016/j.ejpain.2004.11.001

Arcourt, A., Gorham, L., Dhandapani, R., Prato, V., Taberner, F.J., Wende, H., Gangadharan, V., Birchmeier, C., Heppenstall, P.A., Lechner, S.G., 2017. Touch Receptor-Derived Sensory Information Alleviates Acute Pain Signaling and Fine-Tunes Nociceptive Reflex Coordination. Neuron 93, 179–193. https://doi.org/10.1016/j.neuron.2016.11.027

Arendt-Nielsen, L., Fernández-de-las-Peñas, C., Graven-Nielsen, T., 2011. Basic aspects of musculoskeletal pain: from acute to chronic pain. J. Man. Manip. Ther. 19, 186–193. https://doi.org/10.1179/106698111X13129729551903

Argüello, E.J., Silva, R.J., Huerta, M.K., Avila, R.S., 2015. Computational modeling of peripheral pain: a commentary. Biomed. Eng. Online 14, 56. https://doi.org/10.1186/s12938-015-0049-x

Arjmand, N., Shirazi-Adl, A., 2006. Model and in vivo studies on human trunk load partitioning and stability in isometric forward flexions. J. Biomech. 39, 510–521. https://doi.org/10.1016/j.jbiomech.2004.11.030

Arntz, A., Claassens, L., 2004. The meaning of pain influences its experienced intensity. Pain 109, 20–25. https://doi.org/10.1016/j.pain.2003.12.030

Arsiccio, A., Giorsello, P., Marenco, L., Pisano, R., 2020. Considerations on Protein Stability During Freezing and Its Impact on the Freeze-Drying Cycle: A Design Space Approach. J. Pharm. Sci. 109, 464–475. https://doi.org/10.1016/j.xphs.2019.10.022

Artus, M., van der Windt, D.A., Jordan, K.P., Hay, E.M., 2010. Low back pain symptoms show a similar pattern of improvement following a wide range of primary care treatments: A systematic review of randomized clinical trials. Rheumatology 49, 2346–2356. https://doi.org/10.1093/rheumatology/keq245

Atlas, L.Y., Wager, T.D., 2012. How expectations shape pain. Neurosci. Lett. 520, 140–8. https://doi.org/10.1016/j.neulet.2012.03.039

Avin, K.G., Frey Law, L.A., 2011. Age-related differences in muscle fatigue vary by contraction type: a meta-analysis. Phys. Ther. 91, 1153–65. https://doi.org/10.2522/ptj.20100333

Ayturk, U.M., Garcia, J.J., Puttlitz, C.M., 2010. The Micromechanical Role of the Annulus Fibrosus Components Under Physiological Loading of the Lumbar Spine. J. Biomech. Eng. 132, 061007. https://doi.org/10.1115/1.4001032

Bagal, S.K., Chapman, M.L., Marron, B.E., Prime, R., Storer, R.I., Swain, N.A., 2014. Recent progress in sodium channel modulators for pain. Bioorganic Med. Chem. Lett. 24, 3690–3699. https://doi.org/10.1016/j.bmcl.2014.06.038

Bailey, J.F., Liebenberg, E., Degmetich, S., Lotz, J.C., 2011. Innervation patterns of PGP 9.5-positive nerve fibers within the human lumbar vertebra. J. Anat. 218, 263–270. https://doi.org/10.1111/j.1469-7580.2010.01332.x

Balagué, F., Mannion, A.F., Pellisé, F., Cedraschi, C., 2012. Non-specific low back pain. Lancet 379, 482–91. https://doi.org/10.1016/S0140-6736(11)60610-7

Baliki, M.N., Apkarian, A.V., 2015. Nociception, Pain, Negative Moods, and Behavior Selection. Neuron 87, 474–491. https://doi.org/10.1016/j.neuron.2015.06.005

Barrett, J.M., Callaghan, J.P., 2018. A procedure for determining parameters of a simplified ligament model. J. Biomech. 66, 175–179. https://doi.org/10.1016/j.jbiomech.2017.10.037

Barrett, J.M., Gooyers, C.E., Karakolis, T., Callaghan, J.P., 2016. The Impact of Posture on the Mechanical Properties of a Functional Spinal Unit During Cyclic Compressive Loading. J. Biomech. Eng. 138, 081007. https://doi.org/10.1115/1.4033916

Barrot, M., 2012. Tests and models of nociception and pain in rodents. Neuroscience 211, 39–50. https://doi.org/10.1016/j.neuroscience.2011.12.041

Basbaum, A.I., Bautista, D.M., Scherrer, G., Julius, D., 2009. Cellular and Molecular Mechanisms of Pain. Cell 139, 267–284. https://doi.org/10.1016/j.cell.2009.09.028

Bass, C.R., Lucas, S.R., Salzar, R.S., Oyen, M.L., Planchak, C., Shender, B.S., Paskoff, G., 2007. Failure properties of cervical spinal ligaments under fast strain rate deformations. Spine (Phila. Pa. 1976). 32, 7–13. https://doi.org/10.1097/01.brs.0000251058.53905.eb

Bautista, D.M., Sigal, Y.M., Milstein, A.D., Garrison, J.L., Zorn, J.A., Tsuruda, P.R., Nicoll, R.A., Julius, D., 2008. Pungent agents from Szechuan peppers excite sensory neurons by inhibiting two-pore potassium channels. Nat. Neurosci. 11, 772–779. https://doi.org/10.1038/nn.2143.Pungent

Bazrgari, B., Hendershot, B., Muslim, K., Toosizadeh, N., Nussbaum, M.A., Madigan, M.L., 2011. Disturbance and recovery of trunk mechanical and neuromuscular Behaviours following repetitive lifting: Influences of flexion angle and lift rate on creep-induced effects. Ergonomics 54, 1043–1052.

Been, E., Kalichman, L., 2014. Lumbar lordosis. Spine J. 14, 87–97. https://doi.org/10.1016/j.spinee.2013.07.464

Beharriell, T.H., Mavor, M.P., Ramos, W., Mauger, J.F., Imbeault, P., Graham, R.B., 2020. Beyond the mechanical lens: Systemic inflammatory responses to repetitive lifting under varying loads and frequencies. Appl. Ergon. 89, 103199. https://doi.org/10.1016/j.apergo.2020.103199

Beissner, F., Brandau, A., Henke, C., Felden, L., Baumgärtner, U., Treede, R.D., Oertel, B.G., Lötsch, J., 2010. Quick discrimination of Adelta and C fiber mediated pain based on three verbal descriptors. PLoS One 5, 1–7. https://doi.org/10.1371/journal.pone.0012944

Bessou, P., Perl, E.R., 1969. Response of cutaneous sensory units with unmyelinated fibers to noxious stimuli. J. Neurophysiol. 32, 1025–1043. https://doi.org/10.1152/jn.1969.32.6.1025

Bianchi, L., Driscoll, M., 2002. Protons at the gate: DEG/ENaC ion channels help us feel and remember. Neuron 34, 337–340. https://doi.org/10.1016/S0896-6273(02)00687-6

Biedert, R., Lobenhoffer, P., Lattermann, C., Stauffer, E., Müller, W., 2000. Free nerve endings in the medial and posteromedial capsuloligamentous complexes: occurrence and distribution. Knee Surg, Sport. Traumatol, Arthrose 8, 68–72. https://doi.org/10.1007/s001670050188

Bird, S.B., Dickson, E.W., 2001. Clinically significant changes in pain along the visual analog scale. Ann. Emerg. Med. 38, 639–643. https://doi.org/10.1067/mem.2001.118012

Blanchard, E.B., Young, L.D., McLeod, P., 1984. Awareness of Heart Activity and Self-Control of Heart Rate. Psychophysiology 21, 361–362. https://doi.org/10.1111/j.1469-8986.1984.tb02948.x

Bogduk, N., Tynan, W., Wilson, A.S., 1981. The nerve supply to the human lumbar intervertebral discs. J. Anat. 132, 39–56.

Borg, G.A. V., 1982. Psychophysical bases of perceived exertion. Med. Sci. Sports Exerc. 14, 377–381. https://doi.org/10.1249/00005768-198205000-00012

Borzan, J., Zhao, C., Meyer, R.A., Raja, S.N., 2010. A Role for Acid-sensing Ion Channel 3, but Not Acid-sensing Ion Channel 2, in Sensing Dynamic Mechanical Stimuli. Anesthesiology 113, 647–654.

Boschman, J.S., Van Der Molen, H.F., Sluiter, J.K., Frings-Dresen, M.H.W., 2011. Occupational demands and health effects for bricklayes and construction supervisors: A systematic review. Am. J. Ind. Med. 54, 55–77. https://doi.org/10.1002/ajim.20899

Boström, K.J., de Lussanet, M.H.E., Weiss, T., Puta, C., Wagner, H., 2015. A computational model unifies apparently contradictory findings concerning phantom pain. Sci. Rep. 4, 5298. https://doi.org/10.1038/srep05298

Boucher, J.-A., Abboud, J., Descarreaux, M., 2012. The influence of acute back muscle fatigue and fatigue recovery on trunk sensorimotor control. J. Manipulative Physiol. Ther. 35, 662–8. https://doi.org/10.1016/j.jmpt.2012.10.003

Boyle, K.A., Gutierrez-Mecinas, M., Polgár, E., Mooney, N., O'Connor, E., Furuta, T., Watanabe, M., Todd, A.J., 2017. A quantitative study of neurochemically defined populations of inhibitory interneurons in the superficial dorsal horn of the mouse spinal cord. Neuroscience 363, 120–133. https://doi.org/10.1016/j.neuroscience.2017.08.044

Brain, S.D., 2011. TRPV1 and TRPA1 channels in inflammatory pain: Elucidating mechanisms. Ann. N. Y. Acad. Sci. 1245, 36–37. https://doi.org/10.1111/j.1749-6632.2011.06326.x

Braithwaite, I., White, J., Saifuddin, A., Renton, P., Taylor, B.A., 1998. Vertebral end-plate (Modic) changes on lumbar spine MRI: Correlation with pain reproduction at lumbar discography. Eur. Spine J. 7, 363–368. https://doi.org/10.1007/s005860050091

Braz, J.M., Nassar, M.A., Wood, J.N., Basbaum, A.I., 2005. Parallel "pain" pathways arise from subpopulations of primary afferent nociceptor. Neuron 47, 787–793. https://doi.org/10.1016/j.neuron.2005.08.015

Braz, J.M., Solorzano, C., Wang, X., Basbaum, A.I., 2014. Transmitting Pain and Itch Messages: A Contemporary View of the Spinal Cord Circuits that Generate Gate Control. Neuron 82, 522–536. https://doi.org/10.1016/j.neuron.2014.01.018

Breen, Alexander, Hemming, R., Mellor, F., Breen, Alan, 2019. Intrasubject repeatability of in vivo intervertebral motion parameters using quantitative fluoroscopy. Eur. Spine J. 28, 450–460. https://doi.org/10.1007/s00586-018-5849-9

Brereton, L.C., McGill, S.M., 1998. Frequency response of spine extensors during rapid isometric contractions: effects of muscle length and tension. J. Electromyogr. Kinesiol. 8, 227–32.

Brinjikji, W., Diehn, F.E., Jarvik, J.G., Carr, C.M., Kallmes, D.F., Murad, M.H., Luetmer, P.H., 2015. MRI findings of disc degeneration are more prevalent in adults with low back pain than in asymptomatic controls: A systematic review and meta-analysis. Am. J. Neuroradiol. 36, 2394–2399. https://doi.org/10.3174/ajnr.A4498

Britton, N.F., 1996. The role of N-methyl-D-aspartate (NMDA) receptors in wind-up: A mathematical model. Math. Med. Biol. 13, 193–205. https://doi.org/10.1093/imammb/13.3.193

Britton, N.F., Skevington, S.M., 1996. On the mathematical modelling of pain. Neurochem. Res. 21, 1133–1140. https://doi.org/10.1007/BF02532424

Britton, N.F., Skevington, S.M., 1989. A Mathematical Model of the Gate Control Theory of Pain. J. theor. Biol. 137, 91–105.

Brodal, P., 2017. A neurobiologist's attempt to understand persistent pain. Scand. J. Pain 15, 140–147. https://doi.org/10.1016/j.sjpain.2017.03.001

Bushnell, M.C., Ceko, M., Low, L.A., 2013. Cognitive and emotional control of pain and its disruption in chronic pain. Nat. Rev. Neurosci. 14, 502–511.

Busscher, I., Van Dieën, J.H., Van Der Veen, A.J., Kingma, I., Meijer, G.J.M., Verkerke, G.J., Veldhuizen, A.G., 2011. The effects of creep and recovery on the in vitro biomechanical characteristics of human multi-level thoracolumbar spinal segments. Clin. Biomech. 26, 438–444. https://doi.org/10.1016/j.clinbiomech.2010.12.012

Cai, W., Cao, J., Ren, X., Qiao, L., Chen, X., Li, M., Zang, W., 2016. shRNA mediated knockdown of Nav1.7 in rat dorsal root ganglion attenuates pain following burn injury. BMC Anesthesiol. 16, 1–7. https://doi.org/10.1186/s12871-016-0215-0

Callaghan, J.P., McGill, S.M., 2001. Intervertebral disc herniation: Studies on a porcine model exposed to highly repetitive flexion/extension motion with compressive force. Clin. Biomech. 16, 28–37. https://doi.org/10.1016/S0268-0033(00)00063-2

Cao, E., Chen, Y., Cui, Z., Foster, P.R., 2003. Effect of freezing and thawing rates on denaturation of proteins in aqueous solutions. Biotechnol. Bioeng. 82, 684–690.

Carragee, E.J., Alamin, T.F., Miller, J.L., Carragee, J.M., 2005. Discographic, MRI and psychosocial determinants of low back pain disability and remission: A prospective study in subjects with benign persistent back pain. Spine J. 5, 24–35. https://doi.org/10.1016/j.spinee.2004.05.250

Carvalho, C., Caetano, J.M., Cunha, L., Rebouta, P., Kaptchuk, T.J., Kirsch, I., 2016. Open-label placebo treatment in chronic low back pain : a randomized controlled trial. Pain 157, 2766–2772.

Caterina, M.J., Leffler, A., Malmberg, A.B., Martin, W.J., Trafton, J., Peterses-Zeitz, K.R., Kolzenburg, M., Basbaum, A.I., Julius, D., 2000. Impaired nociception and pain sensation in mice lacking the capsaicin receptor. Science (80-.). 288, 306–313.

Caterina, M.J., Schumacher, M.A., Tominaga, M., Rosen, T.A., Levine, J.D., Julius, D., 1997. The capsaicin receptor: A heat-activated ion channel in the pain pathway. Nature 389, 816–824. https://doi.org/10.1038/39807

Cavanaugh, J.M., Ozaktay, A.C., Yamashita, H.T., King, A.I., 1996. Lumbar facet pain: Biomechanics, neuroanatomy and neurophysiology. J. Biomech. 29, 1117–1129. https://doi.org/10.1016/0021-9290(96)00023-1

Cecchi, G.A., Huang, L., Hashmi, J.A., Baliki, M., Centeno, M. V., Rish, I., Apkarian, A.V., 2012. Predictive Dynamics of Human Pain Perception. PLoS Comput. Biol. 8, e1002719. https://doi.org/10.1371/journal.pcbi.1002719

Chalfie, M., 2009. Neurosensory mechanotransduction. Nat. Rev. Mol. Cell Biol. 10, 44–52. https://doi.org/10.1038/nrm2595

Chalhoub, E., Hanson, R.W., Belovich, J.M., 2007. A computer model of gluconeogenesis and lipid metabolism in the perfused liver. AJP Endocrinol. Metab. 293, E1676–E1686. https://doi.org/10.1152/ajpendo.00161.2007

Champely, S., 2017. pwr: Basic Functions for Power Analysis.

Chau, A.M.T., Pelzer, N.R., Hampton, J., Smith, A., Seex, K.A., Stewart, F., Gragnaniello, C., 2014. Lateral extent and ventral laminar attachments of the lumbar ligamentum flavum: Cadaveric study. Spine J.

14, 2467–2471. https://doi.org/10.1016/j.spinee.2014.03.041

Chen, C.-C., Zimmer, Anne, Sun, W.-H., Hall, J., Brownstein, M.J., Zimmer, Andreas, 2002. A role for ASIC3 in the modulation of high-intensity pain stimuli. Proc. Natl. Acad. Sci. U. S. A. 99, 8992–8997. https://doi.org/10.1073/pnas.122245999

Chen, C., Lu, Y., Kallakuri, S., Patwardhan, A., Cavanaugh, J.M., 2006. Distribution of A-d and C-fiber receptors in the cervical facet joint capsule and their response to stretch. J. Bone Jt. Surg. - Ser. A 88, 1807–1816. https://doi.org/10.2106/JBJS.E.00880

Chen, S.Y., Cheng, H.J., 2009. Functions of axon guidance molecules in synapse formation. Curr. Opin. Neurobiol. 19, 471–478. https://doi.org/10.1016/j.conb.2009.09.005

Cherkin, D.C., Sherman, K.J., Balderson, B.H., Cook, A.J., Anderson, M.L., Hawkes, R.J., Hansen, K.E., Turner, J.A., 2016. Effect of mindfulness-based stress reduction vs cognitive behavioral therapy or usual care on back pain and functional limitations in adults with chronic low back pain: A randomized clinical trial. J. Am. Med. Assoc. 315, 1240–1249. https://doi.org/10.1001/jama.2016.2323

Chesterton, L.S., Barlas, P., Foster, N.E., Baxter, D.G., Wright, C.C., 2003. Gender differences in pressure pain threshold in healthy humans. Pain 101, 259–266. https://doi.org/10.1016/S0304-3959(02)00330-5

Choi, J., Dib-Hajj, S.D., Waxman, S.G., 2007. Differential Slow Inactivation and Use-Dependent Inhibition of NaV 1.8 Channels Contribute to Distinct Firing Properties in IB4+ and IB4–DRG Neurons 1258–1265. https://doi.org/10.1152/jn.01033.2006

Cholewicki, J., McGill, S.M., 1996. Mechanical stability of the in vivo lumbar spine implications for injury and chronic low back pain. Clin. Biomech. 11, 1–15.

Cholewicki, J., McGill, S.M., 1994. EMG assisted optimization : A hybrid approach for estimating muscle forces in an indeterminate biomechanical model. J. Biomech. 27, 1287–1289.

Ciubotariu, A., Arendt-Nielsen, L., Graven-Nielsen, T., 2007. Localized muscle pain causes prolonged recovery after fatiguing isometric contractions. Exp. brain Res. 181, 147–58. https://doi.org/10.1007/s00221-007-0913-4

Claude, L.N., Solomonow, M., Zhou, B.-H., Baratta, R. V., Zhu, M.P., 2003. Neuromuscular dysfunction elicited by cyclic lumbar flexion. Muscle and Nerve 27, 348–358. https://doi.org/10.1002/mus.10318

Coderre, T.J., Katz, J., Vaccarino, A.L., Melzack, R., 1993. Contribution of central neuroplasticity to pathological pain: review of clinical and experimental evidence. Pain 52, 259–285. https://doi.org/10.1016/0304-3959(93)90161-H

Colbert, C.M., Johnston, D., 1996. Axonal action-potential initiation and Na+ channel densities in the soma and axon initial segment of subicular pyramidal neurons. J. Neurosci. 16, 6676–86. https://doi.org/8824308

Cole, M.H., Grimshaw, P.N., 2003. Low back pain and lifting: a review of epidemiology and aetiology. Work 21, 173–184.

Cordero-Erausquin, M., Inquimbert, P., Schlichter, R., Hugel, S., 2016. Neuronal networks and nociceptive processing in the dorsal horn of the spinal cord. Neuroscience 338, 230–247. https://doi.org/10.1016/j.neuroscience.2016.08.048

Corey, S.M., Vizzard, M.A., Badger, G.J., Langevin, H.M., 2011. Sensory innervation of the nonspecialized connective tissues in the low back of the rat. Cells Tissues Organs 194, 521–530.

https://doi.org/10.1159/000323875

Costa, L.C.M., Maher, C.G., Hancock, M.J., McAuley, J.H., Herbert, R.D., Costa, L.O.P., 2012. The prognosis of acute and persistent low-back pain: A meta analysis. CMAJ 184, E613–E624. https://doi.org/10.1503/cmaj.111271

Costa, L.C.M., Maher, C.G., McAuley, J.H., Hancock, M.J., Herbert, R.D., Refshauge, K.M., Henschke, N., 2009. Prognosis for patients with chronic low back pain: inception cohort study. BMJ 339, 850. https://doi.org/10.1136/bmj.b3829

Cragg, B.G., Thomas, P.K., 1961. Changes in conduction velocity and fibre size proximal to peripheral nerve lesions. J. Physiol. 157, 315–327.

Craig, A.D., 2003. Pain mechanisms: Labeled lines versus convergence in central processing. Annu. Rev. Neurosci. 26, 1–30. https://doi.org/10.1146/annurev.neuro.26.041002.131022

Craig, A.D., Andrew, D., 2002. Responses of Spinothalamic Lamina I Neurons to Repeated Brief Contact Heat Stimulation in the Cat. J. Neurophysiol. 87, 1902–1914. https://doi.org/10.1152/jn.00578.2001

Criscenti, G., De Maria, C., Sebastiani, E., Tei, M., Placella, G., Speziali, A., Vozzi, G., Cerulli, G., 2015. Quasi-linear viscoelastic properties of the human medial patello-femoral ligament. J. Biomech. 48, 4297–4302. https://doi.org/10.1016/j.jbiomech.2015.10.042

Cummins, T.R., Sheets, P.L., Waxman, S.G., 2007. The roles of sodium channels in nociception: Implications for mechanisms of pain. Pain 131, 243–257. https://doi.org/10.1016/j.jacc.2007.01.076.White

D'Ambrosia, P., King, K.B., Davidson, B.S., Zhou, B.-H., Lu, Y., Solomonow, M., 2010. Pro-inflammatory cytokines expression increases following low- and high-magnitude cyclic loading of lumbar ligaments. Eur. Spine J. 19, 1330–1339. https://doi.org/10.1007/s00586-010-1371-4

Dalton, B.H., Power, G.A., Vandervoort, A.A., Rice, C.L., 2010. Power loss is greater in old men than young men during fast plantar flexion contractions. J. Appl. Physiol. 109, 1441–7. https://doi.org/10.1152/japplphysiol.00335.2010

Dankaerts, W., O'Sullivan, P.B., Burnett, A.F., Straker, L.M., Danneels, L.A., 2004. Reliability of EMG measurements for trunk muscles during maximal and sub-maximal voluntary isometric contractions in healthy controls and CLBP patients. J. Electromyogr. Kinesiol. 14, 333–342. https://doi.org/10.1016/j.jelekin.2003.07.001

Dankaerts, W., O'Sullivan, P.B., Burnett, A.F., Straker, L.M., Davey, P., Gupta, R., 2009. Discriminating healthy controls and two clinical subgroups of nonspecific chronic low back pain patients using trunk muscle activation and lumbosacral kinematics of postures and movements: a statistical classification model. Spine (Phila. Pa. 1976). 34, 1610–1618. https://doi.org/10.1097/BRS.0b013e3181aa6175

Dao, T.T., 2016. Enhanced Musculoskeletal Modeling for Prediction of Intervertebral Disc Stress Within Annulus Fibrosus and Nucleus Pulposus Regions During Flexion Movement. J. Med. Biol. Eng. 36, 583–593. https://doi.org/10.1007/s40846-016-0156-6

De Biasi, S., Rustioni, A., 1988. Glutamate and substance P coexist in primary afferent terminals in the superficial laminae of spinal cord. Proc. Natl. Acad. Sci. U. S. A. 85, 7820–7824. https://doi.org/10.1073/pnas.85.20.7820

De Carvalho, D.E., Soave, D., Ross, K., Callaghan, J.P., 2010. Lumbar Spine and Pelvic Posture Between Standing and Sitting: A Radiologic Investigation Including Reliability and Repeatability of the Lumbar Lordosis Measure. J. Manipulative Physiol. Ther. 33, 48–55.

https://doi.org/10.1016/j.jmpt.2009.11.008

Deering, R., Pashibin, T., Cruz, M., Hunter, S.K., Hoeger Bement, M., 2019. Fatiguing Trunk Flexor Exercise Decreases Pain Sensitivity in Postpartum Women. Front. Physiol. 10, 1–9. https://doi.org/10.3389/fphys.2019.00315

Delitto, A., Erhard, R.E., Bowling, R.W., 1995. A treatment-based classification approach to low back syndrome: identifying and staging patients for conservative treatment. Phys. Ther. 75, 470–485; discussion 485-489. https://doi.org/10.1197/j.jht.2007.12.001

Dempsey, P.G., Hashemi, L., 1999. Analysis of workers' compensation claims associated with manual materials\par handling.\par. Ergonomics 42, 183–95.

Dennett, D., 1978. Why you can't make a machine that feels pain. Synthese 38, 415–456. https://doi.org/10.1007/BF00486638Drescher

Deyo, R.A., Mirza, S.K., 2016. Herniated Lumbar Intervertebral Disk. N. Engl. J. Med. 374, 1763–1772. https://doi.org/10.1056/nejmcp1512658

Dezhdar, T., Moshourab, R.A., Fründ, I., Lewin, G.R., Schmuker, M., 2015. A Probabilistic Model for Estimating the Depth and Threshold Temperature of C-fiber Nociceptors. Sci. Rep. 5, 17670. https://doi.org/10.1038/srep17670

Dib-Hajj, S.D., Yang, Y., Black, J.A., Waxman, S.G., 2013. The NaV1.7 sodium channel: from molecule to man. Nat. Rev. Neurosci. 14, 49–62. https://doi.org/10.1038/nrn3404

Dickey, J.P., McNorton, S., Potvin, J.R., 2003. Repeated spinal flexion modulates the flexion-relaxation phenomenon. Clin. Biomech. 18, 783–789. https://doi.org/10.1016/S0268-0033(03)00166-9

Dimitroulias, A., Tsonidis, C., Natsis, K., Venizelos, I., Djau, S.N., Tsitsopoulos, P., Tsitsopoulos, P., 2010. An immunohistochemical study of mechanoreceptors in lumbar spine intervertebral discs. J. Clin. Neurosci. 17, 742–745. https://doi.org/10.1016/j.jocn.2009.09.032

Doleys, D.M., 2017. Chronic pain as a hypothetical construct: A practical and philosophical consideration. Front. Psychol. 8, 1–7. https://doi.org/10.3389/fpsyg.2017.00664

Drake, J.D.M., Callaghan, J.P., 2009. Intervertebral neural foramina deformation due to two types of repetitive combined loading. Clin. Biomech. 24, 1–6. https://doi.org/10.1016/j.clinbiomech.2008.09.010

Drake, J.D.M., Callaghan, J.P., 2006. Elimination of electrocardiogram contamination from electromyogram signals: An evaluation of currently used removal techniques. J. Electromyogr. Kinesiol. 16, 175–187. https://doi.org/10.1016/j.jelekin.2005.07.003

Du, X., Gamper, N., 2013. Potassium channels in peripheral pain pathways: expression, function and therapeutic potential. Curr. Neuropharmacol. 11, 621–40. https://doi.org/10.2174/1570159X113119990042

Duan, B., Cheng, L., Bourane, S., Britz, O., Padilla, C., Garcia-Campmany, L., Krashes, M.J., Knowlton, W., Velasquez, T., Ren, X., Ross, S.E., Lowell, B.B., Wang, Y., Goulding, M., Ma, Q., 2014. Identification of spinal circuits transmitting and gating mechanical pain. Cell 159, 1417–1432. https://doi.org/10.1016/j.cell.2014.11.003

Dubin, A.E., Patapoutian, A., 2010. Nociceptors: The sensors of the pain pathway. J. Clin. Invest. 120, 3760–3772. https://doi.org/10.1172/JCI42843

Duncan, G., 2017. The Meanings of 'Pain' in Historical, Social, and Political Context. Monist 100, 514–

531. https://doi.org/10.1093/monist/onx026

Dunn, K.M., Jordan, K., Croft, P.R., 2006. Characterizing the course of low back pain: A latent class analysis. Am. J. Epidemiol. 163, 754–761. https://doi.org/10.1093/aje/kwj100

Dvoretzky, A., 1956. On Stochastic Approximation, in: Proceedings of the Third Berkeley Symposium on Mathematical Statistics and Probability. pp. 39–55.

Ebara, S., Latridis, J.C., Setton, L.A., Foster, R.J., Mow, V.C., Weidenbaum, M., 1996. Tensile properties of the non-degenerate human lumbar annulus fibrosus. Spine (Phila. Pa. 1976).

Ebraheim, N.A., Hassan, A., Lee, M., Xu, R., 2004. Functional anatomy of the lumbar spine. Semin. Pain Med. 2, 131–137. https://doi.org/10.1016/j.spmd.2004.08.004

Ehrlich, G.E., 2003. Low back pain. Bull. World Health Organ. 81, 671–676.

El Mestikawy, S., Wallén-Mackenzie, Å., Fortin, G.M., Descarries, L., Trudeau, L.E., 2011. From glutamate co-release to vesicular synergy: Vesicular glutamate transporters. Nat. Rev. Neurosci. 12, 204–216. https://doi.org/10.1038/nrn2969

Ellingson, L.D., Koltyn, K.F., Kim, J.S., Cook, D.B., 2014. Does exercise induce hypoalgesia through conditioned pain modulation? Psychophysiology 51, 267–276. https://doi.org/10.1111/psyp.12168

Enoka, R.M., Duchateau, J., 2008. Muscle fatigue: what, why and how it influences muscle function. J. Physiol. 586, 11–23. https://doi.org/10.1113/jphysiol.2007.139477

Fairbank, J., Gwilym, S.E., France, J.C., Daffner, S.D., Dettori, J., Hermsmeyer, J., Andersson, G.B.J., 2011. The role of classification of chronic low back pain. Spine (Phila. Pa. 1976). 36, S19-42. https://doi.org/10.1097/BRS.0b013e31822ef72c

Fang, X., Djouhri, L., McMullan, S., Berry, C., Waxman, S.G., Okuse, K., Lawson, S.N., 2006. Intense Isolectin-B4 Binding in Rat Dorsal Root Ganglion Neurons Distinguishes C-Fiber Nociceptors with Broad Action Potentials and High Nav1.9 Expression. J. Neurosci. 26, 7281–7292. https://doi.org/10.1523/JNEUROSCI.1072-06.2006

Fick, J.M., Ronkainen, A., Herzog, W., Korhonen, R.K., 2015. Site-dependent biomechanical responses of chondrocytes in the rabbit knee joint. J. Biomech. 48, 4010–4019. https://doi.org/10.1016/j.jbiomech.2015.09.049

Fields, A.J., Liebenberg, E.C., Lotz, J.C., 2014. Innervation of pathologies in the lumbar vertebral end plate and intervertebral disc. Spine J. 14, 513–521. https://doi.org/10.1016/j.spinee.2013.06.075

Finocchietti, S., Mørch, C.D., Arendt-Nielsen, L., Graven-Nielsen, T., 2011. Effects of adipose thickness and muscle hardness on pressure pain sensitivity: Correction. Clin. J. Pain 27, 735–745. https://doi.org/10.1097/AJP.0b013e31820c5353

Flor, H., Nikolajsen, L., Jensen, T.S., 2006. Phantom limb pain: A case of maladaptive CNS plasticity? Nat. Rev. Neurosci. 7, 873–881. https://doi.org/10.1038/nrn1991

Foster, N.E., Hill, J.C., Hay, E.M., 2011. Subgrouping patients with low back pain in primary care: are we getting any better at it? Man. Ther. 16, 3–8. https://doi.org/10.1016/j.math.2010.05.013

Frahm, K., Mørch, C., Grill, W.M., Lubock, N.B., Hennings, K., Andersen, O., 2013. Activation of peripheral nerve fibers by electrical stimulation in the sole of the foot. BMC Neurosci. 14, 116. https://doi.org/10.1186/1471-2202-14-116

François, A., Low, S.A., Sypek, E.I., Christensen, A.J., Sotoudeh, C., Beier, K.T., Ramakrishnan, C., Ritola,

K.D., Sharif-Naeini, R., Deisseroth, K., Delp, S.L., Malenka, R.C., Luo, L., Hantman, A.W., Scherrer, G., 2017. A Brainstem-Spinal Cord Inhibitory Circuit for Mechanical Pain Modulation by GABA and Enkephalins. Neuron 93, 822–839. https://doi.org/10.1016/j.neuron.2017.01.008

Fritz, J.M., Delitto, A., Erhard, R.E., 2003. Comparison of classification-based physical therapy with therapy based on clinical practice guidelines for patients with acute low back pain: a randomized clinical trial. Spine (Phila. Pa. 1976). 28, 1363–1371; discussion 1372. https://doi.org/10.1097/01.BRS.0000067115.61673.FF

Fuchs, P.N., Peng, Y.B., Boyette-Davis, J.A., Uhelski, M.L., 2014. The anterior cingulate cortex and pain processing. Front. Integr. Neurosci. 8, 1–10. https://doi.org/10.3389/fnint.2014.00035

Fung, Y.C., 1994. Mechanical Properties of Real Fluids and Solids, in: A First Course in Continuum Mechanics. Prentice-Hall, pp. 181–208.

Gajsar, H., Nahrwold, K., Titze, C., Hasenbring, M.I., Vaegter, H.B., 2018. Exercise does not produce hypoalgesia when performed immediately after a painful stimulus. Scand. J. Pain 18, 311–320. https://doi.org/10.1515/sjpain-2018-0024

Galbusera, F., Niemeyer, F., Tao, Y., Cina, A., Sconfienza, L.M., Kienle, A., Wilke, H.J., 2021. ISSLS Prize in Bioengineering Science 2021: in vivo sagittal motion of the lumbar spine in low back pain patients—a radiological big data study. Eur. Spine J. https://doi.org/10.1007/s00586-021-06729-z

Gallagher, E.J., Liebman, M., Bijur, P.E., 2001. Prospective validation of clinically important changes in pain severity measured on a visual analog scale. Ann. Emerg. Med. 38, 633–638. https://doi.org/10.1067/mem.2001.118863

Gallagher, K.M., Campbell, T., Callaghan, J.P., 2014. The influence of a seated break on prolonged standing induced low back pain development. Ergonomics 57, 555–62. https://doi.org/10.1080/00140139.2014.893027

Gallagher, S., Heberger, J.R., 2012. Examining the Interaction of Force and Repetition on Musculoskeletal Disorder Risk: A Systematic Literature Review. Hum. Factors 55, 108–124. https://doi.org/10.1177/0018720812449648

Gallagher, S., Marras, W.S., 2012. Tolerance of the lumbar spine to shear: A review and recommended exposure limits. Clin. Biomech. 27, 973–978. https://doi.org/10.1016/j.clinbiomech.2012.08.009

Gallagher, S., Marras, W.S., Litsky, A.S., Burr, D., 2005. Torso Flexion Loads and the Fatigue Failure of Human Lumbosacral Motion Segments. Spine (Phila. Pa. 1976). 30, 2265–2273. https://doi.org/10.1097/01.brs.0000182086.33984.b3

Gandevia, S.C., 2001. Spinal and supraspinal factors in human muscle fatigue. Physiol. Rev. 81, 1725–89.

Garell, P.C., McGillis, S.L., Greenspan, J.D., 1996. Mechanical response properties of nociceptors innervating feline hairy skin. J. Neurophysiol. 75, 1177–1189.

Gedalia, U., Solomonow, M., Zhou, B.-H., Baratta, R. V., Lu, Y., Harris, M., 1999. Biomechanics of increased exposure to lumbar injury caused by cyclic loading. Part 2. Recovery of reflexive muscular stability with rest. Spine (Phila. Pa. 1976). 24, 2461–7.

Geffeney, S.L., Goodman, M.B., 2012. How we feel: Ion channel partnerships that detect mechanical inputs and give rise to touch and pain perception. Neuron 74, 609–619. https://doi.org/10.1016/j.neuron.2012.04.023

Gerling, G.J., Wan, L., Hoffman, B.U., Wang, Y., Lumpkin, E.A., 2018. Computation predicts rapidly

adapting mechanotransduction currents cannot account for tactile encoding in Merkel cell-neurite complexes. PLoS Comput. Biol. 14, 1–21. https://doi.org/10.1371/journal.pcbi.1006264

Gerstner, W., Kistler, W.M., Naud, R., Paninski, L., 2014. Neuronal Dynamics: From single neurons to networks and models of cognition and beyond, 1st ed. Cambridge University Press, Cambridge, UK.

Ghitani, N., Barik, A., Szczot, M., Thompson, J.H., Li, C., Le Pichon, C.E., Krashes, M.J., Chesler, A.T., 2017. Specialized Mechanosensory Nociceptors Mediating Rapid Responses to Hair Pull. Neuron 95, 944-954.e4. https://doi.org/10.1016/j.neuron.2017.07.024

Gillespie, K.A., Dickey, J.P., 2004. Biomechanical role of lumbar spine ligaments in flexion and extension: Determination using a parallel linkage robot and a porcine model. Spine (Phila. Pa. 1976). 29, 1208–1216. https://doi.org/10.1097/00007632-200406010-00010

Goffaux, P., Redmond, W.J., Rainville, P., Marchand, S., 2007. Descending analgesia - When the spine echoes what the brain expects. Pain 130, 137–143. https://doi.org/10.1016/j.pain.2006.11.011

Gooyers, C.E., McMillan, E.M., Noguchi, M., Quadrilatero, J., Callaghan, J.P., 2015. Characterizing the combined effects of force, repetition and posture on injury pathways and micro-structural damage in isolated functional spinal units from sub-acute-failure magnitudes of cyclic compressive loading. Clin. Biomech. 30, 953–959. https://doi.org/10.1016/j.clinbiomech.2015.07.003

Gore, M., Sadosky, A., Stacey, B.R., Tai, K.-S., Leslie, D., 2012. The burden of chronic low back pain: clinical comorbidities, treatment patterns, and health care costs in usual care settings. Spine (Phila. Pa. 1976). 37, E668-77. https://doi.org/10.1097/BRS.0b013e318241e5de

Goubert, D., Danneels, L., Graven-Nielsen, T., Descheemaeker, F., Meeus, M., 2017. Differences in Pain Processing Between Patients with Chronic Low Back Pain, Recurrent Low Back Pain, and Fibromyalgia. Pain Physician 20, 307–318.

Gould, H.J., England, J.D., Soignier, R.D., Nolan, P., Minor, L.D., Liu, Z.P., Levinson, S.R., Paul, D., 2004. Ibuprofen blocks changes in nav 1.7 and 1.8 sodium channels associated with complete freund's adjuvant-induced inflammation in rat. J. Pain 5, 270–280. https://doi.org/10.1016/j.jpain.2004.04.005

Granan, L.P., 2016. The Ising model applied on chronification of pain. Pain Med. (United States) 17, 5–9. https://doi.org/10.1111/pme.12933

Granata, K.P., Rogers, E.L., Moorhouse, K., 2005. Effects of static flexion-relaxation on paraspinal reflex behavior. Clincal Biomech. 20, 16–24. https://doi.org/10.1242/jcs.03292.Multiple

Grant, K.A., Habes, D.J., Tepper, A.J., 1995. Work activities and musculoskeletal complaints among preschool workers. Appl. Ergon. 26, 405–410.

Greffrath, W., Binzen, U., Schwarz, S.T., Saaler-Reinhardt, S., Treede, R.-D., 2003. Co-expression of heat sensitive vanilloid receptor subtypes in rat dorsal root ganglion neurons. NeruoReport 14, 2251–2255. https://doi.org/10.1097/01.wnr.000009571

Gregory, D.E., Callaghan, J.P., 2011. Does vibration inﬂuence the initiation of intervertebral disc herniation?: An examination of herniation occurrence using a porcine cervical disc model. Spine (Phila. Pa. 1976). 36. https://doi.org/10.1097/BRS.0b013e3181d89094

Gregory, N.S., Brito, R.G., Fusaro, M.C.G.O., Sluka, K.A., 2016. ASIC3 Is Required for Development of Fatigue-Induced Hyperalgesia. Mol. Neurobiol. 53, 1020–1030. https://doi.org/10.1007/s12035-014-9055-4

Groh, A.M.R., Fournier, D.E., Battié, M.C., Séguin, C.A., 2021. Innervation of the Human Intervertebral

Disc: A Scoping Review. Pain Med. 22, 1281–1304. https://doi.org/10.1093/pm/pnab070

Gruber, H.E., Hoelscher, G.L., Ingram, J.A., Hanley, E.N., 2012. Genome-wide analysis of pain-, nerve- and neurotrophin -related gene expression in the degenerating human annulus. Mol. Pain 8, 1–18. https://doi.org/10.1186/1744-8069-8-63

Gumbel, E.J., 1941. The Return Period of Flood Flows. Ann. Math. Stat. 12, 163–190.

Guo, D., Hu, J., 2014. Spinal presynaptic inhibition in pain control. Neuroscience 283, 95–106. https://doi.org/10.1016/j.neuroscience.2014.09.032

Haeri, M., Asemani, D., Gharibzadeh, S., 2003. Modeling of pain using artificial neural networks. J. Theor. Biol. 220, 277–284.

Hägg, G.M., Åström, A., 1997. Load pattern and pressure pain threshold in the upper trapezius muscle and psychosocial factors in medical secretaries with and without shoulder/neck disorders. Int. Arch. Occup. Environ. Health 69, 423–432. https://doi.org/10.1007/s004200050170

Hägg, O., Fritzell, P., Nordwall, A., 2003. The clinical importance of changes in outcome scores after treatment for chronic low back pain. Eur. spine J. 12, 12–20. https://doi.org/10.1007/s00586-002-0464-0

Hall, H., McIntosh, G., Boyle, C., 2009. Effectiveness of a low back pain classification system. Spine J. 9, 648–57. https://doi.org/10.1016/j.spinee.2009.04.017

Handwerker, H.O., 2010. Classification of nociceptors - To what purpose? Pain 148, 355–356. https://doi.org/10.1016/j.pain.2009.12.012

Handwerker, H.O., Anton, F., Reeh, P.W., 1987. Discharge patterns of afferent cutaneous nerve fibers from the rat's tail during prolonged noxious mechanical stimulation. Exp. Brain Res. 65, 493–504.

Hansen, B.B., Bendix, T., Grindsted, J., Bliddal, H., Christensen, R., Hansen, P., Riis, R.G.C., Boesen, M., 2015. Effect of lumbar disc degeneration and low back pain on the lumbar lordosis in supine and standing: A cross-sectional MRI study. Spine (Phila. Pa. 1976). 40, 1690–1696. https://doi.org/10.1097/BRS.0000000000001120

Hansson, T., Bigos, S., Beecher, P., Wortley, M., 1985. The lumbar lordosis in acute and chronic low-back pain. Spine (Phila. Pa. 1976).

Harper, A.A., Lawson, S.N., 1985. Electrical properties of rat dorsal root ganglion neurones with different peripheral nerve conduction velocities. J. Physiol. 359, 47–63. https://doi.org/10.1113/jphysiol.1985.sp015574

Harvey, S., Hukins, D., Smith, F., Wardlaw, D., Kader, D., 2016. Measurement of lumbar spine intervertebral motion in the sagittal plane using videofluoroscopy. J. Back Musculoskelet. Rehabil. 29, 445–457. https://doi.org/10.3233/BMR-150639

Hebert, J.J., Koppenhaver, S.L., Walker, B.F., 2011. Subgrouping patients with low back pain: A treatment-based approach to classification. Sports Health 3, 534–542. https://doi.org/10.1177/1941738111415044

Heinricher, M.M., Tavares, I., Leith, J.L., Lumb, B.M., 2009. Descending control of nociception: Specificity, recruitment and plasticity. Brain Res. Rev. 60, 214–225. https://doi.org/10.1016/j.brainresrev.2008.12.009

Hendershot, B., Bazrgari, B., Muslim, K., Toosizadeh, N., Nussbaum, M.A., Madigan, M.L., 2011. Disturbance and recovery of trunk stiffness and reflexive muscle responses following prolonged trunk

flexion: Influences of flexion angle and duration. Clin. Biomech. 26, 250–256. https://doi.org/10.1016/j.clinbiomech.2010.09.019

Hendrich, J., Alvarez, P., Joseph, E.K., Chen, X., Bogen, O., Levine, J.D., 2013. Electrophysiological correlates of hyperalgesic priming in vitro and in vivo. Pain 154, 2207–2215. https://doi.org/10.1016/j.pain.2013.07.004

Henneman, E., Somjen, G., Carpenter, D.O., 1965. Functional significance of cell size in spinal motoneurons. J. Neurophysiol. 28, 560–580.

Hermens, H.J., Freriks, B., Disselhorst-Klug, C., Rau, G., 2000. Development of recommendations for SEMG sensors and sensor placement procedures. J. Electromyogr. Kinesiol. 10, 361–374. https://doi.org/10.1016/S1050-6411(00)00027-4

Heylings, D.J., 1978. Supraspinous and interspinous ligaments of the human lumbar spine. J. Anat. 125, 127–31.

Higuchi, K., Sato, T., 2002. Anatomical study of human lumbar spine innervation. Folia Morphol. (Warsz). 61, 71–79.

Hill, J.C., Afolabi, E.K., Lewis, M., Dunn, K.M., Roddy, E., Van Der Windt, D.A., Foster, N.E., 2016. Does a modified STarT Back Tool predict outcome with a broader group of musculoskeletal patients than back pain? A secondary analysis of cohort data. BMJ Open 6, 1–8. https://doi.org/10.1136/bmjopen-2016-012445

Hill, J.M., 2000. Discharge of group IV phrenic afferent fibers increases during diaphragmatic fatigue. Brain Res. 856, 240–244. https://doi.org/10.1016/S0006-8993(99)02366-5

Hindle, R.J., Pearcy, M.J., Cross, A., 1990. Mechanical function of the human lumbar interspinous and supraspinous ligaments. J. Biomed. Eng. 12, 340–344. https://doi.org/10.1016/0141-5425(90)90010-K

Hingorani, R. V., Provenzano, P.P., Lakes, R.S., Escarcega, A., Vanderby Jr., R., 2004. Nonlinear viscoelasticity in rabbit medial collateral ligament. Ann Biomed Eng 32, 306–312. https://doi.org/10.1023/B:ABME.0000012751.31686.70

Hirsch, C., Ingelmark, B.-E., Miller, M., 1963. The Anatomical Basis for Low Back Pain: Studies on the presence of sensory nerve endings in ligamentous, capsular and intervertebral disc structures in the human lumbar spine. Acta Orthop. Scand. 33, 1–17. https://doi.org/10.3109/17453676308999829

Hjermstad, M.J., Fayers, P.M., Haugen, D.F., Caraceni, A., Hanks, G.W., Loge, J.H., Fainsinger, R., Aass, N., Kaasa, S., 2011. Studies comparing numerical rating scales, verbal rating scales, and visual analogue scales for assessment of pain intensity in adults: A systematic literature review. J. Pain Symptom Manage. 41, 1073–1093. https://doi.org/10.1016/j.jpainsymman.2010.08.016

Hochman, B., Isoldi, F.C., Gonçalves de Freitas, J.O., Lapin, G.A.F., Quieregatto, P.R., Da Silva, E.C.R., Chadi, G., Ferreira, L.M., 2014. Reaction time and replenishment time of SP and CGRP after incision in rat skin. Cent. Eur. J. Biol. 9, 1140–1146. https://doi.org/10.2478/s11535-014-0349-3

Hockley, J.R.F., González-Cano, R., McMurray, S., Tejada-Giraldez, M.A., McGuire, C., Torres, A., Wilbrey, A.L., Cibert-Goton, V., Nieto, F.R., Pitcher, T., Knowles, C.H., Baeyens, J.M., Wood, J.N., Winchester, W.J., Bulmer, D.C., Cendán, C.M., McMurray, G., 2017. Visceral and somatic pain modalities reveal NaV1.7-independent visceral nociceptive pathways. J. Physiol. 595, 2661–2679. https://doi.org/10.1113/JP272837

Hodgkin, A.L., Huxley, A.F., 1952a. A quantitative description of membrane current and its application to

conduction and excitation in nerve. J. Physiol. 117, 500–544. https://doi.org/10.1113/jphysiol.1952.sp004764

Hodgkin, A.L., Huxley, A.F., 1952b. Currents carried by sodium and potassium ions through the membrane of the giant axon of Loligo. J. Physiol. 116, 449–472.

Hoeger Bement, M.K., Weyer, A.D., Hartley, S., Yoon, T., Hunter, S.K., 2009. Fatiguing exercise attenuates pain-induced corticomotor excitability. Neurosci. Lett. 452, 209–213. https://doi.org/10.1016/j.neulet.2009.01.038

Hoffman, M.D., Shepanski, M.A., Ruble, S.B., Valic, Z., Buckwalter, J.B., Clifford, P.S., 2004. Intensity and duration threshold for aerobic exercise-induced analgesia to pressure pain. Arch. Phys. Med. Rehabil. 85, 1183–1187. https://doi.org/10.1016/j.apmr.2003.09.010

Hoheisel, U., Taguchi, T., Treede, R.D., Mense, S., 2011. Nociceptive input from the rat thoracolumbar fascia to lumbar dorsal horn neurones. Eur. J. Pain 15, 810–815. https://doi.org/10.1016/j.ejpain.2011.01.007

Hoogendoorn, W.E., Bongers, P.M., de Vet, H.C., Douwes, M., Koes, B.W., Miedema, M.C., Ariëns, G.A., Bouter, L.M., 2000. Flexion and rotation of the trunk and lifting at work are risk factors for low back pain: results of a prospective cohort study. Spine (Phila. Pa. 1976). 25, 3087–92. https://doi.org/10.1097/00007632-200012010-00018

Howarth, S.J., Callaghan, J.P., 2012. Compressive force magnitude and intervertebral joint flexion/extension angle influence shear failure force magnitude in the porcine cervical spine. J. Biomech. 45, 484–490. https://doi.org/10.1016/j.jbiomech.2011.11.051

Howarth, S.J., Callaghan, J.P., 2009. The rule of 1s for padding kinematic data prior to digital filtering: influence of sampling and filter cutoff frequencies. J. Electromyogr. Kinesiol. 19, 875–81. https://doi.org/10.1016/j.jelekin.2008.03.010

Howarth, S.J., Glisic, D., Lee, J.G.B., Beach, T.A.C., 2013a. Does prolonged seated deskwork alter the lumbar flexion relaxation phenomenon? J. Electromyogr. Kinesiol. 23, 587–593. https://doi.org/10.1016/j.jelekin.2013.01.004

Howarth, S.J., Kingston, D.C., Brown, S.H.M., Graham, R.B., 2013b. Viscoelastic creep induced by repetitive spine flexion and its relationship to dynamic spine stability. J. Electromyogr. Kinesiol. 23, 794–800. https://doi.org/10.1016/j.jelekin.2013.04.002

Hoy, D., Bain, C., Williams, G., March, L., Brooks, P., Blyth, F., Woolf, A.D., Vos, T., Buchbinder, R., 2012. A systematic review of the global prevalence of low back pain. Arthritis Rheum. 64, 2028–2037. https://doi.org/10.1002/art.34347

Huang, J., Han, C., Estacion, M., Vasylyev, D., Hoeijmakers, J.G.J., Gerrits, M.M., Tyrrell, L., Lauria, G., Faber, C.G., Dib-Hajj, S.D., Merkies, I.S.J., Waxman, S.G., 2014. Gain-of-function mutations in sodium channel NaV1.9 in painful neuropathy. Brain 137, 1627–1642. https://doi.org/10.1093/brain/awu079

Huang, J., Vanoye, C.G., Cutts, A., Goldberg, Y.P., Dib-Hajj, S.D., Cohen, C.J., Waxman, S.G., George Jr, A.L., 2017. Sodium channel NaV1.9 mutations associated with insensitivity to pain dampen neuronal excitability. J. Clin. Invest. 127, 2805–2814.

Hursh, J.B., 1939. Conduction velocity and diameter of nerve fibers. Am. J. Physiol. 127, 131–139.

Hven, L., Frost, P., Bonde, J.P.E., 2017. Evaluation of pressure pain threshold as a measure of perceived stress and high job strain. PLoS One 12, 1–9. https://doi.org/10.1371/journal.pone.0167257

Ikeuchi, M., Wang, Q., Izumi, M., Tani, T., 2012. Nociceptive sensory innervation of the posterior cruciate ligament in osteoarthritic knees. Arch. Orthop. Trauma Surg. 132, 891–895. https://doi.org/10.1007/s00402-012-1478-7

Imamura, M., Chen, J., Matsubayashi, R., Targino, R.A., Marcon, F., Bueno, D.K., Hsing, W.T., 2013. Changes in pressure pain threshold in patients with chronic nonspecific low back pain. Spine (Phila. Pa. 1976). 38, 2098–2107. https://doi.org/10.1097/01.brs.0000435027.50317.d7

Isaacs, J.L., Vresilovic, E., Sarkar, S., Marcolongo, M., 2014. Role of biomolecules on annulus fibrosus micromechanics: Effect of enzymatic digestion on elastic and failure properties. J. Mech. Behav. Biomed. Mater. 40, 75–84. https://doi.org/10.1016/j.jmbbm.2014.08.012

Jo, Y.H., Schlichter, R., 1999. Synaptic corelease of ATP and GABA in cultured spinal neurons. Nat. Neurosci. 2, 241–245. https://doi.org/10.1038/6344

Jones, M.D., Valenzuela, T., Booth, J., Taylor, J.L., Barry, B.K., 2017. Explicit education about exercise-induced hypoalgesia influences pain responses to acute exercise in healthy adults: A randomised controlled trial. J. Pain 18, 1409–1416. https://doi.org/10.1016/j.jpain.2017.07.006

Jorgensen, M.J., Marras, W.S., Gupta, P., Waters, T.R., 2003. Effect of torso flexion on the lumbar torso extensor muscle sagittal plane moment arms. Spine J. 3, 363–369. https://doi.org/10.1016/S1529-9430(03)00140-2

Joseph, E.K., Levine, J.D., 2010. Hyperalgesic priming is restricted to isolectin B4-positive nociceptors. Neuroscience 169, 431–435. https://doi.org/10.1016/j.neuroscience.2010.04.082

Joshi, S.K., Mikusa, J.P., Hernandez, G., Baker, S., Shieh, C.C., Neelands, T., Zhang, X.F., Niforatos, W., Kage, K., Han, P., Krafte, D., Faltynek, C., Sullivan, J.P., Jarvis, M.F., Honore, P., 2006. Involvement of the TTX-resistant sodium channel Nav 1.8 in inflammatory and neuropathic, but not post-operative, pain states. Pain 123, 75–82. https://doi.org/10.1016/j.pain.2006.02.011

Julius, D., Basbaum, A.I., 2001. Molecular mechanisms of nociception. Nature 413, 203–210. https://doi.org/10.1038/35093019

Kallakuri, S., Cavanaugh, J.M., Blagoev, D.C., 1998. An immunohistochemical study of innervation of lumbar spinal dura and longitudinal ligaments. Spine (Phila. Pa. 1976). https://doi.org/10.1097/00007632-199802150-00001

Kallakuri, S., Singh, A., Chen, C., Cavanaugh, J.M., 2004. Demonstration of substance P, calcitonin gene-related peptide, and protein gene product 9.5 containing nerve fibers in human cervical facet joint capsules. Spine (Phila. Pa. 1976). 29, 1182–1186. https://doi.org/10.1097/00007632-200406010-00005

Kameda, T., Zvick, J., Vuk, M., Sadowska, A., Tam, W.K., Leung, V.Y., Bölcskei, K., Helyes, Z., Applegate, L.A., Hausmann, O.N., Klasen, J., Krupkova, O., Wuertz-Kozak, K., 2019. Expression and activity of TRPA1 and TRPV1 in the intervertebral disc: Association with inflammation and matrix remodeling. Int. J. Mol. Sci. 20. https://doi.org/10.3390/ijms20071767

Kandel, E., Schwartz, J.H., Jessell, T.M., Siegelbaum, S.A., Hudspeth, A.J., 2013. Principles of Neural Science, 5th ed. McGraw-Hill Companies Inc., New York.

Karayannis, N. V., Jull, G.A., Hodges, P.W., 2016. Movement-based subgrouping in low back pain: Synergy and divergence in approaches. Physiother. (United Kingdom) 102, 159–169. https://doi.org/10.1016/j.physio.2015.04.005

Kashiba, H., Uchida, Y., Senba, E., 2001. Difference in binding by isolectin B4 to trkA and c-ret mRNA-

expressing neurons in rat sensory ganglia. Mol. Brain Res. 95, 18–26. https://doi.org/10.1016/S0169-328X(01)00224-8

Kashiwadani, H., Kanmura, Y., Kuwaki, T., 2017. Application of calibrated forceps for assessing mechanical nociception with high time resolution in mice. PLoS One 12, 1–10. https://doi.org/10.1371/journal.pone.0172461

Kawakami, T., Ishihara, M., Mihara, M., 2001. Distribution Density of Intraepidermal Nerve Fibers in Normal Human Skin. J. Dermatol. 28, 63–70. https://doi.org/10.1111/j.1346-8138.2001.tb00091.x

Keller, A.F., Coull, J.A., Chery, N., Poisbeau, P., De Koninck, Y., 2001. Region-specific developmental specialization of GABA-glycine cosynapses in laminas I-II of the rat spinal dorsal horn. J. Neurosci. 21, 7871–7880. https://doi.org/21/20/7871 [pii]

Kelly, A.M., 2001. The minimum clinically significant difference in visual analogue scale pain score does not differ with severity of pain. Emerg. Med. J. 18, 205–7.

Kemp, J., Despres, O., Dufour, A., 2012. Unreliability of the visual analog scale in experimental pain assessment: a sensitivity and evoked potentials study. Pain Physician 15, E693-9.

Kennedy, D.S., Fitzpatrick, S.C., Gandevia, S.C., Taylor, J.L., 2015. Fatigue-related firing of muscle nociceptors reduces voluntary activation of ipsilateral but not contralateral lower limb muscles. J. Appl. Physiol. 118, 408–418. https://doi.org/10.1152/japplphysiol.00375.2014

Kenntner-Mabiala, R., Weyers, P., Pauli, P., 2007. Independent effects of emotion and attention on sensory and affective pain perception. Cogn. Emot. 21, 1615–1629. https://doi.org/10.1080/02699930701252249

Kidd, B.L., Urban, L.A., 2001. Mechanisms of inflammatory pain. Br. J. Anaesth. 87, 3–11. https://doi.org/10.1093/bja/87.1.3

King, K.B., Davidson, B.S., Zhou, B.-H., Lu, Y., Solomonow, M., 2009. High magnitude cyclic load triggers inflammatory response in lumbar ligaments. Clin. Biomech. 24, 792–798. https://doi.org/10.1016/j.clinbiomech.2009.07.011

Kiter, E., Karaboyun, T., Tufan, A.C., Acar, K., 2010. Immunohistochemical demonstration of nerve endings in iliolumbar ligament. Spine (Phila. Pa. 1976). 35, 101–104. https://doi.org/10.1097/BRS.0b013e3181ae561d

Kiyak, E., 2012. The impact of wool in the patients with chronic non-specific low back pain. Coll. Antropol 36, 623–626.

Knapstad, M.K., Goplen, F.K., Ask, T., Skouen, J.S., Nordahl, S.H.G., 2019. Associations between pressure pain threshold in the neck and postural control in patients with dizziness or neck pain - A cross-sectional study. BMC Musculoskelet. Disord. 20, 1–9. https://doi.org/10.1186/s12891-019-2922-4

Kóbor, I., Gál, V., Vidnyánszky, Z., 2009. Attentional modulation of perceived pain intensity in capsaicin-induced secondary hyperalgesia. Exp. Brain Res. 195, 467–472. https://doi.org/10.1007/s00221-009-1799-0

Kodesh, E., Weissman-Fogel, I., 2014. Exercise-induced hypoalgesia – interval versus continuous mode. Appl. Physiol. Nutr. Metab. 39, 829–834. https://doi.org/10.1139/apnm-2013-0481

Koltyn, K.F., 2000. Analgesia following exercise: a review. Sport. Med. 29, 85–98.

Koltyn, K.F., Brellenthin, A.G., Cook, D.B., Sehgal, N., Hillard, C., 2014. Mechanisms of exercise-induced hypoalgesia. J. Pain 15, 1294–1304. https://doi.org/10.1016/j.jpain.2014.09.006

Koltzenburg, M., Stucky, C.L., Lewin, G.R., 1997. Receptive properties of mouse sensory neurons innervating hairy skin. J. Neurophysiol. 78, 1841–1850. https://doi.org/10.1152/jn.1997.78.4.1841

Kosek, E., Ekholm, J., Hansson, P., 1999. Pressure pain thresholds in different tissues in one body region. The influence of skin sensitivity in pressure algometry. Scand. J. Rehabil. Med. 31, 89–93. https://doi.org/10.1080/003655099444597

Koskinen, M., Hietaharju, A., Kyläniemi, M., Peltola, J., Rantala, I., Udd, B., Haapasalo, H., 2005. A quantitative method for the assessment of intraepidermal nerve fibers in small-fiber neuropathy. J. Neurol. 252, 789–794. https://doi.org/10.1007/s00415-005-0743-x

Kucyi, A., Davis, K.D., 2017. The Neural Code for Pain: From Single-Cell Electrophysiology to the Dynamic Pain Connectome. Neuroscientist 23, 397–414. https://doi.org/10.1177/1073858416667716

Kucyi, A., Moayedi, M., Weissman-Fogel, I., Goldberg, M.B., Freeman, B. V., Tenenbaum, H.C., Davis, K.D., 2014. Enhanced Medial Prefrontal-Default Mode Network Functional Connectivity in Chronic Pain and Its Association with Pain Rumination. J. Neurosci. 34, 3969–3975. https://doi.org/10.1523/JNEUROSCI.5055-13.2014

Kumar, K., Taylor, R.S., Jacques, L., Eldabe, S., Meglio, M., Molet, J., Thomson, S., O'Callaghan, J., Eisenberg, E., Milbouw, G., Buchser, E., Fortini, G., Richardson, J., North, R.B., 2007. Spinal cord stimulation versus conventional medical management for neuropathic pain: A multicentre randomised controlled trial in patients with failed back surgery syndrome. Pain 132, 179–188. https://doi.org/10.1016/j.pain.2007.07.028

Kumar, S., 2001. Theories of musculoskeletal injury causation. Ergonomics 44, 17–47. https://doi.org/10.1080/00140130120716

Labaj, A., Diesbourg, T., Dumas, G., Plamondon, A., Mercheri, H., Larue, C., 2016. Posture and lifting exposures for daycare workers. Int. J. Ind. Ergon. 54, 83–92. https://doi.org/10.1016/j.ergon.2016.05.003

Lacourt, T.E., Houtveen, J.H., van Doornen, L.J.P., 2012. Experimental pressure-pain assessments: Test-retest reliability, convergence and dimensionality. Scand. J. Pain 3, 31–37. https://doi.org/10.1016/j.sjpain.2011.10.003

Langley, C.K., Aziz, Q., Bountra, C., Gordon, N., Hawkins, P., Jones, A., Langley, G., Nurmikko, T., Tracey, I., 2008. Volunteer studies in pain research - Opportunities and challenges to replace animal experiments. The report and recommendations of a Focus on Alternatives workshop. Neuroimage 42, 467–473. https://doi.org/10.1016/j.neuroimage.2008.05.030

Lao, L., Daubs, M.D., Scott, T.P., Lord, E.L., Cohen, J.R., Yin, R., Zhong, G., Wang, J.C., 2015. Effect of Disc Degeneration on Lumbar Segmental Mobility Analyzed by Kinetic Magnetic Resonance Imaging. Spine (Phila. Pa. 1976). 40, 316–322. https://doi.org/10.1097/BRS.0000000000000738

Larson, D.J., Brown, S.H.M., 2018. The effects of trunk extensor and abdominal muscle fatigue on postural control and trunk proprioception in young, healthy individuals. Hum. Mov. Sci. 57, 13–20. https://doi.org/10.1016/j.humov.2017.10.019

Latremoliere, A., Woolf, C.J., 2009. Central Sensitization: A Generator of Pain Hypersensitivity by Central Neural Plasticity. J. Pain 10, 895–926. https://doi.org/10.1016/j.jpain.2009.06.012

Lawson, J.J., McIlwrath, S.L., Woodbury, C.J., Davis, B.M., Koerber, H.R., 2008. TRPV1 Unlike TRPV2 Is Restricted to a Subset of Mechanically Insensitive Cutaneous Nociceptors Responding to Heat. J. Pain 9, 298–308. https://doi.org/10.1016/j.jpain.2007.12.001

Lee, H.M., Liau, J.J., Cheng, C.K., Tan, C.M., Shih, J.T., 2003. Evaluation of shoulder proprioception following muscle fatigue. Clin. Biomech. 18, 843–847. https://doi.org/10.1016/S0268-0033(03)00151-7

Lemley, K.J., Hunter, S.K., Bement, M.K.H., 2015. Conditioned pain modulation predicts exercise-induced hypoalgesia in healthy adults. Med. Sci. Sports Exerc. 47, 176–184. https://doi.org/10.1249/MSS.0000000000000381

Lewandowski, A., 1982. Issues in model validation. Int. Inst. Appl. Syst. Anal. RR-82-37, 1–11.

Lewis, R., Asplin, K.E., Bruce, G., Dart, C., Mobasheri, A., Barrett-Jolley, R., 2011. The role of the membrane potential in chondrocyte volume regulation. J. Cell. Physiol. 226, 2979–2986. https://doi.org/10.1002/jcp.22646

Li, H., Santos, M.S., Park, C.K., Dobry, Y., Voglmaier, S.M., 2017. VGLUT2 Trafficking Is Differentially Regulated by Adaptor Proteins AP-1 and AP-3. Front. Cell. Neurosci. 11, 1–20. https://doi.org/10.3389/fncel.2017.00324

Libet, B., Pearl, D.K., Morledge, D.E., Gleason, C.A., Hosobuchi, Y., Barbaro, N.M., 1991. Control of the transition from sensory detection to sensory awareness in man by the duration of a thalamic stimulus: The cerebral "time-on" factor. Brain 114, 1731–1757. https://doi.org/10.1093/brain/114.4.1731

Lichtman, J.W., Conchello, J.A., 2005. Fluorescence microscopy. Nat. Methods 2, 910–919. https://doi.org/10.1038/nmeth817

Lieberman, M.D., Eisenberger, N.I., 2015. The dorsal anterior cingulate cortex is selective for pain: Results from large-scale reverse inference. Proc. Natl. Acad. Sci. 112, 15250–15255. https://doi.org/10.1073/pnas.1515083112

Lima, L. V., Abner, T.S.S., Sluka, K.A., 2017. Does exercise increase or decrease pain? Central mechanisms underlying these two phenomena. J. Physiol. 595, 4141–4150. https://doi.org/10.1113/JP273355

Lin, G.X., Suen, T.K., Quillo-Olvera, J., Akbary, K., Hur, J.W., Kim, E., Park, E.J., Kim, J.S., 2018. Dimensions of the spinous process and interspinous space: a morphometric study. Surg. Radiol. Anat. 40, 1383–1390. https://doi.org/10.1007/s00276-018-2096-z

Lindstedt, F., Lonsdorf, T.B., Schalling, M., Kosek, E., Ingvar, M., 2011. Perception of thermal pain and the thermal grill illusion is associated with polymorphisms in the serotonin transporter gene. PLoS One 6. https://doi.org/10.1371/journal.pone.0017752

Lis, A.M., Black, K.M., Korn, H., Nordin, M., 2007. Association between sitting and occupational LBP. Eur. spine J. 16, 283–98. https://doi.org/10.1007/s00586-006-0143-7

Little, J.S., Khalsa, P.S., 2005. Human lumbar spine creep during cyclic and static flexion: Creep rate, biomechanics, and facet joint capsule strain. Ann. Biomed. Eng. 33, 391–401. https://doi.org/10.1007/s10439-005-1742-x

Liu, F., Li, C., Liu, S., Genin, G.M., Huang, G., Lu, T., Xu, F., 2015. Effect of viscoelasticity on skin pain sensation. Theor. Appl. Mech. Lett. 5, 222–226. https://doi.org/10.1016/j.taml.2015.11.002

Liu, Y., Fan, X., Wei, Y., Piao, Z., Jiang, X., 2014. Intraepidermal nerve fiber density of healthy human. Neurol. Res. 36, 911–914. https://doi.org/10.1179/1743132814Y.0000000377

Llinás, R.R., 2003. The contribution of Santiago Ramon y Cajal to functional neuroscience. Nat. Rev. Neurosci. 4, 77–80.

Loeser, J.D., Melzack, R., 1999. Pain: an overview. Lancet 353, 1607–9. https://doi.org/10.1016/S0140-6736(99)01311-2

Loeser, J.D., Treede, R.D., 2008. The Kyoto protocol of IASP Basic Pain Terminology. Pain 137, 473–477. https://doi.org/10.1016/j.pain.2008.04.025

Lowitzsch, K., Hopf, H.C., Galland, J., 1977. Changes of sensory conduction velocity and refractory periods with decreasing tissue temperature in man. J. Neurol. 216, 181–188. https://doi.org/10.1007/BF00313619

Lu, X.L., Mow, V.C., 2008. Biomechanics of articular cartilage and determination of material properties. Med. Sci. Sports Exerc. 40, 193–199. https://doi.org/10.1249/mss.0b013e31815cb1fc

Lu, Y., Perl, E.R., 2005. Modular organization of excitatory circuits between neurons of the spinal superficial dorsal horn (Laminae I and II). J. Neurosci. 25, 3900–3907. https://doi.org/10.1523/JNEUROSCI.0102-05.2005

Lu, Y., Perl, E.R., 2003. A specific inhibitory pathway between substantia gelatinosa neurons receiving direct C-fiber input. J. Neurosci. 23, 8752–8758. https://doi.org/23/25/8752 [pii]

MacIsaac, D., Parker, P.A., Scott, R.N., 2001. The short-time Fourier transform and muscle fatigue assessment in dynamic contractions. J. Electromyogr. Kinesiol. 11, 439–49. https://doi.org/10.1016/S1050-6411(01)00021-9

Mackiewicz, K.L., Sarinopoulos, I., Cleven, K.L., Nitschke, J.B., 2006. The effect of anticipation and the specificity of sex differences for amygdala and hippocampus function in emotional memory. Proc. Natl. Acad. Sci. 103, 14200–14205. https://doi.org/10.1073/pnas.0601648103

Mahmood, T., Yang, P.C., 2012. Western blot: Technique, theory, and trouble shooting. N. Am. J. Med. Sci. 4, 429–434. https://doi.org/10.4103/1947-2714.100998

Mainero, C., Zhang, W.T., Kumar, A., Rosen, B.R., Sorensen, A.G., 2007. Mapping the spinal and supraspinal pathways of dynamic mechanical allodynia in the human trigeminal system using cardiac-gated fMRI. Neuroimage 35, 1201–1210. https://doi.org/10.1016/j.neuroimage.2007.01.024

Mammoto, T., Ingber, D.E., 2010. Mechanical control of tissue and organ development. Development 137, 1407–1420. https://doi.org/10.1242/dev.024166

Mansour, Z.M., Lepping, R.J., Honea, R.A., Brooks, W.M., Yeh, H.W., Burns, J.M., Sharma, N.K., 2017. Structural Brain Imaging in People with Low Back Pain. Spine (Phila. Pa. 1976). 42, 726–732. https://doi.org/10.1097/BRS.0000000000001915

Martin, M., Béjar, J., Esposito, G., Chávez, D., Contreras-Hernández, E., Glusman, S., Cortés, U., Rudomín, P., 2017. Markovian Analysis of the Sequential Behavior of the Spontaneous Spinal Cord Dorsum Potentials Induced by Acute Nociceptive Stimulation in the Anesthetized Cat. Front. Comput. Neurosci. 11, 1–13. https://doi.org/10.3389/fncom.2017.00032

Martucci, K.T., 2017. Disentangling mood and pain: A commentary on 2 manuscripts. Pain 158, 4–5. https://doi.org/10.1097/j.pain.0000000000000746

Mattucci, S.F.E., Moulton, J.A., Chandrashekar, N., Cronin, D.S., 2013. Strain rate dependent properties of human craniovertebral ligaments. J. Mech. Behav. Biomed. Mater. 23, 71–79. https://doi.org/10.1016/j.jmbbm.2013.04.005

Maurer, K., Hopf, H.C., Lowitzsch, K., 1977. Hypokalemia shortens relative refractory period of peripheral sensory nerves in man. J. Neurol. 216, 67–71. https://doi.org/10.1007/BF00312818

Mawston, G.A., McNair, P.J., Boocock, M.G., 2007. The effects of prior warning and lifting-induced fatigue on trunk muscle and postural responses to sudden loading during manual handling. Ergonomics 50, 2157–70. https://doi.org/10.1080/00140130701510139

McCormick, D.A., 1989. GABA as an inhibitory neurotransmitter in human cerebral cortex. J. Neurophysiol. 62, 1018–1027. https://doi.org/10.1152/jn.1989.62.5.1018

McGill, S.M., Brown, S., 1992. Creep response of the lumbar spine to prolonged full flexion. Clin. Biomech. 7, 43–46. https://doi.org/10.1016/0268-0033(92)90007-Q

McGill, S.M., Hughson, R.L., Parks, K., 2000. Changes in lumbar lordosis modify the role of the extensor muscles. Clin. Biomech. 15, 777–780. https://doi.org/10.1016/S0268-0033(00)00037-1

Medzhitov, R., 2008. Origin and physiological roles of inflammation. Nature 454, 428–435.

Melia, M., Schmidt, M., Geissler, B., König, J., Krahn, U., Ottersbach, H.J., Letzel, S., Muttray, A., 2015. Measuring mechanical pain: The refinement and standardization of pressure pain threshold measurements. Behav. Res. Methods 47, 216–227. https://doi.org/10.3758/s13428-014-0453-3

Mello, R.G.T., Oliveira, L.F., Nadal, J., 2007. Digital Butterworth filter for subtracting noise from low magnitude surface electromyogram. Comput. Methods Programs Biomed. 87, 28–35. https://doi.org/10.1016/j.cmpb.2007.04.004

Mellor, F.E., Thomas, P.W., Thompson, P., Breen, A.C., 2014. Proportional lumbar spine inter-vertebral motion patterns: a comparison of patients with chronic, non-specific low back pain and healthy controls. Eur. Spine J. 23, 2059–2067. https://doi.org/10.1007/s00586-014-3273-3

Melzack, R., 1999. From the gate to the neuromatrix. Pain 82, S121–S126. https://doi.org/10.1016/S0304-3959(99)00145-1

Melzack, R., 1987. The short-form McGill pain questionnaire. Pain 30, 191–197. https://doi.org/doi: 10.1016/0304-3959(87)91074-8

Melzack, R., 1975. The McGill pain questionnaire: Major properties and scoring methods. Pain 1, 277–299. https://doi.org/10.1016/0304-3959(75)90044-5

Melzack, R., Wall, P.D., 1965. Pain Mechanisms : A New Theory. Science (80-.). 150, 971–979.

Mense, S., Hoheisel, U., 2016. Evidence for the existence of nociceptors in rat thoracolumbar fascia. J. Bodyw. Mov. Ther. 20, 623–628. https://doi.org/10.1016/j.jbmt.2016.01.006

Micalos, P.S., Arendt-Nielsen, L., 2016. Differential pain response at local and remote muscle sites following aerobic cycling exercise at mild and moderate intensity. Springerplus 5, 91. https://doi.org/10.1186/s40064-016-1721-8

Minett, M.S., Nassar, M.A., Clark, A.K., Passmore, G., Dickenson, A.H., Wang, F., Malcangio, M., Wood, J.N., 2012. Distinct Nav1.7-dependent pain sensations require different sets of sensory and sympathetic neurons. Nat. Commun. 3, 791–799. https://doi.org/10.1038/ncomms1795

Mogil, J.S., Davis, K.D., Derbyshire, S.W., 2010. The necessity of animal models in pain research. Pain 151, 12–17. https://doi.org/10.1016/j.pain.2010.07.015

Morikawa, H., Paladini, C.A., 2011. Dynamic regulation of midbrain dopamine neuron activity: Intrinsic, synaptic, and plasticity mechanisms. Neuroscience 198, 95–111. https://doi.org/10.1016/j.neuroscience.2011.08.023

Morinaga, T., Takahashi, K., Yamagata, M., Chiba, T., Tanaka, K., Takahashi, Y., Nakamura, S., Suseki,

K., Moriya, H., 1996. Sensory innervation to the anterior portion of lumbar intervertebral disc. Spine (Phila. Pa. 1976). 21, 1848–1851.

Moseley, G.L., 2017. Innovative treatments for back pain. Pain 158, S2–S10. https://doi.org/10.1097/j.pain.0000000000000772

Moseley, G.L., Butler, D.S., 2015. Fifteen Years of Explaining Pain: The Past, Present, and Future. J. Pain 16, 807–813. https://doi.org/10.1016/j.jpain.2015.05.005

Moseley, G.L., Flor, H., 2012. Targeting cortical representations in the treatment of chronic pain: A review. Neurorehabil. Neural Repair 26, 646–652. https://doi.org/10.1177/1545968311433209

Mow, V.C., Gibbs, M.C., Lai, W.M., Zhu, W.B., Athanasiou, K.A., 1989. Biphasic indentation of articular cartilage-II. A numerical algorithm and an experimental study. J. Biomech. 22, 853–861. https://doi.org/10.1016/0021-9290(89)90069-9

Müller-Schwefe, G., Morlion, B., Ahlbeck, K., Alon, E., Coaccioli, S., Coluzzi, F., Huygen, F., Jaksch, W., Kalso, E., Kocot-Kępska, M., Kress, H.G., Mangas, A.C., Margarit Ferri, C., Mavrocordatos, P., Nicolaou, A., Hernández, C.P., Pergolizzi, J., Schäfer, M., Sichère, P., 2017. Treatment for chronic low back pain: the focus should change to multimodal management that reflects the underlying pain mechanisms. Curr. Med. Res. Opin. 33, 1199–1210. https://doi.org/10.1080/03007995.2017.1298521

Munkhammar, J., Mattsson, L., Rydén, J., 2017. Polynomial probability distribution estimation using the method of moments. PLoS One 12, 1–14. https://doi.org/10.1371/journal.pone.0174573

Murakami, M., Fleischmann, B., De Felipe, C., Freichel, M., Trost, C., Ludwig, A., Wissenbach, U., Schwegler, H., Hofmann, F., Hescheler, J., Flockerzi, V., Cavalié, A., 2002. Pain perception in mice lacking the B3 subunit of voltage-activated calcium channels. J. Biol. Chem. 277, 40342–40351. https://doi.org/10.1074/jbc.M203425200

Murray, C.J.L., Lopez, A.D., 2013. Measuring the Global Burden of Disease. N. Engl. J. Med. 369, 448–457. https://doi.org/10.1056/NEJMra1201534

Murtezani, A., Ibraimi, Z., Sllamniku, S., Osmani, T., Sherifi, S., 2011. Prevalence and Risk Factors for Low Back Pain in Industrial Workers. Folia Med. (Plovdiv). 53, 68–74. https://doi.org/10.2478/v10153-011-0060-3

Muslim, K., Bazrgari, B., Hendershot, B., Toosizadeh, N., Nussbaum, M.A., Madigan, M.L., 2013. Disturbance and recovery of trunk mechanical and neuromuscular behaviors following repeated static trunk flexion: Influences of duration and duty cycle on creep-induced effects. Appl. Ergon. 44, 643–651. https://doi.org/10.1016/j.apergo.2012.12.004

Nagel, T., 1974. What is it like to be a bat? Philos. Rev. 83, 435–450. https://doi.org/10.2307/2176743

Nagi, S.S., Marshall, A.G., Makdani, A., Jarocka, E., Liljencrantz, J., Ridderström, M., Shaikh, S., O'Neill, F., Saade, D., Donkervoort, S., Reghan Foley, A., Minde, J., Trulsson, M., Cole, J., Bönnemann, C.G., Chesler, A.T., Catherine Bushnell, M., McGlone, F., Olausson, H., 2019. An ultrafast system for signaling mechanical pain in human skin. Sci. Adv. 5, 1–11. https://doi.org/10.1126/sciadv.aaw1297

Namer, B., Schick, M., Kleggetveit, I.P., Orstavik, K., Schmidt, R., Jorum, E., Torebjörk, E., Handwerker, H.O., Schmelz, M., 2015. Differential sensitization of silent nociceptors to low pH stimulation by prostaglandin E2 in human volunteers. Eur. J. Pain (United Kingdom) 19, 159–166. https://doi.org/10.1002/ejp.532

Naugle, K.M., Fillingim, R.B., Riley, J.L., 2012. A meta-analytic review of the hypoalgesic effects of exercise. J. Pain 13, 1139–1150. https://doi.org/10.1016/j.jpain.2012.09.006

Naugle, K.M., Naugle, K.E., Fillingim, R.B., Samuels, B., Riley, J.L., 2014. Intensity thresholds for aerobic exercise-induced hypoalgesia. Med. Sci. Sports Exerc. 46, 817–825. https://doi.org/10.1249/MSS.0000000000000143

Nederpelt, I., Bleeker, D., Tuijt, B., IJzerman, A.P., Heitman, L.H., 2016. Kinetic binding and activation profiles of endogenous tachykinins targeting the NK1 receptor. Biochem. Pharmacol. 118, 88–95. https://doi.org/10.1016/j.bcp.2016.08.004

Nelson-Wong, E., Callaghan, J.P., 2010. Is muscle co-activation a predisposing factor for low back pain development during standing? A multifactorial approach for early identification of at-risk individuals. J. Electromyogr. Kinesiol. 20, 256–63. https://doi.org/10.1016/j.jelekin.2009.04.009

Newell, N., Little, J.P., Christou, A., Adams, M.A., Adam, C.J., Masouros, S.D., 2017. Biomechanics of the human intervertebral disc: A review of testing techniques and results. J. Mech. Behav. Biomed. Mater. 69, 420–434. https://doi.org/10.1016/j.jmbbm.2017.01.037

Ng, J.K.F., Parnianpour, M., Kippers, V., Richardson, C.A., 2003. Reliability of electromyographic and torque measures during isometric axial rotation exertions of the trunk. Clin. Neurophysiol. 114, 2355–2361. https://doi.org/10.1016/S1388-2457(03)00249-9

Norman, R.W., Wells, R.P., Neumann, P., Shannon, H., Kerr, M., 1998. A comparison of peak vs cumulative physical work exposure risk factors for the reporting of low back pain in the automotive industry. Clincal Biomech. 13, 561–73.

Norton, G., McDonough, C.M., Cabral, H.J., Shwartz, M., Burgess, J.F., 2016. Classification of patients with incident non-specific low back pain: implications for research. Spine J. 16, 567–576. https://doi.org/10.1016/j.spinee.2015.08.015

Novak, K., De Camargo, A.B., Neuwirth, M., Kothbauer, K., Amassian, V.E., Deletis, V., 2004. The refractory period of fast conducting corticospinal tract axons in man and its implications for intraoperative monitoring of motor evoked potentials. Clin. Neurophysiol. 115, 1931–1941. https://doi.org/10.1016/j.clinph.2004.03.016

O'Neill, S., Manniche, C., Graven-Nielsen, T., Arendt-Nielsen, L., 2007. Generalized deep-tissue hyperalgesia in patients with chronic low-back pain. Eur. J. Pain 11, 415–420. https://doi.org/10.1016/j.ejpain.2006.05.009

O'Sullivan, K., Verschueren, S., Van Hoof, W., Ertanir, F., Martens, L., Dankaerts, W., 2013. Lumbar repositioning error in sitting: healthy controls versus people with sitting-related non-specific chronic low back pain (flexion pattern). Man. Ther. 18, 526–32. https://doi.org/10.1016/j.math.2013.05.005

O'Sullivan, P.B., 2005. Diagnosis and classification of chronic low back pain disorders: maladaptive movement and motor control impairments as underlying mechanism. Man. Ther. 10, 242–55. https://doi.org/10.1016/j.math.2005.07.001

Ochoa, J., Torebjörk, E., 1989. Sensations evoked by intraneural microstimulation of C nociceptor fibres in human skin nerves. J. Physiol. 415, 583–599.

Ochoa, J., Torebjörk, E., 1983. Sensations evoked by intraneural microstimulation of single mechanoreceptor units innervating the human hand. J. Physiol. 342, 633–54.

Ohtori, S., Takahashi, K., Moriya, H., 2003. Calcitonin gene-related peptide immunoreactive DRG neurons innervating the cervical facet joints show phenotypic switch in cervical facet injury in rats. Eur. Spine J. 12, 211–215. https://doi.org/10.1007/s00586-002-0506-7

Olson, M.W., 2014. Comparison of trunk muscle reflex activation patterns between active and passive trunk

flexion-extension loading conditions. Hum. Mov. Sci. 34, 12–27. https://doi.org/10.1016/j.humov.2014.03.004

Osmakov, D.I., Andreev, Y.A., Kozlov, S.A., 2014. Acid Sensing Ion Channels and Their Modulators. Biochem. 79, 1528–1545.

Osteen, J.D., Herzig, V., Gilchrist, J., Emrick, J.J., Zhang, C., Wang, X., Castro, J., Garcia-Caraballo, S., Grundy, L., Rychkov, G.Y., Weyer, A.D., Dekan, Z., Undheim, E.A.B., Alewood, P., Stucky, C.L., Brierley, S.M., Basbaum, A.I., Bosmans, F., King, G.F., Julius, D., 2016. Selective spider toxins reveal a role for Nav1.1 channel ion mechanical pain. Nature 534, 494–499. https://doi.org/10.1038/nature17976

Oxland, T.R., Panjabi, M.M., Southern, E.P., Duranceau, J.S., 1991. An anatomic basis for spinal instability: a porcine trauma model. J. Orthop. Res. 9, 452–62. https://doi.org/10.1002/jor.1100090318

Panjabi, M.M., 2003. Clinical spinal instability and low back pain. J. Electromyogr. Kinesiol. 13, 371–379. https://doi.org/10.1016/S1050-6411(03)00044-0

Park, U., Vastani, N., Guan, Y., Raja, S.N., Koltzenburg, M., Caterina, M.J., 2011. TRP Vanilloid 2 Knock-Out Mice Are Susceptible to Perinatal Lethality But Display Normal Thermal and Mechanical Nociception. J. Neurosci. 31, 11425–11436. https://doi.org/10.1523/JNEUROSCI.1384-09.2011

Parkinson, R.J., Beach, T.A.C., Callaghan, J.P., 2004. The time-varying response of the in vivo lumbar spine to dynamic repetitive flexion. Clin. Biomech. 19, 330–336. https://doi.org/10.1016/j.clinbiomech.2004.01.002

Parkinson, R.J., Callaghan, J.P., 2009. The role of dynamic flexion in spine injury is altered by increasing dynamic load magnitude. Clin. Biomech. 24, 148–154. https://doi.org/10.1016/j.clinbiomech.2008.11.007

Parkinson, R.J., Callaghan, J.P., 2007. Can periods of static loading be used to enhance the resistance of the spine to cumulative compression? J. Biomech. 40, 2944–2952. https://doi.org/10.1016/j.jbiomech.2007.02.007

Parks, W.C., Wilson, C.L., López-Boado, Y.S., 2004. Matrix metalloproteinases as modulators of inflammation and innate immunity. Nat. Rev. Immunol. 4, 617–629. https://doi.org/10.1038/nri1418

Paz, J.T., Mahon, S., Tiret, P., Genet, S., Delord, B., Charpier, S., 2009. Multiple forms of activity-dependent intrinsic plasticity in layer V cortical neurones in vivo. J. Physiol. 587, 3189–3205. https://doi.org/10.1113/jphysiol.2009.169334

Perl, E.R., 2007. Ideas about pain, a historical view. Nat. Rev. Neurosci. 8, 71–80. https://doi.org/10.1038/nrn2042

Petrini, L., Matthiesen, S.T., Arendt-Nielsen, L., 2015. The effect of age and gender on pressure pain thresholds and suprathreshold stimuli. Perception 44, 587–596. https://doi.org/10.1068/p7847

Phillips, C.J., 2009. The Cost and Burden of Chronic Pain. Rev. Pain 3, 2–5. https://doi.org/10.1177/204946370900300102

Pinski, S.E., King, K.B., Davidson, B.S., Zhou, B.-H., Lu, Y., Solomonow, M., 2010. High-frequency loading of lumbar ligaments increases proinflammatory cytokines expression in a feline model of repetitive musculoskeletal disorder. Spine J. 10, 1078–1085. https://doi.org/10.1016/j.spinee.2010.08.030

Pintar, F.A., Yoganandan, N., Myers, T., Elhagediab, A., Sances, A., 1992. Biomechanical properties of human lumbar spine ligaments. J. Biomech. 25, 1351–1356. https://doi.org/10.1016/0021-9290(92)90290-H

Pinto, B.L., Viggiani, D., Callaghan, J.P., 2021. Exposure to Sustained Flexion Impacts Lumbar Extensor Spinae Muscle Fiber Orientation. J. Appl. Biomech. 37, 248–253. https://doi.org/10.1123/jab.2020-0238

Pitcher, G.M., Henry, J.L., 2004. Nociceptive response to innocuous mechanical stimulation is mediated via myelinated afferents and NK-1 receptor activation in a rat model of neuropathic pain. Exp. Neurol. 186, 173–197. https://doi.org/10.1016/j.expneurol.2003.10.019

Platkiewicz, J., Brette, R., 2010. A threshold equation for action potential initiation. PLoS Comput. Biol. 6, 25. https://doi.org/10.1371/journal.pcbi.1000850

Polgár, E., Hughes, D.I., Riddell, J.S., Maxwell, D.J., Puskár, Z., Todd, A.J., 2003. Selective loss of spinal GABAergic or glycinergic neurons is not necessary for development of thermal hyperalgesia in the chronic constriction injury model of neuropathic pain. Pain 104, 229–239. https://doi.org/10.1016/S0304-3959(03)00011-3

Poole, S., Lorenzetti, B.B., Cunha, J.M., Cunha, F.Q., Ferreira, S.H., 1999. Bradykinin B1 and B2 receptors, tumour necrosis factor a and inflammatory hyperalgesia. Br. J. Pharmacol. 126, 649–656.

Price, D.D., McGrath, P.A., Rafii, A., Buckingham, B., 1983. The validation of visual analogue scales as ratio scale measures for chronic and experimental pain. Pain 17, 45–56.

Price, M.P., McIlwrath, S.L., Xie, J., Cheng, C., Qiao, J., Tarr, D.E., Sluka, K.A., Brennan, T.J., Lewin, G.R., Welsh, M.J., 2001. The DRASIC cation channel contributes to the detection of cutaneous touch and acid stimuli in mice. Neuron 32, 1071–1083. https://doi.org/10.1016/S0896-6273(01)00547-5

Prince, K., Campbell, J.A., Picton, P., Turner, S.J., 2005. A Computational Model of Acute Pain. Int. J. Simul. 6, 1–6.

Provenzano, P.P., Lakes, R.S., Corr, D.T., Vanderby, R., 2002. Application of nonlinear viscoelastic models to describe ligament behavior. Biomech. Model. Mechanobiol. 1, 45–57. https://doi.org/10.1007/s10237-002-0004-1

Provenzano, P.P., Lakes, R.S., Keenan, T., Vanderby, R., 2001. Nonlinear ligament viscoelasticity. Ann. Biomed. Eng. 29, 908–914. https://doi.org/10.1114/1.1408926

Qi, Y., Andolfi, L., Frattini, F., Mayer, F., Lazzarino, M., Hu, J., 2015. Membrane stiffening by STOML3 facilitates mechanosensation in sensory neurons. Nat. Commun. 6, 1–13. https://doi.org/10.1038/ncomms9512

Rabey, M., Smith, A., Beales, D., Slater, H., O'Sullivan, P.B., 2017. Pain provocation following sagittal plane repeated movements in people with chronic low back pain: Associations with pain sensitivity and psychological profiles. Scand. J. Pain 16, 22–28. https://doi.org/10.1016/j.sjpain.2017.01.009

Raja, S.N., Carr, D.B., Cohen, M., Finnerup, N.B., Flor, H., Gibson, S., Keefe, F.J., Mogil, J.S., Ringkamp, M., Sluka, K.A., Song, X.-J., Stevens, B., Sullivan, M.D., Tutelman, P.R., Ushida, T., Vader, K., 2020. The revised International Association for the Study of Pain definition of pain. Pain 161, 1976–1982.

Rama, S., Zbili, M., Debanne, D., 2018. Signal propagation along the axon. Curr. Opin. Neurobiol. 51, 37–44. https://doi.org/10.1016/j.conb.2018.02.017

Raoul, S., Faure, A., Robert, R., Rogez, J.-M., Hamel, O., Cuillère, P., Le Borgne, J., 2002. Role of the sinu-vertebral nerve in low back pain and anatomical basis of therapeutic implications. Surg. Radiol. Anat. 24, 366–371. https://doi.org/10.1007/s00276-002-0084-8

Reeh, P.W., Bayer, J., Kocher, L., Handwerker, H.O., 1987. Sensitization of nociceptive cutaneous nerve fibers from the rat's tail by noxious mechanical stimulation. Exp. Brain Res. 65, 505–512. https://doi.org/10.1007/BF00235973

Reynaud, B., Quinn, T.M., 2006. Anisotropic hydraulic permeability in compressed articular cartilage. J. Biomech. 39, 131–137. https://doi.org/10.1016/j.jbiomech.2004.10.015

Rhalmi, S., Yahia, L.H., Newman, N., Lsler, M., 1993. Immunohistochemical study of nerves in lumbar spine ligaments. Spine (Phila. Pa. 1976). 18, 264–267.

Ristanović, D., Stefanović, B.D., Milošević, N.T., Grgurević, M., Stanković, J.B., 2006. Mathematical modeling and computational analysis of neuronal cell images: Application to dendritic arborization of Golgi-impregnated neurons in dorsal horns of the rat spinal cord. Neurocomputing 69, 403–423. https://doi.org/10.1016/j.neucom.2005.04.007

Roberts, M.H., Mapel, D.W., Thomson, H.N., 2015. The impact of chronic pain on direct medical utilization and costs in chronic obstructive pulmonary disease. Clin. outcomes Res. 7, 173–84. https://doi.org/10.2147/CEOR.S80424

Roberts, S., Eisenstein, S.M., Menage, J., Evans, E.H., Ashton, I.K., 1995. Mechanoreceptors in intervertebral discs -morphology, distribution, and neuropeptides. Spine (Phila. Pa. 1976). https://doi.org/10.1097/00007632-199512150-00005

Robertson, D., Willardson, R., Parajuli, D., Cannon, A., Bowdenn, A.E., 2013a. The lumbar supraspinous ligament demonstrates increased material stiffness and strength on its ventral aspect. J. Mech. Behav. Biomed. Mater. 17, 34–43. https://doi.org/10.1016/j.jmbbm.2012.07.009

Robertson, D., Willardson, R., Parajuli, D., Cannon, A., Bowdenn, A.E., 2013b. The lumbar supraspinous ligament demonstrates increased material stiffness and strength on its ventral aspect. J. Mech. Behav. Biomed. Mater. 17, 34–43. https://doi.org/10.1016/j.jmbbm.2012.07.009

Roffey, D.M., Wai, E.K., Bishop, P., Kwon, B.K., Dagenais, S., 2010a. Causal assessment of occupational sitting and low back pain: results of a systematic review. Spine J. 10, 252–61. https://doi.org/10.1016/j.spinee.2009.12.005

Roffey, D.M., Wai, E.K., Bishop, P., Kwon, B.K., Dagenais, S., 2010b. Causal assessment of occupational standing or walking and low back pain: results of a systematic review. Spine J. 10, 262–72. https://doi.org/10.1016/j.spinee.2009.12.023

Rogers, E.L., Granata, K.P., 2006. Disturbed paraspinal reflex following prolonged flexion-relaxation and recovery. Spine (Phila. Pa. 1976). 31, 839–45. https://doi.org/10.1097/01.brs.0000206361.53451.c7

Rolke, R., Baron, R., Maier, C., Tölle, T.R., Treede, R.D., Beyer, A., Binder, A., Birbaumer, N., Birklein, F., Bötefür, I.C., Braune, S., Flor, H., Huge, V., Klug, R., Landwehrmeyer, G.B., Magerl, W., Maihöfner, C., Rolko, C., Schaub, C., Scherens, A., Sprenger, T., Valet, M., Wasserka, B., 2006. Quantitative sensory testing in the German Research Network on Neuropathic Pain (DFNS): Standardized protocol and reference values. Pain 123, 231–243. https://doi.org/10.1016/j.pain.2006.01.041

Roofe, P.G., 1940. Innervation of annulus fibrosus and posterior longitudinal ligament: Fourth and fifth lumbar level. Arch. Neurol. Psychiatry 44, 100–103.

Roseboom, I.C., Rosing, H., Beijnen, J.H., Dorlo, T.P.C., 2020. Skin tissue sample collection, sample homogenization, and analyte extraction strategies for liquid chromatographic mass spectrometry quantification of pharmaceutical compounds. J. Pharm. Biomed. Anal. 191, 113590. https://doi.org/10.1016/j.jpba.2020.113590

Roy, M., Finley, S.D., 2017. Computational model predicts the effects of targeting cellular metabolism in pancreatic cancer. Front. Physiol. 8, 1–16. https://doi.org/10.3389/fphys.2017.00217

Rukwied, R., Weinkauf, B., Main, M., Obreja, O., Schmelz, M., 2013. Inflammation meets sensitization - An explanation for spontaneous nociceptor activity? Pain 154, 2707–2714. https://doi.org/10.1016/j.pain.2013.07.054

Russell, F.A., King, R., Smillie, S.J., Kodji, X., Brain, S.D., 2014. Calcitonin gene-related peptide: physiology and pathophysiology. Physiol. Rev. 94, 1099–1142. https://doi.org/10.1152/physrev.00034.2013

Saeed, A.W., Ribeiro-da-Silva, A., 2012. Non-peptidergic primary afferents are presynaptic to neurokinin-1 receptor immunoreactive lamina I projection neurons in rat spinal cord. Mol. Pain 8, 1. https://doi.org/10.1186/1744-8069-8-64

Sakatani, S., Hirose, A., 2003. The influence of neuron shape changes on the firing characteristics. Neurocomputing 52–54, 355–362. https://doi.org/10.1016/S0925-2312(02)00839-1

Sánchez-Zuriaga, D., Adams, M.A., Dolan, P., 2010. Is activation of the back muscles impaired by creep or muscle fatigue? Spine (Phila. Pa. 1976). 35, 517–25. https://doi.org/10.1097/BRS.0b013e3181b967ea

Santos, D.F. da S. dos, Melo Aquino, B. de, Jorge, C.O., Azambuja, G. de, Schiavuzzo, J.G., Krimon, S., Neves, J. dos S., Parada, C.A., Oliveira-Fusaro, M.C.G., 2017. Muscle pain induced by static contraction in rats is modulated by peripheral inflammatory mechanisms. Neuroscience 358, 58–69. https://doi.org/10.1016/j.neuroscience.2017.06.041

Sasaki, N., Nakayama, Y., Yoshikawa, M., Enyo, A., 1993. Stress relaxation function of bone and bone collagen. J. Biomech. 26, 1369–1376. https://doi.org/10.1016/0021-9290(93)90088-V

Saxler, G., Brankamp, J., Von Knoch, M., Löer, F., Hilken, G., Hanesch, U., 2008. The density of nociceptive SP- and CGRP-immunopositive nerve fibers in the dura mater lumbalis of rats is enhanced after laminectomy, even after application of autologous fat grafts. Eur. Spine J. 17, 1362–1372. https://doi.org/10.1007/s00586-008-0741-7

Schiottz-Christensen, B., Nielsen, G.L., Hansen, V.K., Schodt, T., Sorensen, H.T., Olesen, F., 1999. Long-term prognosis of acute low back pain in patients seen in general practice: a 1-year prospective follow-up study. Fam. Pract. 16, 223–232. https://doi.org/10.1093/fampra/16.3.223

Schmidt, R., Schmelz, M., Forster, C., Ringkamp, M., Torebjörk, E., Handwerker, H.O., 1995. Novel classes of responsive and unresponsive C nociceptors in human skin. J. Neurosci. 15, 333–341.

Schuelert, N., Just, S., Corradini, L., Kuelzer, R., Bernloehr, C., Doods, H., 2015. The bradykinin B1 receptor antagonist BI113823 reverses inflammatory hyperalgesia by desensitization of peripheral and spinal neurons. Eur. J. Pain (United Kingdom) 19, 132–142. https://doi.org/10.1002/ejp.573

Scotti, C., Gobbi, A., Karnatzikos, G., Martin, I., Shimomura, K., Lane, J.G., Peretti, G.M., Nakamura, N., 2016. Cartilage repair in the inflamed joint: considerations for biological augmentation towards tissue regeneration. Tissue Eng. Part B Rev. 22, 149–159. https://doi.org/10.1089/ten.TEB.2015.0297

Seminowicz, D.A., Wideman, T.H., Naso, L., Hatami-Khoroushahi, Z., Fallatah, S., Ware, M.A., Jarzem,

P., Bushnell, M.C., Shir, Y., Ouellet, J.A., Stone, L.S., 2011. Effective Treatment of Chronic Low Back Pain in Humans Reverses Abnormal Brain Anatomy and Function. J. Neurosci. 31, 7540–7550. https://doi.org/10.1523/JNEUROSCI.5280-10.2011

Senkowski, D., Höfle, M., Engel, A.K., 2014. Crossmodal shaping of pain: A multisensory approach to nociception. Trends Cogn. Sci. 18, 319–327. https://doi.org/10.1016/j.tics.2014.03.005

Sharma, M., Langrana, N.A., Rodriguez, J., 1995. Role of ligaments and facets in lumbar spinal stability. Spine (Phila. Pa. 1976). 20, 887–900.

Sherwood, T.W., Frey, E.N., Askwith, C.C., 2012. Structure and activity of the acid-sensing ion channels. AJP Cell Physiol. 303, C699–C710. https://doi.org/10.1152/ajpcell.00188.2012

Shin, G., D'Souza, C., Liu, Y.-H., 2009. Creep and fatigue development in the low back in static flexion. Spine (Phila. Pa. 1976). 34, 1873–8. https://doi.org/10.1097/BRS.0b013e3181aa6a55

Shin, G., Mirka, G.A., 2007. An in vivo assessment of the low back response to prolonged flexion: Interplay between active and passive tissues. Clin. Biomech. 22, 965–71. https://doi.org/10.1016/j.clinbiomech.2007.06.003

Skaggs, D.L., Weidenbaum, M., Latridis, J.C., Ratcliffe, A., Mow, V.C., 1994. Regional variation in tensile properties and biochemical composition of the human lumbar anulus fibrosus. Spine (Phila. Pa. 1976). https://doi.org/10.1097/00007632-199406000-00002

Slugg, R.M., Meyer, R.A., Campbell, J.N., 2000. Response of cutaneous A- and C-fiber nociceptors in the monkey to controlled-force stimuli. J. Neurophysiol. 83, 2179–2191.

Sluka, K.A., 1998. Blockade of N- and P/Q-type calcium channels reduces the secondary heat hyperalgesia induced by acute inflammation. J. Pharmacol. Exp. Ther. 287, 232–7.

Smeets, R.J.E.M., van Geel, A., Kester, A., Knottnerus, J.A., 2007. Physical capacity tasks in chronic low back pain: What is the contributing role of cardiovascular capacity, pain and psychological factors? Disabil. Rehabil. 29, 577–586. https://doi.org/10.1080/09638280600925829

Søgaard, K., Gandevia, S.C., Todd, G., Petersen, N.T., Taylor, J.L., 2006. The effect of sustained low-intensity contractions on supraspinal fatigue in human elbow flexor muscles. J. Physiol. 573, 511–523. https://doi.org/10.1113/jphysiol.2005.103598

Solomonow, M., 2012. Neuromuscular manifestations of viscoelastic tissue degradation following high and low risk repetitive lumbar flexion. J. Electromyogr. Kinesiol. 22, 155–175. https://doi.org/10.1016/j.jelekin.2011.11.008

Solomonow, M., 2011. Time dependent spine stability: the wise old man and the six blind elephants. Clin. Biomech. 26, 219–28. https://doi.org/10.1016/j.clinbiomech.2010.10.010

Solomonow, M., 2004. Ligaments: a source of work-related musculoskeletal disorders. J. Electromyogr. Kinesiol. 14, 49–60. https://doi.org/10.1016/j.jelekin.2003.09.011

Solomonow, M., Zhou, B.-H., Baratta, R. V., Burger, E., 2003. Biomechanics and electromyography of a cumulative lumbar disorder: Response to static flexion. Clin. Biomech. 18, 890–898. https://doi.org/10.1016/S0268-0033(03)00173-6

Solomonow, M., Zhou, B.-H., Baratta, R. V., Lu, Y., Zhu, M.P., Harris, M., 2000. Biexponential recovery model of lumbar viscoelastic laxity and reflexive muscular activity after prolonged cyclic loading. Clin. Biomech. 15, 167–175. https://doi.org/10.1016/S0268-0033(99)00062-5

Song, S.O., Varner, J., 2009. Modeling and analysis of the molecular basis of pain in sensory neurons. PLoS

One 4, e6758. https://doi.org/10.1371/journal.pone.0006758

Sperry, M.M., Ita, M.E., Kartha, S., Zhang, S., Yu, Y.-H., Winkelstein, B.A., 2017. The Interface of Mechanics and Nociception in Joint Pathophysiology: Insights From the Facet and Temporomandibular Joints. J. Biomech. Eng. 139, 021003. https://doi.org/10.1115/1.4035647

Stanton, T.R., Fritz, J.M., Hancock, M.J., Latimer, J., Maher, C.G., Wand, B.M., Parent, E.C., 2011. Evaluation of a treatment-based classification algorithm for low back pain: a cross-sectional study. Phys Ther 91, 496–509. https://doi.org/10.2522/ptj.20100272

Stanton, T.R., Hancock, M.J., Apeldoorn, A.T., Wand, B.M., Fritz, J.M., 2013. What characterizes people who have an unclear classification using a treatment-based classification algorithm for low back pain? A cross-sectional study. Phys. Ther. 93, 345–355.

Staud, R., Koo, E., Robinson, M.E., Price, D.D., 2007. Spatial summation of mechanically evoked muscle pain and painful aftersensations in normal subjects and fibromyalgia patients. Pain 130, 177–187. https://doi.org/10.1016/j.pain.2007.03.015

Staud, R., Price, D.D., Janicke, D., Andrade, E., Hadjipanayis, A.G., Eaton, W.T., Kaplan, L., Wallace, M.R., 2011. Two novel mutations of SCN9A (Nav1.7) are associated with partial congenital insensitivity to pain. Eur. J. Pain 15, 223–230. https://doi.org/10.1016/j.ejpain.2010.07.003

Stefanik, J.J., Frey-Law, L., Segal, N.A., Niu, J., Lewis, C.E., Nevitt, M.C., Neogi, T., 2020. The relation of peripheral and central sensitization to muscle co-contraction: the MOST study. Osteoarthr. Cartil. 28, 1214–1219. https://doi.org/10.1016/j.joca.2020.06.002

Stemper, B.D., Baisden, J.L., Yoganandan, N., Shender, B.S., Maiman, D.J., 2014. Mechanical yield of the lumbar annulus: A possible contributor to instability. J. Neurosurg. Spine 21, 608–613. https://doi.org/10.3171/2014.6.SPINE13401

Sterling, M., Jull, G.A., Wright, A., 2001. The effect of musculoskeletal pain on motor activity and control. J. Pain 2, 135–45. https://doi.org/10.1054/jpai.2001.19951

Sterud, T., Johannessen, H.A., Tynes, T., 2016. Do Work-Related Mechanical and Psychosocial Factors Contribute to the Social Gradient in Low Back Pain? Spine (Phila. Pa. 1976). 41, 1089–1095. https://doi.org/10.1097/BRS.0000000000001451

Sterud, T., Tynes, T., 2013. Work-related psychosocial and mechanical risk factors for neck/shoulder pain: A 3-year follow-up study of the general working population in Norway. Occup. Environ. Med. 70, 296–302. https://doi.org/10.1007/s00420-013-0886-5

Stuart, G., Schiller, J., Sakmann, B., 1997. Action potential initiation and propagation in rat neocortical pyramidal neurons. J. Physiol. 505, 617–632. https://doi.org/10.1152/jn.01288.2006.

Stucky, C.L., Lewin, G.R., 1999. Isolectin B4-positive and -negative nociceptors are functionally distinct. J. Neurosci. 19, 6497–6505.

Tabard-Fougère, A., Rose-Dulcina, K., Pittet, V., Dayer, R., Vuillerme, N., Armand, S., 2018. EMG normalization method based on grade 3 of manual muscle testing: Within- and between-day reliability of normalization tasks and application to gait analysis. Gait Posture 60, 6–12. https://doi.org/10.1016/j.gaitpost.2017.10.026

Tamcan, O., Mannion, A.F., Eisenring, C., Horisberger, B., Elfering, A., Müller, U., 2010. The course of chronic and recurrent low back pain in the general population. Pain 150, 451–457. https://doi.org/10.1016/j.pain.2010.05.019

Tanasescu, R., Cottam, W.J., Condon, L., Tench, C.R., Auer, D.P., 2016. Functional reorganisation in chronic pain and neural correlates of pain sensitisation: A coordinate based meta-analysis of 266 cutaneous pain fMRI studies. Neurosci. Biobehav. Rev. 68, 120–133. https://doi.org/10.1016/j.neubiorev.2016.04.001

Tang, R., Gungor, C., Sesek, R.F., Foreman, K.B., Gallagher, S., Davis, G.A., 2016. Morphometry of the lower lumbar intervertebral discs and endplates: comparative analyses of new MRI data with previous findings. Eur. Spine J. 25, 4116–4131. https://doi.org/10.1007/s00586-016-4405-8

Tatu, K., Costa, T., Nani, A., Diano, M., Quarta, D.G., Duca, S., Apkarian, A.V., Fox, P.T., Cauda, F., 2018. How do morphological alterations caused by chronic pain distribute across the brain? A meta-analytic co-alteration study. NeuroImage Clin. 18, 15–30. https://doi.org/10.1016/j.nicl.2017.12.029

Taylor, J.L., Amann, M., Duchateau, J., Meeusen, R., Rice, C.L., 2016. Neural contributions to muscle fatigue: From the brain to the muscle and back again. Med. Sci. Sports Exerc. 48, 2294–2306. https://doi.org/10.1249/MSS.0000000000000923

Taylor, J.L., Butler, J.E., Gandevia, S.C., 2000. Changes in muscle afferents, motoneurons and motor drive during muscle fatigue. Eur J Appl Physiol 83, 106–115. https://doi.org/10.1007/s004210000269

Taylor, R.S., Buyten, J.P. Van, Buchser, E., 2006. Spinal cord stimulation for complex regional pain syndrome: A systematic review of the clinical and cost-effectiveness literature and assessment of prognostic factors. Eur. J. Pain 10, 91–101. https://doi.org/10.1016/j.ejpain.2005.02.004

Tesarz, J., Hoheisel, U., Wiedenhöfer, B., Mense, S., 2011. Sensory innervation of the thoracolumbar fascia in rats and humans. Neuroscience 194, 302–308. https://doi.org/10.1016/j.neuroscience.2011.07.066

Thiede, M., Liebers, F., Seidler, A., Gravemeyer, S., Latza, U., 2014. Gender specific analysis of occupational diseases of the low back caused by carrying, lifting or extreme trunk flexion-use of a prevention index to identify occupations with high prevention needs. Am. J. Ind. Med. 57, 233–244. https://doi.org/10.1002/ajim.22277

Thomas, J.S., Gibson, G.E., 2007. Coordination and timing of spine and hip joints during full body reaching tasks. Hum. Mov. Sci. 26, 124–140.

Thornton, G.M., Shrive, N.G., Frank, C.B., 2002. Ligament creep recruits fibres at low stresses and can lead to modulus-reducing fibre damage at higher creep stresses: A study in rabbit medial collateral ligament model. J. Orthop. Res. 20, 967–974. https://doi.org/10.1016/S0736-0266(02)00028-1

Tissot, F., Messing, K., Stock, S., 2009. Studying the relationship between low back pain and working postures among those who stand and those who sit most of the working day. Ergonomics 52, 1402–18. https://doi.org/10.1080/00140130903141204

Toda, K., Zeredo, J.L., Fujiyama, R., Okada, Y., Oi, K., Hayashi, Y., Nasution, F.H., 2004. Characteristics of nociceptors in the periodontium - An in vitro study in rats. Brain Res. Bull. 62, 345–349. https://doi.org/10.1016/j.brainresbull.2003.10.005

Todd, K.H., Funk, K.G., Funk, J.P., Bonacci, R., 1996. Clinical significance of reported changes in pain severity. Ann. Emerg. Med. 27, 485–489. https://doi.org/10.1016/S0196-0644(96)70238-X

Toosizadeh, N., Nussbaum, M.A., 2013. Creep deformation of the human trunk in response to prolonged and repetitive flexion: Measuring and modeling the effect of external moment and flexion rate. Ann. Biomed. Eng. 41, 1150–1161. https://doi.org/10.1007/s10439-013-0797-3

Toosizadeh, N., Nussbaum, M.A., Bazrgari, B., Madigan, M.L., 2012. Load-Relaxation Properties of the Human Trunk in Response to Prolonged Flexion: Measuring and Modeling the Effect of Flexion

Angle. PLoS One 7, 1–10. https://doi.org/10.1371/journal.pone.0048625

Torisu, T., Wang, K., Svensson, P., De Laat, A., Fujii, H., Arendt-Nielsen, L., 2006. Effects of muscle fatigue induced by low-level clenching on experimental muscle pain and resting jaw muscle activity: gender differences. Exp. brain Res. 174, 566–74. https://doi.org/10.1007/s00221-006-0497-4

Treede, R.D., Rolke, R., Andrews, K., Magerl, W., 2002. Pain elicited by blunt pressure: Neurobiological basis and clinical relevance. Pain 98, 235–240. https://doi.org/10.1016/S0304-3959(02)00203-8

Troyer, K.L., Estep, D.J., Puttlitz, C.M., 2012. Viscoelastic effects during loading play an integral role in soft tissue mechanics. Acta Biomater. 8, 234–243. https://doi.org/10.1016/j.actbio.2011.07.035

Twomey, L., Taylor, J., 1982. Flexion creep deformation and hysteresis in the lumbar vertebral column. Spine (Phila. Pa. 1976). 7, 116–122.

van den Beuken-van Everdingen, M.H.J., de Graeff, A., Jongen, J.L.M., Dijkstra, D., Mostovaya, I., Vissers, K.C., 2017. Pharmacological Treatment of Pain in Cancer Patients: The Role of Adjuvant Analgesics, a Systematic Review. Pain Pract. 17, 409–419. https://doi.org/10.1111/papr.12459

van den Pol, A.N., 2012. Neuropeptide Transmission in Brain Circuits. Neuron 76, 98–115. https://doi.org/10.1016/j.neuron.2012.09.014

Van Der Houwen, E.B., Baron, P., Veldhuizen, A.G., Burgerhof, J.G.M., Van Ooijen, P.M.A., Verkerke, G.J., 2010. Geometry of the intervertebral volume and vertebral endplates of the human spine. Ann. Biomed. Eng. 38, 33–40. https://doi.org/10.1007/s10439-009-9827-6

van Dieën, J.H., Kingma, I., 2005. Effects of antagonistic co-contraction on differences between electromyography based and optimization based estimates of spinal forces. Ergonomics 48, 411–26. https://doi.org/10.1080/00140130512331332918

van Dieën, J.H., Kingma, I., Van Der Bug, J.C.E., 2003. Evidence for a role of antagonistic cocontraction in controlling trunk stiffness during lifting. J. Biomech. 36, 1829–1836. https://doi.org/10.1016/S0021-9290(03)00227-6

Van Dillen, L.R., Sahrmann, S.A., Norton, B.J., Caldwell, C.A., McDonnell, M.K., Bloom, N.J., 2003. Movement system impairment-based categories for low back pain: stage 1 validation. J. Orthop. Sports Phys. Ther. 33, 126–142. https://doi.org/10.2519/jospt.2003.33.3.126

Van Houdenhove, B., Egle, U., Luyten, P., 2005. The role of life stress in fibromyalgia. Curr. Rheumatol. Rep. 7, 365–370. https://doi.org/10.1007/s11926-005-0021-z

van Tulder, M.W., Assendelft, W.J.J., Koes, B.W., Bouter, L.M., 1997. Spinal radiographic findings and nonspecific low back pain: A systematic review of observational studies. Spine (Phila. Pa. 1976). 22, 427–34.

Veiersted, K.B., Forsman, M., Hansson, G.Å., Mathiassen, S.E., 2013. Assessment of time patterns of activity and rest in full-shift recordings of trapezius muscle activity - Effects of the data processing procedure. J. Electromyogr. Kinesiol. 23, 540–547. https://doi.org/10.1016/j.jelekin.2012.12.004

Veres, S.P., Robertson, P.A., Broom, N.D., 2009. The morphology of acute disc herniation: a clinically relevant model defining the role of flexion. Spine (Phila. Pa. 1976). 34, 2288–96. https://doi.org/10.1097/BRS.0b013e3181a49d7e

Verrills, P., Nowesenitz, G., Barnard, A., 2015. Prevalence and Characteristics of Discogenic Pain in Tertiary Practice: 223 Consecutive Cases Utilizing Lumbar Discography. Pain Med. (United States) 16, 1490–1499. https://doi.org/10.1111/pme.12809

Viggiani, D., Callaghan, J.P., 2018. Hip abductor fatigability and recovery are related to the development of low back pain during prolonged standing. J. Appl. Biomech. 34, 39–46. https://doi.org/10.1123/jab.2017-0096

Viggiani, D., Gallagher, K.M., Sehl, M., Callaghan, J.P., 2017. The distribution of lumbar intervertebral angles in upright standing and extension is related to low back pain developed during standing. Clin. Biomech. 49, 85–90. https://doi.org/10.1016/j.clinbiomech.2017.09.003

Viidik, A., 1972. Simuhaneous Mechanical and Light Microscopic Studies of Collagen Fibers. Z Anat Entwickl Gesch 136, 204–212. https://doi.org/10.1007/BF00519178

Villemure, C., Bushnell, M.C., 2009. Mood influences supraspinal pain processing separately from attention. J. Neurosci. 29, 705–715. https://doi.org/10.1523/JNEUROSCI.3822-08.2009

Voglar, M., Wamerdam, J., Kingma, I., Sarabon, N., Diee, J.H. Van, 2016. Prolonged Intermittent Trunk Flexion Increases Trunk Muscles Reflex Gains and Trunk Stiffness. PLoS One 11, e0162703. https://doi.org/10.1371/journal.pone.0162703

Vos, T., Flaxman, A.D., Naghavi, M., Lozano, R., Michaud, C., Ezzati, M., Shibuya, K., Salomon, J.A., Abdalla, S., Aboyans, V., Abraham, J., Ackerman, I., Aggarwal, R., Ahn, S.Y., Ali, M.K., Alvarado, M., Anderson, H.R., Anderson, L.M., Andrews, K.G., Atkinson, C., Baddour, L.M., Bahalim, A.N., Barker-Collo, S., Barrero, L.H., Bartels, D.H., Basáñez, M.G., Baxter, A., Bell, M.L., Benjamin, E.J., Bennett, D., Bernabé, E., Bhalla, K., Bhandari, B., Bikbov, B., Abdulhak, A. Bin, Birbeck, G., Black, J.A., Blencowe, H., Blore, J.D., Blyth, F., Bolliger, I., Bonaventure, A., Boufous, S., Bourne, R., Boussinesq, M., Braithwaite, T., Brayne, C., Bridgett, L., Brooker, S., Brooks, P., Brugha, T.S., Bryan-Hancock, C., Bucello, C., Buchbinder, R., Buckle, G., Budke, C.M., Burch, M., Burney, P., Burstein, R., Calabria, B., Campbell, B., Canter, C.E., Carabin, H., Carapetis, J., Carmona, L., Cella, C., Charlson, F., Chen, H., Cheng, A.T.A., Chou, D., Chugh, S.S., Coffeng, L.E., Colan, S.D., Colquhoun, S., Colson, K.E., Condon, J., Connor, M.D., Cooper, L.T., Corriere, M., Cortinovis, M., De Vaccaro, K.C., Couser, W., Cowie, B.C., Criqui, M.H., Cross, M., Dabhadkar, K.C., Dahiya, M., Dahodwala, N., Damsere-Derry, J., Danaei, G., Davis, A., De Leo, D., Degenhardt, L., Dellavalle, R., Delossantos, A., Denenberg, J., Derrett, S., Des Jarlais, D.C., Dharmaratne, S.D., Dherani, M., Diaz-Torne, C., Dolk, H., Dorsey, E.R., Driscoll, T., Duber, H., Ebel, B., Edmond, K., Elbaz, A., Ali, S.E., Erskine, H., Erwin, P.J., Espindola, P., Ewoigbokhan, S.E., Farzadfar, F., Feigin, V., Felson, D.T., Ferrari, A., Ferri, C.P., Fèvre, E.M., Finucane, M.M., Flaxman, S., Flood, L., Foreman, K., Forouzanfar, M.H., Fowkes, F.G.R., Franklin, R., Fransen, M., Freeman, M.K., Gabbe, B.J., Gabriel, S.E., Gakidou, E., Ganatra, H.A., Garcia, B., Gaspari, F., Gillum, R.F., Gmel, G., Gonzalez-Medina, D., Gosselin, R., Grainger, R., Grant, B., Groeger, J., Guillemin, F., Gunnell, D., Gupta, R., Haagsma, J., Hagan, H., Halasa, Y.A., Hall, W., Haring, D., Haro, J.M., Harrison, J.E., Havmoeller, R., Hay, R.J., Higashi, H., Hill, C., Hoen, B., Hoffman, H., Hotez, P.J., Hoy, D., Huang, J.J., Ibeanusi, S.E., Jacobsen, K.H., James, S.L., Jarvis, D., Jasrasaria, R., Jayaraman, S., Johns, N., Jonas, J.B., Karthikeyan, G., Kassebaum, N., Kawakami, N., Keren, A., Khoo, J.P., King, C.H., Knowlton, L.M., Kobusingye, O., Koranteng, A., Krishnamurthi, R., Laden, F., Lalloo, R., Laslett, L.L., Lathlean, T., Leasher, J.L., Lee, Y.Y., Leigh, J., Lim, S.S., Limb, E., Lin, J.K., Lipnick, M., Lipshultz, S.E., Liu, W., Loane, M., Ohno, S.L., Lyons, R., Ma, J., Mabweijano, J., MacIntyre, M.F., Malekzadeh, R., Mallinger, L., Manivannan, S., Marcenes, W., March, L., Margolis, D.J., Marks, G.B., Marks, R., Matsumori, A., Matzopoulos, R., Mayosi, B.M., McAnulty, J.H., McDermott, M.M., McGill, N., McGrath, J., Medina-Mora, M.E., Meltzer, M., Mensah, G.A., Merriman, T.R., Meyer, A.C., Miglioli, V., Miller, M., Miller, T.R., Mitchell, P.B., Mock, C., Mocumbi, A.O., Moffitt, T.E., Mokdad, A.A., Monasta, L., Montico, M., Moran, A., Morawska, L., Mori, R., Murdoch, M.E., Mwaniki, M.K., Naidoo, K., Nair, M.N., Naldi, L., Narayan, K.M.V., Nelson, P.K., Nelson, R.G., Nevitt, M.C., Newton, C.R., Nolte, S., Norman, P., Norman, R., O'Donnell, M., O'Hanlon, S., Olives, C., Omer, S.B., Ortblad, K., Osborne, R., Ozgediz, D., Page, A., Pahari, B., Pandian, J.D., Rivero, A.P., Patten,

S.B., Pearce, N., Padilla, R.P., Perez-Ruiz, F., Perico, N., Pesudovs, K., Phillips, D., Phillips, M.R., Pierce, K., Pion, S., Polanczyk, G. V., Polinder, S., Pope, C.A., Popova, S., Porrini, E., Pourmalek, F., Prince, M., Pullan, R.L., Ramaiah, K.D., Ranganathan, D., Razavi, H., Regan, M., Rehm, J.T., Rein, D.B., Remuzzi, G., Richardson, K., Rivara, F.P., Roberts, T., Robinson, C., De Leòn, F.R., Ronfani, L., Room, R., Rosenfeld, L.C., Rushton, L., Sacco, R.L., Saha, S., Sampson, U., Sanchez-Riera, L., Sanman, E., Schwebel, D.C., Scott, J.G., Segui-Gomez, M., Shahraz, S., Shepard, D.S., Shin, H., Shivakoti, R., Singh, D., Singh, G.M., Singh, J.A., Singleton, J., Sleet, D.A., Sliwa, K., Smith, E., Smith, J.L., Stapelberg, N.J.C., Steer, A., Steiner, T., Stolk, W.A., Stovner, L.J., Sudfeld, C., Syed, S., Tamburlini, G., Tavakkoli, M., Taylor, H.R., Taylor, J.A., Taylor, W.J., Thomas, B., Thomson, W.M., Thurston, G.D., Tleyjeh, I.M., Tonelli, M., Towbin, J.A., Truelsen, T., Tsilimbaris, M.K., Ubeda, C., Undurraga, E.A., Van Der Werf, M.J., Van Os, J., Vavilala, M.S., Venketasubramanian, N., Wang, M., Wang, W., Watt, K., Weatherall, D.J., Weinstock, M.A., Weintraub, R., Weisskopf, M.G., Weissman, M.M., White, R.A., Whiteford, H., Wiebe, N., Wiersma, S.T., Wilkinson, J.D., Williams, H.C., Williams, S.R.M., Witt, E., Wolfe, F., Woolf, A.D., Wulf, S., Yeh, P.H., Zaidi, A.K.M., Zheng, Z.J., Zonies, D., Lopez, A.D., Murray, C.J.L., Moradi-Lakeh, M., 2012. Years lived with disability (YLDs) for 1160 sequelae of 289 diseases and injuries 1990-2010: A systematic analysis for the Global Burden of Disease Study 2010. Lancet 380, 2163–2196. https://doi.org/10.1016/S0140-6736(12)61729-2

Vuillerme, N., Pinsault, N., 2007. Re-weighting of somatosensory inputs from the foot and the ankle for controlling posture during quiet standing following trunk extensor muscles fatigue. Exp. Brain Res. 183, 323–327. https://doi.org/10.1007/s00221-007-1047-4

Vydyanathan, A., Wu, Z., Chen, S., Pan, H., 2005. A-Type Voltage-Gated K+ Currents Influence Firing Properties of Isolectin B4-Positive But Not Isolectin B4-Negative Primary Sensory Neurons. J. Neurophysiol. 93, 3401–3409. https://doi.org/10.1152/jn.01267.2004.

Waddell, G., Burton, A.K., 2001. Occupational health guidelines for the management of low back pain at work: evidence review. Occup. Med. (Lond). 51, 124–35.

Wager, T.D., Atlas, L.Y., Lindquist, M.A., Roy, M., Woo, C.-W., Kross, E., 2013. An fMRI-Based Neurologic Signature of Physical Pain. N. Engl. J. Med. 368, 1388–1397. https://doi.org/10.1056/NEJMoa1204471

Wai, E.K., Roffey, D.M., Bishop, P., Kwon, B.K., Dagenais, S., 2010. Causal assessment of occupational lifting and low back pain: results of a systematic review. Spine J. 10, 554–66. https://doi.org/10.1016/j.spinee.2010.03.033

Wang, Y., 2008. The functional regulation of TRPV1 and its role in pain sensitization. Neurochem. Res. 33, 2008–2012. https://doi.org/10.1007/s11064-008-9750-5

Wasner, G., Lee, B.B., Engel, S., McLachlan, E., 2008. Residual spinothalamic tract pathways predict development of central pain after spinal cord injury. Brain 131, 2387–2400. https://doi.org/10.1093/brain/awn169

Weidenbaum, M., Latridis, J.C., Foster, R.J., Van Mow, C., Acaroglu, E.R., Setton, L.A., 1995. Degeneration and aging affect the tensile behavior of human lumbar anulus fibrosus. Spine (Phila. Pa. 1976). https://doi.org/10.1097/00007632-199512150-00010

Weisshaar, C.L., Kras, J. V., Pall, P.S., Kartha, S., Winkelstein, B.A., 2017. Ablation of IB4 non-peptidergic afferents in the rat facet joint prevents injury-induced pain and thalamic hyperexcitability via supraspinal glutamate transporters. Neurosci. Lett. 655, 82–89. https://doi.org/10.1016/j.neulet.2017.07.006

Wester, J.C., Contreras, D., 2013. Biophysical mechanism of spike threshold dependence on the rate of rise of the membrane potential by sodium channel inactivation or subthreshold axonal potassium current. J. Comput. Neurosci. 35, 1–17. https://doi.org/10.1007/s10827-012-0436-2

Wetzel, C., Pifferi, S., Picci, C., Gök, C., Hoffmann, D., Bali, K.K., Lampe, A., Lapatsina, L., Fleischer, R., Smith, E.S.J., Bégay, V., Moroni, M., Estebanez, L., Kühnemund, J., Walcher, J., Specker, E., Neuenschwander, M., Von Kries, J.P., Haucke, V., Kuner, R., Poulet, J.F.A., Schmoranzer, J., Poole, K., Lewin, G.R., 2017. Small-molecule inhibition of STOML3 oligomerization reverses pathological mechanical hypersensitivity. Nat. Neurosci. 20, 209–218. https://doi.org/10.1038/nn.4454

White III, A.A., Panjabi, M.M., 1990. Physical properties and functional biomechanics of the spine, in: Clinical Biomechanics of the Spine. Lippincott Williams & Wilkins, pp. 3–76.

Williams, A.C.D.C., Craig, K.D., 2016. Updating the definition of pain. Pain 157, 2420–2423. https://doi.org/10.1097/j.pain.0000000000000613

Winkelstein, B.A., DeLeo, J.A., 2004. Mechanical thresholds for initiation and persistence of pain following nerve root injury: mechanical and chemical contributions at injury. J. Biomech. Eng. 126, 258–63. https://doi.org/10.1115/1.1695571

Winter, D.A., 2009. Biomechanics and Motor Control of Human Movement, Biomechanics and Motor Control of Human Movement: Fourth Edition. John Wiley & Sons, Inc., Hoboken, NJ, USA. https://doi.org/10.1002/9780470549148

Wooldridge, J.M., 2001. Applications of generalized method of moments estimation. J. Econ. Perspect. 15, 87–100. https://doi.org/10.1257/jep.15.4.87

Woolf, A.D., Pfleger, B., 2003. Burden of major musculoskeletal conditions. Bull. World Health Organ. 81, 646–656. https://doi.org/S0042-96862003000900007 [pii]

Woolf, C.J., Ma, Q., 2007. Nociceptors-Noxious stimulus detectors. Neuron 55, 353–364. https://doi.org/10.1016/j.neuron.2007.07.016

Woolf, C.J., Salter, M.W., 2000. Neuronal plasticity: Increasing the gain in pain. Science (80-.). 288, 1765–1768. https://doi.org/10.1126/science.288.5472.1765

Wynne-Jones, G., Cowen, J., Jordan, J.L., Uthman, O., Main, C.J., Glozier, N., Van Der Windt, D., 2014. Absence from work and return to work in people with back pain: A systematic review and meta-analysis. Occup. Environ. Med. 71, 448–458. https://doi.org/10.1136/oemed-2013-101571

Xia, T., Frey Law, L.A., 2008. A theoretical approach for modeling peripheral muscle fatigue and recovery. J. Biomech. 41, 3046–52. https://doi.org/10.1016/j.jbiomech.2008.07.013

Xu, F., Lu, T.J., Seffen, K.A., 2008a. Biothermomechanical behavior of skin tissue. Acta Mech. Sin. 24, 1–23. https://doi.org/10.1007/s10409-007-0128-8

Xu, F., Wen, T., Lu, T.J., Seffen, K.A., 2008b. Modeling of Nociceptor Transduction in Skin Thermal Pain Sensation. J. Biomech. Eng. 130, 041013. https://doi.org/10.1115/1.2939370

Xu, Y., Bach, E., Orhede, E., 1997. Work environment and low back pain: the influence of occupational activities. Occup. Environ. Med. 54, 741–5.

Yahia, L.H., Newman, N., Rivard, C.H., 1988. Neurohistology of lumbar spine ligaments. Acta Orthop. 59, 508–512. https://doi.org/10.3109/17453678809148773

Yang, G., Marras, W.S., Best, T.M., 2011. The biochemical response to biomechanical tissue loading on the low back during physical work exposure. Clin. Biomech. 26, 431–437.

https://doi.org/10.1016/j.clinbiomech.2011.01.005

Yang, H., Jekir, M.G., Davis, M.W., Keaveny, T.M., 2016. Effective modulus of the human intervertebral disc and its effect on vertebral bone stress. J. Biomech. 49, 1134–1140. https://doi.org/10.1016/j.jbiomech.2016.02.045

Yang, H., Meijer, H.G.E., Doll, R.J., Buitenweg, J.R., van Gils, S.A., 2015. Computational modeling of Adelta-fiber-mediated nociceptive detection of electrocutaneous stimulation. Biol. Cybern. 109, 479–491. https://doi.org/10.1007/s00422-015-0656-4

Yasaka, T., Tiong, S.Y.X., Hughes, D.I., Riddell, J.S., Todd, A.J., 2010. Populations of inhibitory and excitatory interneurons in lamina II of the adult rat spinal dorsal horn revealed by a combined electrophysiological and anatomical approach. Pain 151, 475–488. https://doi.org/10.1016/j.pain.2010.08.008

Yingling, V.R., Callaghan, J.P., McGill, S.M., 1999. The porcine cervical spine as a model of the human lumbar spine: An anatomical, geometric, and functional comparison. J. Spinal Disord. 12, 415–423.

Yoshimura, M., Jessell, T., 1990. Amino acid-mediated EPSPs at primary afferent synapses with substantia gelatinosa neurones in the rat spinal cord. J. Physiol. 430, 315–335.

Yoshimura, M., Nishi, S., 1995. Primary afferent-evoked glycine- and GABA-mediated IPSPs in substantia gelatinosa neurones in the rat spinal cord in vitro. J. Physiol. 482, 29–38. https://doi.org/10.1113/jphysiol.1995.sp020497

Yung, M., Mathiassen, S.E., Wells, R.P., 2012. Variation of force amplitude and its effects on local fatigue. Eur. J. Appl. Physiol. 112, 3865–79. https://doi.org/10.1007/s00421-012-2375-z

Zbili, M., Rama, S., Debanne, D., 2016. Dynamic Control of Neurotransmitter Release by Presynaptic Potential. Front. Cell. Neurosci. 10, 1–6. https://doi.org/10.3389/fncel.2016.00278

Zemp, R., Fliesser, M., Wippert, P.M., Taylor, W.R., Lorenzetti, S., 2016. Occupational sitting behaviour and its relationship with back pain - A pilot study. Appl. Ergon. 56, 84–91. https://doi.org/10.1016/j.apergo.2016.03.007

Zhang, J.-M., An, J., 2007. Cytokines, inflammation and pain. Int Anesth. Clin 45, 27–37. https://doi.org/10.1097/AIA.0b013e318034194e.Cytokines

Zhou, S.H., McCarthy, I.D., McGregor, A.H., Coombs, R.R.H., Hughes, S.P.F., 2000. Geometrical dimensions of the lower lumbar vertebrae - analysis of data from digitised CT images. Eur. Spine J. 9, 242–248. https://doi.org/10.1007/s005860000140

Zito, K., Svoboda, K., 2002. Activity-dependent synaptogenesis in the adult mammalian cortex. Neuron 35, 1015–1017. https://doi.org/10.1016/S0896-6273(02)00903-0

Appendix A – Screening Form for Studies 1 and 2

HEALTH SCREENING FORM

Participant Code: _____

This questionnaire asks some questions about your health status, this information will guide us with your entry into the study.

Contraindications to participation in this study include:

1. Low back or lower pain that required medical intervention or time off from work in the last 12 months
2. Diagnosed psychiatric, neurological, or chronic pain disorder that affects your pain sensitivity
3. Taking pain medications
4. History of fainting

Past Relevant Health History (Check all that apply):

Musculoskeletal Disorders:

- ☐ Back Injury/Pain, please specify: _____
- ☐ Hip Injury/Pain, please specify: _____
- ☐ Knee Injury/Pain, please specify: _____
- ☐ Ankle Injury/Pain, please specify: _____
- ☐ Scoliosis
- ☐ Spondylolisthesis
- ☐ Scheuermann's Disease
- ☐ Shin Splints

Cardiovascular Disorders:

- ☐ Heart Murmur
- ☐ Disease of the Arteries
- ☐ Heart Attack
- ☐ High Blood Pressure
- ☐ Congenital Heart Disease
- ☐ High Cholesterol
- ☐ Heart Disease

Respiratory Disorders:

- ☐ Emphysema
- ☐ Asthma
- ☐ Pneumonia
- ☐ Bronchitis

Psychological Disorders:

- ☐ Major Depressive Disorder
- ☐ Schizophrenia
- ☐ Other: _____
- ☐ Bipolar Disorder
- ☐ Generalized Anxiety Disorder

Neurological and Chronic Pain Disorders:

☐	Neuropathy (any)	☐	Neuropathic Pain
☐	Fibromyalgia	☐	Chronic Regional Pain Syndrome
☐	Congenital Insensitivity to Pain	☐	Nerve Impingement
☐	Whiplash	☐	Other: _____

Other:

☐	Fainting	☐	Arthritis
☐	Dizziness		

Current Relevant Health History (Check all that apply):

☐	Irregular Heartbeat	☐	Fatigue
☐	Chest Pain	☐	Persistent Coughing
☐	Wheezing (Asthma)	☐	Dizziness
☐	Back pain/injury	☐	Shoulder pain/injury
☐	Leg Pain/injury		

Dietary Intake within the Past 24 Hours (Circle Yes/No for each):

Alcohol	Yes	No
Caffeine	Yes	No
Vitamin Supplements	Yes	No
Fast Food	Yes	No
Deep-Fried Foods	Yes	No
Sweets or Desserts	Yes	No
Candies or Chocolate Bars	Yes	No

If you answered yes to any of the above, please use this space to list what foods/supplements and rough quantities:

Appendix B – Electromyography Preparation

Table B-1 describes the muscle sites used in this thesis.

Table B-1: Muscle Sites for Electromyography

Muscle Site	Landmarking and Orientation
Lumbar Erector Spinae	Placed 5 cm lateral to the L3 spinous process, oriented along the superior-inferior axis (Ng et al., 2003).
Tibialis Anterior	Placed along the line connecting the tip of the fibula to the medial malleolus over the largest bulk of the muscle (Hermens et al., 2000).

Once the muscle site was located, the following steps were carried out:

1. Shave the area to remove hair and dead skin with a disposable razor
2. Lightly rub skin with an abrasive cloth (KimWipes, Kimberley-Clark Inc., Irving, TX, USA) coated in isopropyl alcohol
3. Apply two silver/silver-chloride electrodes (Model 272S, Noraxon Inc., Scottsdale, AZ, USA) over the muscle site
4. Secure electrodes with medical fabric tape (Hypafix, BSN Medical, Hamburg, Germany)

Participants performed maximal voluntary contractions and quiet resting trials to normalize myoelectric signals for each muscle. For maximal voluntary contractions, participants were instructed to gradually build up force to their maximum effort over five seconds against isometric resistance. Details on the maximal contractions used in this thesis are in Table B-2. Quiet rest trials consisted of five seconds of relaxed prone lying. Both recorded measures for electromyography preparation were visually inspected for artifacts; trials with artifacts present were discarded and recollected.

Table B-2: Maximal Voluntary Contraction Protocols

Muscle Site	Maximal Voluntary Contraction
Lumbar Erector Spinae Dankaerts et al., (2004)	• Participant lay prone on a table with legs secured to the table and trunk suspended over table edge in relaxed flexion. • Participants slowly extended trunk upwards with arms crossed in front of their chest. • Isometric manual resistance was provided by the experimenter when the participant's trunk reached horizontal. • Participant develops maximum force.
Tibialis Anterior Tabard-Fougère et al., (2018)	• Participant seated on a table with test leg hanging over the edge. • Participant's ankle was held in a neutral posture by experimenter. • Participants maximally dorsiflexed their ankle against manual resistance.

Appendix C – Pressure Algometer Development and Reliability

As documented in Section 3.3.2, the pressure algometers used in Chapters 3 and 4 consisted of a linear motor, a load cell, an indenter, and a shared power supply. All components and an example of use on the lower back with all parts assembled are depicted in Figure C-1, the figure caption has further details.

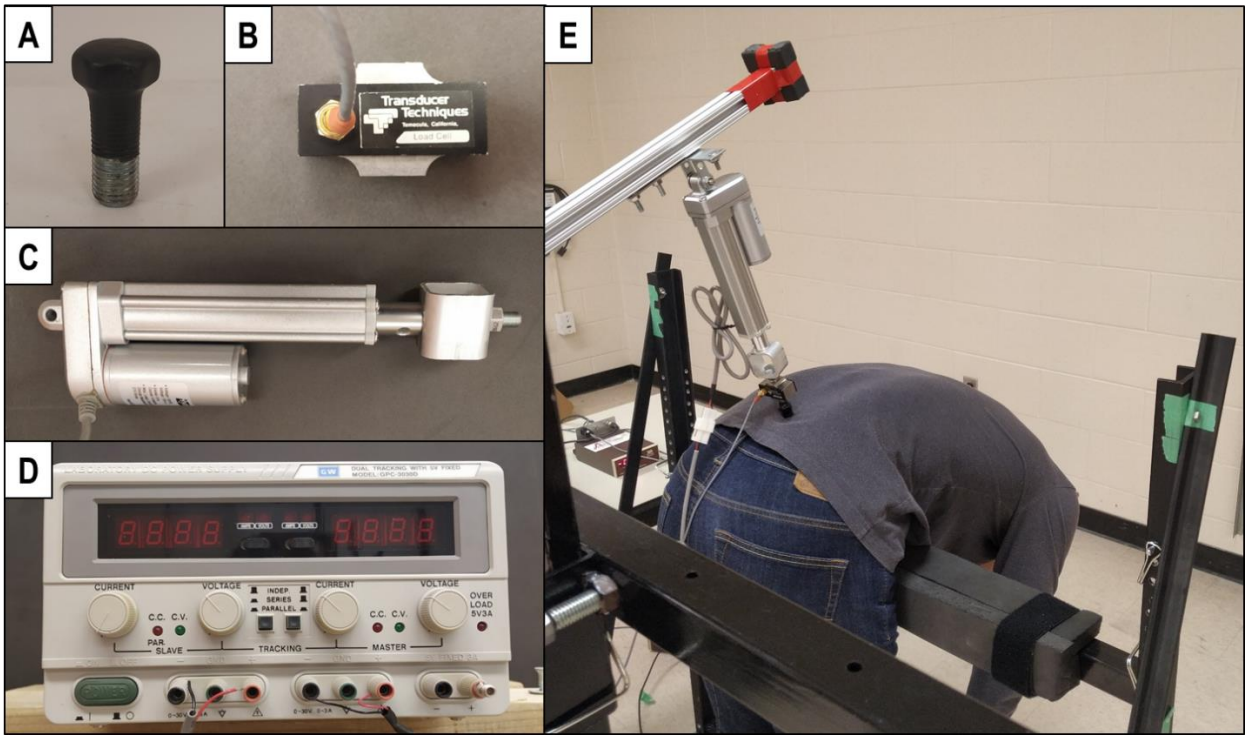

Figure C-1: Components and Assembly of the Pressure Algometer. The indenter (Panel A) was a shaved down 7/16" by 1" hexagonal bolt dipped in black multipurpose rubber coating (Plasti Dip, Blaine, MN, USA). Assuming a regular hexagon and a measured side length of 10.759 mm after coating, the approximate contact area was computed to be 1.003 cm^2. The load cell (Panel B) was threaded on both ends to screw into the indenter and linear motor (Panel C). Load cell signals were amplified and conditioned (visible in Panel E background; Strain Gauge Conditioner 3270, Daytronic Corporation, Miamisburg, OH, USA) prior to sampling. The linear motor was powered by a power supply (Panel D) and mounted to one of two frames. The motor had an upper force limit of 1200 N and a maximum displacement of 101.6 mm; the voltage setting dictated the displacement rate, the motor drew more current with greater loads to a maximum current of 4.6 A. A press-button switch (not pictured; see Figure 3-1 Panel B) was put in series between the power supply and the motor. The full assembly in use is depicted in Panel E and Figure C-2.

The rate of pressure application has varied between 0.05 MPa/s (Chesterton et al., 2003; Gajsar et al., 2018; Stefanik et al., 2020) and 0.59 MPa/s (Finocchietti et al., 2011) in previous studies using pressure algometry, with 0.1 MPa/s being a common choice (Deering et al., 2019; Lacourt et al., 2012; Melia et al., 2015). With the exception of two sources (Finocchietti et al., 2011; Melia et al., 2015), groups have used handheld pressures that approximate their reported pressure application rates. Communication delays between the participant and experimenter and an uneven rate of pressure application hinder pressure-pain thresholds determined by these methods. Also, the lack of real-time time-varying pressure feedback greatly hinders sub-threshold stimuli perceptions beyond the above limitations. This work used a displacement-control motor to improve over handheld methods, however an appropriate displacement rate needed to be

determined prior to testing. This involved predicting a displacement rate—indicated by the power supply's voltage, from a desired pressure application rate using regression equations unique to each motor.

Forces measured through the load cell on the algometer (MLP-300-CO, Transducer Technologies, Temecula, CA, USA) were converted into pressures by dividing by the area of the indenter, displacements were measured using infrared emitting diodes (Optotrak Certus, Northern Digital Inc., Waterloo, ON, Canada) placed on the stationary and moving aspects of the motor. Trials were taken for each of the two algometers applying pressures to the L3/L4 intervertebral space in the configuration shown in Panel E of Figure C-1 by modulating the voltage input on the power supply. The rate of pressure development dP/dt and the motor velocity v from the linear region of the trial were computed for each trial and presented in Table C-1, the regression equations built off those data to determine power supply settings for the pressure algometers are presented in Table C-2.

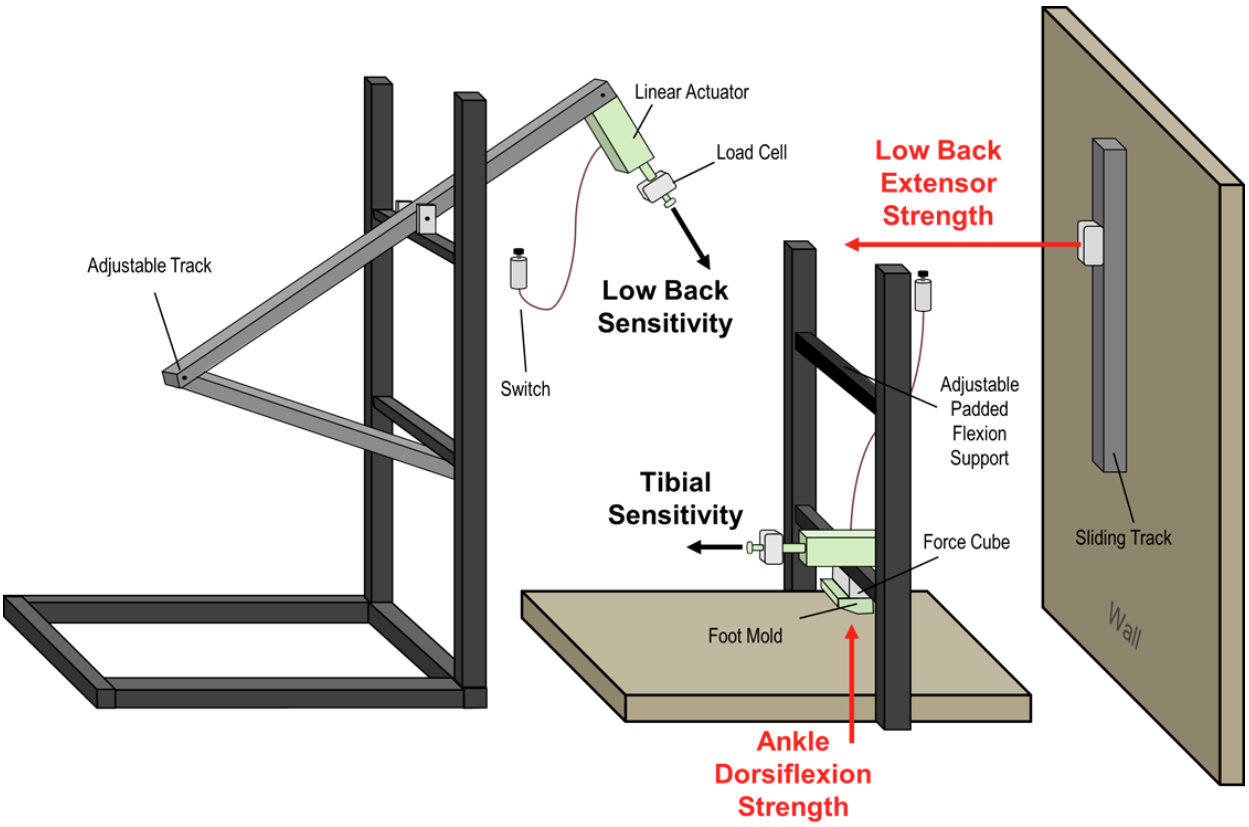

Figure C-2: Illustration of Pressure Algometers in the Context of the Instrumentation of Chapters 3 and 4. The low back pressure algometer (left) could be slid away from or towards the participant, who either stood on or sat with their feet on a wooden platform (middle). When assessing low back sensitivity, an experimenter moved the low back pressure algometer into position, then stood on base frame and guided the actuator to prevent any reactive motion and ensure that pressures were applied perpendicular to the participant's skin. See Chapters 3 and 4 for additional details on experimental protocol. There are two unlabeled load cells in gray: one for the tibial pressure algometer (middle) and one on the sliding track used to measure low back extensor strength (right).

Table C-1: Motor Velocities (v) and Rates of Pressure Development (dP/dt) for a Distribution of Supply Voltages.

Motor 1 (L3/L4)			Motor 2 (Mid-Tibia)		
Supply Voltage	v *(mm/s)*	dP/dt *(MPa/s)*	*Supply Voltage*	v *(mm/s)*	dP/dt *(MPa/s)*
5.8	2.44	0.095	6.0	2.45	0.102
6.2	2.64	0.164	6.3	2.56	0.083
6.7	2.87	0.188	6.8	2.83	0.123
7.1	3.05	0.137	7.2	3.03	0.170
7.5	3.27	0.186	7.6	3.14	0.152
8.3	3.65	0.185	7.9	3.35	0.165
8.7	3.85	0.174	8.3	3.55	0.213
9.0	3.97	0.177	8.6	3.64	0.208
9.6	4.29	0.154	9.2	3.97	0.148
10.1	4.51	0.177	9.4	4.05	0.165
10.6	4.76	0.265	10.0	4.38	0.272
11.2	5.07	0.248	10.5	4.57	0.224
11.8	5.32	0.339	10.8	4.72	0.246
			11.2	4.96	0.277
			11.4	5.01	0.277
			12.0	5.32	0.214

Table C-2: Outputs of Regression Equation Fitting Voltages to Velocities and Rates of Pressure Development. In each equation, "x" represents the supply voltage and the output is the corresponding measure.

	Motor 1 (L3/L4)		Motor 2 (Mid-Tibia)	
	Volt-v	*Volt-*dP/dt	*Volt-*v	*Volt-*dP/dt
Equation	$0.483x - 0.364$	$0.0250x - 0.0251$	$0.481x - 0.453$	$0.0272x - 0.0538$
R^2	~1.000	0.619	0.999	0.719

The minimum voltage designated by the supplier was 6.0 V. Setting voltages below this value occasionally produced uneven velocities despite being close to a target pressure rate of 0.1 MPa/s. As a result, a target rate of 0.2 MPa/s was chosen since it occupied the middle of the possible range of voltage inputs (6-12 V). This pressure rate corresponded to a velocity of 3.99 mm/s and a supply voltage of 9.0 V for the L3/L4 algometer; and a velocity of 4.03 mm/s and a supply voltage of 9.3 V for the mid-tibial motor.

The reliability of pressure-pain threshold measures using the above components and parameters was assessed using Baseline and Pre-Exposure data from Chapters 3 and 4 (Figures 3-2 and 4-1). Pressure-pain thresholds from those time points were processed as per Section 3.3.2. Intra-session reliability was tested by comparing the average of the three Baseline pressure-pain thresholds the Pre-Exposure pressure-pain threshold on that testing session. Inter-session reliability compared both the average Baseline and Pre-

Exposure measures between sessions for participants common to both sessions. Intraclass Correlations and root-mean-square residuals were computed for both comparisons and shown in Table C-3.

Table C-3: Reliability Measures for Pressure-Pain Thresholds using the Custom Pressure Algometers. The Intra-session comparison had n = 152, k = 2; the Inter-session comparison used n = 148, k = 2 for measures.

	Intraclass Correlation Coefficient		**RMS Residual (MPa)**
	Consistency	*Agreement*	
Intra-session	0.880	0.869	0.223
Inter-session	0.721	0.720	0.325

Appendix D – Solutions and Suppliers for Western Blotting

Abbreviations are described in Chapter 6.

Antibody Information

Table D-1: Primary Antibody Information for Chapter 6

Target	Host	Product Code	Supplier
PGP9.5	Rabbit	AB10404	Abcam PLC, Cambridge, UK
CGRP	Goat	PA185250	Fisher Scientific, Ottawa, ON, Canada
B1R	Mouse	H00000623-M04	Fisher Scientific, Ottawa, ON, Canada
ASIC3	Rabbit	PIPA577734	Fisher Scientific, Ottawa, ON, Canada

All secondary antibodies were HRP-positive, IgG immunoreactive, from Bio-Rad Laboratories, Montreal, QC, Canada.

Stock Solutions

1. **Muscle Lysis Buffer (20mM HEPES, 10mM NaCl, 1.5mM MgCl, 1mM DTT, 20% Glycerol, 0.1% Triton X-100), pH 7.4**

2.383 g	HEPES (4-(2-hydroxyethyl)-1-piperazineethanesulfonic acid)
0.2922 g	NaCl
0.0714 g	MgCl
0.077125 g	DTT (DL-Dithiothreitol)
100 mL	100% Glycerol
500 µL	Triton X-100

- Add all contents to 300mL double-distilled water.
- Adjust pH to 7.4.
- Top up to a final volume of 500mL with double-distilled water.
- Store at 4°C.

2. **Transfer Buffer**

6.055 g	Tris Base
28.53 g	Glycine
400 mL	Methanol

- Add distilled water up to a final volume of 2L.
- Store at 4°C.

3. 0.5M Tris-HCl, pH 6.8

7.88 g	Tris-HCl

- Dissolve in 80 mL double-distilled water.
- Adjust pH to 6.8 with NaOH.
- Bring volume up to 100 mL with double-distilled water.
- Store at room temperature.

4. 0.2M EDTA, pH 7.5

3.722 g	EDTA (Ethylenediaminetetraacetic acid)

- Dissolve in 30 mL double-distilled water.
- Adjust pH to 7.5.
- Bring volume up to 50 mL with double-distilled water.
- Store at room temperature.

5. 20% SDS

10 g	SDS (Sodium Dodecyl Sulphate)

- Dissolve in 30 ml of double-distilled water; may need heat.
- Bring volume up to 50 mL with double-distilled water.
- Store at room temperature.

6. Sample Buffer

10 g	Sucrose
7.5 mL	20% SDS
200 µL	0.5M Tris-HCl, pH 6.8
200 µL	0.2M EDTA, pH 7.5
0.62 g	DTT
200 µL	1% Bromophenol Blue

- Bring volume up to 20 mL with double-distilled water.
- Freeze in 500 uL aliquots @ -80°C.

7. 4 x Running Gel Buffer Stock; pH 8.8

36.32 g	Tris Base
0.8 g	SDS
2 mL	12M HCl

- Dissolve in 150 mL distilled water.
- Adjust pH to 8.8 with HCl.
- Bring volume to 200 mL with double distilled H_2O.
- Filter the solution through a Whatman No.1 filter paper.
- Store at 4°C.

8. 4 x Stacking Gel Buffer Stock; pH 6.8

12.12 g	Tris Base
0.8 g	SDS

- Dissolve in 160mL double-distilled water.
- Adjust pH to 6.8 with HCl.
- Bring volume to 200 mL with double-distilled water.
- Filter the solution through a Whatman No.1 filter paper.
- Store at 4°C.

9. 30% Acrylamide

60 g	Acrylamide
1.6 g	Bisacrylamide

- Dissolve in 120mL of double-distilled water.
- Adjust final volume to 200mL with double-distilled water.
- Filter the solution through a Whatman No.1 filter paper.
- Store at 4°C.

10. 10 x TBS (Tris buffered saline), pH 7.5

48.44 g	Tris Base
160.3 g	NaCl
76 mL	1M HCl

- Dissolve in 1.5L distilled water.
- Adjust pH to 7.5.
- Adjust to a final volume of 2L with distilled water.
- Store at 4°C.

11. 1 x TBS-T;

- Add 200mL of 10X TBS-T to container.
- Make to a final volume of 2L with distilled water.
- Add 2 mL of Tween-20.
- Store at room temperature

Chemicals

Table D-2: Chemical Products and Suppliers.

Chemical/Solution (Product)	Supplier
1% Bromophenol Blue	Millipore Sigma, Oakville, ON, Canada
100% Glycerol	BioShop Canada Inc, Burlington, ON, Canada
12M/1M HCl	
Acrylamide	
Ammonium Persulfate	
BCA Stock (B9643)	Millipore Sigma, Oakville, ON, Canada
Bisacrylamide	BioShop Canada Inc, Burlington, ON, Canada
BSA	
DTT: DL-Dithiothreitol	
ECL (Clarity Western Blotting Substrates)	Bio-Rad Laboratories, Montreal, QC, Canada
EDTA: Ethylenediaminetetraacetic acid	Millipore Sigma, Oakville, ON, Canada
Glycine	BioShop Canada Inc, Burlington, ON, Canada
HEPES	
Ladder (Precision Plus protein Kaleidoscope Pre-stained Protein Standards)	Bio-Rad Laboratories, Montreal, QC, Canada
Methanol	BioShop Canada Inc, Burlington, ON, Canada
MgCl	
NaCl	
Ponceau: (Ponceau S Solution)	
Protease Inhibitor (Product No 11697498001)	Cedarlane Labs, Burlington, ON, Canada
SDS: Sodium Dodecyl Sulphate	BioShop Canada Inc, Burlington, ON, Canada
TEMED	
Tris Base	
Tris-HCl	
Triton X-100	

Appendix E – Derivation of Tissue Model Constants

The collagenous tissue model based off Barrett and Callaghan (2017) required the mechanical derivation of three parameters in both a pre-creep and post-creep state: a linear stiffness k; a mean fibre resting length μ; and a spread of fibre lengths η. Additionally, a time constant τ and a decay magnitude constant β were required to model viscoelastic changes in each tissue. Human lumbar spine tissues were harvested and subjected to mechanical testing, with the resulting load-deformation curves fit to derive these parameters.

Tissues were harvested from 5 fresh-frozen cadavers (3 female; age 84.0 ± 10.5 years; Table E-1). All cadavers were screened for pathogens and contraindications for dissection as per the University of Waterloo School of Anatomy guidelines. Cadavers were stored at -20°C and thawed to 4°C over the course of 3-4 days for dissection. Following isolation of the lumbar spine and surrounding passive tissues, specimens were re-frozen at -20°C until mechanical testing. Once tissues thawed to room temperature on the mechanical testing date, the posterior annulus fibrosus (AF) and supraspinous-interspinous ligament complex (SILC) were dissected away from the joint. AF and SILC samples were harvested as bone-tissue-bone complexes and randomized into two testing streams. AF samples were split into left and right halves if too thick to be clamped anterior-posteriorly (and were instead clamped medial-laterally) but were otherwise left intact. SILC were harvested from up to four locations based on specimen integrity and ability to fit the sample into the clamps needed for testing (Figure E-1).

Table E-1: Available Cadaveric Donor Characteristics.

Donor ID	Age (years)	Sex	Cause of Death
20128	85	M	Prostate Cancer
20129	83	F	End Stage Bronchiectasis
20130	67	M	Coronary Artery Disease
20131	100	F	COPD, Respiratory Disease
20132	85	F	Seizure Disorder, Brain Mass

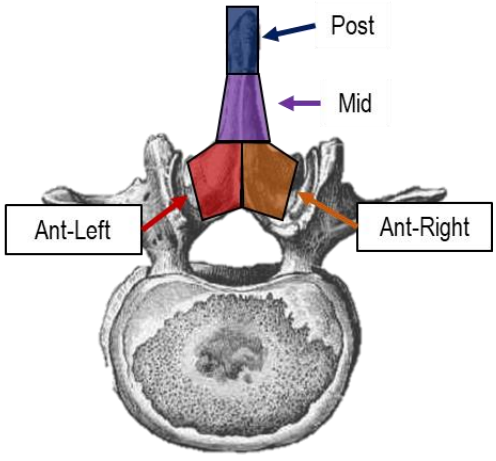

Figure E-1: Supraspinous-Interspinous Ligament Complex Harvesting Regions. Post and Mid occupied the spinous process, while Ant-Left and Ant-Right included regions of the complex connected to the lamina of the vertebral arch.

Common to both testing streams, samples had their soft-tissue cross-sectional areas measured with a 2D laser displacement sensor (LJ-V7080, Keyence Corporation, Osaka, Japan) and underwent 20 cycles of a 10% strain cyclical pre-load 2 Hz (Bass et al., 2007). For the first testing stream, samples underwent displacement-controlled failure tests at a 5% strain per second. For the second testing stream, samples underwent a 30-minute stress relaxation test before undergoing the same failure test as in the first testing stream. Tissues were held at an estimated strain corresponding to 11.1° of intervertebral flexion (Viggiani et al., 2017) determined by multiplying the posterior distance between the tissue and the centre of the vertebral body by 0.1937 radians (equivalent to 11.1°). Both streams used a load cell (Mini40, ATI Industrial Automation, Apex, NC, USA) mounted to a robot arm (Motoman HGS II, Yaskawa Electric Corporation, Kitakyushu, Japan) controlled through custom-written C++ in Visual Studio (version 16.8, Microsoft Corporation, Seattle, WA, USA). Loads in N were sampled directly from the load cell at 100 Hz; displacements were sampled directly from the robotic arm at 100 Hz.

The load-displacement curves from the failure tests (first and second streams) were fit to Equation 9 in Barrett and Callaghan (2017) to derive k, μ, and η (Equation E-1). $F(x(t))$ is a function of tissue displacement $x(t)$ over time, and erf is the error-function. To determine the tissue properties k, μ, and σ, the result of Equation F-1 was fit to the load profiles using the `optimize.curve_fit` function in the `scipy` library in Python (v 3.6.3). Note that Equation E-1 is mathematically equivalent to Equation 7-10, however this form is expressed purely relative to tissue displacements, $x(t)$, while the variant presented in Chapter 7 is expressed in terms of displacement z-scores, $z(t)$.

$$F\big(x(t)\big) = \frac{k\eta}{\sqrt{2\pi}} \exp\left(-\frac{\big(\mu + x(t)\big)^2}{2\eta^2}\right) + \frac{k\big(\mu + x(t)\big)}{2}\left[\operatorname{erf}\left(\frac{\mu + x(t)}{\sqrt{2}\eta}\right) + 1\right] \tag{E-1}$$

The viscoelastic constants τ and β were determined by fitting the load-time profile of the stress-relaxation test to the Kohlrausch-Williams-Watts function $\psi(t)$ (Sasaki et al., 1993) (Equation E-2). The constants F_0 and F_1 in Equation E-2 represent the initial and final loads measured during the stress-relaxation test.

$$\psi(t) = F_1 + (F_0 - F_1)\exp\left[-(t/\tau)^{\beta}\right] \tag{E-2}$$

The sample cross-sectional areas and the outcomes of the curve-fitting procedures are presented in Tables E-2 (AF) and E-3 (SILC), sorted by donor ID, joint level, and region.

Table E-2: Tissue Properties for the Annulus Fibrosus Samples. ID refers to the donor identification number from Table E-1; see text for region definitions. Blank entries for τ and β indicate samples in the first data stream, others were in the second data stream.

ID	Level	Region	CSA (mm^2)	k (N/mm)	η (mm)	μ (mm)	τ (s)	β (unitless)
20129	L2/L3	Left	120.6	2.015	0.001	-0.536	0.269	0.217
20129	L2/L3	Right	139.6	20.782	0.452	-2.088		
20130	L1/L2	Whole	140.5	41.684	0.000	-0.913		
20131	L2/L3	Whole	58.8	1.870	1.234	-1.910	0.124	0.228
20132	L3/L4	Left	99.3	228.935	1.366	-7.818	0.007	0.156
20132	L3/L4	Right	81.9	30.602	0.351	-2.014	42.265	0.453

Table E-3: Tissue Properties for the Supraspinous-Interspinous Ligament Complex Samples. ID refers to the donor identification number from Table E-1; see Figure E-1 for region definitions. Blank entries for τ and β indicate samples in the first data stream, others were in the second data stream.

ID	Level	Region	CSA (mm^2)	k (N/mm)	η (mm)	μ (mm)	τ (s)	β (unitless)
20128	L1/L2	Ant-Left	34.1	31.322	1.719	-5.920		
20128	L1/L2	Ant-Right	43.3	17.039	1.415	-2.337		
20129	L1/L2	Mid	21.3	7.377	0.860	-5.439		
20129	L1/L2	Post	47.9	21.072	0.783	-3.468		
20129	L2/L3	Mid	49.6	17.403	0.601	-8.195	13.308	0.345
20130	L1/L2	Ant-Left	84.6	37.993	0.700	-3.435		
20130	L2/L3	Ant-Left	136.6	43.264	2.310	-6.109	0.854	0.234
20131	L2/L3	Mid	103.6	1.872	0.489	-5.570	4.987	0.335
20132	L3/L4	Mid	151.5	32.342	0.907	-7.954	0.583	0.229

Due to the wide range of values and small number of samples within each tissue type and region, the median values (Table E-4) were chosen and used in Chapter 7 when applicable.

Table E-4: Median Tissue Properties used in the Nociceptive Model. AF – Annulus Fibrosus; SILC – Supraspinous-Infraspinous Ligament Complex.

Tissue	CSA (mm^2)	k (N/mm)	η (mm)	μ (mm)	τ (s)	β (unitless)
AF	109.9	25.692	0.401	-1.962	0.197	0.223
SILC	49.6	21.072	0.860	-5.570	2.921	0.285

Appendix F – Smooth Interpolation Technique

The functions constructed in the Chapter 7 required combining two or more functions into a single waveform with a continuous first derivative. The following interpolation technique was employed with the general form of Equation F-1.

$$y(t) = f(t) + h(t)[g(t) - f(t)] \tag{F-1}$$

The output $y(t)$ is a smoothed shape connecting two functions of time (t), $f(t)$ and $g(t)$.There is no restriction on the shape of $f(t)$ or $g(t)$ so long as the two intersect each other or come arbitrarily close to intersecting each other at some time point t_0. The resulting output $y(t)$ will be mostly equal to $f(t)$ for $t < t_0$, and be mostly equal to $g(t)$ for $t > t_0$. The function $h(t)$ must have the bounds $[0, 1]$, smoothly move between those bounds, and be shifted along the time-axis such that $h(t) = 0.5$ at or around $t = t_0$. A $\tanh(x)$ function was modified for this purpose in the thesis, however the error function, logistic function, or another similar one would be suitable. The general form of the $\tanh(x)$ function used for $h(t)$ is shown in Equation F-2:

$$h(t) = \frac{1}{2}[1 + \tanh(t - t_0)] \tag{F-2}$$

This "base" version in Equation F-2 takes roughly 5 seconds to pass from 0 to 1, which can be interpreted as 5 seconds to transition from the first input function $f(t)$ to the second input function $g(t)$. This long period relative to most of the simulated data employing this technique (~ 10 seconds) makes the resulting output function $y(t)$ very skewed. Therefore, a "squish" factor, h_0, was included that causes the transition from $f(t)$ to $g(t)$ to occur more quickly (Equation F-3). Figure 7-2 depicts how h_0 affects the resulting shape of $y(t)$.

$$h(t) = \frac{1}{2}[1 + \tanh(h_0(t - t_0))] \tag{F-3}$$